Modeling the Land-Hydrology-Atmosphere Interface

Aaron Boone

Habilitation à Diriger les Recherches
Institut National Polytechnique - Toulouse

Spécialité: Sciences de la Terre et de l'Univers

Thèse dirigée par **Jean-François Mahfouf**
CNRM, Météo-France, Toulouse

Modeling the Land-Hydrology-Atmosphere Interface

Aaron A. Boone

Soutenue le 27 Mai 2016
devant le jury composé de:

Isabelle Braud, DR IRSTEA, IRSTEA, Lyon	Rapporteur
Mehrez Zribi, DR CNRS, CESBIO, Toulouse	Rapporteur
Sonia Seneviratne, Pr ETH, Zurich, Suisse	Rapporteur
Eric Martin, IPEF, IRSTEA, Aix	Examinateur
Serge Chauzy, Pr Univ Paul Sabatier, Toulouse	Président
Jean-François Mahfouf, IPEF, CNRM-Météo-France, Toulouse	Directeur de thèse

UMR 3589 Centre National de Recherches Météorologiques
GMME/MOSAYC
Météo-France
14 ave G Coriolis, 31075 TOULOUSE CEDEX, France
aaron.boone@meteo.fr

Remerciements

List of Acronyms-1 of 4

AEJ	African Easterly Jet
ALMIP	AMMA Land surface Inter-comparison Project
ARTS	AMIP2 mesoscale River RouTing Scheme
AMETHYST	Assessment of changes in MEdiTerranean HYdro-resources
AMMA	African Monsoon Multidisciplinary Analysis
AMMA-CATCH	AMMA-Couplage de l'Atmosphère Tropicale et du Cycle Hydrologique
AMSR-E	Advanced Microwave Scanning Radiometer for Earth Observing System
ANOVA	ANalysis Of VAriance
ANR	L'Agence Nationale de la Recherche
AROME	Applications of Research to Operations at Mesoscale
ARPEGE	Action de Recherche Petite Echelle Grande Echelle
CABLE	Community Atmosphre Biosphere Land Exchange model
CAM	Community Atmospheric Model (NCAR)
CEN	Centre d'Etude de la Neige (Météo-France)
CERFACS	Centre Européen de Recherche et de Formation Avancée en Calcul Scientifique
CESBIO	Centre d'Etudes Spatiales de la BIOsphère
CHS	Continental Hydrologic System
CLM	Common Land Model
CMEM	Community Microwave Emission Model
CMIP	Coupled Model Intercomparison Project Phase
CNES	Centre Nationale d'Etudes Spatiales
CNRM	Centre National de Recherches Meteorologiques
CPU	central processing unit
CROCUS	detailed multi-layer snow process model developed at CEN, Météo-France
DA	Data Assimilation
DWI	deep water infiltration
ECMWF	European Centre for Medium-Range Weather Forecasts
ECMWF-FC	ECMWF ForeCast
ECOCLIMAP	ECOlogical CLImate MAP physiographic database
EKF	Extended Kalman Filter
ERA	ECMWF Interim Re-Analysis
ESM	Earth System Model

List of Acronyms-2 of 4

FLake	freshwater lake model
GCM	Global Climate (or Circulation) Model
GEWEX	Global Energy and Water Cycle Exchanges project
GLASS	Global Land-Atmosphere System Study
GLDAS	Global Land Data Assimilation System
GMGEC	Groupe de Météorologie de Grande Echelle et Climat (at CNRM)
GRACE	Gravity Recovery and Climate Experiment
GSWP	Global Soil Wetness Project
HIRLAM	High Resolution Local Area Modelling for numerical weather prediction
HWSD	Harmonized World Soil Database
HYDRO-WEB	Produits/Services d'Observations et d'Archives/Hydrologie (LEGOS)
HyMAP	The Hydrological Modeling and Analysis Platform
IGBP	International Geosphere-Biosphere Programme
INRA	Institut National de la Recherche Agronomique
IOP	Intensive Observing Period
IPCC	Inter-governmental Panel on Climate Change
ISBA	Interactions between the Surface Biosphere Atmosphere
ISBA-3L	ISBA 3-layer Force Restore hydrology option
ISBA-Ags	ISBA photosynthesis option
ISBA-DIF	ISBA soil multi-layer diffusion option
ISBA-ES	ISBA multi-layer Explicit Snow option
ISBA-MEB	ISBA Multi-Energy-Balance (explicit vegetation canopy) option
JAS	July-August-September (average)
JJAS	June-July-August-September (average)
JULES	Joint UK Land Environment Simulator
LAG	Lagrangean rainfall product
LAI	Leaf Area Index
LDAS	Land Data Assimilation System
LEGOS	Laboratoire d'Etudes en Géophysique et Océanographie Spatiales
LERMA	Laboratory for Studies of Radiation and Matter in Astrophysics et Atmospheres

List of Acronyms-3 of 4

LMTG	Laboratoire des Mécanismes et Transferts en Géologie
LGGE	Laboratoire de Glaciologie et Géophysique de l'Environnement
LS3MIP	Land Surface, Snow and Soil Moisture Model Intercomparison Project
LSA-SAF	Land Surface Analysis Satellite Applications Facility
LSCE	Laboratoire des Sciences du Climat et l'Environnement
LTHE	Laboratoire d'études des Transferts en Hydrologie et Environnement
LULC	Land Use Land Cover
LULCC	Land Use Land Cover Change
LSM	land surface model
MEB	ISBA Multi-Energy-Balance (explicit vegetation canopy) option
MEB-L	ISBA-MEB option with forest Litter
MELDAS	Mexican Land Data Assimilation System
MEM	Microwave Emission Model
Meso-NH	Mesoscale-Non-Hydrostatic model
MIP	Model Inter-comparison Project
MOCAM-UA	Multiobjective Complex Evolution optimization algorithm
MODCOU	Distributed Groundwater model
MOSAYC	Modélisation surface-atmosphère-hydrologie couplées team at CNRM
MOSES	U.K. Meteorological Office Surface Exchange Scheme
MSE	Laboratoire HydroSciences Montpellier
NASA	National Aeronautics and Space Administration
NASA-GSFC	NASA Goddard Space Flight Center
NASA-JPL	NASA Jet Propulsion Laboratory
NASA-MAP	NASA-GSFC Mesoscale Atmospheric Processes branch
NCAR	National Center for Atmospheric Research (USA)
NRMSE	Normalized Root Mean Square Error
NS	Nash-Sutcliff statistical metric
NSIDC	National Snow and Ice Data Center (USA)
NWP	Numerical Weather Prediction
ORCHIDEE	Organising Carbon and Hydrology In Dynamic Ecosystems
OSSE	Observing System Simulation Experiment
PILPS	Project for the Intercomparison of Land surface Parameterization Schemes

List of Acronyms- 4 of 4

PLACE	Parameterization for Land-Atmosphere-Cloud-Exchange
PAPIT	Programa de Apoyo a Proyectos de Investigacion e Innovacion Technologica
PLUMBER	The Plumbing of Land Surface Models
RAPID	the Routing Application for Parallel computatIon of Discharge
RCA	Rossby Centre Regional Climate Model
RCM	Regional Climate Model
RMSE	Root Mean Square Error
Rhône-AGG	Rhône AGGregation land surface model intercomparison project
ROSES	NASA Research Opportunities in Space and Earth Sciences
SAFRAN	Système d'Analyse Fournissant des Renseignements Atmosphériques Ã la Neige
SCFA	Snow Covered Fractional Area
SIM	SAFRAN-ISBA-MODCOU distributed hydrometeorological model
SiSPAT	Simple Soil Plant Atmosphere Transfer
SMHI	Swedish Meteorological and Hydrological Institute
SnowMIP	Snow Model Intercomparison Project
SOP	Special Observing Period
SURFEX	SURFace EXternalisé (surface offline and coupling platform)
SVAT	Soil-Vegetation-Atmosphere Transfer scheme
SWOT	Surface Water Ocean Topography satellite mission
THI	Thiessen (nearest-neighbor) rainfall product
TOSCA	Terre, Océan, Surfaces continentales, Atmosphère (CNES research opportunities)
TRIP	Total Runoff Integrating Pathways
TRMM	Tropical Rainfall Measuring satellite Mission
UCLA	University of California at Los Angeles, USA
UNAM	Universidad Nacional Autònoma de México
VIC	Variabile Infiltration Capacity model
WAM	West African Monsoon
WAMME	West African Monsoon Modeling and Evaluation
WCRP	World Climate Research Programme
WMO	World Meteorological Organization
WRF	non-hydrostatic Weather Research and Forecast model

Contents

1 Introduction **9**
- 1.1 Parameterizing the land surface . . . 9
- 1.2 Research Themes . . . 11

2 The improved representation of land surface and hydrological processes **13**
- 2.1 Introduction . . . 13
- 2.2 Surface hydrological processes . . . 15
  - 2.2.1 Improved vadose-zone water transfer . . . 15
  - 2.2.2 Soil phase changes . . . 16
  - 2.2.3 Explicit physically-based snowpack . . . 17
- 2.3 Multi-Energy Budget: MEB . . . 19
  - 2.3.1 MEB model . . . 20
  - 2.3.2 Evaluation at the local scale . . . 23
  - 2.3.3 Evaluation for multiple climates, forest types . . . 27

3 Land surface Model Inter-comparison Projects **31**
- 3.1 Introduction . . . 31
- 3.2 Coupled Land-hydrology MIP: The Rhône AGGregation project . . . 33
  - 3.2.1 Project Objectives . . . 33
  - 3.2.2 Main Conclusions . . . 34
- 3.3 Coupled Land-atmosphere MIP: The WAMME project . . . 37
  - 3.3.1 Overview, Objectives and Methodology . . . 37
  - 3.3.2 Main Conclusions . . . 38
- 3.4 Offline Land MIP: ALMIP . . . 41
  - 3.4.1 ALMIP1: Regional Scale . . . 41
  - 3.4.2 ALMIP2: Meso-Scale . . . 47

4 Improved Hydrological Modeling using Remote sensing data **57**
- 4.1 Introduction . . . 57
- 4.2 Improving hydrological modeling: The SWOT mission . . . 57
  - 4.2.1 Research Objectives . . . 58
  - 4.2.2 Strategy . . . 59
  - 4.2.3 Regional Scale Hydrology . . . 60

4.2.4 Large to Global Scale Hydrology 62

5 Prospectives **70**
5.1 Land surface and hydrological modeling 70
5.1.1 Lakes and closing the water cycle 71
5.1.2 Anthropization 71
5.1.3 Vegetation processes 72
5.2 Land surface intercomparison projects 73
5.3 Hydrology from space: SWOT 74
5.3.1 River storage and discharge 74
5.3.2 Lake storage and exchanges 74

6 Bibliography **76**

7 Curriculum Vitae **92**
7.1 Formation 92
7.2 Expérience professionnelle 92
7.3 Encadrement d'étudiants 93
7.3.1 Thèse 93
7.3.2 Post-Doc 93
7.3.3 Comité du thèse 94
7.3.4 Jury de thèse 94
7.4 Divers 95
7.5 Responsabilités 95
7.6 Participation à l'organisation de conférences, ateliers 96
7.7 Liste de Publications 96
7.7.1 Revues à comité de lecture 96
7.7.2 Actes de colloques à comité de lecture 106
7.7.3 Chapitres d'ouvrages 106
7.7.4 Publications dans des revues sans comité (depuis 2001) 107
7.7.5 Communications à des congrès, symposium 109
7.7.6 Séminaires, Workshops 114

8 Selected Publications **117**

Chapter 1

Introduction

1.1 Parameterizing the land surface

My research thematic focuses on the improved representation and understanding of land surface and hydrological processes and their coupling with the atmosphere. To accomplish this goal, the strategy is to improve the surface component (the land surface model or LSM) of atmospheric and hydrological numerical models and the coupling, notably for those models used at Centre National de Recherches Meteorologiques (CNRM), for research, operational weather forecasting, climate research, regional scale operational hydrological analysis and for building surface reanalysis datasets for research and applications. The main function of the LSM in this context is to partition the incoming solar and longwave atmospheric radiation and precipitation fluxes into the different storage and flux components of the surface energy and water budgets. As such, it represents vadose-zone hydrology, snowpack evolution, soil heat transfer and freeze-thaw cycles, and vegetation mass, heat and chemical (e.g. Carbon) exchanges with the soil, snow and the atmosphere. When confronted with, forced by or incorprating observations, LMSs can be used as a basis to improve our understanding and, as a result, prediction.

The LSM is both a conceptual and a mathematical representation of those surface processes for which we have a basic fundamental understanding. In addition to adequately describing the processes, the problem of constructing a LSM parameterisation must be approached across scales, where processes are resolved in such models from the local (or the parcel, as small as on the order of 10s of m), to the mesoscale (100m to several km), regional (km to 10s of km), to global (10s to 100s of km). Of course, the aforementioned discrete scale definitions are somewhat artificial and result either from historical reasons and/or for convenience, as the actual processes are continuous across scales. The research community is supporting the idea of *seamless prediction*, in which a single earth system model can be applied over all of the aforementioned scales. This requires new thinking and model development since many models have been designed in the past with a specific range of scale in mind. Thus, such parameterizations must account for scale change either statistically, through scaled input parameters, or a combination of both. Therefore, a combination of theory, modeling, analysis and observations (data from field campaigns, re-analysis data-sets and satellite-based data) at multiple scales have been used to address the essential science questions posed within my research.

Generally speaking, the research community has a fundamental knowledge of how to model certain surface processes using very detailed approaches, however, progress is made seemingly slowly at times in fully coupled or spatially distributed models since such numerical modeling must strike a sometimes delicate balance between computational usage or efficiency, the ability to accurately define input parameters, and the complexity of the physical parameterization. Such factors weigh heavily for both operational applications (where tight schedules for getting products to end users must be respected) and climate research (where simulations can take months of CPU time, which is a resource in itself to be shared among researchers). And of course, academic research sometimes requires simulations over large domains using dense computational grids for significant integration periods. In order to strike a balance, researchers use the strategy of developing a parameterization which only considers what are deemed to be the first order processes (or even only those for which we have reasonable estimates of input parameters). Such models are usually developed and bench-marked based on more complex process-based schemes. As our understanding of processes, computational resources and the availability of observational or satellite data sets all increase, complexity can be added. This is the approach I have taken (as do many researchers in both the French and inter-national communities) in my work at both National Aeronautics and Space Administration-Goddard Space Flight Center (NASA-GSFC) and CNRM.

It is widely accepted that the best way to improve our understanding of a given system using models is to adopt a multi-model approach, since each particular model (whether it be an LSM, hydrological or even a fully coupled atmospheric model) has its particular biases and deficiencies, or conversely, strengths. For this reason, I have participated in and lead several international multi-model intercomparison studies. The mains goals have been both to identify where LSMs might have weaknesses for (or even an absence of) certain critical processes and then to provide advice for improvements, and to get a more robust multi-model vision (by considering LSM uncertainty) of surface states and fluxes for a particular region over a given time frame.

Finally, In the face of climate change, improved simulations by earth system models are needed to better understand the potential feedbacks for both mitigation and adaptation strategies to be developed for society, since such model simulations are the basis for the reports by the Inter-governmental Panel on Climate Change (IPCC). A part of the needed improvements resides in obtaining a better understanding of which land surface and hydrological processes have potentially the largest feedback with the atmosphere, and the nature of the coupling itself. For example, some of the Coupled Model Intercomparison Project Phase 5 (CMIP5: Taylor et al., 2012) models did not include interactive vegetation, which removes one of the potentially important feedback mechanisms (via changes in vegetation coverage on climate and Carbon sinks). Part of the problem is that such models introduce considerable degrees of freedom in terms of numerous additional (and sometimes difficult to define) parameters, and that potential feedbacks in a global climate model (GCM) can be exaggerated or even false owing to interactions with other parameterizations in the model which have their own biases or other errors. Therefore, considerable work has been done in the international and national communities, notably at CNRM, to improve the Carbon cycle in the SURFace EXternalisé (SURFEX: Masson et al., 2013) platform used in the Action de Recherche Petite Echelle Grande Echelle climate (ARPEGE-Climat) model. Part of this work also necessitates improving the representation of

vegetation in a consistent manner, and its coupling with soil and snow processes. This has been one of the core subjects of my research. Finally, climate warming in the lower atmosphere is predicted to be largest in high latitude regions, where feedbacks with the snow cover and the permafrost are critical. Significant effort has been undertaken at CNRM to improve the snow and soil parameterizations and their interactions with vegetation in the Interactions between the Surface Biosphere Atmosphere (ISBA) LSM in the SURFEX platform.

1.2 Research Themes

The work presented in this dissertation is broken into three sections covering the following topics:

1. land surface model physics developments and evaluation
2. improved process understanding and modeling within the context of both offline and online model intercomparison studies
3. the use of satellite-based data to improve large scale hydrological and land surface modeling and estimates of surface states and fluxes.

Chapter 2 presents an overview of the different LSM development work that I have done, mainly within the ISBA LSM at CNRM. Four improvements and new parameterizations were made during my thesis, a sub-root zone soil layer (ISBA-3L) which is currently used in the operational weather forecast model AROME at Météo-France, a multi-layer soil diffusion option for soil heat and liquid water transfer (ISBA-DIFfusion) which has undergone continuous improvements since its development and is now used in the ARPEGE climate model at Météo-France, a scheme to model soil ice (which can be used with ISBA-DIF or with the Force-Restore soil option), and a multi-layer snow process model (ISBA-ES: Explicit Snow) which has also undergone continuous improvements and is used in ARPEGE-Climat. All of the aforementioned schemes are also available for use within the Mesoscale research model Meso-NH. I have continuously worked on improving and evaluating these schemes, not to mention using them in numerous diverse applications, with different researchers both at CNRM and other laboratories. Most recently, I have lead an initiative to develop an explicit vegetation scheme which separates the vegetation canopy from the soil and also includes an explicit forest litter scheme. This scheme represents the culmination of the aforementioned physics improvements in moving away from the conceptual Force-Restore approach to a more explicit representation of surface processes. The vegetation scheme is at the heart of the LSM as it is coupled to all of the aforemtnioned parameterizations. This part of my research is part of the ongoing community-wide effort to continually improve the representation of and surface and hydrological processes which are of importance towards obtaining a better understanding of the fully coupled atmosphere-land-ocean system with the ultimate goal of improving prediction from short (hours to days), medium (7 days to seasonal) to climate (annual to hundreds of years) time scales.

Chapter 3 presents a summary of my work as a part of different international model intercomparison projects (MIPs). During my career, I have participated in or lead multiple international

LSM MIPs in offline mode: Project for the Intercomparison of Land surface Parameterization Schemes (PILPS), Global Soil Wetness Project (GSWP), Snow Model Intercomparison Project (SnowMIP), Rhône-AGGregation project (Rhône-AGG), ALMIP, and The Plumbing of Land Surface Models (PLUMBER), or coupled with the atmosphere: West African Monsoon Modeling and Evaluation (WAMME) and African Monsoon Multidisciplinary Analyses (AMMA). These projects addressed a number of scientific issues, among which are related to i) the ability of LSMs to simulate surface and below-surface states and fluxes for a range climate conditions and surface characteristics, ii) the coupling with hydrology, iii) the influence of land surface processes on the atmosphere and the attendent feedbacks, and the iv) the scaleability of certain simulated surface processes. For example, the focus of the international African Multidisciplinary Monsoon Analysis (AMMA) LSM Intercomparison Project (ALMIP), which I have been running since 2006 (ALMIP phase 2 since 2009 with a French core group of 5 other researchers), is to improve our understanding and modeling of land surface and hydrological processes in West Africa, in particular, in regions where the combination of water scarcity, population growth and potential climate change are posing big challenges to regional resource managers and decision makers. In addition, when forced by satellite products, notably rainfall and physiographic data, multi-model land surface models product outputs that are akin to a reanalysis and can be used to gain a more accurate view of a particular system, obtain a measure of model uncertainty, and even help improve the representation of surface processes in fully coupled models.

In Chapter 4, an overview of methodologies to optimally combine satellite data and the hydrological component of land surface models is presented. I have lead several studies as a part of the upcoming joint CNES-NASA Surface Water Ocean Topography (SWOT) satellite mission, which will provide global estimates of inland surface water storage change as products or by combination with models (e.g. using calibration or data assimilation) using altimetry. Thus, models must be prepared to ingest SWOT data by launch. Once the satellite is launched, near-real time hydrological analysis systems will also need to be ready in gest this data in an optimal fashion at the global scale.

In the final chapter, Chapter 5, I present a brief prospective of my research priorities and how they attempt to address scientific issues and questions identified by the French and international communities.

Chapter 2

The improved representation of land surface and hydrological processes

2.1 Introduction

Land surface models (LSMs) were originally implemented in numerical weather prediction (NWP) models to provide interactive lower boundary conditions for atmospheric radiation and turbulence schemes, therefore they compute the fluxes of heat, mass and momentum between the land and the atmosphere. In the past two decades, LSMs have evolved considerably to include more physical processes in order to meet the growing demands of both the research and the user communities. Processes such as photosynthesis and the associated Carbon fluxes, aerosol emissions, soil moisture prediction (estimate of drought severity, initial values for flash flood prediction), vegetation phenology (biomass evolution, net primary production), surface runoff and exchanges with ground water, atmosphere-lake exchanges, snow pack dynamics and coverage, and near surface urban meteorology. The LSM parameterization treats unresolved scale-dependent processes as a function of some grid-average state variable though a combination of conceptual models, empirical relationships, theory and fundamental mathematical laws.

I began my research career in 1992 at NASA-GSFC working on improving and developing a coupled 1D land surface-PBL model (Wetzel and Boone, 1995; Boone and Wetzel, 1996) called the Parameterization for Land-Atmosphere-Cloud-Exchange (PLACE). My work centered on improving the representation of soil heterogeneity (e.g. Boone and Wetzel, 1999), soil heat and mass transfer, and cold-season processes. PLACE was then incorporated into two research mesoscale models to study the influence of soil moisture conditions on deep convection. Since my arrvial in France in 1997, I have been working with researchers at CNRM, Météo-France with the main objective of improving the Interactions between the Surface Biopshere Atmosphere (ISBA: Noilhan and Planton, 1989; Noilhan and Mahfouf 1996) LSM, as part of the SURFac Externalisé (SURFEX: Masson et al., 2013) platform, for operational numerical weather prediction, climate simulations, hydrological monitoring systems, land surface reanalysis and research applications. Several new schemes were developed within ISBA during my PhD work (Section 2.2), but since that time, considerable work has been ongoing by PhD students, post-doctoral fellows and CNRM researchers to continuously update, evaluate and improve the

schemes presented herein, along with testing the schemes in operational hydrometeorological modeling systems and various numerical weather prediction models. This will be described in this Chapter. In addition, a new development is also presented (Section 2.3), which will be the focus of a considerable amount of my research activity in upcoming years. An illustration of the modeled processes which I have developed and have continued to collaborate on is shown in Fig. 1.

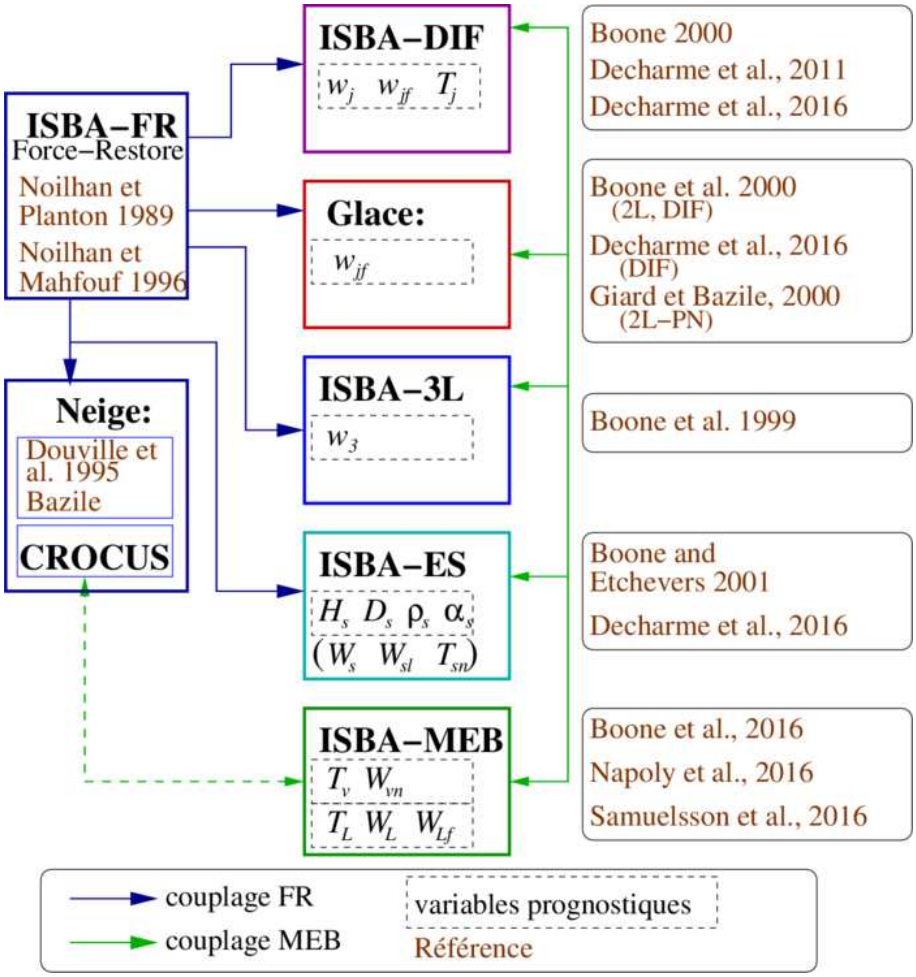

Figure 2.1: Schematic representation of the surface processes modeled within ISBA as a part of SURFEX. My model development work centers around the natural land surface, including vadose zone soil hydrology, soil heat transfer and freeze-thaw processes, snow, and vegetation.

2.2 Surface hydrological processes

2.2.1 Improved vadose-zone water transfer

The original two-layer Force-Restore hydrological model (Noilhan and Planton, 1989) consists in a single bulk soil layer (generally having a thickness on the order of 50 cm to several m) coupled to a superficially thin surface soil layer which is meant to represent the daily cycle of drying and moistening at the surface. Thus, the model simulates so-called fast processes which occur at sub-diurnal timescales which are pertinent to short term numerical weather prediction, a realistic simulation of soil evaporation, and provides a longer term water storage reservoir which provides a source for transpiration and a certain degree of memory in the ground. This scheme was based on the pioneering work of Deardorff (1977, 1978). However, limitations to this two-layer approach were found through participation in the international land model intercomparison Global Soil Wetness Project (GSWP: Dirmeyer 1997). It was determined that the computation of the soil water index (SWI) and the partitioning of precipitation between runoff and evapotranspiration within ISBA should be improved by distinguishing between a plant root-extraction layer and a sub-root zone soil layer (Douville 1997). As a result, a third hydrological soil layer was added to ISBA (Boone et al., 1999) which included a root zone diffusion force-restore coefficient (to permit capillary rise into the root zone) which was parameterized as a function of soil texture and calibrated based on the results of an explicit multi-layer soil model. A root-zone gravitational drainage term based on Mahfouf and Noilhan (1996) was also added. This option is named ISBA-3L (three hydrological layers). This option became the default for hydrology and was used in numerous research projects. For example, tt has been used up until the present time within the operational version of the hydrometeorological model SAFRAN-ISBA-MODCOU (SIM: Habets et al., 2008) and it is currently used in the non-hydrostatic operational numerical weather prediction system AROME at Météo-France (Seity et al., 2010).

Development of the ISBA-3L scheme has essentially ended (although it will continue to be a model option under the SURFEX for the foreseeable future) in favor of the explicit soil diffusion scheme called ISBA-DIFfusion (ISBA-DIF: Boone et al., 2000; Decharme et al., 2011; Decharme et al., 2016). This option consists in an explicit multi-layer diffusion scheme for heat transfer, and the Richard's equation for vertical soil water transfer. Compared to the Force-Restore approach, this model can represent the sometimes significant near surface gradients of heat and moisture, permits the use of an explicit vertically varying root zone distribution, facilitates the use of satellite data and computing various soil moisture diagnostics since the soil grid geometry is explicitly defined, and allows for consideration of a heterogeneous soil property (texture) profile. ISBA-DIF was originally developed as a detailed reference for the Force-Restore approach, and it became an ISBA option for specific research projects. But since that time, efforts have been initiated to implement this scheme into operational hydrometeorological models (such as SIM), the basis for road condition forecast modeling (Bouilloud et al., 2009) and coupled to the detailed snow scheme CROCUS used for operational avalanche forecasting (Brun et al., 2012) at Météo-France. Efforts have also been undertaken to include it within numerical weathr prediction models (such as the Mesoscale-Non-Hydrostatic model, Meso-NH: Lafore et al. 1998). For example, it will be the default scheme used in Action de Researche Petite Echelle Grande Echelle (ARPEGE: Courtier and Geleyn 1988) Climat, notably for the

upcoming Coupled Model Intercomparison Project Phase 6 (CMIP6) exercise.

Since its original development, the scheme has been improved upon and undergone extensive evaluation at the local (Decharme at al., 2011; Best et al., 2015; Haughton et al., 2016), the regional (Habets et al., 2003; Boone et al., 2009a,b; de Rosnay et al., 2009) and the global scale (Decharme et al., 2016). The main improvements compared to the original model of Boone et al. (2000) are increased vertical resolution, the addition of a Green-Ampt based infiltration scheme (needed owing to the combination of higher vertical resolution and potentially larger time steps, such as those use in ARPEGE-Climat), and a simplified vertical interpolation scheme for computing inter-facial fluxes (owing to the higher vertical resolution). These improvements have been shown to improve results in terms of local scale soil moisture, turbulent fluxes and river discharge (when coupled to a lateral transfer scheme: a recent example is Getirana et al., 2014b).

As a final note, in terms of processes, ISBA-DIF only considers (explicitly) vertical mass transfer along the liquid water gradient (expressed as matric potential) and gravitational drainage (i.e. flow induced owing to departures from hydrostatic equilibrium), and heat transfer along the thermal gradient. LSMs exist which model a much more complete set of soil heat and mass vertical transfer processes (such as the Simple Soil Plant Atmosphere Transfer LSM, SiSPAT, Braud et al., 1995) based on the work of Philip and De Vries (1975) and Milly (1982), but the inclusion of such processes makes the model more complicated for large scale (in the limit, global scale) applications (in part, owing to defining needed parameters) and data assimilation for operational weather forecasting. But, such problems are not absolute limits. It is likely that ISBA-DIF will continue to include more such processes in the future as further advances are made in terms of assembling needed spatially distributed input parameters and data assimilation, and as fully coupled earth system models incorporate an ever increasing range of processes.

2.2.2 Soil phase changes

Soil water freezing processes are critical for numerical weather prediction over cold regions. The most evident example comes from simulating future projections of the climate: permafrost changes could be brought on by climate change, thereby causing significant feedbacks between the surface in terms of water storage, snowpack evolution, greenhouse gas release, and heat transfer and storage. Cox et al. (1999) incorporated soil freezing physics into the U.K. Meteorological Office Surface Exchange Scheme (MOSES) LSM coupled to a climate model and obtained improved atmospheric simulations for high-latitude regions, primarily from the latent heating from soil water phase changes. Giard and Bazile (2000) obtained improved forecast scores from the inclusion of a soil ice scheme in the operational NWP model ARPEGE. However, the ability to generalize those results (from single LSMs) needed to be examined, thus the first LSM-community wide effort to study this problem was initiated by Schlosser et al. (2000). They analyzed simulations by 21 research and operational LSMs under the auspices of the Project for the Intercomparison of Land-Surface Parameterization Schemes (PILPS; Henderson-Sellers et al. 1995) for an 18-yr off-line simulation for a cold continental site (Valdai, Russia). It was determined that the parameterization of frozen soil (or lack of such a parameterization) was a cause for considerable model disagreement in predicted soil moisture and surface fluxes.

The treatment of soil freezing processes was also shown to have substantial effects on model simulated variability (over the 18-year period considered).

Soil phase changes (herein referring changes between solid and liquid phases of water) were neglected in the original version of ISBA used for atmospheric modeling. In response to the need to incorporate some notion of soil freeze-thaw into ISBA, soil water phase changes were added to both the ISBA 3L (Force-Restore) and DIF options in Boone et al. (2000), and this method was based on soil temperature falling below the freezing point for simplicity. At roughly the same time, Giard and Bazile (2000) also included soil freezing in the Force-Restore operational version of the NWP version of ARPEGE, and some exchanges were made with this group, notably on the minimum number of layers required (two) and on the definition of a characteristic timescale for freezing. But in addtion to the thermal effects modeled in Giard and Bazile (2000), Boone et al. (2000) also included the hydrological impact of ice (decreasing pore-space for liquid transfer) owing to the objective of improving hydrology for long term integrations. This scheme was tested in conjunction with the explicit snow scheme option at the regional scale for the first time by Habets et al. (2003). It was also used to simulate soil temperatures and permafrost coverage over Siberia in Boone et al. (2006). This study showed that the inclusion of ancillary data into a satellite data-based snow retrieval algorithm, such as LSM-simulated soil temperatures, can significantly improve derived snow depth computed from Special Sensor Microwave/Imager (SSM/I) data.

In the last few years, the Gibbs free-energy method has been added to the soil freezing scheme (as discussed in Decharme et al., 2016). This method is more physically realistic, in that water can exist in the liquid state at lower temperatures (below freezing) for more fine grained soils. For example, this scheme was recently evaluated in offline mode driven by ERA-Interim (European Centre for Medium-Range Weather Forecasts, ECMWF, Interim Re-Analysis: Dee et al., 2011) reanalysis data (using ISBA-DIF) over Eurasia coupled to the detailed snow model CROCUS (Brun, 1989, 1992; Vionnet et al., 2012), and was shown to produce robust estimates of the soil temperatures at a 20 cm depth for 96 stations over a multi-year period extending from 1979-1993 (Brun et al., 2013). In addition, the soil freezing front is influenced by model grid resolution, thus for an accurate modeling of freeze thaw it is of interest to have a relatively high soil grid vertical resolution near the surface where gradients of temperature are generally the largest. This was one of the motivations for recently increasing the soil-grid vertical resolution in ISBA-DIF (Decharme et al., 2016) as discussed in Section 2.2.1. As a result of this work, ISBA-DIF with soil-freezing using the Gibbs-free energy concept (and hydrological modifications) will be used in several applications: i) ARPEGE Climat for the CMIP6 and related projects, ii) the new default in the operational SIM platform, iii) the Global Soil Wetness Project phase 3 (GSWP3: Ek and Boone, 2015) 100-year multi-model surface reanalysis, among others.

2.2.3 Explicit physically-based snowpack

The snow cover is known to have a profound effect on the land surface primarily through modification of the surface albedo, roughness, and the insulating capacity of the snow. Snow coverage varies greatly in both time and space and modulates the radiative fluxes and the fluxes of heat, momentum, and moisture between the surface and atmosphere. The hydrological cycle also is

influenced, because a large component of the precipitation enters the soil significantly lagged in time because of storage by the snow cover.

Several snow-scheme intercomparison studies were done around the turn of the last century to address issues related to the current state of snow modeling used by the atmospheric research community. Slater et al. (2001) inter-compared 18-yr local scale simulations by 21 Soil-Vegetation-Atmosphere Transfer (SVAT) models that represented the full range of snow scheme complexity for a cold continental region in Russia under the auspices of PILPS. They found that considerable model variability exists for the snow simulations, with sublimation being one of the major sources of differences at this site. Essery et al. (1999) compared simulations of snow at a micro-meteorological site by two climate model snow schemes, a model for hydrological forecasting and an operational avalanche prediction model. They found the models simulated similar snow cover duration but differed with respect to the timing and amount of peak snow mass and the temporal distribution of runoff. These projects laid the groundwork and provided much of the motivation for the Snow Model Intercomparison Project phase 1 (SnowMIP: Etchevers et al., 2004), which focused on multi-model simulations for different climates over multi-year periods. The overall conclusion of these studies (along others) was that considerable disparity exists in terms of the simulation of the snowpack among LSMs, and there is a need to make progress in understanding the key processes the improving the models.

In response, an initiative was undertaken at Météo-France to improve upon the relatively simple LSM snow schemes used for spatially distributed hydrometeorological modeling and coupled atmospheric applications. Three general model complexity classifications can be used to describe the LSM snow component that are used by the atmospheric research community.

- The first class consists of relatively simple so-called force-restore schemes in which the snow is modeled using composite snow-soil layer(s) (e.g., Douville et al. 1995; Yang et al. 1997). There is also another group of schemes that falls into this relatively simple class, which uses a single explicit snow layer to differentiate the thermal properties and surface fluxes of the snow cover from that of the soil (e.g., Verseghy 1991; Slater et al. 1998; Sud and Mocko 1999).

- The second class of schemes consist of detailed internal-snow-process schemes such as those of Anderson (1976), Brun et al. (1989, 1992), Jordan (1991), and Lehnings et al. (1998). These models use multiple layers with a relatively fine vertical resolution and have detailed physical parameterization schemes. Their use in atmospheric models, however, has been limited by their relatively large computational expense.

- A third class of so-called intermediate-complexity schemes are based on the internal-snow-process (class 2) models. However, they use simplified versions of the physical parameterization schemes describing what are deemed to be the most important processes from the complex models and the minimum number of layers required to resolve the large thermal and density gradients within the snow cover (Loth et al. 1993; Lynch-Stieglitz 1994; Sun et al. 1999). The intended application of these schemes is for full coupling within atmospheric models.

The third strategy was used to develop the ISBA Explicit Snow (ISBA-ES: Boone and Etchevers, 2001; Decharme et al., 2016) scheme.

ISBA-ES has had several improvements added in recent years, the sum of which are described in Decharme et al. (2016). These improvements were inspired by the CROCUS snow process model developed at the Centre d'Etudes de la Neige (CEN), Météo-France (Vionnet et al., 2012). The original ISBA-ES scheme consisted in 3 layers, which was determined to be the minimum necessary to be able to model key features of the snowpack, with an upper thin layer to resolve the diurnal cycle, a deep layer which could be saturated by liquid water for extended time periods, and an intermediate layer which is characterized by a potentially significant number of freeze-thaw events (and has a *memory* of a day to weeks). The scheme also enabled the retention (and potential refreezing) of liquid water, which proved to be especially important for distributed hydrological applications (Boone et al., 2004). New improvements include increased vertical resolution, especially at the snowpack base (owing to potentially large temperature gradients which can sometimes arise in lower portions of the snowpack), the same method to compute compaction and the thermal conductivity as CROCUS, snow sublimation by the wind (an option), and an improved multi-spectral representation of the snow albedo. This latter change is based on a simplified treatment from CROCUS, but it has been shown to give the same basic (improved) response. In addition, this multi-spectral albedo approach enables a full radiative coupling with the new explicit vegetation scheme (see Section 2.3).

ISBA-ES is currently still better adapted for operational weather forecasting and climate prediction than CROCUS owing to its relative simplicity and computational efficiency, however, CROCUS is better adapted for detailed snow process studies and operational avalanche forecasting. In the future, it is possible that the two schemes will eventually merge into a single multi-option scheme within SURFEX. In terms of applications, ISBA-ES has been used in the operational version of SIM for several years already (Habets et al., 2008), in addition to numerous research (e.g. Boone et al., 2006; Biancamaria et al., 2009) and intercomparison projects with a focus on snow and cold season processes (e.g.s Boone et al., 2004; Habets et al, 2003; Etchevers et al., 2004; Rutteri et al., 2009). As is the case for ISBA-DIF, ISBA-ES will be used in the same upcoming applications (listed at the end of Section 2.2.2). Finally, ISBA-ES was also recently incorporated into the Organising Carbon and Hydrology In Dynamic Ecosystems (ORCHIDEE) land surface model (Wang et al., 2013). The model was re-coded and adapted to the ORCHIDEE coding rules and certain physics, and was shown to give results very close to ISBA-ES for multiple local scale sites.

2.3 Multi-Energy Budget: MEB

There is continuous work to improve the representation of the land surface processes in the ISBA LSM within SURFEX. The so-called composite soil-vegetation Force-Restore approach used within the atmospheric models at CNRM, Météo-France approach has proven its value since its inception by Noilhan and Planton (1989): it was necessary to have a relatively simple and economical approach since both CPUs and the availability of spatially distributed parameters needed by the land surface model (LSM) were limited compared to today. But now, most LSMs are pushing towards improved realism in terms of snowpack, soil and vegetation processes, ow-

ing to an increasing number of observations at the local scale, constantly improving satellite data-sets and the associated methodologies to best exploit such data, improved computing resources, and in response to the user community via climate services (and seasonal forecasts, drought indexes, etc...). The representation of bio-geochemistry has also become much more sophisticated in recent years, so that we have reached the conceptual limits of using of a bulk soil-vegetation scheme for the coupled Carbon and dynamic vegetation options now available with ISBA-SURFEX.

In response to these issues, a collaboration began in 2008 in which several research groups have engaged in developing an explicit representation of the vegetation in ISBA. The main partners are the French laboratories CNRM and Centre d'Etudes Spatiales de la Biosphère (CESBIO), and the Swedish Meteorological and Hydrological Institute (SMHI), through a collaboration under the auspices of the High-Resolution Limited Area Model (HIRLAM) international consortium. The vegetation parameterization has become a focal point for improvements for several reasons:

- for data assimilation, it is known that it is best to distinguish the soil, vegetation canopy and snow surface temperatures since they can have very different amplitudes and phases in terms of the diurnal cycle
- it has become evident that the only way to simulate the snowpack beneath forests in a robust and a physically consistent manner (i.e. lessening the dependence of forest snow cover on highly empirical and poorly constrained snow fractional cover parameterizations, among other things) and including certain key processes (such as canopy interception and unloading of snow) is to include a forest canopy above or buried by the ground-based snowpack
- for accurately modeling canopy radiative transfer, within or below canopy turbulent fluxes and soil heat fluxes
- to make a more consistent photosynthesis and dynamic vegetation model (including explicit Carbon stores for the vegetation, litter and soil in a consistent manner)
- the explicit treatment of litter layer, which has a significant impact on ground heat fluxes and soil temperatures (and freezing), and by extension, the turbulent heat fluxes.

A new parameterization has been developed called the ISBA Multi-Energy Budget (MEB: Boone et al., 2017; Napoly et al., 2017) scheme, in order to account for all of the above issues.

2.3.1 MEB model

MEB is based on the classic two-source model for snow-free conditions which considers explicit energy budgets (for computing fluxes) for the soil the vegetation. The vegetation canopy is represented using the so-called big-leaf method which lumps the entire vegetation canopy into a single leaf for computing energy budgets and the fluxes. A reference model using this representation in France is SiSPAT (Braud et al., 1995), which has been used extensively for

offline local scale process-based studies (e.g. Boulet et al., 2004; Velluet et al., 2014). This approach has been implemented with success within coupled land-atmosphere models (e.g. Xue et al., 1991; Sellers 1996; Dickinson et al., 1998; Lawrence et al., 2011). But in contrast to the aforementioned models, when snow is present on the ground, MEB is extended to a three-source model using the same basic principles for resistance pathways. Finally, in the limit as the snow becomes deep enough to bury the vegetation, MEB collapses to a single snow energy budget which is coupled directly to the atmosphere (the notion of a canopy air space vanishes as the canopy becomes totally buried by snow).

ISBA-MEB has been developed taking the same strategy which has been used historically for ISBA: inclusion of the key first order processes while maintaining a system which has minimal input data requirements and computational cost while being consistent with other aspects of ISBA (with the ultimate goal of being used in coupled numerical weather forecast and climate models, and spatially distributed monitoring and hydrological modeling systems). The original vegetation canopy model was taken from the SMHI regional climate model (RCM), and reformulated (to be as consistent as possible with existing ISBA parameterizations) and then incorporated onto ISBA. SMHI had already been using such a model for forests owing to the importance of modeling explicit snow-canopy interactions in Nordic regions for both meteorology and hydrology. The canopy turbulence scheme, longwave radiation transmission function and snow interception formulations are taken from the Rossby Centre Regional Climate Model (RCA3) LSM used at SMHI as described by Samuelsson et al. (2006, 2011). ISBA-MEB has several new features compared to the original SMHI scheme:

- a snow fraction which can gradually bury the vegetation vertically thereby transitioning the turbulence coupling from the canopy air space directly to the atmosphere (using a fully implicit numeric scheme)
- the use of the detailed solar radiation transfer scheme from ISBA-Ags which is a multi-layer model that considers two spectral bands, direct and diffuse flux components and the concept of sunlit and shaded leaves (Carrer et al., 2013)
- a more detailed treatment of canopy snow processes and a coupling with the ISBA physically-based multi-layer snow scheme,
- a reformulation of the turbulent exchange coefficients within the canopy air space for stable conditions
- a fully implicit Jacobean matrix for the longwave fluxes from multiple surfaces (snow, below-canopy snow-free ground surface, vegetation canopy)
- an explicit forest litter layer model (which also acts as the below-canopy surface energy budget when litter covers the soil)

In terms of numerical aspects, all of the energy budgets are implicitly coupled with each other, and with the atmosphere using the coupling method by Best et al. (2004) which was first proposed by Polcher et al. (1998). Scientific papers have been submitted which describe in detail the overall model concept, assumptions, mathematics and numerics (Boone et al., 2017), the

new litter option and local scale evaluation (Napoly et al., 2017) and the evaluation for sites with a significant snow component (Samuelsson et al., 2018). In this chapter, a brief overview of results and key differences with the default ISBA scheme are given. Two schematics are shown in Fig. 2.2 to illustrate the main conceptual differences between the classic composite ISBA scheme and ISBA-MEB. The composite soil-vegetation ISBA scheme with an explicit snowpack is shown on the left-hand side of the schematic, while that corresponding to ISBA-MEB is on the right-hand side. The figure illustrates the maximum possible of three fully (implicitly) coupled surface energy budgets for the bulk vegetation canopy, T_v, snow-free surface (soil or litter), T_g, and snowpack, T_n, and the various resistance pathways for the turbulent fluxes. Compared to the resistances for the classic two-source model (snow-free ground surface and canopy air, r_{ag-c}, non-snow buried vegetation canopy and canopy air, r_{avg-c}, and canopy air with the atmosphere, r_{ac-N}), ISBA-MEB includes up to three additional resistances in the presence of ground-based snowpack corresponding to; i) the snow surface and canopy air, r_{an-c}, ii) the snow-covered part of the canopy and the canopy air, r_{avn-c}, and iii) the snow surface directly with the overlying atmosphere, r_{an-N}.

The ground surface in forest regions is generally covered by a litter layer consisting of dead leaves and or needles, branches, fruit, and other organic material. It is generally on the order of several to 10s of centimeters thick (based on a literature survey in Napoly et al., 2017). In reality, the thickness can vary in time and space owing to numerous factors (decay and compression rates, wind transport, etc.), but such data is not currently a part of standard spatially distributed

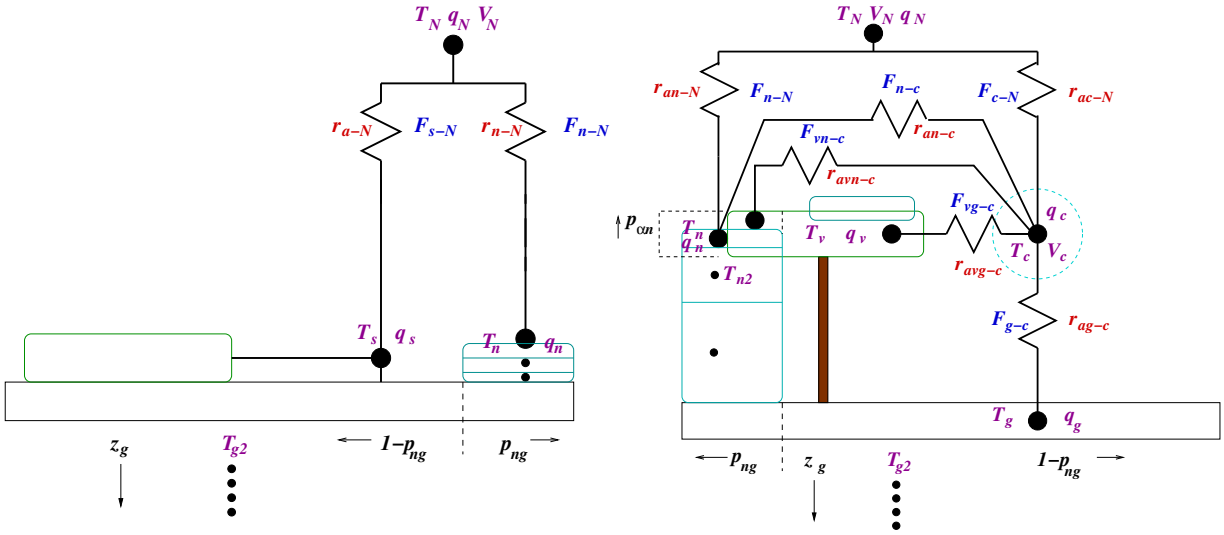

Figure 2.2: A schematic representation of the composite soil-vegetation ISBA scheme with an explicit snowpack (ISBA-ES): left-hand side. The ISBA-MEB schematic is shown on the right. The turbulent resistance pathways are shown. State variables are in purple, and resistances are in red. Snow is indicated using turquoise. Atmospheric variables (lowest model level) are indicated using the N subscript.

input data for LSM schemes. Therefore, in the current study, this layer is modeled by default using a constant thickness (although it can be specified as a monthly varying input parameter if the required observational data exists). This layer is generally accepted to have the following properties:

- has a strong insulating effect (thereby having a strong impact on the energy exchanges with the soil below) owing to its particular thermal properties (leading to a relatively low thermal diffusivity)
- causes a significant reduction of ground evaporation (capillary rise into this layer is negligible)
- constitutes an interception reservoir for liquid water (rainfall, snow melt and canopy drip) which can also lose water by evaporation

Indeed, the impact of this layer has been shown to have substantial impact on hydrological (Putuhena and Cordery 1996, Guevara-Escobar et al. 2007, Gerrits et al. 2007) and thermal (Andrade et al. 2010) processes. For simplicity, no radiation transmission through this layer is currently modeled, thus all net radiation at the surface is available for turbulent or ground heat fluxes.

Some LSMs have introduced parameterizations for litter (Enrique et al., 1999; Ogé et al. 2002, Wilson et al. 2012), but the approach can be very different from one to another depending on their complexity. The simplest approach is to modify or add an additional ground resistance, while the alternative is to model the litter using an explicit single or multi-layer model. All of these approaches were initially tested for ISBA-MEB, and in keeping with both the explicit nature of the model and to improve coupling with the Carbon module (which considers a Carbon storage by litter), it was decided to use an explicit litter layer approach. But in an effort to just model the first order effect as simply as possible, and because the typical litter thicknesses reported in the literature are sufficient to resolve the diurnal cycle, currently a single layer approach is used. Litter thickness sensitivity testing is described in Section 2.3.2.

2.3.2 Evaluation at the local scale

Part of the ongoing ISBA-MEB evaluation is for local scale sites which are characterized by a comprehensive set of observations and detailed site descriptions. In this section, some results for three such forested French sites which encompass a range in climate conditions is presented. A short summary of basic characteristics is shown in Table 2.1, a more detailed description can be found in Napoly et al. (2017). There is very little snow at these sites, thus this impact is not discussed herein (and the evaluation for cold sites is the subject of an ongoing evaluation by Samuelsson et al., 2016). ISBA-MEB results are compared to the baseline composite version of ISBA, and using two MEB options. The first corresponds to the classic two-source (MEB: in the absence of snow) model with a vegetation canopy overlying a bare-soil. The second option includes a ground based litter layer (MEB-L). All of the results reported here use the most recent version of ISBA-DIF (Decharme et al., 2016) for the soil, the ISBA-Ags scheme (Calvet et al., 1998) for computing photosynthesis and canopy resistance, and the Carrer et al.

(2013) shortwave radiative transfer scheme. Vegetation parameters were determined using the SURFEX default ECOCLIMAP land cover (save for variables measured at each site, such as Leaf Area Index, LAI, etc.) and the Harmonized World Soil Database (HWSD) soil data bases (see Napoly et al., 2017 for more details).

Finally, the idea is to validate the model using prescribed or observed parameters as much as possible. The only adjusted (compared to values not prescribed by ECOCLIMAP or from field measurements) parameters were: the wilting point and field capacity water contents were estimated using observed soil moisture, and the shortwave radiation parameters were adjusted slightly to increase absorption for all three of the sites. The only calibrated parameter was the litter thickness since its value was uncertain for two of the three sites. Generally speaking, this parameter is currently not defined in global databases such as ECOCLIMAP, thus it must be determined as a secondary parameter (i.e. defined empirically based on existing parameters), or as a new class specific parameter for look-up tables. Thus, sensitivity tests were carried out on litter thickness and they are discussed later in this section.

Site	**Bray**	**Puéchabon**	**Barbeau**
Years	2006-2008	2006 and 2008	2013
Vegetation type	Maritime pine, Grass	Green Oak	Sessile Oak
Climate	Maritime	Mediterranean	Temperate
Forest type	Evergreen Needle-leaf	Evergreen Broadleaf	Deciduous Broadleaf
Mean vegetation height (m)	18	5.5	27
Mean T (C^o)	12.9	13.5	10.7
Rainfall (mm y^{-1})	997	872	680
Location	44.7N, 0.7W	43.7N, 3.5E	48.4N, 2.7E
Altitude (m)	62	270	90

Table 2.1: Summary of the vegetation characteristics, climate, location and altitude of each of the three local scale sites.

Flux evaluation

Extensive analysis was undertaken for each of the three sites in Napoly et al. (2017). As an example, the monthly average diurnal cycle turbulent and ground fluxes simulated by ISBA, MEB and MEB-L are shown in Fig. 2.3 for the Puéchabon site for 2006. The thick black solid curves indicate the observed sensible, H, latent, LE, and ground, G heat fluxes, while the dashed black curves represent the Bowen-ratio adjusted observed LE and H values. This adjustment method essentially assumes that the et radiation error is relatively small, and that the Bowen ratio computed from the un-adjusted observations is relatively accurate (see Napoly et al., 2017, for further discussion). Thus, simulated values falling within the gray zone are considered to be within the error of the measured fluxes. Overall, ISBA and the two MEB versions perform fairly well for this site (and the other two, not shown) in terms of H and LE. But several results were

consistent across the sites and can be summarized from Napoly et al. (2017) as:

- latent heat flux is generally well simulated for all model versions despite being slightly underestimated. While the total evapotranspiration, E, is somewhat similar between ISBA, MEB and MEB-L, the partitioning of E into transpiration, E_{tr}, evaporation of canopy-intercepted water, E_r, and ground evaporation, E_g, differ. With MEB and MEB-L, E_{tr} makes up a larger portion of E

- the shading effect of the canopy layer (MEB) in addition to the low thermal diffusivity of the litter layer (MEB-L) greatly reduced and improved the ground heat flux and soil temperature amplitudes. The improvement in G for all three sites is shown in Fig. 2.4, with MEB-L consistently giving the best results by a significant margin

- the standard ISBA model is found to underestimate the amplitude of the sensible heat flux and to have a peak too late in the day. The two versions of MEB give a better phasing of the simulated and observed H (closer to the solar diurnal cycle) owing to the reduced canopy heat capacity (which only represents the vegetation in MEB, but is a larger composite value in ISBA)

- the reduced ground heat flux in MEB and MEB-L compared to ISBA mainly lead to increased and improved sensible heat fluxes, while having relatively less impact on evapotranspiration. This effect can be seen in Fig. 2.3 at Puéchabon in February through June, for which LE is very low thus the decreased MEB-L G translates mostly into increased H compared to ISBA

- the main difference between ISBA and MEB-L occurs during spring for the deciduous forest site where the litter layer acts to significantly limit soil evaporation, whereas ISBA (and to a lesser extent MEB without explicit litter) overestimate evapotranspiration due to strong ground evaporation. In fact, MEB-L therefore reduces a known long standing problem with ISBA (at least in terms of the forested sites studied herein)

- the litter layer improved the simulation of surface soil moisture for several cold events in which ISBA and MEB both simulated soil freezing through several layers. MEB-L simulated warmer soil temperatures and negligible soil freezing, which was consistent with the observed liquid water content. This will be further explored for cold forest sites which have the needed observations

As mentioned above, MEB and MEB-L simulate considerably lower E_g than ISBA. Part of the reason is the lower (and more conceptually consistent) roughness length used by MEB in the explicit computation of this flux, since ISBA uses an aggregated surface roughness (which can be well over 10s of cm in forests). In addition, measurements of transmitted energy through the canopy compare well to values simulated by MEB (as seen in Napoly et al., 2017), which strongly conditions the maximum possible ground evaporation. ISBA often simulates ground evaporation exceeding these values (ISBA E_g generally exceeds the surface R_{net} simulated by MEB for example), which doesn't seem realistic. Indeed, it has long been suspected that ISBA

overestimates ground evaporation in forests. Indeed, an attempt to fix this was done by fixing large values of the vegegtaion cover fraction for forest covers in ECOCLIMAP, *veg*, to somewhat tuned values to limit this excessive E_g. MEB does not use the *veg* concept, as it is used to partition E into E_g and E_v in ISBA (where vegetation evapotranspiration is expressed as $E_v = E_r + E_{tr}$). So this can be seen as an improvement and further validation of this will be pursued.

Litter thickness sensitivity tests

There are currently only two new primary parameters introduced by MEB (all of the other parameters, such as vegetation canopy height, separate soil and vegetation albedo for different spectral bands, etc...are already computed in ECOCLIMAP, but were aggregated as a pre-processing step for ISBA). They are the longwave transmission coefficient (which is currently fixed as a constant for all vegetation classes) and the litter layer thickness (when using option MEB-L). After surveying the literature, there seems to be relatively little agreement on the value for this parameter, and further, assigning it as a class dependent value (for different forest types) seems dubious currently: thus we simply inherit the nominal constant value from RCA3 (Samuelsson

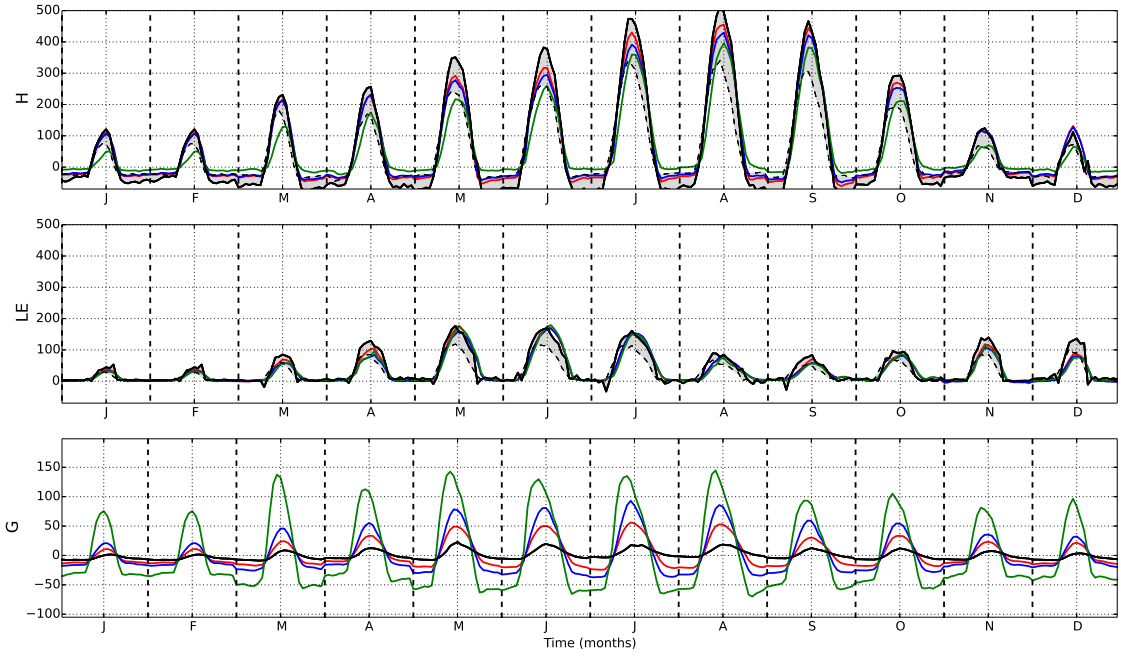

Figure 2.3: Composite diurnal cycles by month at Puéchabon in 2006. MEB-L is in red, MEB in blue, ISBA (composite) in green, the measurements are represented by the dashed black line and Bowen-ratio adjusted measurements are represented by solid black curves.

et al., 2011). For the litter thickness, however, a literature survey (Napoly et al., 2017) revealed that values tend to be in the range of 1 to 10 cm. Thus, sensitivity tests were undertaken to see how sensitive the model is to values within (and slightly outside of) this range. The results of these tests are shown in Fig. 2.5, where the RMSE of G (W m^{-2}) for each site is plotted as a function of litter thickness (for values ranging from 0 (corresponding to MEB) to 10 cm, using increments of 1 cm. Consistent with the results shown in Fig. 2.4, G is improved with MEB compared to ISBA, and further improved with MEB-L for any value of litter thickness over the tested range (as seen in Fig. 2.5). And as mentioned, these improved G values translated consistently into improved H as discussed in Section 2.3.2. Note there are two curves for each site, using different (extreme) values of one of the key shortwave radiation transmission parameters. These results results show that above approximately 3 cm, the errors are relatively low and only slightly increase as thicknesses approach 10 cm. Indeed, it is possible that for values above 6 to 10 cm, a multiple layer model might be better than the bulk approach, thus current, the default is set to 3 cm. But overall, it can be seen that as a first order effect, the inclusion of a litter layer improves results compared to no-litter for a nominal thickness value which can be approximated as a constant across the sites. Future work will continue in order to determine whether this parameter should be varying as a function of vegetation cover and time.

2.3.3 Evaluation for multiple climates, forest types

Another local scale offline evaluation of MEB has been done using the recently developed benchmark tool developed at Météo-France. It uses a quality controlled subset of flux data from the FluxNet network (Baldocchi et al . 2001). The FluxNet database has been used for LSM evaluation by several widely used models: some examples for widely used LSMs are Stockli et al. (2008) with CLM, Blyth et al. (2009) with JULES, and Ukkola et al. (2015) with CABLE. It has also been used in the recent Plumbing of land surface models (PLUMBER) international

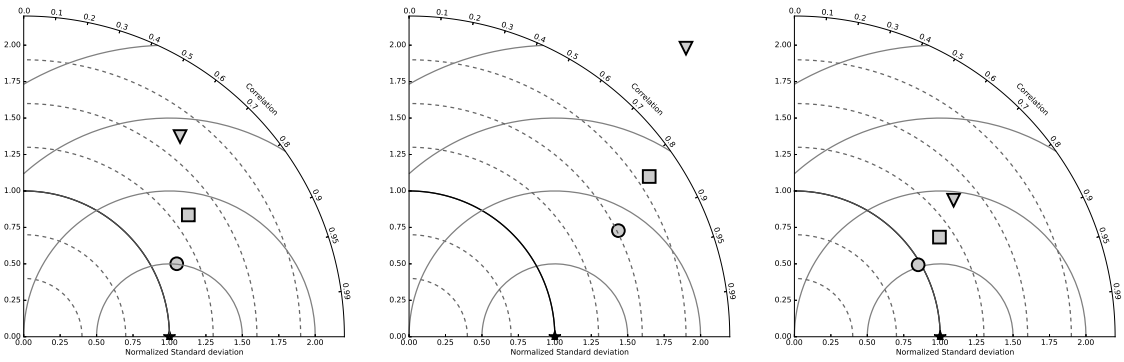

Figure 2.4: Ground heat flux plotted on Taylor diagrams for (from left to right) for the LeBray, Puéchabon and Barbeau sites. The points correspond to ISBA (composite: triangle), ISBA-MEB (square) and ISBA-MEB-L (circle).

multi-LSM intercomparison project (Best et al., 2015; Haughton et al., 2016). An overview of the benchmark evaluation is presented herein: it is described in more detail in Napoly et al. (2017).

Many sites are available within the FluxNet database, however in the current study, only those sites and years with an energy balance closure of 20 % (or less) before adjustment of the turbulent heat flux are retained. Ground heat flux was assumed to represent 3% of net radiation when not available (this is close to the average value over the three French sites and is consistent with the estimate given by Monteith, 1973). After screening, 39 forested sites remain which gives a total of 179 years of observations for the sites shown in Fig. 2.6. The method used to gap fill missing atmospheric forcing data is described in Vuichard et al. (2015). The three French sites used in Section 2.3.2 have been removed in this analysis.

ISBA and MEB-L were both run using ECOCLIMAP parameters and a fixed litter thickness for MEB-L of 0.03 m: no calibration or tuning was performed for either model version. The same model options were used for the benchmark as for the three French sites: the most recent version of ISBA-DIF (Decharme et al., 2016) for the soil, the ISBA-Ags scheme (Calvet et al.,

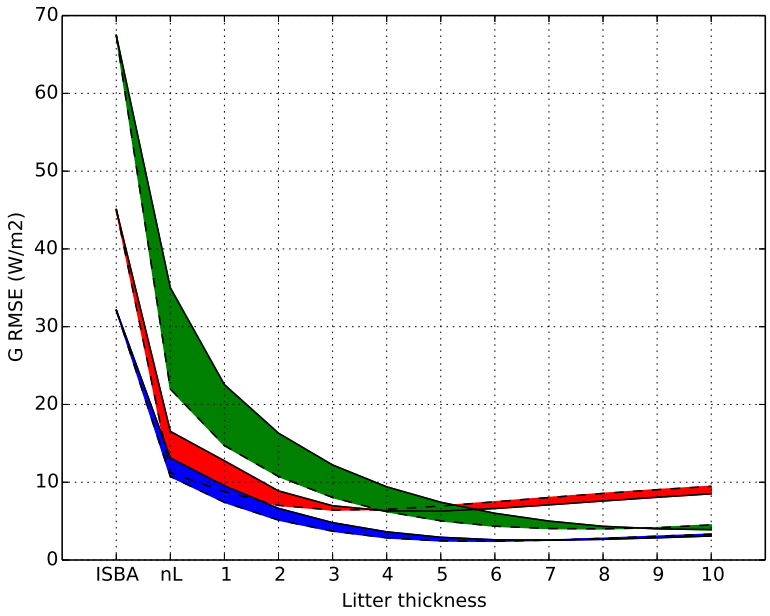

Figure 2.5: Root mean square error (RMSE) in G (ground heat flux) as a function of litter thickness (m) for MEB-L. A thickness of 0 corresponds to MEB (nl=No litter), and results for ISBA are shown for comparison. Each site is represented by a color: Le Bray (red), Puéchabon (green) and Barbeau (blue). Finally, there are two curves for each site, and each corresponds to a different parameter value for shortwave transmission through the canopy.

1998) for computing photosynthesis and canopy resistance, and the Carrer et al. (2013) shortwave radiative transfer scheme. A summary of the simulation statistics are shown graphically in Fig.s 2.7-2.8. The root mean squared error (RMSE: W m^{-2}), explained variance (or correlation squared, R^2), and absolute error (AE: W m^{-2}) are shown as MEB-L verses ISBA for each site for *LE* (Fig. 2.7) and *H* (Fig. 2.8). The average value over all sites is shown as a dashed horizontal line for MEB-L and a vertical line for ISBA. A point falling within the grey shaded area in Fig.s 2.7-2.8 indicates that the score is better for MEB-L than ISBA, and the corresponding percentage of points in the gray zone is shown at the top of each panel (for the given statistic).

In terms of *LE*, there is a slight improvement in terms of R^2 and RMSE for MEB-L, but the gains are nearly offset by points for which the simulation is worse using MEB-L: overall, the results are nearly neutral. There is a slightly worse bias using MEB-L, however, the average bias is quite small for both models. In terms of *H*, however, the results are considerably improved using MEB-L. Not only are considerably more points showing improved results in terms of R^2 and RMSE, the values are considerably improved for MEB-L. The average bias is nearly zero. The important point is that these results are very consistent with what was seen in Section 2.3.2 for the three well-instrumented French sites: MEB-L results in a fairly consistent and significant improvement in *H*, while impacting the total *LE* less. The recent PLUMBER project (Best et al., 2015; Haughton et al., 2016) showed that LSMs generally have the most difficulty simulating *H*. The inclusion of an explicit litter layer significantly and consistently improved *H* (owing to the lower vegetation heat capacity in MEB, but seemingly more-so to the improved *G*) for the French sites and for the FluxNet sites with ISBA-MEB-L, so this might be one possible solution to the general *H* problem.

Finally, note that many of the identified improvements in MEB compared to ISBA described in this section and listed in Section 2.3.2 are not related to a problem with ISBA per say, but more

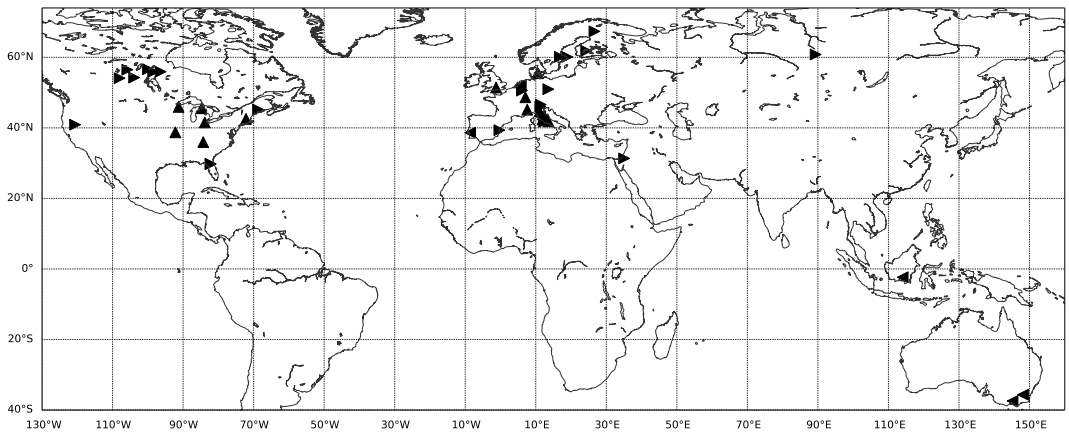

Figure 2.6: The location of the FluxNet sites used in the ISBA-MEB evaluation. Sites correspond to forests with an energy budget closure error less than 20 %.

to the inclusion of more explicit processes (in favor of composite and aggregated approaches) in MEB. The next step is to see how these modifications translate to fully coupled atmospheric and Carbon processes, where ISBA has already proven its value and good performance.

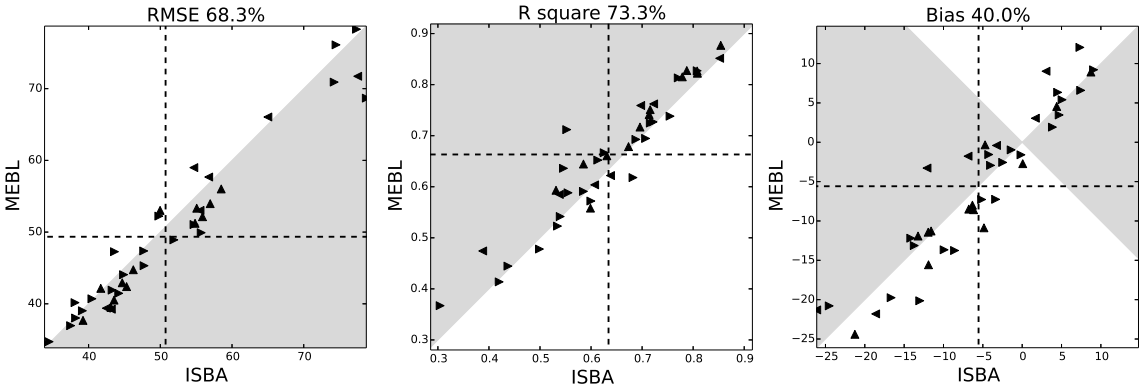

Figure 2.7: Scatter plot of RMSE, R^2 and AE computed with the latent heat flux (*LE*) for each site and year. The abscissa corresponds to the ISBA model and the ordinate to the MEB-L. The intersection of the dashed lines corresponds to the average of all sites/years. Figures over each graphs correspond to the number of years MEB-L has statistical results superior to ISBA. Each point corresponds to a given year for each site shown in Fig. 2.6, for a total of 118 years.

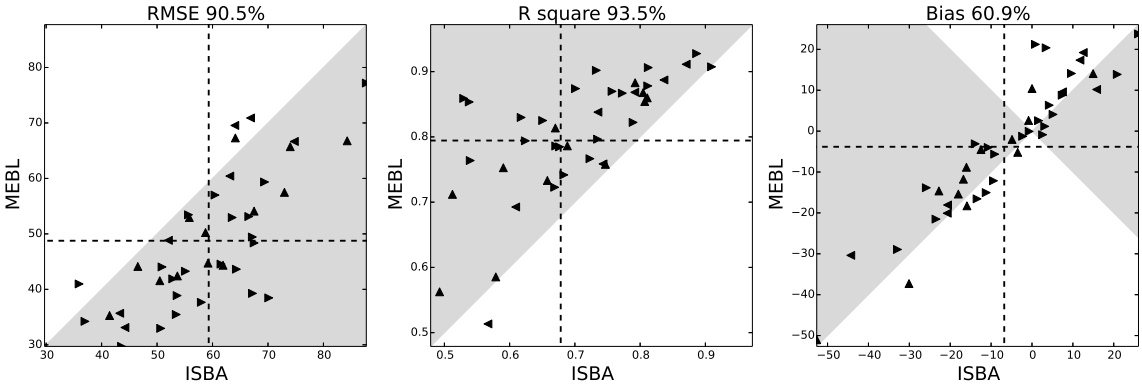

Figure 2.8: As in Fig. 2.7 except for the sensible heat flux, *H*.

Chapter 3

Land surface Model Inter-comparison Projects

3.1 Introduction

There have been a significant number of international land surface inter-comparison projects, most of which have operated under the auspices of the Global Energy and Water EXchanges (GEWEX) project, which is supported by the World Climate Research Programme (WCRP) within the World Meteorological Organization (WMO). These projects have been run in offline mode (i.e. decoupled from an atmospheric model), mainly in order to avoid the additional complexity of including the feedbacks with the atmosphere. Model parameterization development has greatly benefited in the past two decades from these international collaborative efforts. Also, model simulations form a tpye of multi-model analysis, the basic idea is that given the highest quality estimate of atmospheric forcing, what are the best estimates of the fluxes and state variables. Such ensembles also provide a measure of LSM uncertainty. These projects were done in so-called stand-alone mode (uncoupled with an atmospheric host model) using a blend of observational and model output data as (input) time varying boundary conditions.

The first international offline land MIP was the Project for the Intercomparison of Land surface Parameterization Schemes (PILPS: Henderson-Sellers et al., 1993, 1995) which began in the 1990s using climate model generated atmospheric forcing at a grid point. PILPS then continued in multiple phases, and evolved to use observed atmospheric forcing with evaluation data comprised of observed surface fluxes and state variables, such as soil moisture for mid-latitude sites (Chen et al., 1997). Additional PILPS experiments were extended to cold regions in order to evaluate soil freezing and snow parameterizations in LSMs (Schlosser et al., 1999). In latter experiments, PILPS was extended to the basin scale using spatially distributed atmospheric forcings and river discharge to evaluate the models for mid (Wood et al., 1998) and high latitude catchments (Bowling et al., 2003).

In the spirit of PILPS, the Global Soil Wetness Project (Dirmeyer, 2011) was initiated with simulations covering the entire globe. Results from this project represented the first offline multi-model analysis of land surface state variables and fluxes. The most recent phase of GSWP (3) has been initiated, and I am currently participating in this project using ISBA with several colleagues

at CNRM. In addition, several other GEWEX supported intercomparison projects have been done with specific focus, such as the Snow Model Intercomparison Project (SnowMIP: Etchevers et al., 2004; Rutteri et al., 2009) which focused on snow processes for multiple local scale sites and annual cycles, the Rhône-AGGregation project (Rhône-AGG: Boone et al., 2004) which focused on the regional scale water budget and coupled land surface hydrological processes across a range of spatial scales, and the African Monsoon Multidisciplinary Analyses (AMMA: Redelsperger et al., 2006) Land surface Model Intercomparison Project (ALMIP: Boone et al., 2009a) which sought to improve the understanding of critical land surface processes over west Africa at the regional scale. Owing to the success of ALMIP, a second phase was initiated (ALMIP2: Boone et al. 2009b) which focused on land surface processes along an eco-climatic gradient in west Africa, again as a part of the AMMA project. During the course of my research, I have participated in every PILPS study but one, all three GSWP phases, and both SNOWMIP experiments. I have lead or co-lead two of the aforementioned international offline projects; the Rhône-AGG and ALMIP (phases 1 and 2).

Offline studies have their limitations, since the impacts of such parameterizations on the coupled system can not be fully understand in offline mode. In response, there is a growing effort in the scientific community to promote efforts to evaluate such schemes in fully coupled mode (van den Hurk et al., 2011), despite the additional complexity. I have also done work to examine the feedbacks between the land surface (soil moisture) and the atmosphere using fully coupled models in terms of PBL cloud development (Wetzel and Boone, 1997), convection (Lynn et al., 2001; Baker et al., 2001), and the feedback of the land surface and the atmosphere over West Africa using a 2-D idealized West African Monsoon (WAM) model (Peyrille et al., 2016). Owing to these experiences and the ALMIP work within AMMA, I co-lead a MIP within the international West African Monsoon Modeling and Evaluation (WAMME: Xue et al., 2010, 2016) in which the impact of land-use land cover change (LULCC) on the WAM was studied (Boone et al., 2016).

In this chapter, I will give a brief overview of the Rhône-AGG and WAMME-LULCC MIPs, and a more in depth overview of ALMIP, since this project involved a large number of international and French colleagues and was the catalyst for my participation in WAMME.

3.2 Coupled Land-hydrology MIP: The Rhône AGGregation project

The Rhône-Aggregation (Rhône-AGG) LSM intercomparison project (Boone et al., 2004) was an initiative within the GEWEX Global Land-Atmosphere System Study (GLASS) panel of the WCRP. It was a intermediate step leading up to GSWP2. This project made use of the Rhône modeling system, which was developed by the French research community in order to study the continental water cycle on a regional scale. Many French laboratories participated in the development of the Rhone modeling system (see the listing in Boone et al., 2004). There were two main goals of this study, the first was to investigate how multiple state-of-the-art LSMs simulate the water balance for several annual cycles compared to data from a dense observation network consisting of daily discharge from over 145 gauges and daily snow depth from 24 sites. LSM runoff was fed to the MODCOU distributed hydrological model for computing the river discharge. The second goal was to examine the impact of changing the spatial scale on the simulations. The basin domain and the location of the main river gauges and snow observation sites are shown in Fig. 3.1.

This project differs from the aforementioned PILPS projects owing to the much higher spatial resolution of the gridded atmospheric forcing and surface parameters, the large within-basin range in vegetation types (Mediterranean, maritime-continental, and alpine), the large grid-box average altitude gradient (3000 m over a horizontal distance of approximately 300 km), and the comparatively large quantity of observational data for evaluating the schemes. A list of the 15 participant LSMs is given in Table 3.1.

3.2.1 Project Objectives

The objective of exploring LSM-scaling issues addresses one of the key questions to come out of the La Jolla International Geosphere-Biosphere Programme (IGBP)/GEWEX workshop (Dolman and Dickinson 1997): How are the simulations from a wide range of LSMs - currently used in Global Climate Models (GCMs), atmospheric models, or for local-scale studies - impacted by changing the spatial resolution? The Rhône-AGG project attempts to address this issue along with others, and so the main scientific questions of this project are:

1. How do the various LSMs simulate the discharge compared to the observed values for the entire basin and for various sub-basins for several annual cycles
2. Are the sub-grid parameterizations for surface runoff and drainage scale-dependent
3. How do the varying aggregation or explicit tiling methods impact the results
4. How does soil moisture scale in the LSMs
5. What is the impact of grid resolution on the simulated snow water equivalent (SWE) and the associated snow melt runoff

Three sets of experiments designed to examine the impact of scaling. The control experiment (Exp1) consists of running the LSM on the default high-resolution grid (8x8 km) In Exp2a,

simulations are run at a 1^o resolution (approximately 69 km) which roughly corresponds to a GCM grid box size. The purpose of these simulations is to examine the impact of up-scaling on the water and energy budget components. In Exp2b, the schemes are run as in Exp2a, but for 57 boxes defined by overlaying a $1/2^o$ x $1/2^o$ grid. The purpose of this experiment is to examine an intermediate spatial scale, which might be more typical of a NWP model.

3.2.2 Main Conclusions

A total of 60 3-year simulations (3 resolutions and 20 model configurations since 5 models performed 2 runs with different options: see Boone et al., 2004, for more details) were analyzed.

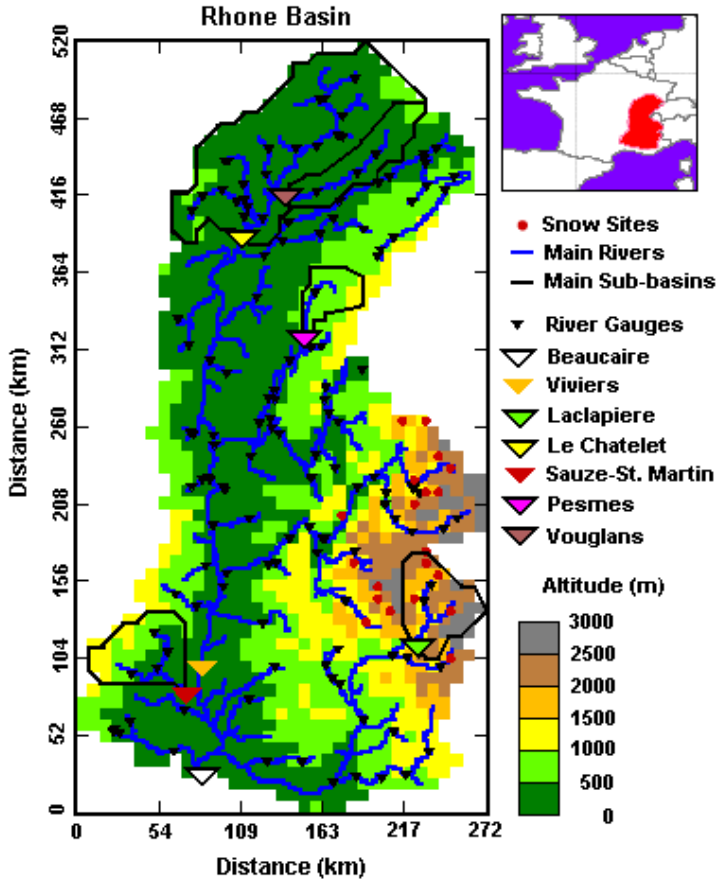

Figure 3.1: The Rhône model domain with gridded topography at 500 m intervals. The 145 gauging station locations (filled triangles) and the snow observation sites (filled red circles). The major rivers are shown in blue. The three sub-basins given special treatment in Rhône-AGG are outlined, along with two used for model calibration. (upper right) The basin location relative to France.

LSM	Country	Institute, Acronym
ISBA	France	CNRM Interactions between Soil Biosphere Atmosphere
NOAH	USA	NCEP, Oregon State Univ., Air Force, NWS Hydrologic Res. Lab.
COLA-SSiB	USA	Center for Ocean Land Atmosphere Studies, Simple Biosphere Model
MOSES-PDM	UK	Met Office Surface Exchange Scheme Probability Distributed Moisture
ECMWF	UK	European Centre for Medium-Range Weather Forecasts scheme
NSIPP	USA	NASA Seasonal to Interannual Prediction Project Catchment Model
VIC	USA	Varible Infiltration Capacity Model
MECMWF	UK	Modified ECMWF scheme
SWAP	Russia	Soil Water Atmosphere Plants
VISA	USA	Versatile Integrator of SurfaceâAtmospheric processes
SPONSOR	Russia	Semidistributed Parameterization Scheme of Orography Induced Hydrology
CLASS	Canada	Canadian Land Surface Scheme
ORCHIDEE	France	Laboratoire de Meteorologie Dynamique (LMD) surface model
SIBUC	Japan	Simple Biosphere Model Including Urban Canopy
CHASM	Australia	Chameleon Surface Model

Table 3.1: The Rhône-AGG participant LSMs.

Some of the key results were:

- LSMs generally have the highest spatial variability in the more water-stressed southern portion of the basin where the most significant inter-LSM differences occur: LSMs with saturated sub-grid fractions have the largest spatial variability (since some part of the grid box is always evaporating at the potential rate, even if for a small region)
- No significant systematic inter-model differences in the overall water budget or surface energy balance components in the control experiment can be attributed to the use of single tile versus multiple tiles except for snow cover (which was improved using the special tile case of explicit sub-grid elevation banding)
- The statistically best snow simulations, compared to data at 24 observation sites were obtained by LSMs having so-called explicit snow schemes
- The LSMs simulate the total flow volume and the monthly discharge at Viviers, which comprises over 80% of the total Rhone discharge, reasonably well on the monthly timescale. However, at the daily timescale, LSMs using sub-grid runoff formulations generally perform better than schemes without sub-grid runoff. However, an overestimation of this quantity was found to be far more detrimental to the simulation accuracy than an underestimation

- sub-grid runoff was found to be especially important for discharge at the daily timescale and for smaller scale basins.
- Only five of the LSMs are able to simulate the discharge with some skill on a monthly basis for a high Alpine basin (the Durance), all of them having explicit snow schemes which produce the best depth simulations for the six observation sites within this basin. Composite snow schemes generally simulate too much snow melt before the observed springtime discharge peak (peak runoff generally occurs 2 to 4 weeks early)
- LSMs that only permit runoff when the soil water is above the holding capacity (two LSMs; therefore there is no slow runoff component) or those which simulate most of the runoff as fast-response or surface runoff (three LSMs) generally did not simulate the daily discharge as well as the other LSMs for the Rhône sub-basins
- The magnitude of the response of LSMs to up-scaling varies greatly among models, although the trends tend to be similar for most schemes. Several basin-averaged quantities scale reasonably well, such as evapotranspiration and drainage, with total relative differences generally less than 10% when moving from 8 km to 1^o (approximately 69 km)
- Surface runoff is significantly decreased with increasing grid resolution in most LSMs primarily because of the up-scaling of the precipitation forcing. Thus there is a need for the implementation and improvement of sub-grid precipitation algorithms in large-scale LSM applications.
- Soil moisture scales very well (to within 5% at the 1^o resolution for 13 of the 15 LSMs) because evaporation changes are generally offset by runoff changes with the opposite sign. The LSMs tend to equilibrate to specific model-preferred soil moisture states
- The SWE is the variable the most strongly affected by scaling: SWE is reduced in 13 of the 15 LSMs by 25% to 60% when moving to a 1^o resolution. Snowfall was held constant, thus the decrease in SWE resulted in earlier ablation as a consequence of the relatively warmer atmospheric forcing over snow-covered areas
- The only scheme that explicitly considers sub-grid elevation effects on the forcing (VIC) minimizes the impact of scaling on SWE, and it was the therefore the only LSM to scale SWE well at the most coarse resoltion

The conclusions regarding the impacts of scaling on runoff (especially sub-grid surface runoff), turbulent flux partitioning, soil moisture and SWE (both scaling and complexity) provided an incentive for LSM developers to address such scaling issues in their models. At the very least, this work could serve as a guide for helping the interpretation of results when a LSM is applied over a wide range of spatial scales. Finally, this work also lead to two other studies which used the Rhône-AGG LSM outputs to study the differences in LSM simulations related to their complexity (Fox et al., 2006), and the experimental setup and input data to further examine the impact of changing spatial scale on terrestrial water storage (Stockli et al., 2007). The dataset is part of the SIM system (Habets et al., 2008), and is used both operationally and for research purposes at CNRM.

3.3 Coupled Land-atmosphere MIP: The WAMME project

There is increasing evidence from numerical studies that anthropogenic LULCC can potentially induce significant variations on the local to regional scale climate (Pielke et al. 2011). However, the IPCC's Fifth Assessment lacked a comprehensive evaluation of the relative impact of biogeophysical feedbacks of LULCC on regional climate (Mahmood et al. 2013). This is primarily due to over-simplifications and limits to how some key biogeophysical surface processes are represented in the LSM component of GCMs, and how LULC is represented in such models. The recent Land-Use and Climate Identification of robust impacts (LUCID) experiment (Pitman et al. 2009; de Noblet-Ducoudré et al. 2012) examined the biogeophysical impacts of prescribed, global-scale LULCC using an ensemble of coupled GCMs and LSMs. The goal was to identify impacts that were statistically robust, primarily in terms of being detectable, common among the different models, and above the modelsâ internal variability.

Part of my work within AMMA and the international West African Monsoon Modeling and Evaluation (WAMME: Xue et al., 2010, 2016) project is oriented towards obtaining a better understanding of land-atmosphere coupling where is is strongest (such as West Africa, see for e.g. Koster et al., 2004), and the impacts of surface changes on the regional climate in West Africa. Improved prediction of precipitation is one of the major challenges facing the earth system modeling community, especially in areas with limited water resources such as West Africa. To this end, I was the co-principal investigator of an initiative within the framework of WAMME Phase 2 (WAMME2) international project, which examined the impact of land-use induced land cover change (LULCC) on the WAM. This has been done as a numerical model study using multiple physical parameterization options within the non-hydrostatic Weather Research and Forecast (WRF) model (Hagos et al., 2014), and using several global climate models (Xue et al., 2016; Boone et al., 2016).

3.3.1 Overview, Objectives and Methodology

The population of the Sahel region of West Africa has approximately doubled in the past 50 years, and could potentially double again by the middle of this century. This has led to the northward expansion of agricultural areas at the expense of natural savanna, leading to widespread land use land cover change (LULCC). Because there is strong evidence of significant surface-atmosphere coupling in this region, one of the main goals of the West African Monsoon Modeling and Evaluation (WAMME) Project Phase II is to provide basic understanding of LULCC on the regional climate, and to evaluate the sensitivity of the seasonal variability of the West African Monsoon (WAM) to LULCC.

The prescribed LULCC is based on historical changes from 1950 through 1990, representing a maximum feasible degradation scenario in the past half century. It is applied to 5 state of the art GCMs (see Table 3.2) over a 6-year simulation period. Multiple GCMs are used because the magnitude of the impact of LULCC depends on model-dependent coupling strength between the surface and the overlying atmosphere, the magnitude of the surface biophysical changes, and how the key processes linking the surface with the atmosphere are parameterized within a particular model framework. Land cover maps and surface parameters may vary widely among models; therefore a special effort was made to impose consistent biogeophysical responses of

surface parameters to LULCC using a simple experimental setup. The prescribed LULCC corresponds to degraded vegetation conditions. The main changes were confined to the Sahel region of West Africa (between 10^o and 15^o N, and from 35^o E to the West African coast) and a zone mainly covering Ghana based on the historical LULCC dataset by Hurtt et al. (2006). The GCM models were then run for 6 years using climatological sea surface temperature (SST) forcing (see Boone et al., 2016, for more details).

GCM	**Institute**	**LSM**
UCLA-AGCM	UCLA, USA	SSiB
UCLA-GSM (GFS)	UCLA, USA	SSiB
CAM5 (NCAR)	Univ. Connecticut, USA	CLM
GMAO (GOES-5)	NASA-GSFC, USA	CLSM
HadGEM	UK Met. Office, UK	MOSES

Table 3.2: The WAMME2-LULCC participant GCMs and LSMs. A more complete model description along with points of contact and references is given in Boone et al. (2016).

3.3.2 Main Conclusions

The main and most consistent effect of LULCC (corresponding to degradation only in this study) on the surface parameters among the GCMs was to decrease the *LAI* and increase the total albedo in the domain where LULCC was imposed. The albedo controls the total enthalpy flux exchange with the atmosphere (a larger albedo implies less energy available for surface turbulent fluxes of heat and/or moisture, and therefore, moist convection), while the *LAI* modulates the Bowen ratio (defined as the ratio of sensible to latent heat flux) to a degree which depends on the vegetation coverage. It should be pointed out that in the seminal paper by Charney et al. (1977), a dramatic albedo change (0.21 over the entire longitudinal band centered over the Sahel) was prescribed in order to obtain a significant atmospheric response. This specification has been used as evidence to discredit the potential role of LULCC in terms of Sahel drought. Later observation-based studies (e.g. Nichsolson et al., 1998; Govaerts and Lattanzio, 2008) have suggested that albedo changes over the Sahel of around 0.1 (with locally higher values upwards of 0.15 in the latter study) over the period of several decades are possible. The changes in this study are consistent with those values: the model with the maximum albedo increase has a maximum local peak value of 0.15 with an average increase over the entire LULCC zone of approximately 0.07. The albedo increases in the other models is even more modest (Boone et al., 2016).

The impact of the LULCC on the atmosphere (in terms of a precipitation feedback response) was confined to West Africa, which is consistent with studies showing that the effects of LULCC tend to be local to regional for the most part (Pitman et al., 2009; de Noblet et al., 2012). The overall impact of LULCC on the WAM for the five-year simulation herein can be summarized as follows:

- Reducing the Leaf Area Index (*LAI*) increases the Bowen ratio in regions where transpiration and evaporation from intercepted canopy water are occurring. In all of the regions

where *LAI* (and evaporation) decreases (above some relatively low threshold), the rainfall also decreases. This response is common to all the models. Therefore in such regions, resulting decrease in *LE* is the main cause for reduced rainfall, rather than the reverse.

- The increase in albedo reduces the net radiation, thus the energy available for the turbulent surface fluxes are also decreased, but the partitioning of this energy loss is modulated by the *LAI* change. In models with moderate *LAI* changes, latent heat flux is reduced during the wet season in regions receiving rainfall. For models with large *LAI* changes, the reduction in latent heat can exceed the reduction in net radiation caused by the albedo change (owing to large changes in Bowen ratio), thus the sensible heat flux increases. In the dry season or in dry regions (north of the area receiving rainfall), the increase in albedo (reduction in surface net radiation) translates nearly directly into a decrease in sensible heat flux (and there is little to no impact on overall monsoon rainfall).

- The model specific simulated WAM location influences the impact of the LULCC. The models with the WAM (defined here as the zone with peak JAS rainfall) located furthest to the north (CAM5) experienced a shift in the overall monsoon position owing to LULCC. This feature is seen as a statistically significant JAS precipitation difference dipole pattern. Two other models (with monsoons located further south) also had a dipole pattern, but rainfall increases were not statistically significant. But the main (and statistically robust) impact in all of the models is a lowering of monsoon rainfall within the LULCC zone: the CAM5 was the only model for which this effect extended outside of this zone (to the north). For the models with a more southerly peak monsoon rainfall (HadGEM and GMAO), there was essentially no southward shift and only a rainfall reduction.

- In this WAMME study, the goal is to favor consistent changes in the values of the biogeophysical parameters over changes in a particular modelâs LULC, since how vegetation classes and their associated parameter values are defined can vary tremendously between different models. Collaborations were engaged with each modeling group in order to ensure the LULCC experiment not only had a consistent change in the spatial distribution of LULCC and the vegetation types, but also in terms of the vegetation characteristics and parameters, which provide the real forcing at the land surface in the LULCC experiment. But despite these efforts, this remains a challenging task mainly owing to how LULC and the associated biogeophysical parameters are defined in the models.

This was essentially a pilot multi-model study for obtaining a better understanding of the effects of LULCC over West Africa. A small number of GCMs, climatological SST forcing resulting in a multi-year ensemble, and a relatively simple methodology for representing LULCC were used in order to focus on elucidating the first order physical mechanisms. Based on the results, it can be inferred that the use of climatological land cover can lead to inconsistencies and errors in GCM studies for West Africa, given the high sensitivity to the surface properties in this region which have a large inter-annual variability, notably the *LAI*. Inconsistencies can also arise between locations where LULCC is imposed and those of the simulated monsoon (thereby potentially influencing the magnitude of the impact of LULCC). Finally, it is suggested that future work should be undertaken to evaluate whether the sign and strength of the feedbacks

between the surface and the atmosphere simulated by large scale atmospheric models are consistent with observations. A follow-on project is anticipated for which the impact of LULCC will be explored over all major monsoon regions for a longer time period using more models (and large ensembles).

3.4 Offline Land MIP: ALMIP

West Africa has been subjected to extreme climatic variability over the last half century. Seasonal to inter-annual prediction of the west-African monsoon, which is the main precipitation driving mechanism, has therefore become a research topic of utmost importance, however, a thorough understanding of this complex system has proved illusive. The deficiencies with respect to modeling the African monsoon arise from both the paucity of observations at sufficient space-time resolutions, and because of the complex interactions of the relevant processes at various temporal and spatial scales between the biosphere, atmosphere and hydrosphere over this region.

The AMMA project was organized in recent years with the main goal of obtaining a better understanding of the intra-seasonal and inter-annual variability of the WAM, which was to be accomplished through an extended period of intensive observations and field campaigns together with model developments and improvements. In particular, land-atmosphere coupling is theorized to be significant in this region. The magnitude of the north-south gradient of surface fluxes (related to soil moisture and vegetation) exerts a strong influence on the position of the tropical front and possibly the strength of the monsoon and the African Easterly Jet (AEJ). A high priority goal of AMMA is therefore to better understand and model the influence of the spatio-temporal variability of surface processes on the atmospheric circulation patterns and the regional water cycle.

The strategy proposed in AMMA to develop a better understanding of fully coupled system is to break the various components into more manageable portions which will then provide insight into the various important processes. The first step is to begin with the land surface in off-line or uncoupled (without atmospheric feedbacks) mode. The idea is to force state-of-the-art land surface models with the best quality and highest (space and time) resolution data available in order to better understand the key processes and their corresponding scales. The AMMA project therefore affords the possibility to improve the understanding of critical land surface processes over west Africa within the context of an LSM intercomparison project (ALMIP).

ALMIP has 2 phases, the first being conducted over the regional scale (domain shown in Fig. 3.2) at 0.5 degree spatial and 3 hourly temporal resolutions for a several year period (2002-2007). ALMIP phase 2 (ALMIP2) was run at the mesoscale (0.05 degree and 30 minute forcing) over 3 sub-domains within the AMMA-Couplage de l'Atmosphère Tropicale et du Cycle Hydrologique (AMMA-CATCH: Lebel et al., 2009) transect: the simulation domains encompassing the supersites in Mali, Niger and Benin are shown in blue, orange and red, respectively, in Fig. 3.2. A brief overview and some highlights of the 2 phases are given in the next two sections.

3.4.1 ALMIP1: Regional Scale

Objectives

The multi-model offline technique has been used by numerous intercomparison projects (see Section 3.1). The idea is to force state-of-the-art land surface models with the best quality and highest (space and time) resolution data available to better understand the key processes and

their corresponding scales (Boone and de Rosnay, 2007). The ALMIP has the following main scientific objectives:

1. inter-compare results from an ensemble of state-of-the-art models and study model sensitivity to different parameterizations and forcing inputs
2. determine which processes are missing, or are not adequately modeled, by the current generation of LSMs over this region
3. examine how the various LSM respond to changing the spatial scale (three scales will be analyzed: local, mesoscale, and regional)
4. develop a multi-model climatology of ârealisticâ high-resolution (multi-scale) soil moisture, surface fluxes, and water and energy budget diagnostics at the surface
5. LSMs simulate the vegetation response to the atmospheric forcing on seasonal and interannual time scales.

The LSMs and the participating institutes are listed in Table 3.3: for further details on model structure and the associated references can be found in Boone et al. (2009a).

The input forcing database is composed of land surface parameters, atmospheric state variables, precipitation, and downwelling radiative fluxes based on a blend of numerical weather prediction model output, satellite based products and field data. Three experiments explored the

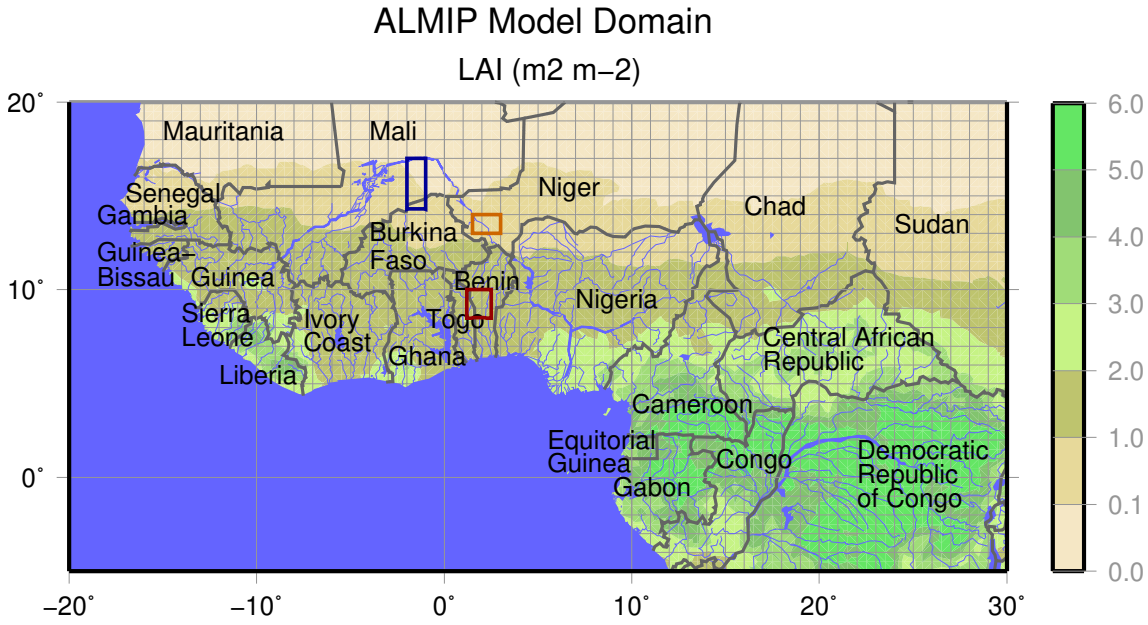

Figure 3.2: ALMIP model domain. The climatological average *LAI* (m^2 m^{-2}) from ECOCLIMAP is contoured. The blue, orange and red sub-domains correspond to the Mali, Niger and Benin AMMA-CATCH supersite domains.

LSM	Institute
TESSEL	ECMWF, Reading, UK
CTESSEL	ECMWF, Reading, UK
HTESSEL	ECMWF, Reading, UK
ORCHIDEE-CHOIS	IPSL, Paris, France
ORCHIDEE-CWRR	IPSL, Paris, France
ISBA	CNRM, Météo-France
ISBA-DIF	CNRM, Météo-France
JULES	CEH, Wallingford, UK
SETHYS	CETP/LSCE, Vélizy/Gif-sur-Yvette
IBIS	ISE, Montpellier, U Wisc., Madison, USA
NOAH	CETP/LSCE (NCEP)
CLSM	UPMC, Paris, France
MSHE	U. of Copenhagen, Denmark
SSiB	LETG, Nantes, France; UCLA, USA
SWAP	IWP, Moscow, Russia

Table 3.3: Listing of models participating in ALMIP. The institute indicates where the ALMIP model simulation was performed.

LSM sensitivity to different input meteorological forcings (notably precipitation, which is the most critical field).

Results and Evaluation

One of the most critical land surface fields is evapotranspiration (E). This flux forms the critical link between land surface (hydrology) and the atmosphere. The meridional gradient of E is a maximum in this region during the monsoon season, and this is a key feature of the WAM as it influences the regional scale atmospheric circulation and convection. The June to September (JJAS) average total evapotranspiration, E, (kg m^{-1} d^{-1}) for 2006 using TRMM rainfall as forcing is shown in Fig. 3.3 for each LSM (panels a-n), along with the multi-model average in panel o. Despite using the same atmospheric forcing and harmonized vergetation and soil parameters, significant inter-model differences exist. For example, in part of the Sahel, E generally varies between models by a factor of approximately 3 (with locally higher values). Since E is one of the main pathways for coupling between the surface and the atmosphere in this region, it is hypothesized that the inter-LSM differences are likely making a contribution to the differences in GCM simulated coupling strength over this region, for example, as seen in Koster et al. (2004). Thus there is a need to better understand and quantify these differences (Boone et al., 2009a). The multi-model average E difference (TRMM-forced less ECMWF-FC rainfall forced: FC corrsesponds to ForeCast) is shown in Fig. 3.3, panel p. This shows the WAM position errors in the ECMWF-FC model (which is seen as the main raninfall area being too far south). This highlights the fact that certain satellite rainfall products are still far superior to model produced (short term forecasts here, but ECMWF and NCEP reanalysis products also suffer from rela-

tively large errors) rainfall estimates in this region, and this obviously has a tremendous impact on the simulated surface fluxes.

Gao and Dirmeyer (2006) showed the advantages and improved realism of using a multi-LSM model average to study simulated surface properties. In ALMIP, the multi-model average and spread were evaluated using field data, and satellite products, and these fields were used as a multi-model ensemble average re-analysis for multiple studies. As an example of an evaluation using local scale data, the ALMIP multi-model average and spread were compared to field data from the AMMA field campaign. Comparing local flux data with model output over a grid square presents a scale problem. It is generally only useful if the grid-square surface parameters and forcing data are consistent with those observed at the local scale since there can be significant sub-grid heterogeneity on the grid-square scale. Surface flux data for three local scale sites located within the Mali super-site square (blue box in Fig. 3.2) was spatially aggregated over

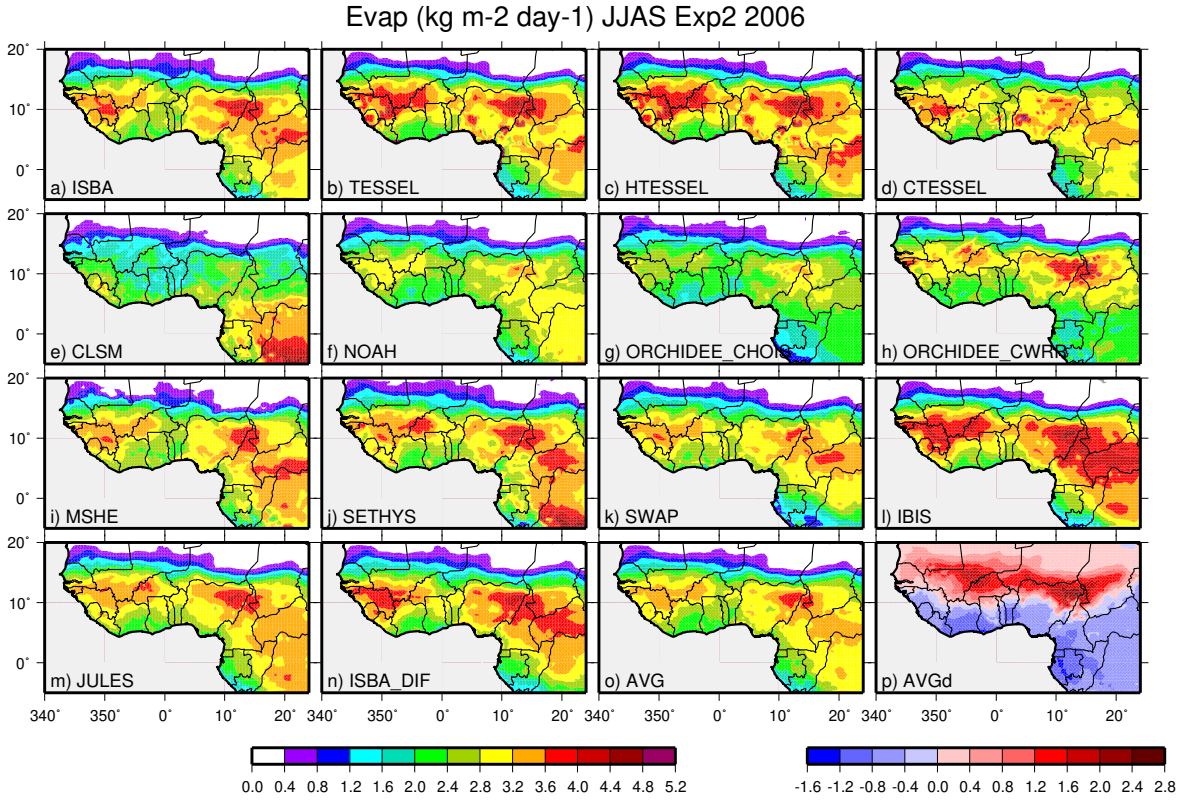

Figure 3.3: The JJAS average total evapotranspiration (kg m^{-1} d^{-1}) for 2006 using TRMM rainfall as forcing. The multi-model average is shown in panel o. The multi-model average difference (TRMM-forced less ECMWF-FC forced) is shown in panel p.

an area of approximately 60x60 km^2, which was the typical of the grid size of more coarse global-scale NWP models, typical RCMs and relatively high-resolution GCMs. The spatially aggregated *observed H* was computed using different weighting schemes based on the spatial coverage of the dominant vegetation type at each site, and the ranges in the soil types, the surface albedo, and the coverage of standing water using remotely sensed data (Timouk et al. 2009). Each of the three observation sites used in the aggregation has a very different land cover type: Kelma is a low-lying marsh during the wet season and ensuing months (hence,the negative *H* values); Eguerit is very dry and rocky (soils quickly drain, thus *H* remains relatively high all year); and Agoufou has sparse, low vegetation. This is the dominant vegetation coverage over the mesoscale area, and the ALMIP land cover for this grid box from Ecoclimap (87% bare soil and 13% tropical grassland) is most consistent with the characteristics of this site. The LSM average simulated *H* response to the wet season and the subsequent dry down are similar to the dynamic of the observed aggregated *H* flux, but it is quite different from 2 of the 3 local scale sites contained within the square (see Fig. 6 in Boone et al., 2009a). This highlights the need to evaluate spatially distributed LSM fluxes with observed fluxes which represent similar surface areas and covers (as those used in the LSMs).

In terms of comparing LSM with satellite based data, generally two approaches are used. The first is to use a forward modeling approach to transform an LSM variable into a satellite measured quantity, such as brightness temperature. This was done for ALMIP using the ALMIP Microwave Emission Model (MEM) as discussed in Boone et al. (2009a). MEM couples ALMIP soil moisture and temperature outputs to the Community Microwave Emission Model (CMEM; de Rosnay et al. 2009). It permits a quantification of the relative impact of land surface modeling and radiative transfer modeling on the simulated brightness temperature background errors. ALMIP MEM brightness temperatures were evaluated for 2006 against Advanced Microwave Scanning Radiometer for Earth Observing System (AMSR-E) C-band data provided by the National Snow and Ice Data Center (NSIDC). For a more in-depth analysis of these results, see de Rosnay et al. (2009).

A second approach of comparing LSM with satellite based data is to make a more direct intercomparison between LSM outputs and a satellite product. The Gravity Recovery and Climate Experiment (GRACE) satellite mission accurately measures gravity field variations, which are inverted to retrieve terrestrial water storage variations. Knowledge of the land surface water storage is important for estimating vegetation growth, and it may hold a key to increasing long-range atmospheric predictability over West Africa. A comparison of the soil moisture storage change anomaly derived from the GRACE satellite product to two simulations by the ALMIP LSMs over the Sahel from 2005 to 2006 is shown in Fig. 3.4. Exp.3 results (the default, driven by TRMM) compare quite well with GRACE. The Exp.1 results are quite poor, but this was related to the precipitation forcing which was based on NWP-FC data (see panel p of Fig. 3.3). Further details can be found in Grippa et al. (2011).

Proxy Surface re-analysis

In terms of the value of the project to the international community, the multi-model surface analysis output from ALMIP has been used in a significant number of peer reviewed publications; the project overview (Boone et al., 2009a), the impact of improved soil moisture on weather

forecasting (Agusti-Panareda, 2009), the WAM water cycle (Bock et al., 2010; Meynadier et al., 2010), within the Regional Climate Model (RCM) and GCM intercomparison project WAMME (Boone et al., 2010; Xue et al., 2010) and AMMA-Cross (Hourdin et al., 2010), in terms of the Nitrogen budget of Sahelian dry savannas (Delon et al., 2009), in evaluation of regional atmospheric models (Dominguez et al., 2008; Steiner et al., 2009), in comparison with GRACE satellite estimates (Grippa et al., 2011), in an intercomparison of simulated rainfall and evapotranspiration associated with a mesoscale convective system (Guichard et al., 2010), to explore the drying down of Sahelian soils after precipitation events (Lohou et al., 2014), in a study to characterize the hydrological functioning of the Niger (Pedinotti et al., 2012), an intercomparison, of LSM brightness temperature using a forward model (de Rosnay et al., 2008), and a model study of dust emission (Tulet et al., 2008). The ALMIP input data has also been used in some

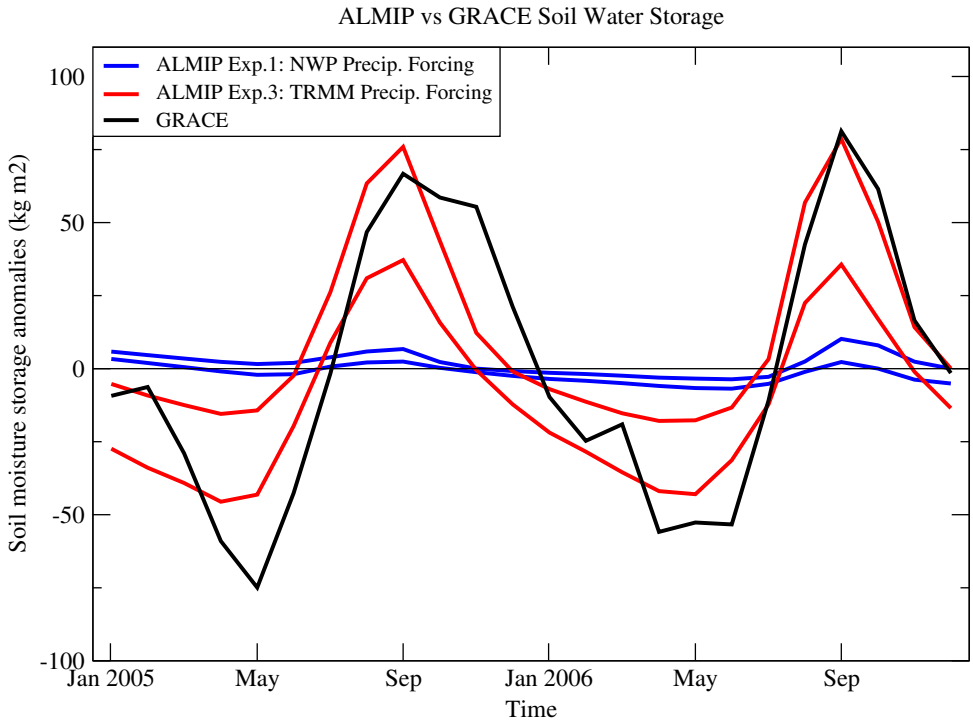

Figure 3.4: Comparison of the soil moisture storage change anomaly derived from the GRACE satellite product (black curve) to two simulations by the ALMIP LSMs over the Sahel from 2005 to 2006. The blue lines en- closed the mean plus the root-mean-square difference for results from experiment 1 (using NWP rainfall forcing). The red lines correspond to results from experiment 3 (using TRMM rainfall input). Taken from Boone et al. (2009a), and based on the study by Grippa et al. (2011).

studies, for example, to examine vegetation dynamics over West Africa (Yin et al., 2014a,b).

An example of using ALMIP offline data as a proxy re-analysis of the surface turbulent fluxes (Boone et al., 2010) for the Phase 1 of the WAMME project (Xue et al., 2010) is shown in Fig. 3.5 for two years, 2004-2005. The two *A* symbols correspond to the multi-model ALMIP average (for two different years distinguished by color), and the boxes correspond to the multi-model spread (here defined as the range in LSM annual average values). The diagonal lines correspond to lines of constant net radiation (the multi-model ALMIP average: the spread is quite small and is thus not shown). It is taken as a proxy of the true net radiation (since the downwelling components and surface albedo were based on satellite data products and the ALMIP-simulated upwelling longwave radiation had comparatively little spread). All of the other symbols correspond to different RCM and GCM simulated values (see Boone et al., 2010, for the corresponding symbols and model names). The ALMIP results showed a certain degree of inter-model variability, however, as expected, it is relatively small compared to that simulated by the fully coupled models. Most of the WAMME models simulate a Bowen ratio which is considerably less than that of the ALMIP multi-model average. To the south of the Sahel, the Bowen ratio was quite low in most models (below 0.1 for large areas), while ALMIP values (which agreed with local scale observational data) reveals that average Bowen ratios in the same region rarely fell below approximately 0.3 for the same time (average) periods considered. This is turn, could have an impact on model simulated planetary boundary layer depths, convective available potential energy , etc. in this region which is the core of the monsoon (using the definition of peak rainfall). Part of the reason for this problem could be related to the generally excessive rainfall simulated by the WAMME models, however, the exact reasons for this need to be determined so that future work on this subject was suggested by Boone et al. (2010).

3.4.2 ALMIP2: Meso-Scale

Objectives

In ALMIP Phase 2, the focus is on the mesoscale and local scale (Boone et al, 2009b). LSMs are being evaluated using observational data from three heavily instrumented supersites from the AMMA-Couplage de l'Atmosphère Tropicale et du Cycle Hydrologique (CATCH) observing system (Mali, Niger, and Bénin). The AMMA-CATCH window covers a north-south transect encompassing a large eco-climatic gradient. Experiments have been performed at the mesoscale for each of the three super sites, using a grid resolution of approximately 5 km. The simulations cover the years 2005-2008, so that they encompass the 2005-2007 Intensive Observing Period (IOP) with a special focus on the analysis during the Special Observing Period (SOP) in 2006. In addition to evaluation using field data, LSM simulations have been compared to results from detailed vegetation process and hydrological models that have already been extensively validated over this region. Finally, the results will be used in conjunction with those from ALMIP-1 in an effort to evaluate the effect of scale change on the representation of the most important processes from the local to the regional scale.

A coordinated set of model experiments over the three AMMA-CATCH sites provide good idea of the contrasting characteristics and processes in the Sahel and Soudano-Guinean regions. The typical endorheic nature of the surface hydrology of the two Sahelian sites (Mali and Niger)

for which catchments are limited to scales on the order of a few tens of square kilometers, includes both high runoff-prone and infiltration-prone surfaces. This is in contrast to the large hydrological catchments over the Benin site. Each site observing system provides both forcing (i.e., micro-meteorological description and soil and vegetation properties) and validation data (surface fluxes, soil moisture, water table, and runoff). In addition, remote sensing images have been processed in order to infer land surface properties at the mesoscale, such as land cover, leaf area index maps, land surface temperature, albedo, and superficial soil moisture.

The main scientific questions to be addressed in ALMIP Phase 2 are:

1. Which local or mesoscale processes are missing or not adequately modeled by the current generation of LSMs over this region (infiltration over crusted soils, endoric hydrology...)?

2. How do the various LSM respond to changing the spatial scale? The relation between

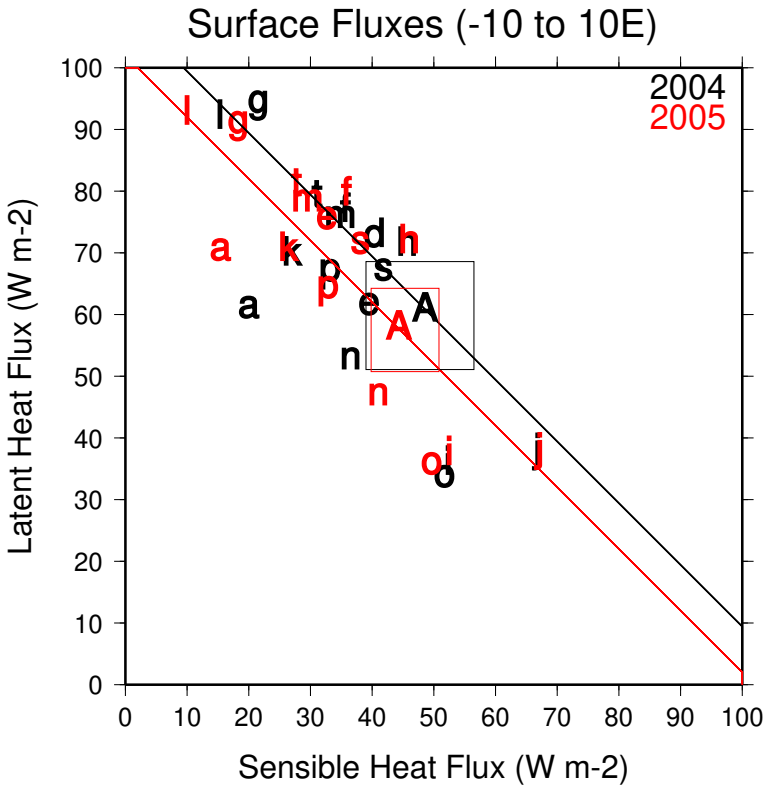

Figure 3.5: Annual average latent verses sensible heat fluxes from the WAMME RCM and GCM models, and ALMIP. The A symbols correspond to the multi-model ALMIP average, and the boxes correspond to the multi-model spread (here defined as the range in LSM annual average values). The colors correspond to the two years. The diagonal lines correspond to lines of constant net radiation (the multi-model ALMIP average: the spread is quite small and is thus not shown). All of the other symbols correspond to different RCM and GCM simulated values (see Boone et al., 2010, for the corresponding symbols and model names).

meso and regional scales will be made using ALMIP Phase 1 results.

3. Can relatively simple LSMs simulate the vegetation response to the atmospheric forcing on seasonal time scale (for several annual cycles) for the diverse climates/vegetation covers?

4. How can LSM simulate mesoscale hydrology given their relatively simple representation of such processes?

5. What are the impacts of uncertainties/differences in the precipitation on the surface fluxes and hydrological responses of the LSM models?

Over 20 land surface and hydrological model groups from the international community participating in ALMIP2, with contributions from several other groups (such as the USDA etc.). A list of the participant LSMs is shown in Table 3.4.

LSM	**Institute**
CHTESSEL	ECMWF, Reading, UK
ORCHIDEE	LSCE, Gif-sur-Yvette, France
ISBA	CNRM, Météo-France; HSM, Montpellier
JULES	CEH, Wallingford; UKMO, Exeter, UK
SETHYS	LSCE, Gif-sur-Yvette
NOAH	CETP/LSCE (NCEP)
CLSM-UPMC	UPMC, Paris, France
CLSM-NASA	GMAO, NASA-GSFC, USA
STEP	GET, Toulouse, France
SWAP	IWP, Moscow, Russia
MOSAIC (LIS)	NASA-GSFC, USA
NOAH (LIS)	NASA-GSFC, NCEP, USA
SiBUC	Hydro. and Wat. Res. Res., Kyoto, Japan
SPONSOR	Inst. Geog., RAS, Moscow, Russia
MATSIRO	Univ. of Tokyo, Japan
CLM	Natl. Taiwan Univ., Taipei

Table 3.4: Listing of LSMs participating in ALMIP2. The institute indicates where the ALMIP model simulation was performed.

The input forcing data is always a critical aspect of such modeling exercises. ALMIP2. Several state-of-the-art or new data sets were used in ALMIP2, and moreover two specific data sets have been developed for use by ALMIP2. Most LSMs use climatological physiographic data sets as input, but owing to the significant vegetation inter-annual variability in this region, notably in the Sahel, a specific land cover dataset which accounts for this was developed using the ECOCLIMAP methodology (Kaptué et al., 2011). In terms of forcing, ECMWF-FC state variables were interpolated using a classical two-dimensional scheme, and thermodynamic variables were adjusted hypsometrically to the higher resolution topography of ALMIP2. The

downwelling radiative fluxes from the LSA-SAF project (Trigo et al., 2011) were interpolated from their native 3 km grid to the 0.05^o ALMIP2 grid (thus, relatively little information was lost to smoothing owing to interpolation effects). Arguably the most important time varying forcing input is the precipitation. Two rainfall data sets were prepared using data from the dense rain gauge network over each mesoscale super-site. The first uses the classic nearest-neighbor or Thiessen (THI) method. This is sometimes the preferred method for hydrology over such regions since there is essentially no smoothing of the rain fields, but there can be considerable extrapolation in regions with relatively few rain gauges. A new method was also developed, which consisted in a combined krigged-Lagrangean rainfall (LAG: Vischel et al., 2011). The classic krigging technique was used for disorganized convection, but a Lagrangean method was used when coherent structures (squall lines) were present. The impact of each on surface state variables, fluxes and hydrology was studied in ALMIP2.

Analysis

Preliminary results of the mesoscale analysis were presented at the ALMIP2 Workshop at Météo-France in February, 2013. The results have also been presented at numerous conferences by A. Boone, the other members of the French ALMIP2 Core Working group. Publications are being submitted to the ALMIP Special Collection in the Journal of Hydrometeorology in 2016.

An example of a multi-model inter-comparison result is shown in Fig. 3.6: the ratio of surface (fast response) runoff to total rainfall (ordinate) is plotted verses the ratio of the drainage (slow response) to the rainfall (abscissa) averaged over a 3-year period and over the entire domain for the Niger mesoscale square. Each symbol represents a particular model: larger symbols represent the simulated runoff ratios using Lagrangian rainfall as input, smaller symbols correspond to Thiessen (or so-called *nearest-neighbor*) rainfall input. First, runoff ratios vary widely among the schemes, which strongly influences the simulated Bowen ratio and soil water content. The inter-model differences are larger than in ALMIP1: this is likely due to the larger rainfall rates which increases the spread among models owing to the non-linear treatment of both runoff and through-flow. The effect of Thiessen rainfall is generally to increase runoff in all of the models, however, each model tends to retain its propensity to generate either mostly surface or drainage flow. Thus, inter-model variability in runoff exceeds that resulting from using two different techniques to interpolate the rainfall (both in space and time). Surface runoff ratios, R_r, range from approximately 0.03 to 0.52 among the LSMs, which is a rather large spread. Drainage flow R_r ranges from 0 to about 0.18, which is in line with the relatively low rainfall and high potential evaporation demand. The spread in surface runoff is quite significant, since this water is assumed to leave the system (theoretically entering a hydrographic network) thus before evaporation from the gound or transpiration. This implies that parameterization exerts a strong control on the Bowen ratio and the recycling of rainfall with the atmosphere.

The impact of scaling has been examined by comparing results from ALMIP1 (0.5 degree, 3 hour time step forcing) with those of ALMIP2 (0.05, 30 minute time step). Despite the non-linearity of evaporation within a grid box (notably with respect to input precipitation and soil

moisture), monthly average evapotranspiration scales quite well, especially as one moves southward towards less water-limited climates (Benin). A similar result was also found by Boone et al. (2004) for the Rhône basin, even though West African precipitation events generally have shorter characteristic correlation length scales and smaller time-scales owing to the large convective component. However, surface runoff does not scale as well. An example of the impact of changing the spatial scale of the land surface model computational grid cell is shown in Fig. 3.7 for monthly average surface runoff. ALMIP2 results have been up-scaled (using linear averaging) to the corresponding ALMIP1 grid cell for each plot. Note that the monthly grid average ALMIP2 rainfall compares very favorably with that of ALMIP1 (explained variance above 0.9 with a bias less than 10 %). The ALMIP2 precipitation forcing has considerably higher spatial

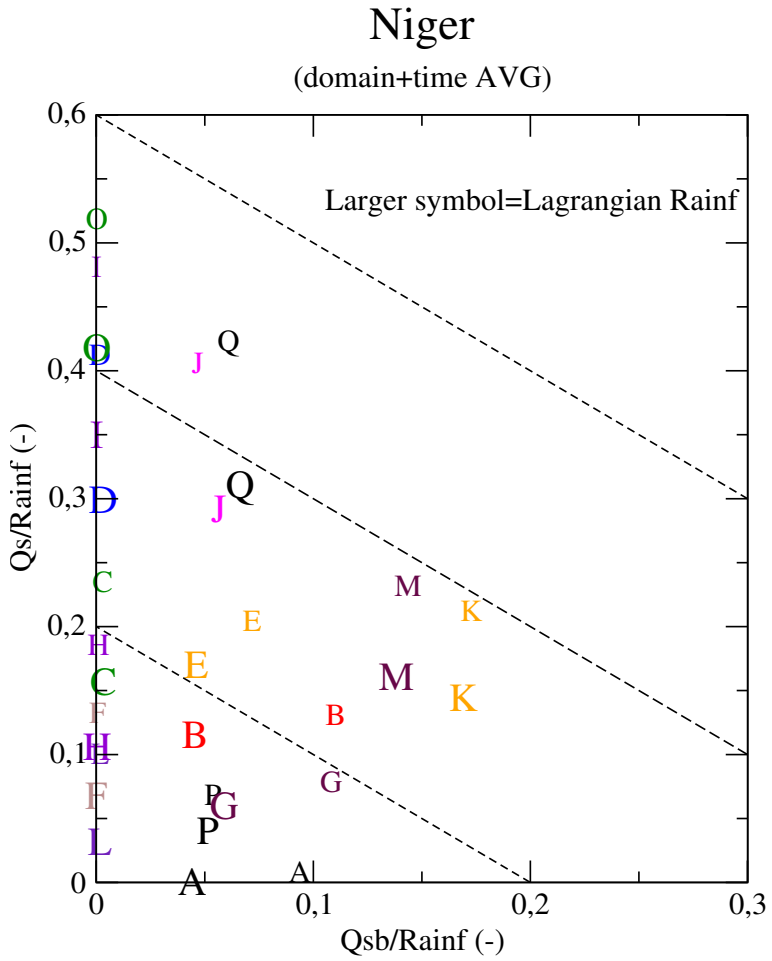

Figure 3.6: The ratio of surface (fast response) runoff to total rainfall (ordinate) is plotted verses the ratio of the drainage (slow response) to the rainfall (abscissa) averaged over a 3-year period and over the entire domain for the Niger mesoscale square. Each symbol represents a particular model: larger symbols represent the simulated runoff ratios using Lagrangian rainfall as input, smaller symbols correspond to Thiessen (or *nearest-neighbor*) rainfall input.

and temporal resolution than that for ALMIP1: it is much closer to the characteristic convective time and spatial scales in this region. It was found that the model surface runoff parameterizations provide similar model average rainfall in the regions receiving the most precipitation (to the south), but the scale dependence becomes more significant in the more rainfall-limited regions (north). However, for all three sites, the inter-LSM runoff spread increases considerably for the higher resolution ALMIP2 rainfall (i.e. the more intense and smaller duration, the larger the disagreement among models).

Further analysis by the different working groups is ongoing, but some general conclusions of the mesoscale phase of ALMIP2 can be summarized to date as

- the inter-model variance exceeds the inter annual variability (for a given variable), and also the variability caused by using two different (but fairly standard) rainfall interpolation methods
- the Bowen ratio varies greatly among the models, however, there is a consistent change among the sites (i.e. as one moved north, the sensible heat flux component of the Bowen ratio increases)

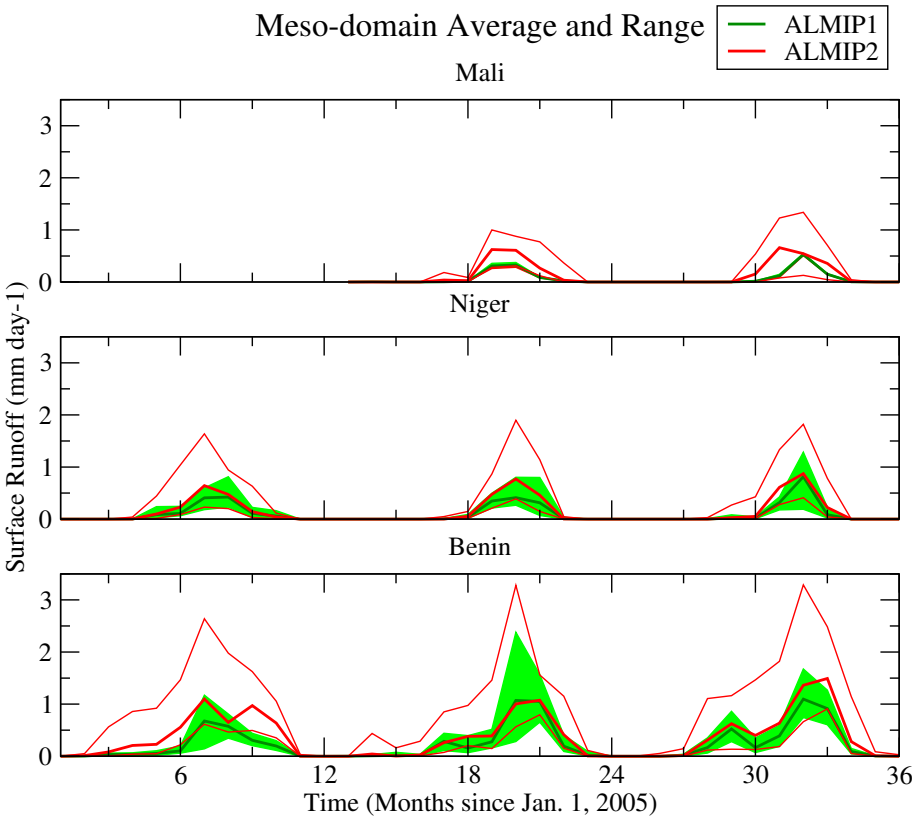

Figure 3.7: ALMIP1 (green) and ALMIP2 (red) multi-model average (thick lines) and spread (thin lines) of surface runoff for the three mesoscale super-sites for several annual cycles.

- surface runoff dominates the total runoff component for most of the models, but is highly variable among the models
- the relationship between the evaporation-precipitation and run off-precipitation ratios for each individual LSM change relatively little across the sites, despite very different climates
- the canopy interception evaporation is fairly small for all models and sites, however, the partitioning of the evapotranspiration between baresoil evaporation and transpiration varies greatly among the models.
- Thiessen rainfall input generally causes more runoff, most most models either increase either surface runoff or drainage in response (i.e. the runoff component ratio doesn't change much for a given scheme),
- Evaporation scales well compared to ALMIP1, however, runoff does not: this points to the need to develop better sub-grid runoff parameterizations which focus on rainfall characteristics.

Several areas which need attention (for one reason, since they could potentially have an impact on prediction by atmospheric models) for future testing and model developments were identified: i) significant interactions with groundwater occur in some locations and this is generally not modeled, ii) endoric processes, which of key importance to the hydrological functioning in this region, are not modeled, iii) lateral fluxes and ponding are generally not represented, iv) deep rooting plants are generally not considered (which is a particular problem during the dry season), v) and soil crusting (a hydrophobic effect which can significantly reduce infiltration and thus water recycling with the atmosphere) is not modeled by any of the LSMs. It should be noted that many of these process are known to be present in many semi-arid regions of the world, not just in the Sahel. It is recommended that the impact on water recycling and coupling to the land surface should be studied.

LSM Hydrology

In addition to the mesoscale inter-comparisons of fluxes and model state variables, several other supplemental studies are being done. For example, a study (Getirana, et al., 2014a) evaluated the water balance simulated by ISBA over the upper Ouémé River basin, in Benin, Western Africa using the AMIP2 mesoscale River RouTing Scheme (ARTS). ARTS is based on the non-linear Muskingum-Cunge method coupled with two linear reservoirs which simulate the time delay of both surface runoff, τ_s (s), and baseflow, τ_b (s), which are produced by land surface models. Based on the evidence of a deep water table recharge in this region, a reservoir representing the deep water infiltration (DWI: kg m^{-2} s^{-1}) is implemented in ARTS. A schematic is shown in Fig. 3.8. The scheme was developed and evaluated using ISBA, but it was made in such a way that it can be applied using the output runoff components of a standard LSM.

The next step was to use ARTS within ALMIP2 in oder to examine their ability to simulate basic runoff processes for this basin and to get a multi-model picture of the basin scale water

budget. Thus, the hydrological processes and water budget components of the basin have been simulated for all of the LSMs over the period 2005-2008 during which rainfall and streamflow data were intensively collected over the study area during the AMMA field campaign. LSM simulated surface runoff and drainage were input into the ARTS, then optimal ARTS parameter sets were determined for three optimization experiments which were performed using daily streamflow at five gauges within the basin as in Getirana et al. (2014a).

A comparison between the four-year average daily discharge resulting from using the THI and LAG precipitation products (Fig. 3.9) shows that the more complex interpolation process used in LAG increased the overall performance of models in simulating streamflows at all gauging stations used to evaluate streamflows within the basin. The corresponding Nash-Sutcliff, NS, and NRMSE are shown in Fig. 3.10: the significant improvement (reduction in NRMSE and substational overall increase in NS) are seen as the shift upwards and to the left of the model points. It is demonstrated that most LSMs have significant errors in the simulated TR, resulting in misrepresentation of streamflows during the beginning of wet seasons. For example, the 4 year average discharge annual cycle is shown in for each LSM (used optimized ARTS parameters) for THI and LAG rainfall inputs. All but 3 LSMs for THI and 4 LSMs for LAG rainfall simulate streamflow several months too soon (as soon as rainfall begins). This suggests that processes related to infiltration in such hydroclimatic and pedologic conditions should be better parameterized. All but 3 LSMs showed an evident need for the representation of DWI. As stated in Getirana et al. (2014a), DWI should be considered as a temporary solution until LSMs are improved to represent more detailed hydrological processes in the basin, notably more realistic groundwater representations. This will likely be a subject for new model development in up-

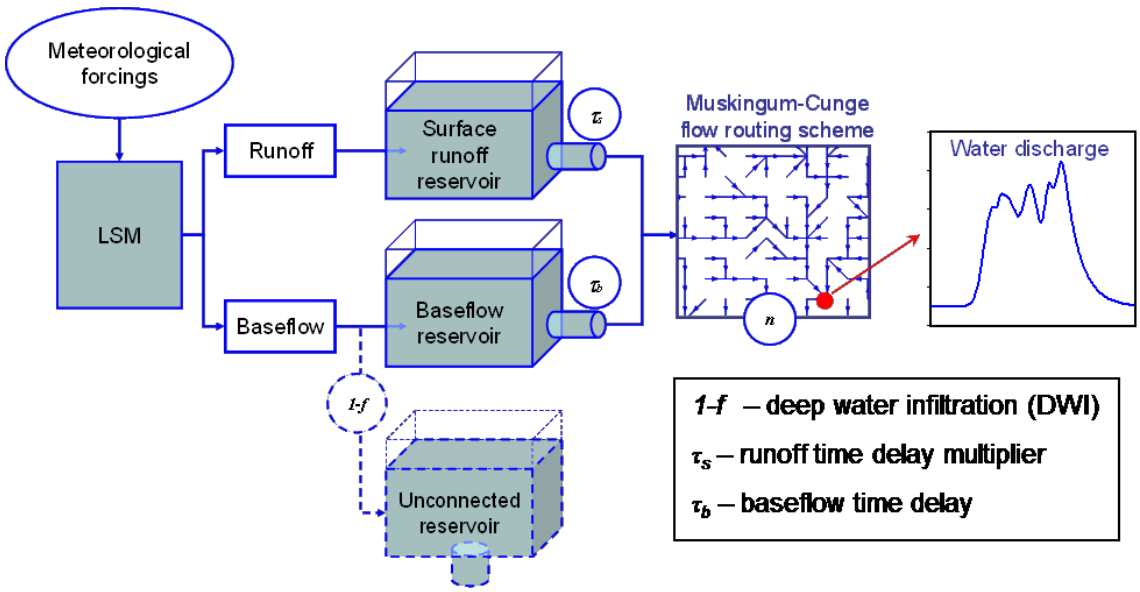

Figure 3.8: Schematic diagram of the ARTS scheme used to compute discharge from ALMIP2 LSM runoff components.

coming years within the international community. Finally, ARTS is considered to be a fairly generic scheme that can be applied to many basins to a first order approximation to transform LSM runoff into discharge. This scheme formed the basis for the global scale river routing scheme called Hydrological Modeling and Analysis Platform (HyMAP: Getirana et al., 2012), which has been applied in an international LSM intercomparison project over the Amazon basin (Getirana et al., 2014b).

Project Status

An international workshop took place in Toulouse in 2013, and a special collection (publication) proposition within the Journal of Hydrometeorology has been accepted. ALMIP2 is one of the core GEWEX-GLASS supported projects. Several other parallel studies (in addition to the aforementioned hydrology coupling study) are also being done by other members of the ALMIP2 French and International working groups. Upwards of 10 papers are anticipated to be submitted to the J. of Hydrometeorology ALMIP2 Special collection. Finally, ALMIP2 will continue to be a model test-bed. For example, work was recently done to develop a methodology to improve downwelling solar radiation owing to a more robust accounting of aerosols (Dramé et al., 2015): it is planned to study the impact of this on the surface fluxes and vegetation phenology in the future.

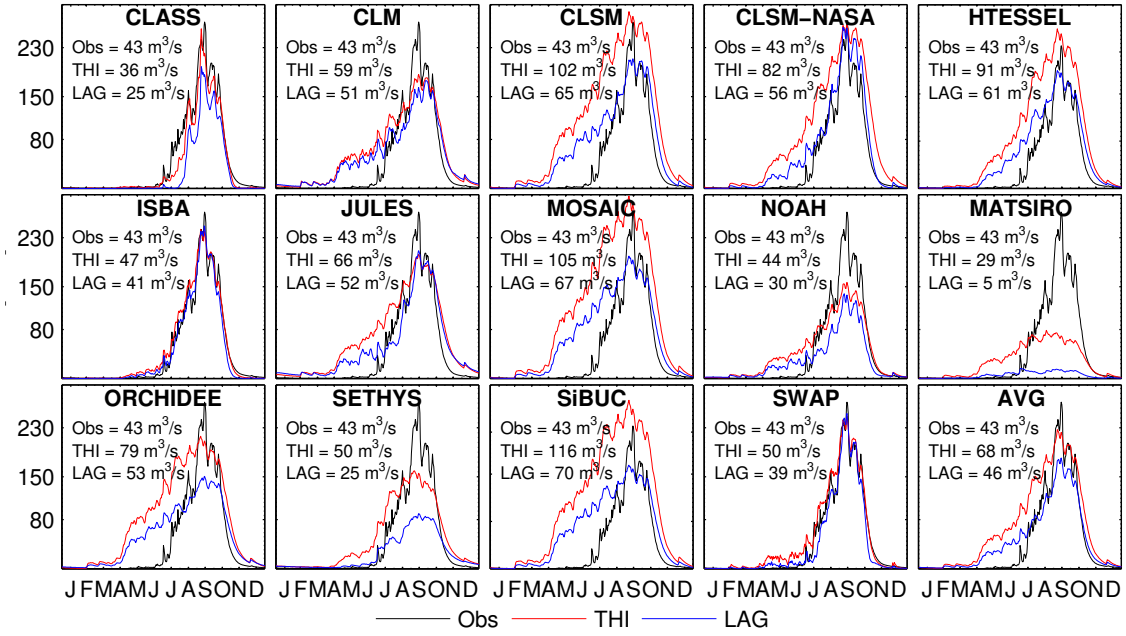

Figure 3.9: Daily discharge annual cycle (averaged from 2005-2008) at the Bétérou station (m^3 s^{-1}) for each LSM after routing using ARTS. The average discharge is shown for the observations (Obs), and simulated for the THI and LAG input rainfall data (Getirana et al., 2017).

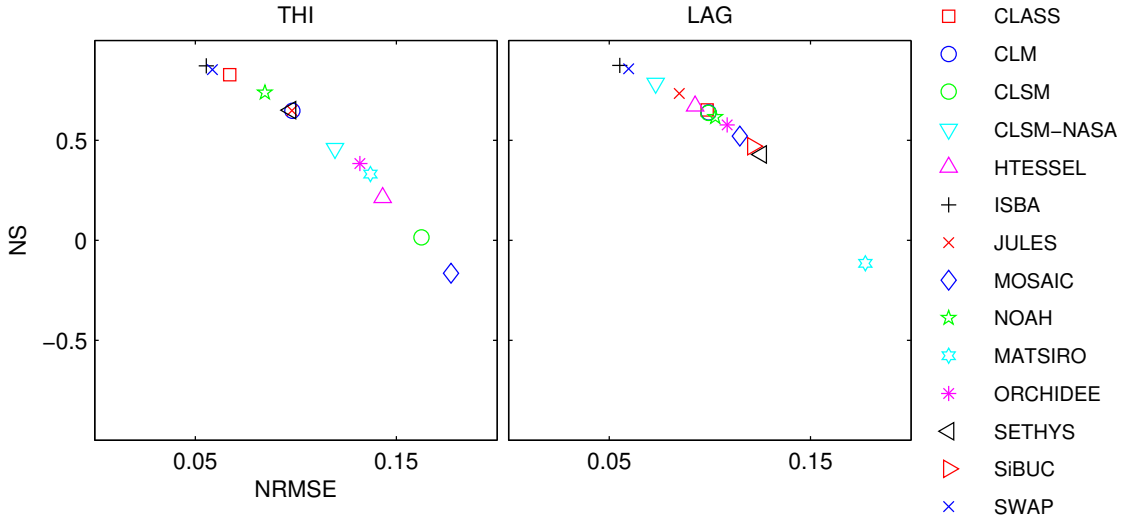

Figure 3.10: Best objective functions resulting from optimization runs for experiments using Thiessen (THI) and kriging-Lagrangean (LAG) based precipitation products. NS represents the Nash-Sutcliff statistical metric, and NRMSE represents the normalized root mean square error: statistics are for the entire period and computed at the river outlet at Bétéroux (Getirana et al., 2017).

Chapter 4

Improved Hydrological Modeling using Remote sensing data

4.1 Introduction

The literature abounds with land surface and hydrological studies utilizing remote sensing data. The main value of remote sensing data is that it can be used to evaluate or improve time-varying spatially distributed estimates of surface and hydrological fluxes and states. Remote sensing data can also be used to indirectly improve model-based estimates of states and fluxes through calibration of model parameters. For example, satellite-based altimetry estimates have been used to make virtual discharge observations which were then used to calibrate parameters within large scale spatially distributed hydrological models. Satellite data can also be assimilated into land surface or hydrological models in order to optimally estimate model parameters or to adjust the model trajectory of certain prognostic variables. I have been investigating such strategies with colleagues and students over the last decade under the auspices of the Surface Water Ocean Topography (SWOT) joint CNES-NASA satellite mission preparation. As the satellite has yet to be launched, these studies have so far focused on using virtual data under fairly idealized conditions in order to explore different optimization and assimilation strategies. The idea is to gradually improve the accuracy and performance of such techniques by including more realistic representations of the associated errors (model, data), model physics, and better satellite simulators, so that by launch, algorithms will be ready to optimally ingest the satellite data in order to improve our understanding of the the global scale hydrological cycle.

4.2 Improving hydrological modeling: The SWOT mission

Satellite-based altimetry is increasingly used for the monitoring of components of the hydrological cycle. Several altimetric satellites have been launched in the past to measure water surface elevations such as ERS-1 (1991), TOPEX/Poseidon (1992), ERS-2 (1995), Jason-1 (2001), Envisat (2002), Jason-2 (2008), and the Satellite with Argos and Ka-band altimeter (SARAL; 2013) (Biancamaria et al. 2010; Santos da Silva et al. 2010). They provide information at the global

scale, and of special important, for ungauged basins. However, they have two important limitations for hydrology which are i) their long revisit time (between 10 and 30 days; Biancamaria et al. 2010), and ii) their coarse spatial resolution. The first nadir altimeters were unable to observe rivers less than 1 km wide and their track spacing was relatively poor.

One of the objectives of the CNES-NASA sponsored Surface Water Ocean Topography (SWOT) mission is to develop the capability to produce estimates of discharge for observable rivers and wetland fluxes over the entire globe at unparalleled spatial resolutions. The SWOT mission (Alsdorf et al. 2007) is a swath mapping Ka-band radar interferometer (Fu et al., 2012) that will provide global measurements of water surface elevation 2 to 10 times per 21 day repeat cycle depending on the location for rivers at least wider than 5O to 100 m and water extent above 250 m x 250 m (Rodriguez, 2015). The vertical resolution of SWOT over rivers will be around 10 cm (as a function of reach averaging), and data will be provided from 78^o S to 78^o N latitude. Thus, SWOT will be the first altimetric mission to provide spatially distributed products for basins ranging in area from 50,000 to 200,000 km^2 at a high temporal frequency over most of the globe (Pavelsky et al. 2014). Such information should go a long way in improving understanding of the role of the spatio-temporal variability of river flows and wetlands within the global water cycle. Currently, no model system exists which is able to produce reliable global estimates of discharge and lake water storage, mostly owing to a lack of data with sufficient spatial and temporal coverage. There is an urgent need to be able to better predict the impacts of global climate change on our fresh water resources. Indeed, the need for more research and improved modeling of the global hydrological cycle are needed to address the GEWEX grand science questions (GEWEX, 2012), and SWOT was mentioned as being one of the key observing systems which will help in this regard. There is a very large degree of uncertainty related to the impact of climate change on the water cycle (IPCC, 2014). Therefore, such a mission constitutes a significant step in spatial hydrology and has implications for improving the representation of hydrological processes at the global scale, which then could improve our estimates of the impact of climate change on the world's freshwater resources. This, in turn, could even be extended to improving water resource management applications.

4.2.1 Research Objectives

The main objective of this large scale work is to develop a methodology for using SWOT data to improve the representation of regional to global scale hydrological processes in Earth System Models (ESMs) in order to better understand the global hydrological cycle. A Terre, Océan, Surfaces continentales, Atmosphère (TOSCA: funding framework of the French Space Agency, Centre National d'Études Spatiales: CNES) project which centers on the theme of obtaining a better understanding of global river and lake water storage and fluxes using SWOT has been recently accepted of which I am the principle investigator entitled *Towards an improved understanding of the global hydrological cycle using SWOT measurements*. In addition, this proposal includes membership on the SWOT Science Team (ST), which runs from 2015-2019 (tentative launch date in 2020). I was previously a member of the science definition team (SDT) which ended in 2015, and I have been involved in SWOT (under the support of TOSCA) since the inception of SWOT. The current TOSCA project is a joint effort between CNRM (MOSAYC and GMGEC teams), LEGOS, CERFACS in France, and in the US: UCLA (Los Angeles, CA),

NASA-JPL (Pasadena, CA), and Northeastern Univ. (Boston, MA), the latter three American partners are affiliated through the Research Opportunities in Earth and Space Science (ROSES: a NASA funding framework). The basic methodology can be summarized in three steps:

- improve and develop physics that is adapted for using SWOT data which is amenable for application in regional scale distributed to regional/global scale earth system models.
- construct data assimilation and calibration strategies which will allow for improved discharge and floodplain extent prediction and the determination of spatially distributed parameters required for such models
- use SWOT data to improve model physics related to the processes (and the feed backs between the land surface and rivers/floodplains/aquifers) in such models

These three steps comprise the necessary procedure to improve large scale hydrology in earth system models using SWOT.

4.2.2 Strategy

Simulating SWOT data

Since SWOT observations are not yet available, different assimilation methods are tested under the framework of an Observing System Simulation Experiments (OSSE). An OSSE consists in simulating data that would be observed by the future measurement platform using a numerical model to generate a proxy *virtual observations* for data assimilation (DA) experiments. The main objective of an OSSE is to validate the DA method by using ideal conditions. It is assumed that the state of the system and the error statistics of the model and observations are known and correctly described, which is not the case in real-world conditions. In the studies described herein, the hydrometeorological model is used to represent the true state of the hydrological system, also referred to as the reference simulation. For this so-called *truth*, the model and its parameters are assumed to be perfect. An error is then added to this true state to build the virtual observations.

Regional and Large Scale Approaches

Three hydrometeorological model platforms have been used at different spatial scales in this study, each in order to address specific aspects of the research. At the mesoscale, the SIM model (using a variable grid resolution ranging between 1 to 8 km) was used. This system is used for near-real time operational hydrometeorological monitoring over France (in this study, the focus is on the Garonne river basin in south-western France). This system is of interest since there is a considerable amount of observational data available to both force and evaluate the model, and it can be used to test the ability of the methodologies to scale between this and more coarse resolutions (such as thse used in river routing models in ESMs).

At the large scale (regional to global), the ISBA-Total Runoff Integrating Pathways (ISBA-TRIP) and The Hydrological Modeling and Analysis Platform (HyMAP) models (using a grid

resolution of 0.5^o) were used. ISBA-TRIP (Decharme et al., 2008) is used in the ARPEGE ESM at Météo-France, thus it is of interest to show how SWOT can be beneficial for such systems (eventually, in coupled mode for climate projections for example). This model also includes feedbacks with the land surface (via floodplains). The goal is to improve model input parameters, and test the same methodology used at the mesoscale for SIM. HyMAP (Getirana et al., 2012) is also a global scale model, but this model has been mainly designed for near-real time global scale offline monitoring. The formulation includes slightly more dynamics than ISBA-TRIP, and it incorporates anthropogenic effects. The goal here is to optimize input parameters with the longer term goal of correcting the trajectory of state variables using SWOT in near-real time.

4.2.3 Regional Scale Hydrology

The objective of the study by Haëfliger et al. (2015) was to evaluate the quality of simulated river water levels in the Garonne River basin (with a surface area of approximately 56,000 km^2) in southwestern France, with the ultimate goal of being able to use SWOT measured water levels. In this basin, SWOT will have a revisit time of about 5 days. The simulations for this work were produced using a distributed regional scale hydro-meteorological modeling framework based on SIM which is composed of i) high quality atmospheric forcing (SAFRAN), ii) a LSM (ISBA), iii) a hydro-geological model (MODCOU) iv) and a new addition compared to SIM in Habets et al. (2008): an explicit river network module (RAPID: David et al., 2011). The modeling framework has been calibrated over France (as discussed in detail in Habets et al., 2008).

The existing RAPID parameters (i.e. temporally-constant but spatially-variable Muskingum parameters) were first updated in the Garonne River Basin based on estimations made using a lagged cross correlation method applied to the observed hydrographs. In a second step, the model equations governing river flow were modified to use a time-variable parameter kinematic or kinematic-diffusive wave equation for routing in order to represent spatially varying wave celerities. These modifications, in turn, require the definition of values for the river-channel hydraulic parameters. The results showed that the variable flow velocity scheme gave better results compared to the original Muskingum method in RAPID. Also, simulated water height errors (compared to observations) ranged from 50-60 cm in the improved Muskingum method and 40-50 cm using a kinematic-diffusive wave method. Simulated discharge was also improved: the values simulated by the model were comparable to those obtained with a high-resolution hydrodynamic model which includes the full 1-D Saint-Venant equations. It is more difficult to simulate water levels than discharge because of the strong dependence on the choice of hydraulic parameters and their spatial variability, but spatial-averaging over a minimum river reach lead to good results (Haëfliger et al., 2015).

In the second phase of this work (Haëfliger et al., 2016), the data assimilation methodology of Pedinotti et al. (2014), which was used to develop a data assimilation strategy using SWOT data for the Niger basin, was adapted for the Garonne modeling system. The method consists in applying a data assimilation approach, the Extended Kalman Filter (EKF) algorithm, to correct the Strickler coefficient, K_{str} (or equivalently, to correct the Manning coefficient which is $n = 1/K_{str}$). River water level and K_{str} are related through Manning's equation. Typical values for

K_{str} within natural river channels range from a maximum of about 10 (rocky river bottom), to about 50 for a relatively smooth channel. The OSSE set up for this study showed the capacity of the system to calibrate the spatially variable K_{str} about the (known) *truth*. Results from several numerical experiments can be summarized as follows (the numbers correspond to the experiment):

1. The assimilation of water levels was performed (default configuration). The parameters converge to the truth after about 2 years, with an average water level error of $\pm$ 5 cm and $\pm$ 1 for K_{str}. The choice of the increment value (the difference between the analysis and the a priori value of the Manning coefficient) has an impact on the convergence speed

2. The importance of the atmospheric forcing on the convergence of the K_{str} was shown. An error of $\pm$ 10 % of the input water flow (from ISBA into the routing scheme) impacts the K_{str} errors to a relatively small degree ($\pm$ 1.5) and thus was found to have a minor impact on the river flows.

3. The assimilation of water level anomalies (differences) instead of water levels (which are equivalent to river depths), was studied. The bathymetry is not known in MODCOU (and, in general, is rarely known for most rivers). The quality of the convergence is slightly lower ($\pm$ 1.7 K_{str}) and the time of convergence is longer (approximately 3 years) than in Exp.1.

4. More realistic SWOT error measurements were introduced, which varied in time and space, and which were functions of the surface area of the observed reach, the look angle of the satellite, the wind speed, and the intra-day variability of the water content in the troposphere. A statostical summary of all of these factors is given in Haëfliger et al.

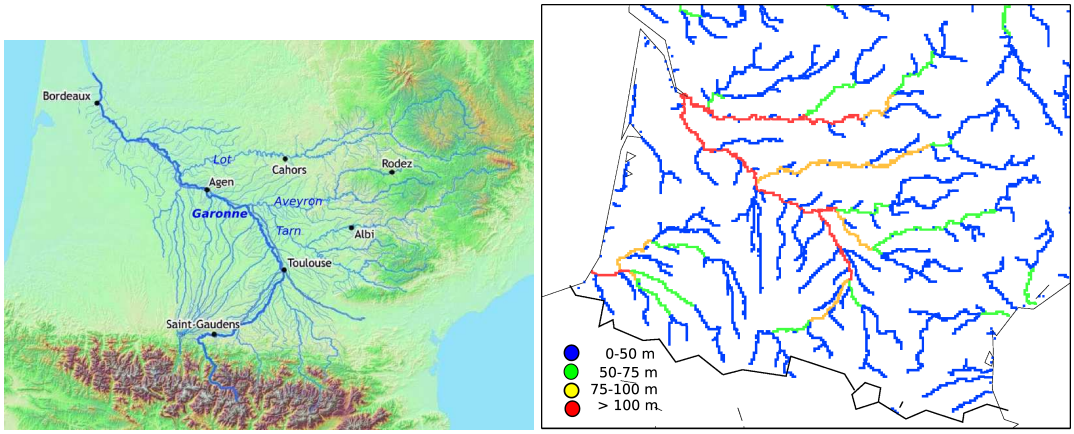

Figure 4.1: Left-hand panel: the Garonne river basin and the main tributaries (domain of the regional scale study). Right-hand panel: river widths computed in the system over the Garonne catchment, considering three river width classes where virtual SWOT products are assimilated : 50-75 m river widths (green), 75-100 m river widths (green), $>$ 100 m river widths (red).

(2016). Of note, the impact of the last factor had a time dependence since convergence of the algorithm was faster during the winter months than the summer months because of the relatively lower tropospheric water content variability

The methodology was found to perform in a similar manner (in terms of overall quality and basic conclusions) as in Pedinotti et al. (2014) despite the difference in resolution and location (climate, soils, etc...). Finally, the study mentions that the measurement error description should be investigated in more detail. The SWOT simulator (Durand et al., 2010, 2014) would provide better instrument error estimates, however, it is currently adapted to much higher spatial resolutions than used herein. But in response, part of the future TOSCA-ROSES collaboration will focus on expanding the simulator capabilities for use in systems such as the one presented here, thus this will open the door to further refinements of this system.

4.2.4 Large to Global Scale Hydrology

In the first phase of this work, the coupled global land-surface hydrological model ISBA-TRIP model was tested and improved for the Niger application (Pedinotti et al., 2012) as a part of the AMMA Project. The Niger basin (model domain) is shown in Fig. 4.2 along with sites with observed discharge (in orange). Physical processes were improved (such as including a simple new deep water reservoir), and the model performance was evaluated using both in-situ discharge measurements, and remotely sensed data (gravimetric data from GRACE, inundated

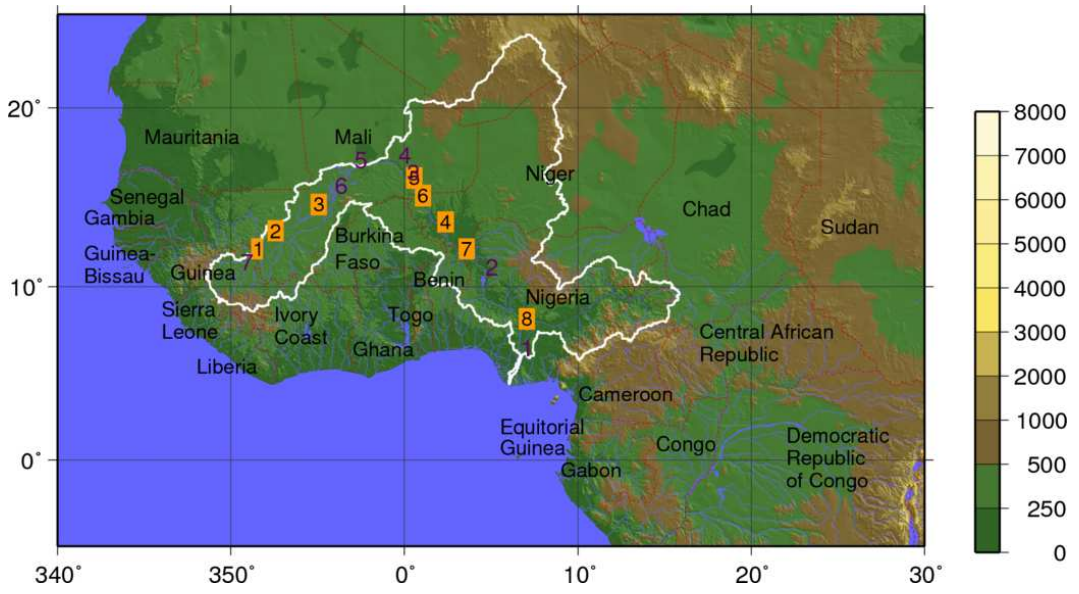

Figure 4.2: The Niger River basin: the white contour marks the boundary. The squares correspond to the discharge observation measurements at the following locations: (1) Ba- nankoro, (2) Koulikoro, (3) Ke Macina, (4) Niamey, (5) Ansongo, (6) Kandadji, (7) Malanville and (8) Lokoja. Terrain elevations are from ETOPO2 (m).

zone coverage using products from C. Prigent, LERMA, and F. Papa ,LMTG, and F. Crétaux, LEGOS). A schematic of ISBA-TRIP is shown in Fig. 4.3. The 0.5^o resolution version was used in the studies presented in this section. Of particular relevance to SWOT, the model simulated river heights were shown to be consistent with altimetric data from HYDRO-WEB (LEGOS). This implies that the fairly simple model is capable of producing height changes which are consistent with remotely sensed values. In addition, numerous sensitivity tests were performed concerning both boundary condition inputs (notably precipitation) and key model parameters in order to quantify the model uncertainty. The goal of this work was to show the potential for using SWOT to improve global hydrological modeling systems (intended for ESMs and offline scenarios). The next step was to develop a methodology for optimally combining SWOT data with the numerical model (the next section).

Data assimilation methodologies

The second part of this study aims to investigate the potential of SWOT data for parameter optimization for large scale river routing models which are typically employed in Land Surface Models (LSM) for global scale applications. The method consists in applying a data assimilation approach, the Extended Kalman Filter (EKF) algorithm, to correct the Manning roughness co-

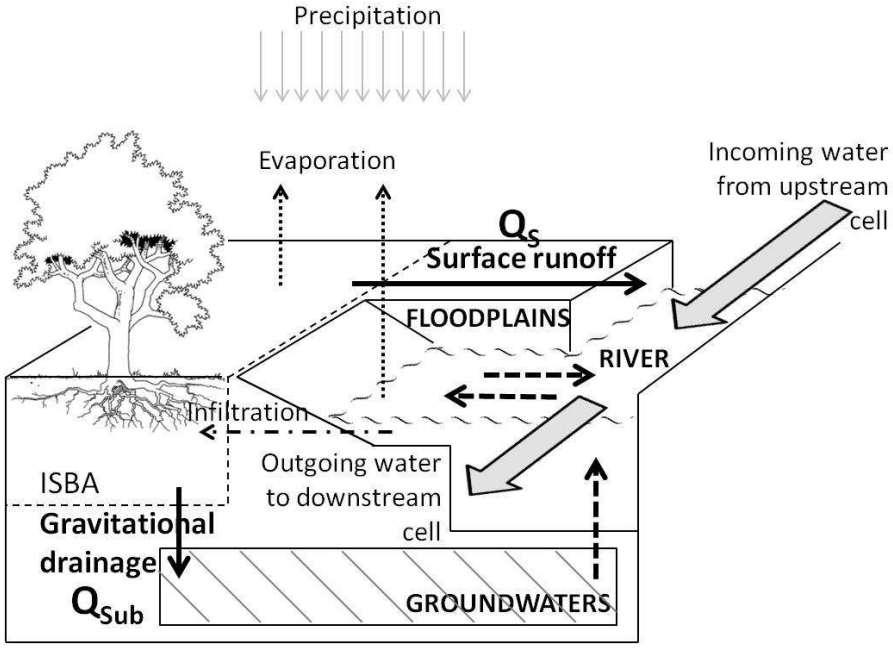

Figure 4.3: The ISBA-TRIP coupled model for a given grid cell. ISBA surface runoff, Q_s, flows into the river/surface reservoir S, ISBA gravitational drainage, $Qsub$, feeds groundwater reservoir G. The surface water is transferred from one cell to another following the TRIP river routing network. Taken from Emery et al. (2016).

efficient, n, of the ISBA-TRIP Continental Hydrologic System (CHS) applied to the Niger basin (Pedinotti et al., 2014). Indeed, parameters such as n, used within such large scale models to describe water basin characteristics, are generally derived from geo-morphological relationships, which might have locally significant errors.

In this study, the purpose of the DA algorithm is to retrieve an optimal set of model parameters starting with the background parameters, by assimilating the virtual observations. It uses the OSSE approach, similar to what was discussed in the previous section. The SWOT observations were generated using a relatively simple simulator developed by Biancamaria et al. (2011). Based on the prescribed orbit and swath, the simulator provides an ensemble of SWOT tracks

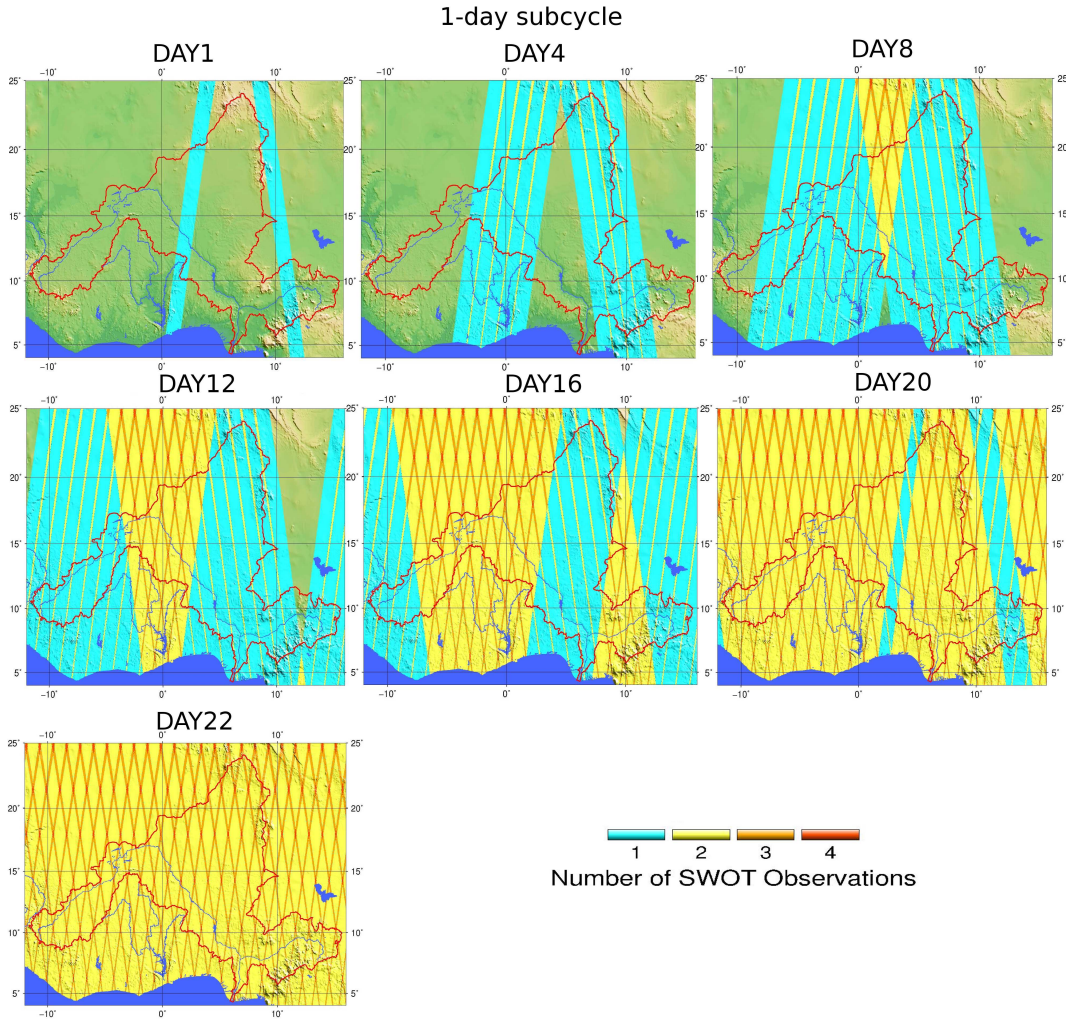

Figure 4.4: The 22-day repeat, 871 km altitude, 1-day sub-cycle orbit coverage, data issued from the SWOT data simulator (Pedinotti et al., 2014).

and related dates (Fig. 4.4) to which different assumed errors can be added.

It is assumed that modeling errors are only due to uncertainties in n. The true values of n are then supposed to be known and are used to generate synthetic SWOT observations over the period 2002-2003. The reference n values range from 0.045 (Niger river outlet in southern Nigeria), gradually increasing to approximately 0.095 (upstream values furthest from the river outlet in Niger and Cameroon to the east, and in Guinea in the westernmost extremities of the basin: see Fig. 4.2). The impact of the assimilation system on the Niger basin hydrological cycle is then quantified. The optimization of the n using the EKF algorithm over an 18 month period leads to a significant improvement of the river water levels. The relative bias of the water level is globally improved (a 30 % reduction along the entire river reach), as shown in Fig. 4.5 for both 1-day and 3-day subcycle orbits. Note that both orbits were tested as a part of a SWOT science team investigation, but for this particular application, no clear advantage for either orbit was found (Pedinotti et al., 2014). The relative bias of the n is also reduced (40 % reduction) and it converges towards an optimal value despite potential problems related to equifinality. Discharge is also improved by the assimilation, but to a lesser extent than for

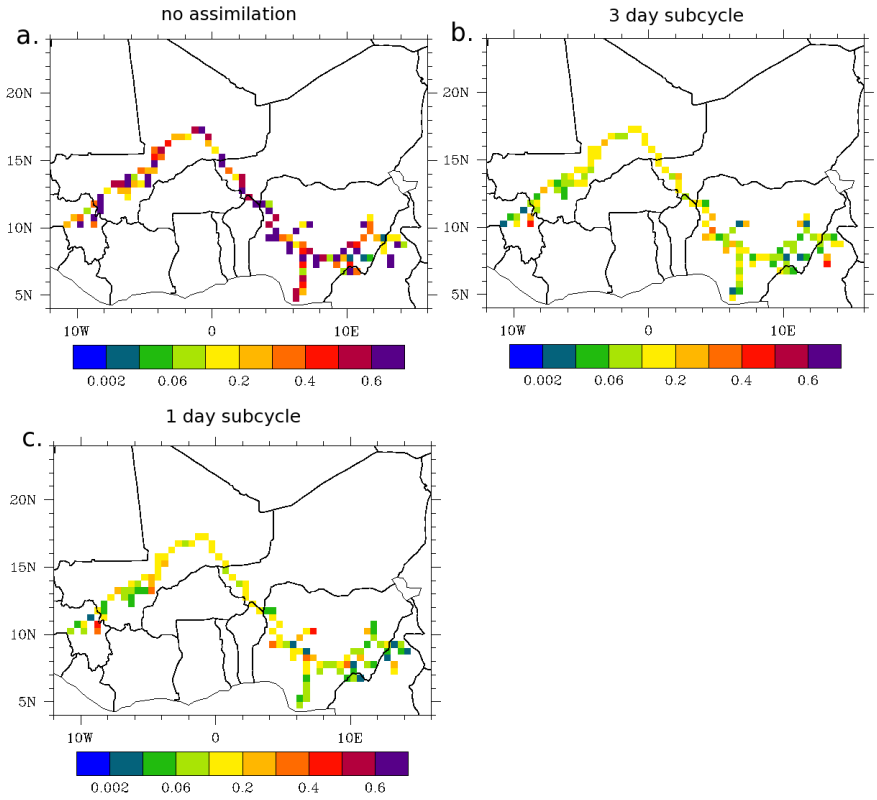

Figure 4.5: Relative error of water levels (m) averaged over the period of assimilation. Errors are reduced for both the 1 and 3 day sub-cycle orbits (Pedinotti et al., 2014).

the water levels. Moreover, the method allows a better prediction of the occurrence of flood events (Fig. 4.6), and the intensity of flood events in the inner delta (Fig. 4.7). It also shows skill in simulating the maxima and minima of the water storage anomalies in several continental reservoirs, especially the groundwater and the aquifer reservoirs. This is significant since flood frequency is not as directly impacted by the assimilation as river height. Results obtained in this preliminary study demonstrate SWOT potential for global hydrologic modeling, especially to improve model parameters.

In the current phase of this work, the data assimilation and optimization methodologies developed for the Niger basin using the ISBA-TRIP configuration are being extended over several large-scale basins with an eye towards global scale applications. This work is being done within the context of a PhD thesis in collaboration with LEGOS (Emery et al., 2016). Again, the goal of this project is to show how hydrological parameters and processes in a large scale hydrological model (typical of those being increasingly applied in ESMs) can be improved owing to SWOT. Part of this research is to test different data assimilation strategies, in addition to the EKF approaches used by Pedinotti et al. (2014) and Haëfliger et al. (2016). As a preliminary step

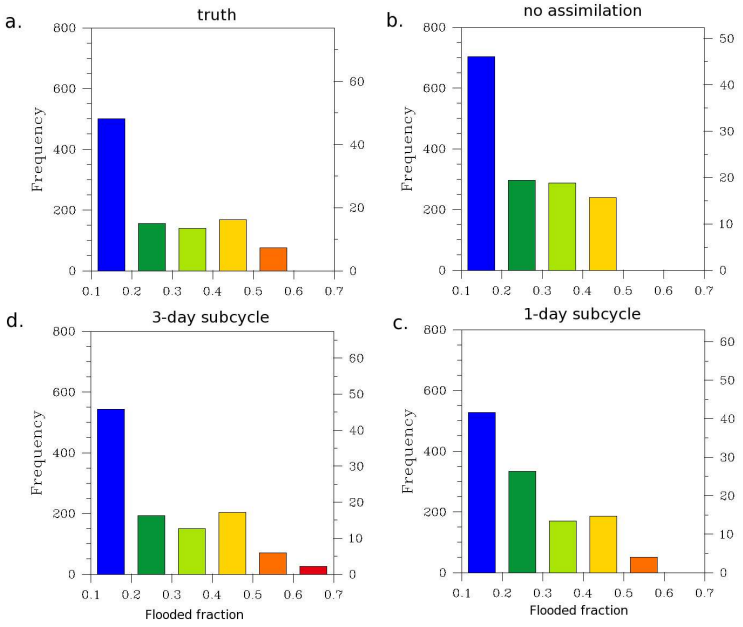

Figure 4.6: Flood frequency over the delta classified by intensity (flooded fraction). Only the pixels with a flooded fraction higher than 10 % are considered for the calculation. The open loop (no-assimilation, panel b) shows that the number of flood events were significantly overestimated. Runs using assimilation for both the 1-day and 3-day orbits improved the flood frequency estimates (Pedinotti et al., 2014).

towards testing a more diverse array of data assimilation methods, a detailed Sensitivity Analysis (SA) was undertaken. SA can be a powerful tool to both identify the most sensitive (and therefore significant) parameters, and to understand the hydrological model structure and its response to perturbations to (or uncertainties in) these parameters. SA can be seen as the study of how uncertainty in the model output can be attributed to different sources of uncertainty in the model inputs. A sensitivity analysis based on ANalysis Of VAriance (ANOVA) was applied to ISBA-TRIP over the Amazon basin (Emery et al., 2016).

The model output variance is synthetically generated by considering uncertain parameters as random variables. Using an ensemble of parameter sets, ANOVA determines the contribution of each parameter to the unconditional variance. Details on the specific ANOVA approach selected and the main assumptions are given in Emery et al. (2016). The goal of this study is to analyze the ISBA-TRIP large-scale hydrological model sensitivity over a large scale river basin, and the

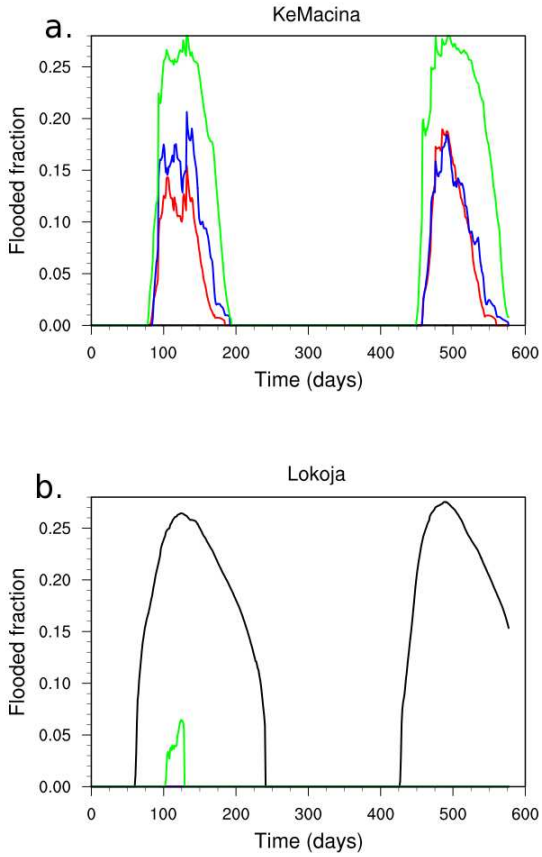

Figure 4.7: Flooded fraction versus time at Ke Macina and Lokoja, for the truth (red), with no assimilation (black), with assimilation for 3-day sub cycles (blue) and 1-day sub cycles (green). Note that in Lokoja, there is no flooded fraction represented for the truth and for the run with assimilation with a 3-day sub cycle, while the open-loop run erroneously simulates a significant event (Pedinotti et al., 2014).

Amazon River basin was selected. An output model variance decomposition method was used to identify key river routing model parameters during a three years period (2008-2010). Two analyses were carried out to evaluate the sensitivity of model parameters at different spatial scales. The first considered parameters whose uncertainty was defined at the entire catchment scale. The second used the same parameters (and the associated uncertainties) which were spatially distributed over homogeneous sub-basins within the Amazon River basin based on geological and hydrological divisions.

The results for the first part of the study show that geo-morphological parameters explain around 95 % of the water height variance with purely additive contributions, all year long, with the river Manning coefficient dominating the impact (40 %). Other significant contributions are from the river bed slope (35 %) and the river width (20 %). The results also show that discharge is sensitive to the groundwater time constant which makes up more than 90 % of its variance. The discharge is also sensitive to geo-morphological parameters (to a somewhat lesser degree) during the transition periods (rising or falling hydrographs). In terms of the second part of the study, the Amazon basin was next sub-divided to nine relatively homogeneous sub-basins. This was done in order to see if a more economical approach could be used (i.e. avoiding to need to define parameters for each pixel). The sensitivity analysis was therefore carried out for regionalized parameter-correcting coefficients, and the main results show that region specific parameters impact water height, while upstream parameters mainly affect discharge.

This platform will be extended to other river basins situated in other climatic zones, such as the Mississippi (mid-latitude) or the McKenzie (high latitude). In addition, it will be of great interest to study the impact of the atmospheric forcing (more precisely precipitation) and the initial conditions of the hydrological reservoir state variables.

Calibration methodologies

While the aforementioned works seek to improve model parameter estimates for eventual inclusion into earth system models, an additional project was begun in which the goal was to move towards a global scale near-real time river-height (storage) and discharge model analysis system which can incorporate river height estimates directly into the model in order to improve the trajectory of this variable. This work was done within the context of a CNES-financed post-doctoral study. The first step, consisted in the development of the hydrological-hydrodynamic model HyMAP. This model differs from ISBA-TRIP mainly in that it considers additional processes, such as runoff and baseflow time delays to reach the river network (a proxy for lateral flow processes), flow dynamics of floodplains, and evaporation from surface water and inundated zones. It can also include anthropogenic effects (although this feature was not used in the current study).

HyMAP is composed of four modules: i) surface and subsurface runoff time delays, ii) river-floodplain interface, iii) flow routing in river channels and flood-plains, and iv) evaporation from floodplains. The model is discretized using 0.25 degree grid cells over the continents. Input data are comprised of LSM fast (surface) and slow (baseflow) runoff components. The corresponding water mass is then routed through a prescribed river network to oceans or inland seas. The river network is represented by river channel and floodplain reservoirs in each grid cell. At each time step, the inflow water is redistributed between these two reservoirs following stage-volume

relationships derived from the topography for each grid cell. Note that the only lateral (pixel-to-pixel) exchanges are through the river network, since the floodplain water storage evolves locally (currently). River discharge is computed for each computational grid cell using the diffusive wave equation which is a simplified version of the one-dimensional St. Venant momentum equation (acceleration and advection are neglected). It is assumed that this approximation is appropriate for the spatial scale considered in the global application.

In addition to using a data assimilation strategy to optimize model parameters (as in the previous section), a more classical (in terms of hydrological science) optimal model parameter estimation methodology was tested over a large basin (the Amazon basin was used in Getirana et al., 2013). The Multi-objective Complex Evolution optimization algorithm (MOCOM-UA: Yapo et al., 1998) was used to optimize one parameter (subsurface runoff time delay) and other three parameter multipliers or factors (for determining n for rivers, river width, and bank-full height) by minimizing two objective functions for the 2002 to 2006 period. Calibration experiments were performed by combining water discharge observations and Envisat data to evaluate the potential of using radar altimetry in the automatic calibration. The first experiment used daily discharge observations, the second combined discharge with altimetric data, and the other two were driven by radar altimetry data, at 16 or four virtual stations, depending on the experiment. The calibration process was validated against discharge observations at five gauging stations located on the main tributaries. Results demonstrate that reasonable parameters can be obtained by using radar altimetry in an optimization procedure with reasonable computational costs. However, there was evidence of equifinality among model parameters. There are future plans to continue to collaborate on this project through the NASA-ROSES framework, and the work will center on i) introducing data assimilation (based on the methods herein) into HyMAP for near-real time monitoring and further ii) studying the benefits and disadvantages of calibration verses assimilation for a near-real time monitoring system.

Chapter 5

Prospectives

My research prosepctives are focused on LSM and hydrological model development for LSMs, and applications. An overview of my planned for for the next 5-10 years is given herein.

5.1 Land surface and hydrological modeling

Despite considerable progress in the past two decades in terms of representing land surface processes in greater detail, certain issues linger. Some examples are:

- Models still can produce very different Bowen ratios, in particular in water-limited regions, and this is one of the key aspects of the land surface which modulates the coupling with the atmosphere. These differences are related to differences in soil water update by bare soil and transpiration, but they are also strongly modulated by the representation of sub-grid hydrology.
- Sub-grid snow covered fractional area, SCFA, is highly empirical in most coupled land-atmosphere models, with little or no consideration of some of the main features controlling snow spatial distribution (sub-grid variability of elevation and exposition). Shortcomings in the SCFA can offset much of the gains made from using more sophisticated physics. In addition, there is a strong coupling between vegetation and the snowpack, and shortcomings have been identified through MIPs (e.g. SNOWMIP2, Rutteri et al., 2009)
- LSMs are increasingly including detailed phenology parameterizations for short to seasonal forecast timescales, but inclusion of such schemes will likely contribute to more inter-model spread over the foreseeable (or longer) future since they have many (difficult to directly observe in many cases) empirical parameters. Such schemes also likely require more sophisticated representations of the vegetation in LSMs as they evolve. This is important since, not only do they have considerable feedbacks with other aspects of the land surface, but with the atmosphere as well.
- Coupling with groundwater and the representation of lateral transfer processes are still neglected in most LSMs, and such processes are key to hydrological functioning in many

regions of the globe. Also, the coupling among the soil, lakes, rivers, and wetlands is still in its early stages or not complete in most ESMs

This is by no means a comprehensive list. Some of the focal points of my future research concerning the land surface and hydrology are highlighted herein.

5.1.1 Lakes and closing the water cycle

It has become necessary to add a lake mass model to SURFEX, coupled to Flake (currently in SURFEX: Salgado and Le Moigne, 2010), for a more complete water cycle. This implies an explicit coupling between rivers and lakes in terms of mass exchange, to include dams for storing irrigation water, and to be able to utilize height change data from SWOT over lakes. FLake is currently a conceptual thermal lake model who's main objective is to compute surface flux exchanges of mass and heat between lakes and the atmosphere, but it currently represents an infinite source of mass. While being well adapted for NWP, arguably it is less suitable for long term climate integration (if one assumes climate change can impact lake levels). Part of my work in upcoming years will be to add this to SURFEX, and a working group within HIRLAM has been established in order to undertake this work as part of an international collaboration. There will also be a collaborative effort to develop a lake mass model under the auspices of the newly started TOSCA proposal (with partners at UCLA and NASA-JPL; see Section 5.3 for a discussion of the linkages with SWOT). Finally, having an explicit lake model will permit the coupling (via mass exchanges) with other reservoirs on the SURFEX platform, such as a global scale groundwater reservoir and rivers and floodplains via TRIP.

5.1.2 Anthropization

In face of increasing human pressure on already limited water resources in semi-arid regions such as western and northern Africa, and northern Mexico, there is an urgent need to obtain a better understanding of key water cycle processes for better water security, especially since some of these regions are also deemed to be areas more likely to have even more drying in current climate change scenarios. Improved understanding could then translate into better modeling and thus prediction on seasonal to longer (climate) time scales. The improvement of the representation of anthropization in land surface and hydrological models has been highlighted as a primary research objective by the Global Energy and Water cycle Exchanges project (GEWEX: Harding et al., 2015) which is supported by the World Climate Research Programme (WCRP) within the World Meteorological Organization (WMO). This is required to better understand and estimate the human imprint on the hydrological cycle and to aid in developing mitigation and adaptation strategies.

There is a new research initiative at CNRM to focus on improving the parameterization of irrigation in SURFEX. This implies explicit modeling of the principal types of irrigation in a simple but robust manner (drip, flooding and sprinkler irrigation) and appropriately coupling this irrigation with the water sources (rivers, ground water and reservoir/lake storage) and the soil and vegetation. Furthermore, certain methods of irrigation (like inundation), will be more straightforward to model in a reasonable manner with the incorporation of an explicit vegetation

cover available as ISBA-MEB. Thus, I plan to work on coupling aspects with lakes and the explicit vegetation and testing the new irrigation methodologies developed within his research program. This work has already begun within the Agence Nationale de la Recherche (ANR) project Assessment of changes in MEdiTerranean HYdro-resources in the South: river basin Trajectories (AMETHYST) as some of the local scale sites are irrigated and work on these sites with ISBA-MEB has been initiated both at CNRM and CESBIO. The REGARD project (MOSAYC is one of the participants) is preparing SURFEX to include anthropogenic influences for the Garonne basin. This is a first step towards a more generalized approach.

The impact of anthropization within semi-arid regions is the subject of a collaboration which has now been submitted as a proposal in Mexico in collaboration with CESBIO and the Universidad Nacional Autònoma de México (UNAM). The idea is to evaluate and contribute to the new developments mentioned in the previous paragraph. The northern part of Mexico is an ideal testbed for improving our understanding of both the water needs for irrigation (evaporative, ground water uptake, links with reservoirs...), and studying the interactions of this irrigation with the atmosphere owing to the vast surface surface area of irrigated agriculture in this region, and the extensive observational network. The idea is to construct a dedicated Mexican Land Data Assimilation System (MELDAS), based to a certain degree on similar efforts in France (LDAS-France which has been developed in the VEGEO team at CNRM, which will be extended globally in the upcoming years) and the US (for example, GLDAS: Global Land Data Assimilation System). As an added value, we plan to add irrigated surfaces to this setup (which doesn't exist over Mexico in GLDAS for example), with fractions estimated from a combination of satellite and ground based data. Discussions have been started with national hydrological agencies in order to gauge their interest in collaborating on such a system (with a potential for a dedicated hydrological application, like SIM), and a proposal has been submitted to Programa de Apoyo a Proyectos de Investigacion e Innovacion Technologica (PAPIT) lead by UNAM partners.

5.1.3 Vegetation processes

Recently at CNRM, ISBA has seen significant improvements in terms of the soil, snowpack, Carbon and the vegetation (see Chapter 2). The schemes will continue to evolve and I will continue collaborating with colleagues, both national and international, in the upcoming years. In upcoming years, many partners of CNRM using SURFEX will be able to use the new ISBA-MEB as it is available in the recently released SURFEX Version 8 (SURFEXv8). Since ISBA-MEB will be used in both our offline hydrological applications (e.g. Safran-ISBA-MODCOU or SIM: Habets et al., 2008) in addition to ARPEGE Climat in the upcoming years (and eventually into numerical weather prediction, or NWP, at Météo-France), several key research priorities have been identified at CNRM. First, there is a need to link ISBA-MEB with ISBA-Ags, in theory to improve photosynthesis, plant phenology and dynamic vegetation modeling. This is a large (and likely multi-year) task, and will be done within the framework of a close collaboration between the MOSAYC (surface, hydrology), GMGEC (surface, dynamic vegetation, climate) and VEGEO (vegetation) teams at CNRM, along with SMHI (surface, NWP, regional climate). ISBA-MEB will also need to be generalized (in terms of processes, parameters and numerical aspects) to model crops and grasslands, since in its current form it is mainly applicable to forests. This work will be done with the aforementioned teams, but also with CESBIO and potentially

with INRA (Avignon). CESBIOs contribution is also needed in terms of improving ISBA-MEB for semi-arid conditions, and this work has been initiated already within the AMETHYST project. In a more general sense, work on validating ISBA-MEB coupled with ISBA-ES and eventually CROCUS will also be undertaken (this began in 2015 in collaboration with CEN). The impact of ISBA-MEB on fully coupled simulations will be studied, likely starting in 2016. First tests will be with ARPEGE Climate, but also with AROME and or MesoNH for case studies, such as Carbo-Europe.

Finally, discussions have begun on the potential evolutions of ISBA-MEB over the next 5-10 years: they include separating certain processes/computations between sunlit and shaded vegetation, and adding an understory layer (mainly for compatibility with evolutions in the Carbon modeling community). Another discussion is underway to possibly significantly enhance an existing forest site in France with additional measurements to evaluate specific aspects of the existing scheme or newer features. Note that other potential partners have been explicitly mentioned here, but as time evolves there can also be potential collaborations with MSE, LTHE, LSCE or LGGE for example owing to their respective expertise and a history of successful collaborative efforts. Multi-layer canopy schemes have been developed (Wang and Jarvis, 1990; Leuning et al., 1995), and extending MEB to include more canopy layers in the future is possible (within the context of improved photosynthesis and Carbon flux modeling for example). But such schemes are more computationally expensive and require more parameters, thus their inclusion in a GCM or even a NWP model must be further studied. Some schemes have been developed which reflect a compromise by using a two-big leaf (2 canopy layer) approach (Dai et al., 2004), and such methods will also be studied in upcoming years.

5.2 Land surface intercomparison projects

The ALMIP2 Special collection of papers in the J. of Hydrometeor. is to be published in the 2016-2017 time frame. This signals the end of phase 2 of ALMIP. We are currently discussing possible follow-on projects. The main focus would be to implement the processes identified in ALMIP2 as essential (which are currently poorly modeled or missing altogether in current LSMs and hydrological models) into one or two LSMs (potentially coupled to hydrological models). This could even be extended to examining the impact in a fully coupled model (ARPEGE for example). We are currently discussing this possibility within the French ALMIP2 Working group. Note that, however, even if a new ANR ALMIP2 follow-on project is not developed, AMMA data and ALMIP2 lessons will be used to improve and further evaluate ISBA within the SURFEX platform at Météo-France over the next several years (the implementation of soil crusting, deep rooting plants, temporary ponds, have all been identified as potential subject to work on, likely through thesis work and/or in collaboration with various ALMIP2 partners, such as GET and MSE).

The GSWP3 was kicked-off in 2015, which is being run by H. Kim (Univ. Of Tokyo, Japan) with the support of GEWEX. Simulations have been done as part of a sub-group performing fast track runs to verify the forcing inputs. It covers an approximate 100 year historical run period (1900-present). GSWP3 is being coordinated with Land Surface, Snow, Soil-Moisture Model Intercomparison Project (LS3MIP: Seneviratne et al., 2014) and CMIP6. CNRM will

also participate in both LS3MIP and CMIP6, so GSWP3 is an important effort.

Owing to my experience from leading several MIPs, and to what I feel is the great importance of such projects, I will still remain active in such projects in upcoming years either as a participant or in some leadership role.

5.3 Hydrology from space: SWOT

5.3.1 River storage and discharge

The first action centers around using SWOT measurements to obtain improved river storage and discharge estimates on the global scale. The strategy has been to develop data assimilation and calibration methods to determine optimal spatially distributed parameters which are difficult to measure or unknown, such as the Manning coefficient. Ongoing work will be centered around continued improvements of existing methodologies and making new developments to optimally ingest SWOT data. Such methods can also be extended towards sequentially correcting the model state when observations are available in order to develop a near-real time analysis system. This work will continue after SWOT launch (tentatively for 2020).

In parallel, another goal of this study is to continue to improve the assimilation method by including more realistic observation errors. In terms of estimating actual SWOT measurements, synthetic SWOT data have been generated from a reference model integration with a very basic simulator: extracting along track and passage time values, on top of which a Gaussian error is added. The generation of more realistic SWOT-like data should be further pursued using the High Resolution scientific SWOT simulator, under development at NASA-JPL and CNES. This software will be used with simplifying assumptions and at a relatively coarse resolution in order to obtain reasonable first order estimates of instrument and other types of errors, but layover errors will not be possible at this coarse resolution. The synthetic SWOT data will be used in the framework of identical twin DA experiments, meaning that the reference model is the same as the model used in the DA process and that there is an optimal set of model parameters that allows the model to simulate the observations. While being very useful for development of the DA scheme, such an approach is obviously quite simple compared to using actual SWOT measurements. The next step is to use river heights simulated by an independent river routing models, and this work will be done within multiple international collaborations (within the NASA ROSES SWOT-ST framework) for several large-scale contrasting basins (with the ultimate goal of extending the method over the globe).

5.3.2 Lake storage and exchanges

Another theme of the accepted TOSCA proposal focuses on improving lake storage and extent estimates within global climate models using SWOT measurements. The first step is to develop a storage reservoir coupled to the FLake model, which is used in many operational NWP centers throughout the world. This will be done in collaboration with UCLA and HIRLAM partners (as discussed in Section 5.1). In terms of the TOSCA-SWOT project, comparison with a detailed hydrodynamic model, TELEMAC (in collaboration with CERFACS and LNHE at EDF RandD), is planned if enough geographical data are available to set up a 3D hydrodynamics model over

areas of interest. The idea is to do parallel model improvements and development of methods to optimally use SWOT measurements under the auspices of a model intercomparison project. The ultimate goal is to show that SWOT will permit the improvement in input continental hydrological model parameters and process representation for both lakes and rivers, and also result in a better understanding of their interactions at the global-scale.

Chapter 6

Bibliography

Agusti-Panareda, A., G. Balsamo, and A. Beljaars, 2009: Impact of improved soil moisture on the ECMWF precipitation forecast in West Africa. Geophys. Res. Letters. doi: 10.1029/2010GL044748

Alsdorf, D. E., E. Rodriguez, and D. P. Lettenmaier, 2007 : Measuring surface water from space, Rev. Geophys., 45 (2), RG2002, doi:10.1029/2006RG000197

Anderson, E. A., 1976: A point energy and mass balance model of a snow cover. NOAA Tech. Rep. NWS 19, 150 pp.

Andrade, J. A. V., F. M. G. D. Abreu, and M. A. V. Madeira, 2010: Influence of litter layer removal on the soil thermal regime of a pine forest in a Mediterranean climate. Revista Brasileira de Ciencia do Solo, 34(5), 1481-1490.

Baker, R. D., B. H. Lynn, A. Boone, W.-K. Tao, and J. Simpson, 2001: The influence of soil moisture, coastline curvature, and land-breeze circulations on sea-breeze-initiated precipitation. J. Hydrometeor., 2, 193-211.

Baldocchi, D., E. Falge, L. Gu, R. Olson, D. Hollinger, S. Running, and J. Fuentes, 2001: FLUXNET: a new tool to study the temporal and spatial variability of ecosystem-scale carbon dioxide, water vapor, and energy flux densities. Bull. Amer. Met. Soc., 82 (11), 2415-2434.

Best, M. J., Beljaars, A., Polcher, J., and Viterbo, P., 2004: A proposed structure for coupling tiled surfaces with the planetary boundary layer. J. Hydrometeorol., 5, 1271-1278.

Best, M.J., G. Abramowitz, H. Johnson, A.J. Pitman, A. Boone, M. Cuntz, B. Decharme, P.A. Dirmeyer, J. Dong, M. Ek, V. Haverd, B.J.J.M van den Hurk, G.S. Nearing, B. Pak, C. Peters-Lidard, J.A. Santanello Jr., L. Stevens, N. Vuichard, 2015: The plumbing of land surface models. J. Hydrometeor., 16, 1425-1442.

Biancamaria, S., P. Bates, A. Boone, and N. Mognard, 2009: Large-scale coupled hydrologic and hydraulic modelling of an arctic river: the Ob river in Siberia. J. Hydrology, 379, 136-150.

Biancamaria, S., K. M. Andreadis, M. Durand, E. A. Clark, E. Rodriguez, N. M. Mognard, D. E. Alsdorf, D. P. Lettenmaier and Y. Oudin, 2010: Preliminary characterization of SWOT hydrology error budget and global capabilities. IEEE J. Selected Topics Appl. Earth Obs. and Rem. Sens., 3, 6Â19.

Biancamaria, S., M. Durand, K. Andreadis, P. Bates, P., A. Boone, N. Mognard, E. Rodriguez, D. Alsdorf, D. Lettenmaier, and E. Clark, 2011: Assimilation of virtual wide swath altimetry to improve Arctic river modeling. Remote Sens. Environ., 115, 373-381. doi:10.1016/j.rse.2010.09.008

Blyth, E., J. Gash, A. Lloyd, M. Pryor, G. P. Weedon, J. Shuttleworth, 2010: Evaluating the JULES land surface model energy fluxes using FLUXNET data. J. Hydrometeor., 11 (2), 509-519.

Bock, O., F. Guichard, R. Meynadier, S. Gervois, A. Agusta-Panareda, A. Beljaars, A. Boone, M. Nuret, J.-L. Redelsperger, P. Roucou, 2010: The large scale water cycle of the West African Monsoon. Atmos. Sci. Let., 12, 51-57, doi: 10.1002/asl.288.

Boone, A. and P. J. Wetzel, 1996: Issues related to low resolution modeling of soil moisture: Experience with the PLACE model. Glob. Plan. Change, 13, 161-181.

Boone, A. and P. J. Wetzel, 1999: A simple scheme for modeling sub-grid soil texture variability for use in an atmospheric climate model. J. Met. Soc. Japan, 77(1B), 317-333.

Boone, A., J.-C. Calvet, and J. Noilhan, 1999: Inclusion of a Third Soil Layer in a Land-Surface Scheme using the Force-Restore method. J. Appl. Meteor., 38, 1611-1630.

Boone, A., V. Masson, T. Meyers, and J. Noilhan, 2000: The influence of the inclusion of soil freezing on simulations by a soil-vegetation-atmosphere transfer scheme. J. Appl. Meteor., 9, 1544-1569.

Boone, A., and P. Etchevers, 2001: An intercomparison of three snow schemes of varying complexity coupled to the same land-surface model: Local scale evaluation at an Alpine site. J. Hydrometeor., 2, 374-394.

Boone, A., F. Habets, J. Noilhan, D. Clark, P. Dirmeyer, S. Fox, Y. Gusev, I. Haddeland, R. Koster, D. Lohmann, S. Mahanama, K. Mitchell, O. Nasonova, G.-Y. Niu, A. Pitman, J. Polcher, A. B. Shmakin, K. Tanaka, B. van den Hurk, S. Vérant, D. Verseghy, P. Viterbo and Z.-L. Yang, 2004: The Rhone-Aggregation Land Surface Scheme Intercomparison Project: An Overview. J. Climate, 17, 187-208

Boone, A., N. Mognard, B. Decharme, H. Douville, M. Grippa, and K. Kerrigan, 2006: Impact of simulated soil temperatures on the estimation of snow depth over Siberia from SSM/I compared to a multi-model climatology. Remote Sens. Env., 101, 482-494.

Boone, A. and P. deRosnay, 2007: AMMA forcing data for a better understanding of the West African monsoon surface-atmosphere interactions. Quantification and Reduction of Predictive Uncertainty for Sustainable Water Resource Management. IAHS Publ., 313, July 2007, 231-241.

Boone, A., P. de Rosnay, G. Basalmo, A. Beljaars, F. Chopin, B. Decharme, C. Delire, A. Ducharne, S. Gascoin, M. Grippa, F. Guichard, Y. Gusev, P. Harris, L. Jarlan, L. Kergoat, E. Mougin, O. Nasonova, A. Norgaard, T. Orgeval, C. OttlÃ©, I. Poccard-Leclercq, J. Polcher, I. Sandholt, S. Saux-Picart, C. Taylor, and Y. Xue, 2009a: The AMMA Land Surface Model Intercomparison Project. Bull. Amer. Meteor. Soc., 90(12), 1865-1880
doi:10.1175/2009BAMS2786.1

Boone, A., A. C. V. Getirana, J. Demarty, B. Cappelaere, S. Galle, M. Grippa, T. Lebel, E. Mougin, C. Peugeot and T. Vischel, 2009b: The African Monsoon Multidisciplinary Analyses (AMMA) Land surface Model Intercomparison Project Phase 2 (ALMIP2). GEWEX News, Novemeber, 19(4), 9-10.

Boone, A., Y. Xue, I. Poccard-Leclerq, J. Feng, and P. de Rosnay, 2010: Evaluation of the WAMME model surface fluxes using results from the AMMA land-surface model intercomparison project. Clim. Dynamics, 35 (1), 127-142. doi 10.1007/s00382-009-0653-1

Boone, A., S. Samuelsson, S. Golvik, A. Napoly, E. Brun, B. Decharme, L. Jarlan, and Co-Authors, 2017: The Interactions bewteen Soil-Biosphere-Atmosphere (ISBA) land surface model Multi-Energy Balance (MEB) option in SURFEX: Model concepts and formulation. Geosci. Model Dev., 10, 1-30. doi:10.5194/gmd-10-1-2017

Boone, A., Y. Xue, F. De Sales, R. Comer, S. Hagos, S. Mahanama, K. Schiro, G. Song, G. Wang and C. R. Mechoso, 2016: The regional impact of Land-Use Land-cover Change (LULCC) over West Africa from an ensemble of global climate models under the auspices of the WAMME2 project. Clim. Dyns., 10.1007/s00382-016-3252-y

Bouilloud, L., E. Martin, F. Habets, A. Boone, P. Le Moigne, J. Livet, M. Marchetti, A. Foidart, L. Franchisteguy, S. Morel, J.Noilhan, and P.Pettre, 2009: Road surface condition forecasting in France. J. App. Meteor., doi: 10.1175/2009JAMC1900.1

Boulet, G., A. Chehbouni, I. Braud, B. Duchemin, and A. Lakhal, 2004: Evaluation of a two-stage evaporation approximation for contrasting vegetation cover. Wat. Res. Res., 40, W12507, doi:10.1029/2004WR003212

Bowling, L.C., D.P. Lettenmaier, B. Nijssen, L.P. Graham, et al. 2003, Simulation of high

latitude hydrological processes in the Torne-Kalix basin: PILPS Phase 2(e) 1: Experiment description and summary intercomparisons, Glob. Plan. Change, 38, 1-30.

Braud I., Dantas-Antonino A. C., Vauclin M., Thony J. L., Ruelle P., 1995: A Simple Soil Plant Atmosphere Transfer model (SiSPAT).Development and field verification. J. Hydrology, 166, 213-250.

Brun, E., E. Martin, V. Simon, C. Gendre, and C. Coléou, 1989: An energy and mass model of snow cover suitable for operational avalanche forecasting. J. Glaciol., 35, 333â342.

Brun, E., P. David, M. Sudul, and G. Brunot, 1992: A numerical model to simulate snow-cover stratigraphy for operational avalanche forecasting. J. Glaciol., 38, 13â22

Brun, E., V. Vionnet, S. Morin, A. Boone, E. Martin, S. Faroux, P. Le Moigne, and J.-M. Willemet, 2012: Le modèle de manteau neigeux Crocus et ses applications (The snow pack model CROCUS and it's applications). La Météorologie, 76, 44-54.

Brun, E., V. Vionnet, B. Decharme, Y. Peings, R. Valette, A. Boone, F. Karbou and S. Morin, 2013: Simulation of northern Eurasian local snow depth, mass and density using a detailed snowpack model and meteorological reanalyses. J. Hydrometeor., 14, 203-219.

Calvet, J.-C., Noilhan, J., Roujean, J.-L., Bessemoulin, P., Cabelguenne, M., et al. 1998: An interactive vegetation SVAT model tested against data from six contrasting sites. Agric. For. Meteorol., 92, 73-95.

Carrer, D., J.-L. Roujean, S. Lafont, J.-C. Calvet, A. Boone, B. Decharme, C. Delire and J.-P. Gastellu-Etchegorry, 2013: A canopy radiative transfer scheme with explicit FAPAR for the interactive vegetation model ISBA-A-gs: impact on carbon fluxes. J. Geophys. Res.-Biogeosciences, 118, doi:10.1002/jgrg.20070.

Charney, J. G., W. J. Quirk, S.-H. Chow, and J. Kornfield, 1977: A comparative study of the effects of albedo change on drought in semi-arid regions. J. Atmos. Sci., 34, 1366-1385.

Chen, T. H., A. Henderson-Sellers, P. C. D. Milly, A. J. Pitman, A. C. M. Beljaars, J. Polcher, F. Abramopoulos, A. Boone, S. Chang, F. Chen, Y. Dai, C. E. Desborough, R. E. Dickinson, L. Duemenil, M. Ek, J. R. Garratt, N. Gedney, Y. M. Gusev, J. Kim, R. Koster, E. Kowalczyk, K. Laval, J. Lean, D. Lettenmaier, X. Liang, J.-F. Mahfouf, H.-T. Mengelkamp, K. Mitchell, O. N. Nasonova, J. Noilhan, A. Robock, C. Rosenweig, J. Schaake, C. A. Schlosser, J.-P. Schulz, Y. Shao, A. B. Shmakin, D. L. Verseghy, P. Wetzel, E. F. Wood, Y. Xue, Z.-L. Yang, and Q. Zeng, 1997: Cabauw experimental results from the project for intercomparison of landsurface schemes (PILPS). J. Climate, 10, 1194-1215.

Courtier, P., and J.-F. Geleyn, 1988: A global numerical weather prediction model with variable

resolution. Applications to the shallow water equations. Quart. J. Roy. Meteor. Soc., 114, 1321â1346.

Cox, P. M., R. A. Betts, C. B. Bunton, R. L. H. Essery, P. R. Rowntree, and J. Smith, 1999: The impact of new land surface physics on the GCM simulation of climate and climate sensitivity. Climate Dyn., 15, 183â203.

Dai, Y., R. E. Dickinson, and Y.-P. Wang, 2004: A two-big-leaf model for canopy temperature, photosynthesis, and stomatal conductance. J. Climate, 17, 2281-2299.

David, C.H., F. Habets, D. R. Maidment and Z.-L. Yang, 2011: RAPID applied to the SIM France model. Hydrol. Process., 25 , 3412â 3425.

Deardorff, J. W., 1977: A parameterization of ground surface moisture content for use in atmospheric prediction models. J. Appl. Meteor., 16, 1182â1185.

Deardorff, J. W., 1978: Efficient prediction of ground surface temperature and moisture, with inclusion of a layer of vegetation. J. of Geophys. Res., 83, 1889-1903.

Decharme, B., H. Douville, C. Prigent, F. Papa, and F. Aires, 2008: A new river flooding scheme for global climate applications: Off-line evaluation over South America. J. Geophys. Res., 113, D11110, doi:10.1029/2007JD009376

Decharme, B., A. Boone, C. Delire and J. Noilhan, 2011: Local evaluation of the ISBA soil multilayer diffusion scheme using four pedotransfer functions. J. Geophys. Res., doi:10.1029/2011JD016002.

Decharme, B., E. Brun, A. Boone, C. Delire, P. Le Moigne and S. Morin, 2016: Impacts of snowpack properties and soil organic carbon content on snow characteristics and soil temperature profiles simulated by the ISBA land surface model. Cryosphere, 10, 853-877. doi:10.5194/tc-10-853-2016.

Dee, D. P., and Coauthors, 2011: The ERA-Interim reanalysis: Configuration and performance of the data assimilation system. Quart. J. Roy. Meteor. Soc., 137, 553-597.

Delon, C., C. Galy-Lacaux, A. Boone, C. Liousse, D. Serca, M. Adon, B. Diop, A. Akpo, F. Lavenu, E. Mougin, and F. Timouk, 2010: Atmospheric Nitrogen budget in Sahelian dry savannas. Atmos. Chem. and Phys., 10, 2691-2708.

De Vries, D.A., 1975. Heat transfer in soils. In: D.A. de Vries and N.H. Afgan (Editors), Heat and Mass Transfer in the Biosphere. Wiley, New York, pp. 5-28.

Dickinson, R. E., M. Shaikh, R. Bryant, and L. Graumlich, 1998: Interactive canopies for a

climate model. J. Climate, 11, 2823â2836.

Dirmeyer, P. A., 1997: The Global Soil Wetness Project. GEWEX News, 7, 3â6.

Paul A. Dirmeyer, 2011: A History and Review of the Global Soil Wetness Project (GSWP). J. Hydrometeor., 12, 729â749, doi: 10.1175/JHM-D-10-05010.1.

Dolman, A. J., and R. Dickinson, 1997: Land surface parameterizations - soil - vegetation - atmosphere transfer schemes workshop. Conclusions and working group reports. GEWEX Tech. Rep., IGPO, Series Pub. No. 31, La Jolla, CA, 77 pp.

Dominguez, M., M. A. Gaertner, P. de Rosnay and T. Losada, 2008: A regional climate model simulation over West Africa: parameterization tests and analysis of land surface fields. Clim. Dynamics, doi: 10.1007/s00382-010-0769-3

Douville, H., J.-F. Royer, and J.-F. Mahfouf, 1995: A new snow parameterization for the Météo-France climate model. Part 1: Validation in stand-alone experiments. Climate Dyn., 12, 21â35.

Douville, H., 1997: Validation and sensitivity of the global hydrologic budget in stand-alone simulations with the ISBA land-surface scheme. Note Trav. 55, GMGEC, Météo-France, 52 pp.

Drame, M. S., X. Ceamanos, J.-L. Roujean, A. Boone, J.-P. Lafore, D. Carrer, and O. Geoffroy, 2015: On the importance of aerosol composition for estimating incoming solar radiation: Focus on the Western African stations of Dakar and Niamey during the dry season. Atmosphere, 6, 1608-1632; doi:10.3390/atmos6111608

Durand, M., E. Rodriguez, E. A. Douglas and M. Trigg, 2010: Estimating River Depth From Remote Sensing Swath Interferometry Measurements of River Height, Slope, and Width. IEEE J. Selected Topics Appl. Earth Obs. and Rem. Sens., 3, 20-31.

Durand, M., J. Neal, E. Rodríguez, M. A. Konstantinos, L. C. Smith, Y. Yoon, 2014: Estimating reach-averaged discharge for the River Severn from measurements of river water surface elevation and slope. J. Hydrology, 511, 92-104.

Ek, M. and A. Boone, 2015: GLASS Panel meeting. GEWEX News, 25(3), 16-18.

Enrique, G. S., I. Braud, J.-L. Thony, M. Vauclin, P. Bessemoulin, and J.-C. Calvet, 1999: Modelling heat and water exchanges of fallow land covered with plant-residue mulch. Agricultural and Forest Meteorology, 97(3), 151-169.

Essery, R., E. Martin, H. Douville, A. Fernandez, and E. Brun, 1999: A comparison of four snow models using observations from an alpine site. Climate Dyn., 15, 583-593.

Etchevers, P., E. Martin, R. Brown, C. Fierz, Y. Lejeune, E. Bazile, A. Boone, Y.-J. Dai, R. Essery, A. Fernandez, Y. Gusev, R. Jordan, V. Koren, E. Kowalczyk, N. O. Nasonova, R. D. Pyles, A. Schlosser, A. B. Shmakin, T. G. Smirnova, U. Strasser, D. Verseghy, T. Yamazaki and Z.-L. Yang, 2004: Validation of the energy budget of an alpine snowpack simulated by several snow models (SNOWMIP project). Annals of Glaciology, 38, 150-158.

Fox, S., A. Pitman, A. Boone and F. Habets, 2006: The relationship between inter-model differences and surface energy balance complexity in the Rhone Aggregation Intercomparison Project. J. Hydrometeor., 7, 81-100.

Fu, L.-L., D. E. Alsdorf, R. Morrow, E. RodrÃguez, N. M. Mognard, 2012: SWOT: the Surface Water and Ocean Topography Mission. JPL Publication 12-05, http://swot.jpl.nasa.gov /files /swot /$SWOT_MSD_1202012.pdf$

Gao, X., and P. A. Dirmeyer, 2006: A multimodel analysis, validation, and transferability study of global soil wetness products. J. Hydrometeor, 7, 1218â1236.

Giard, D., and E. Bazile, 2000: Implementation of a new assimilation scheme for soil and surface variables in a global NWP model. Mon. Wea. Rev., 128, 997-1015.

Gerrits, A.M.J., Savenije, H.H.G., Hoffmann, L. and Pfister, L., 2007: New technique to measure forest floor interception - an application in a beech forest in Luxembourg. Hydrology Earth Sys. Sci., 11, 695-701.

Getirana, A. C. V., A. Boone, D. Yamazaki, B. Decharme, F. Papa, and N. Mognard, 2012: The Hydrological Modeling and Analysis Platform (HyMAP): evaluation in the Amazon basin. J. Hydrometeor., 13, 1641-1665. doi: http://dx.doi.org/10.1175/JHM-D-12-021.1

Getirana, A. C. V., A. Boone, D. Yamazaki and N. Mognard, 2013: Automatic calibration of global flow routing scheme parameters driven by spatial altimetry data: evaluation in the Amazon basin. Wat. Res. Res., 49, 1-16. doi:10.1002/wrcr.20077.

Getirana, A. C. V., A. Boone, and C. Peugeot, 2014a: Evaluating LSM-based water budgets over a West African basin assisted with a river routing scheme, J. Hydrometeor., 15, pp. 2331-2346. doi:http://dx.doi.org/10.1175/JHM-D-14-0012.1

Getirana, A. C. V., E. Dutra, M. Guimberteau, J. Kam, H.-Y. Li, B. Decharme, Z. Zhang, A. Ducharne, A. Boone, G. Balsamo, M. Rodell, A. M. Toure, Y. Xue, C. D. Peters-Lidard, S. V. Kumar, K. Arsenault, G. Drapeau, L. R. Leung, J. Ronchail, and J. Sheffield, 2014b: Water Balance in the Amazon Basin from a Land Surface Model Ensemble. J. Hydrometeor., 15, pp. 2586-2614. doi:10.1175/JHM-D-14-0068.1

Getirana, A., A. Boone, C. Peugeot, and the ALMIP-2 Working Group, 2017: Streamflows over

a West African basin from the ALMIP-2 model ensemble. J. Hydrometeor., 18, 1831-1845. doi:10.1175/JHM-D-16-0233.1

Govaerts Y., and A. Lattanzio, 2008: Estimation of surface albedo increase during the eighties Sahel drought from Meteosat observations. Glob. Plan. Change, 64, 139-145.

Grippa, M., L. Kergoat, F. Frappart, Q. Araud, A. Boone, P. De Rosnay, J.-M. Lemoine, S. Gascoin, G. Balsamo, C. Ottlé, B. Decharme, S.Saux-Picart and G. Ramillien, 2011: Land water storage changes over West Africa estimated by GRACE and land surface models. Wat. Res. Res., 47 , W05549. doi:10.1029/2009WR008856.

Guevara-Escobar, A., E. Gonzalez-Sosa, M. Ramos-Salinas, and G. D. Hernandez-Delgado, 2007: Experimental analysis of drainage and water storage of litter layers. Hydrology Earth Sys. Sci., 11 (5), 1703-1716.

Guichard, F., and co-authors, 2010 : An intercomparison of simulated rainfall and evapotranspiration associated with a mesoscale convective system over West Africa, Wea. and Forcasting, 25, 37-60. doi: 10.1175/2009WAF2222250.1

Habets, F., A. Boone, and J. Noilhan, 2003: Simulation of a Scandinavian basin using the diffusion transfer version of ISBA. Glob. Plan. Change, 38, 137-149.

Habets, F., A. Boone, J.L Champeaux, P. Etchevers, E. Leblois, E. Ledoux, P. Le Moigne, E. Martin, S. Morel, Q. Segui, F. Rousset-Regimbeau, P. Viennot, 2008: The SAFRAN-ISBA-MODCOU hydrometeorological model applied over France. J. Geophys. Res., 113, doi:10.1029/2007JD008548.

Haëfliger, V., E. Martin, A. Boone, F. Habets, C.H. David, P.A. Garambois, H. Roux, and S. Ricci, L. Berthon, and A. Thévenin, 2015: Evaluation of regional-scale water level simulations using various river routing schemes within a hydrometeorological modelling framework for the preparation of the SWOT mission. J. Hydrometeor. doi:http://dx.doi.org/10.1175/JHM-D-14-0107.1

Haëfliger, V., E. Martin, A. Boone, S. Ricci, S. Biancamaria, 2019: Assimilation of virtual SWOT water levels in a regional hydrometeorological model. Water, 11(1), 78; https://doi.org/10.3390/w11010078

Hagos, S., L. R. Leung, Y. Xue, A. Boone, , F. de Sales, N. Neupane, M. Huang, and J.-H. Yoon, 2014: On the Response of the African Monsoon Precipitation to Land Use Change in Regional Model Simulations. Clim. Dyn., 43, 2765-2775. doi: 10.1007/s00382-014-2092-x

Harding, R., J. Polcher, A. Boone, M. Ek, H. Wheater, and A. Nazemi, 2015: Anthropogenic Influences on the Global Water Cycle - Challenges for the GEWEX Community. GEWEX News, 27(4), 6-8.

Haughton, N., G. Abramowitz, A. J. Pitman, D. Or, M. J. Best, H. R. Johnson, G. Balsamo, A. Boone, M. Cuntz, B. Decharme, P. A. Dirmeyer, J. Dong, M. Ek, Z. Guo, V. Haverd, B. J. van den Hurk, G. S. Nearing, B. Pak, C. Peters-Lidard, J. A. Santanello Jr., L. Stevens, and N. Vuichard, 2016: The plumbing of land surface models: why are models performing so poorly? J. Hydrometeor., 17, 1705-1723. doi:JHM-D-15-0171.1

Henderson-Sellers, A., Z.-L. Yang, and R. E. Dickinson, 1993: The Project for Intercomparison of Land-surface Parameterization Schemes. Bull. Amer. Meteor. Soc., 74, 1335â1349.

Henderson-Sellers et al, 1995, The project for intercomparison of land surface parameterisaton schemes PILPS) Phases 2 and 3, Bull. Amer. Meteor. Soc., 76, 489-503

Hourdin, F., F. Guichard, F. Favot, P. Marquet, A. Boone, J.-P. Lafore and J.-L. Redelsperger, P. Ruti, A. Dell'Aquila, T. L. Doval, A. K. Traore, and H. Gallee, 2010: AMMA-Model Intercomparison Project. Bull. Amer. Meteor. Soc., 91(1), 95-104.

Hurtt G. C., S. Frolking, M. G. Fearon, B. Moore III, E. Shevliakova, S. Malyshev, S. W. Pacala, and R. A. Houghton RA, 2006: The Underpinnings of Land-use History: Three Centuries of Global Gridded Land-Use Transitions, Wood Harvest Activity, and Resulting Secondary Lands. Glob. Change Biol., 12, 1208-1229 doi: 10.1111/j.1365-2486.2006.01150.x

IPCC, 2014: Climate Change Synthesis Report. Contribution of Working Groups I, II and III to the Fifth Assessment Report of the Intergovernmental Panel on Climate Change [Core Writing Team, R.K. Pachauri and L.A. Meyer (eds.)]. IPCC, Geneva, Switzerland, 151 pp.

Jordan, R., 1991: A one-dimensional temperature model for a snow cover. CRREL Special Rep. 91-1b, Cold Regions Research and Engineering Laboratory, Hanover, NH, 49 pp.

Kaptué-Tchuente, A. T., A. Begue, J.-L. Roujean, S. O. Los, J. Morisette, A. Boone, J.-F. Mahfouf and B. Daouda, 2011: A new characterisation of the land surface heterogeneity of Africa for use in Land Surface Models. J. Hydrometeor., 12(6), 1321-1336. doi:10.1175/JHM-D-11-020.1.

Koster R, and The GLACE Team, 2004: Regions of strong coupling between soil moisture and precipitation. Science, 305, 1138â1140

Lafore, J. P., J. Stein, N. Asencio, P. Bougeault, V. Ducrocq, J. Duron, C. Fischer, P. Hereil, P. Mascart, J. P. Pinty, J. L. Redelsperger, E. Richard, and J. Vila-Guerau de Arellano, 1998: The Meso-NH Atmospheric Simulation System. Part I: Adiabatic formulation and control simulations. Annales Geophysicae, 16, 90-109.

Lawrence, D.M., K.W. Oleson, M.G. Flanner, P.E. Thornton, S.C. Swenson, P.J. Lawrence, X. Zeng, Z.-L. Yang, S. Levis, K. Sakaguchi, G.B. Bonan, and A.G. Slater, 2011: Parameteriza-

tion improvements and functional and structural advances in version 4 of the Community Land Model. J. Adv. Model. Earth Sys., 3, doi: 10.1029/2011MS000045.

Lebel, T., T. Lebela, B. Cappelaere, S. Galle, N. Hanan, L. Kergoat, S. Levis, B. Vieux, L. Descroix, M. Gosset, E. Mougin, C. Peugeot, and L. Seguis, 2009: AMMA-CATCH studies in the Sahelian region of West Africa: An overview. J. Hydro., 375, 3â13

Lehnings, M., P. Bartlet, and B. Brown, 1998: Operational use of a snowpack model for the avalanche warning service in Switzerland: Model development and first experiences. Nor. Geotech. Inst., 203, 169â174.

Lohou, F., L. Kergoat, F. Guichard, A. Boone, B. Cappelaere, J.-M. Cohard, J. Demarty, S. Galle, C. Peugeot, D. Ramier, C. Taylor and F. Timouk, 2014: Surface response to rain events throughout the West African monsoon. Atmos. Chem. Phys., 14, 3883-3898. doi:10.5194/acp-14-3883-2014

Loth, B., H.-F. Graf, and J. M. Oberhuber, 1993: Snow cover model for global climate simulations. J. Geophys. Res., 98, 10451â10464.

Leuning, R., F. X. Dunin, and Y.-P. Wang, 1995: A two-leaf model for canopy conductance, photosynthesis and partitioning of available energy. II. Comparison with measurements. Agr. For. Meteor., 91, 113-125.

Lynch-Stieglitz, M., 1994: The development and validation of a simple snow model for the GISS GCM. J. Climate, 7, 1842â1855.

Lynn, B. H., D. Stauffer, P. Wetzel, W.-K. Tao, P. Alpert, N. Perlin, D. Baker, R. Munoz, A. Boone and Y. Jia, 2001: Improved Simulation of Florida Summer Convection Using the PLACE Land Model and a 1.5-Order Turbulence Parameterization Coupled to the Penn State/NCAR Mesoscale Model. Mon. Wea. Rev., 129, 1441-1461.

Mahfouf, J.-F., and J. Noilhan, 1996: Inclusion of gravitational drainage in a land surface scheme based on the forceârestore method. J. Appl. Meteor., 35, 987â992.

Mahmood R., R. S. Pielke Sr., K. G. Hubbard, D. Niyogi, P. A. Dirmeyer, C. McAlpine C, A. M. Carleton, R. Hale, S. Gameda, A. Beltran-Przekurat, B. Baker B, R. McNider, D. R. Legates, M. Shepherd, J. Du, P. D. Blanken, O. W. Frauenfeld, U. S. Nair, S. Fall, 2014: Land cover changes and their biogeophysical effects on climate. Int. J. Climatol., 34, 929â953.

Masson, V., P. Le Moigne, E. Martin, S. Faroux, A. Alias, R. Alkama, S. Belamari, A. Barbu, A. Boone, F. Bouyssel, P. Brousseau, E. Brun, J.-C. Calvet, D. Carrer, B. Decharme, C. Delire, S. Donier, R. El Khatib, K. Essaouini2, A.-L. Gibelin, H. Giordani, F. Habets, M. Jidane, G. Kerdraon, E. Kourzeneva, S. Lafont, C. Lebeaupin, A. Lemonsu, J.-F. Mahfouf, P. Marguinaud, M.

Moktari, S. Morin, G. Pigeon, R. Salgado, Y. Seity, F. Taillefer, G. Tanguy, P. Tulet, B. Vincendon, V. Vionnet and A. Voldoire, 2013: The SURFEXv7.2 externalized platform for the simulation of Earth surface variables and fluxes. Geosci. Model Dev., 6, 929-960, doi:10.5194/gmd-6-929-2013.

Meynadier, R., O. Bock, F. Guichard, A. Boone, P. Roucou, J.-L. Redelsperger, 2010: Investigation of the West African Monsoon water cycle. Part I: A hybrid water budget dataset. J. Geophys. Res., 115, doi:10.1029/2010JD013917.

Milly, P.C.D., 1982. Moisture and heat transport in hysteretic inhomogeneous porous media: a matric head-based formulation and a numerical model. Water Resour. Res., 18: 489-498.

Monteith, J.L., 1973. Principles of Environmental Physics. American Elsevier, New York, 241 pp.

Napoly, A., A. Boone, P. Samuelsson, S. Gollvik, E. Martin, B. Decharme, D. Carrer, L. Jarlan, and R. Seferian, 2017: The importance of a detailed description of forest canopy exchanges for land surface modelling. Geosci. Model Dev., 10, 1621-1644. doi:10.5194/gmd-10-1621-2017

Nicholson, S. E., C. J. Tucker, M. B. Ba, 1998: Desertification, drought, and surface vegetation: an example from the West African Sahel. Bull. Amer. Meteor. Soc., 79, 1-15.

de Noblet-Ducoudré, N., J. Boisier, A. Pitman, G. Bonan, V. Brovkin, F. Cruz, C. Delire, V. Gayler, B. van den Hurk, D. Lawrence, M. van der Molen, C. Muller, C. Reick, B. Strengers, and A. Voldoire, 2012: Determining robust impacts of land-use induced land-cover changeson surface climate over North America and Eurasia; Results from the first set of LUCID experiments. J. Climate, 25, 3261-3281. doi:10.1175/JCLI-D-11-00338.1

Noilhan, J., and S. Planton, 1989: A simple parameterization of land surface processes for meteorological models. Mon. Wea. Rev., 117, 536â549.

Noilhan, J. and J.-F. Mahfouf, 1996: The ISBA land surface parameterization scheme. Glob. Plan. Change, 13, 145â159.

Ogée, J., and Y. Brunet, 2002: A forest floor model for heat and moisture including a litter layer. J. Hydrology, 255 (1), 212-233.

Pavelsky, P., M. Durand, K. M. Andreadis, R. E. Beighley, R. C. D. Paiva, G. H. Allen and Z. F. Miller, 2014: Assessing the potential global extent of SWOT river discharge observations, J. Hydro., 519, 1519-1525.

Pedinotti, V., A. Boone, B. Decharme, J.F. Crétaux, N. Mognard, G. Panthou, F. Papa and B.A. Tanimou, 2012: Evaluation of the ISBAÂTRIP continental hydrological system over the Niger

basin using in situ and satellite derived datastes. Hydrol. Earth Syst. Sci., 16, 1745-1773.

Pedinotti, V., A. Boone, S. Ricci, S. Biancamaria and N. Mognard, 2014: Assimilation of satellite data to optimize large scale hydrological model parameters : A case study for the SWOT mission, Hydrol. Earth Syst. Sci., 18, 4485â4507.

Peyrille, P., J.-P. Lafore and A. Boone, 2016: The annual cycle of the West African Monsoon in a two-dimensional model: Mechanisms of the rainband migration. Q. J. Roy. Met. Soc., 142, 1473-1489. doi:10.1002/qj.2750.

Pielke R. A. Sr, A. Pitman, D. Niyogi, R. Mahmood, C. McAlpine, F. Hossain, K. K. Goldewijk, U. Nair, R. Betts, S. Fall, M. Reichstein, P. Kabat and N. de Noblet, 2011: Land use/land cover changes and climate: modeling analysis and observational evidence. WIREs Clim. Change, doi:10.1002/wcc.144

Pitman A. J., N. de Noblet-Ducoudré, F. T. Cruz, E. L. Davin, G.B. Bonan, V. Brovkin, M. Claussen, C. Delire, L. Ganzeveld, V. Gayler and co-authors, 2009: Uncertainties in climate responses to past land cover change: First results from the LUCID intercomparison study. Geophys. Res. Let., 36:L14814 doi:10.1029/2009GL039076.

Polcher, J., and CO-authors, 1998: A proposal for a general interface between land-surface schemes and general circulation models. Global and Plan. Change, 19, 261â276.

Putuhena, W. M., and I. Cordery, 1996: Estimation of interception capacity of the forest floor. J. Hydrology, 180 (1), 283-299.

Redelsperger, J.-L., C. D. Thorncroft, A. Diedhiou, T. Lebel, D. J. Parker, and J. Polcher, 2006: African Monsoon Multidisciplinary Analysis: An international research project and field campaign. Bull. Amer. Meteor. Soc., 87, 1739â1746.

Rodríguez E., 2015: Surface Water and Ocean Topography Mission (SWOT), Science Requirements Document. JPL document D-61923. https://swot.jpl.nasa.gov/files/swot/$SRD_0$21215.pdf.

de Rosnay, P., M. Drusch, A. Boone, G. Balsamo, B. Decharme, P. Harris, Y. Kerr, T. Pellarin, J. Polcher, and J.-P. Wigneron (2009), AMMA Land Surface Model Intercomparison Experiment coupled to the Community Microwave Emission Model: ALMIP-MEM, J. Geophys. Res., 114, D05108, doi:10.1029/2008JD010724.

Rutteri, N., R. Essery, J. Pomeroy, N. Altimir, K. Andreadis, I. Baker, A. Barr, P. Bartlett, A. Boone, H. Deng, H. Douville, E. Dutra, K. Elder, C. Ellis, X. Feng, A. Gelfan, A. Goodbody, Y. Gusev, D. Gustafsson, R. Hellstrom, Y. Hirabayashi, T. Hirota, T. Jonas, V. Koren, A. Kuragina, D. Lettenmaier, W.-P. Li, C. Luce, E. Martin, O. Nasonova, J. Pumpanen, R. D. Pyles, P. Samuelsson, M. Sandells, G. Schadler, A. Shmakin, T. G. Smirnova, M. Stahli, R. Stockli,

U. Strasser, H. Su, K. Suzuki, K. Takata, K. Tanaka, E. Thompson, T. Vesala, P. Viterbo, A. Wiltshire, K. Xia, Y. Xue, and T. Yamazaki, 2009: Evaluation of forest snow processes models (SnowMIP2). J. Geophys. Res., 114, D06111, doi:10.1029/2008JD011063.

Salgado, R. and P. Le Moigne, 2010: Coupling of the flake model to the SURFEX externalized surface model. Boreal Environment Research, 15, 231-244.

Samuelsson P., Gollvik S. and Ullerstig A. 2006. The land-surface scheme of the Rossby Centre regional atmospheric climate model (RCA3). Report in Meteorology 122. SMHI, SE-60176 Norrköping, Sweden, 25 pp.

Samuelsson, P., Jones, C., Willèn, U., Ullerstig, A., Gollvik, S., Hansson, U., Jansson, C., Kjellström, E., Nikulin, G. and Wyser, K. 2011. The Rossby Centre Regional Climate Model RCA3: model description and performance. Tellus 63A. doi: 10.1111/j.1600-0870.2010.00478.x

Santos da Silva, J., S. Calmant, F. Seyler, O. Correa Rotunno Filho, G. Cochonneau and W. Joao Mansur (2010): Water levels in the Amazon basin derived from the ERS2 and ENVISAT radar altimetry missions. Rem. Sens. Environ., 114, 2160-2181.

Schlosser, C. A., A. G. Slater, A. Robock, A. J. Pitman, K. Y. Vinnkov, A. Henderson-Sellers, N. A. Speranskaya, K. Mitchell, A. Boone, H. Braden, F. Chen, P. Cox, P. de Rosnay, C. E. Desborough, R. E. Dickinson, Y.-J. Dai, Q. Duan, J. Entin, P. Etchevers, N. Gedney, Y. M. Gusev, F. Habets, J. Kim, V. Koren, E. Kowalczyk, O. N. Nasonova, J. Noilhan, J. Schaake, A. B. Shmakin, T. G. Smirnova, D. Verseghy, P. Wetzel, Y. Xue, and Z.-L. Yang, 1999: Simulations of a boreal grassland hydrology at Valdai, Russia: PILPS Phase 2(d). Mon. Wea. Rev., 128, 301-321.

Seity Y., P. Brousseau , S. Malardel , G. Hello , P. Bénard, F. Bouttier , C. Lac , and V. Masson , 2010: The AROME-France Convective-Scale Operational Model. Mon. Wea. Rev., 139, 976-991, doi: 10.1175/2010MWR3425.1.

Seneviratne, S. I., B. van den Hurk, D. Lawrence, G. Krinner, G. Hurtt, H. Kim, C. Derksen, T. Oki, A. Boone, M. Ek, V. Brovkin, P. Dirmeyer, H. Douville, P. Friedlingstein, S. Hagemann, R. Koster, N. de Noblet-Ducoudre and A. Pitman, 2014: Land processes, forcings, and feedbacks in climate change simulations: The CMIP6 LandMIPs. GEWEX News, 24(4), Nov., 2014

Sellers, P. J., and Coauthors, 1996: A revised land surface parameterization (SiB2) for atmospheric GCMs. Part I: Model formulation. J. Climate, 9, 676-705.

Slater, A. G., A. J. Pitman, and C. E. Desborough, 1998: The vali- dation of a snow parameterization designed for use in general circulation models. Int. J. Climatol., 18, 595-617.

Slater, A. G., C. A. Schlosser, C. E. Desborough, A. J. Pitman, A. Henderson-Sellers, A. Robock,

K. Ya. Vinnikov, K. Mitchell, A. Boone, H. Braden, F. Chen, P. M. Cox, P. de Rosnay, R. E. Dickinson, Y.-J. Dai, Q. Duan, J. Entin, P. Etchevers, N. Gedney, Ye. M. Gusev, F. Habets, J. Kim, V. Koren, E. A. Kowalczyk, O. N. Nasonova, J. Noilhan, S. Schaake, A. B. Shmakin, T. G. Smirnova, D. Verseghy, P. Wetzel, Y. Xue, Z.-L. Yang, Q. Zeng, 2001: The Representation of Snow in Land Surface Schemes: Results from PILPS 2(d). J. Hydrometeor., 2, 7-25.

Steiner, A., J. Pal, S. Rauscher, J. Bell, N. Diffenbaugh, A. Boone, L. Sloan and F. Giorgi, 2009: Land surface coupling in regional climate simulations of the West African monsoon. Clim. Dynamics, doi 10.1007/s00382-009-0543-6.

Stockli, R., P. L. Vidale, A. Boone, and C. Schar, 2007: Impact of scale and aggregation on the terrestrial water exchange: integrating land surface models and rhone catchment observations. J. Hydrometeorol., 8(5), 1002-1015.

Stockli, R., D. M. Lawrence, G. Y. Niu, K. W. Oleson, P. E. Thornton, Z. L. Yang, and S. W. Running, 2008: Use of FLUXNET in the Community Land Model development. J. Geophys. Res.: Biogeosciences, 113, G01025, doi:10.1029/2007JG000562

Sud, Y. C., and D. M. Mocko, 1999: New snow-physics to complement SSiB, Part I: Design and evaluation with ISLSCP Initiative I datasets. J. Meteor. Soc. Japan, 77(1B), 335-348.

Sun, S., J. Jin, and Y. Xue, 1999: A simple snow-atmosphere-soil transfer (SAST) model. J. Geophys. Res., 104, 19587â19579.

Taylor K. E. , Ronald J. Stouffer , Gerald A. Meehl , 2011: An Overview of CMIP5 and the Experiment Design. Bull. Amer. Meteor. Soc., 93, 485â498, doi: 10.1175/BAMS-D-11-00094.1.

Timouk, F., L. Kergoat, E. Mougin, C.R. Lloyd, E. Ceschia, J.-M. Cohard, P. de Rosnay, P. Hiernaux, V. Demarez, and C.M. Taylor, 2009: Response of sensible heat flux to water regime and vegetation development in a central Sahelian landscape. J. Hydrol., 375, 178-189

Trigo, I. F., C. C. DaCamara, P. Viterbo, J.-L. Roujean, F. Olesen, C. Barroso, F. Camacho-de Coca, D. Carrer, S. C. Freitas, J. García-Haro, B. Geiger, F. Gellens-Meulenberghs, N. Ghilain, J. Meliá, L. Pessanha, N. Siljamo, and A. Arboleda, 2011: The Satellite Application Facility on Land Surface Analysis. Int. J. Remote Sens., 32, 2725-2744, doi:10.1080/01431161003743199

Tulet, P., M. Mallet, V. Pont, J. Pelon, and A. Boone, 2008: The 7-12 March dust storm over West Africa: Mineral dust generation and vertical layering in the atmosphere. J. Geophys. Res., 113, D00C08, doi:10.1029/2008JD009871.

Ukkola, A. M., A. J. Pitman, M. Decker, M. G. De Kauwe, G. Abramowitz, J. Kala, and Y. P. Wang, 2015: Modelling evapotranspiration during precipitation deficits: Identifying critical processes in a land surface model. Hydrology Earth System Sci. Disc., 12, 10789-10825.

van den Hurk, B., M. Best, P. Dirmeyer, A. Pitman, J. Polcher, J. Santanello , 2011: Acceleration of Land Surface Model Development over a Decade of Glass. Bull. Amer. Meteorol. Soc., 92, 1593â1600, doi: 10.1175/BAMS-D-11-00007.1.

Velluet, C., J. Demarty, B. Cappelaere, I. Braud, H. B.-A. Issoufou, N. Boulain, D. Ramier, I. Mainassara, G. Charvet, M. Boucher, J.-P. Chazarin, M. Oi, H. Yahou, B. Maidaji, F. Arpin-Pont , N. Benarrosh, A. Mahamane, Y. Nazoumou, G. Favreau, and J. Seghieri, 2014: Building a field- and model-based climatology of local water and energy cycles in the cultivated Sahel - Annual budgets and seasonality Hydrology Earth System Sci. Disc., 11 (5), 4753-4808. doi: 10.5194/hessd-11-4753-2014,

Vischel T., G. Quantin, T. Lebel, J. Viarre, M. Gosset, F. Cazenave and G. Panthou, 2011: Generation of high resolution rainfields in West Africa: evaluation of dynamical interpolation methods. J. of Hydrometeor., 12, 1465-1482. doi:http://dx.doi.org/10.1175/JHM-D-10-05015.1

Vionnet, V., E. Brun, S. Morin, A. Boone, S. Faroux, P. L. Moigne, E. Martin, and J.-M. Willemet, 2012: The detailed snowpack scheme Crocus and its implementation in SURFEX v7.2. Geosci. Model Dev., 5, 773â791.

Verseghy, D. L., 1991: CLASSâa Canadian land surface scheme for GCMs. I: Soil model. Int. J. Climatol., 11, 111-133.

Vuichard, N., and D. Papale, 2015: Filling the gaps in meteorological continuous data measured at FLUXNET sites with ERA-Interim reanalysis. Earth System Science Data, 7 (2), 157-171.

Wang Y. P., and P. G. Jarvis PG, 1990: Description and validation of an array model â MAESTRO. Agric. For. Meteorol., 51, 257-280.

Wang, T., C. Ottlé, A. Boone, P. Ciais, E. Brun, S. Morin, G. Krinner and S. Piao, 2013: Evaluation of a new snow scheme in ORCHIDEE land surface model. J. Geophys. Res., 118, 6064-6079.

Wetzel, P. J. and A. Boone, 1995: A parameterization for Land-Atmosphere-Cloud-Exchange (PLACE): Documentation and testing of a detailed process model of the partly cloudy boundary layer over heterogeneous land. J. Climate, 8, 1810-1837.

Wilson, T. B., T. Meyers, J. Kochendorfer, M. C. Anderson, and M. Heuer, 2012: The effect of soil surface litter residue on energy and carbon fluxes in a deciduous forest. Agric. For. Meteorol., 161, 134-147.

Wood, E. F., D. Lettenmaier, X. Liang, D. Lohmann, A. Boone, S. Chang, F. Chen, Y. Dai, C. Desborough, Q. Duan, M. Ek, Y. Gusev, F. Habets, P. Irannejad, R. Koster, O. Nasanova, J.

Noilhan, J. Schaake, A. Schlosser, Y. Shao, A. Shmakin, D. Verseghy, J. Wang, K. Warrach, P. Wetzel, Y. Xue, Z.-L. Yang and Q. Zeng, 1998: The Project for Intercomparison of Land-Surface Parameterization Schemes (PILPS) Phase-2c Red-Arkansas River Basin experiment: 3. experiment description and summary intercomparisons. Glob. Plan. Change, 19, 115-139.

Xue, Y., P. J. Sellers, J.L. Kinter and J. Shukla, 1991: A sipmlified biosphere mdoel for global climate studies. J. Climate, 4, 345-364.

Xue, Y., K.-M. Lau, K. H. Cook, D. Rowell, A. Boone, J. Feng, T. Bruecher, F. De Sales, P. Dirmeyer, L. M. Druyan, A. Fink, M. Fulakeza, Z. Guo, S. M. Hagos, S. S. Ibrah, K.-M. Kim, A. Kitoh, A. Konare, V. Kumar, P. Lonergan, M. Pasqui, I. Poccard-Leclercq, N. Mahowald, W. Moufouma-Okia, P. Pegion, J. K. Schemm, S. D. Schubert, A. Sealy, W. M. Thiaw, A. Vintzileos, E. K. Vizy, S. Williams, M.-L. C. Wu, 2010: The West African Monsoon Modeling and Evaluation project (WAMME) and its First Model Intercomparison Experiment. Clim. Dyn., doi: 10.1007/s00382-010-0778-2

Xue, Y., F. De Sales, W. K.-M. Lau, A. Boone, K.-M. Kim, F. Kucharsk, G. Wang, M. Hosaka, M., S. Li, K. Schiro, R. Comer, S. Mahanama, G. Song, M. Chin, L. M. Druyan, P. A. Dirmeyer, Y. Gu, S. M. Hagos, E. Kalnay, A. Kito, R. D. Koster, R. Leung, N. M. Mahowald, C. R. Mechoso, D. Rowell, I. Seidou Sanda, W. Thiaw, Z. Zhang, and N. Zeng, 2016: West African monsoon decadal variability and surface-related forcings: Second West African Monsoon Modeling and Evaluation Project Experiment (WAMME II). Clim. Dyns., doi: 10.1007/s00382-016-3224-2.

Yang, Z.-L., R. E. Dickinson, A. Robock, and K. Y. Vinnikov, 1997: Validation of the snow submodel of the Biosphere-Atmosphere Transfer Scheme with Russian snow cover and meteorological observations data. J. Climate, 10, 353-373

Yapo, P. O., H. V. Gupta, and S. Sorooshian, 1998: Multi-objective global optimization for hydrologic models. J. Hydrol., 204, 83â97.

Yin, Z., S. C. Dekker, B. J. J. M. van den Hurk, and H. A. Dijkstra, 2014: Effects of vegetation structure on biomass accumulation in a Balanced Optimality Structure Vegetation Model (BOSVM v1.0) Geosci. Model Dev., 7, 821-845. doi:10.5194/gmd-7-821-2014

Yin, Z., S. C. Dekker, B. J. J. M. van den Hurk, and H. A. Dijkstra, 2014: Bimodality of woody cover and biomass across the precipitation gradient in West Africa. Earth Syst. Dynam., 5, 257-270. doi:10.5194/esd-5-257-2014

ï»¿

Chapter 7

Curriculum Vitae

Aaron Anthony Boone
Né le 27 juin 1966, à Louisville, KY, EU
Marié, 4 enfants, femme française
Nationalité américaine
Fonction : Chargé de Recherche CNRS, CR1
en poste à l'UMR CNRM-GAME
Adresse professionnelle:
CNRM-GAME, Météo-France
42 ave G Coriolis
31057 Toulouse
email: aaron.boone@meteo.fr

7.1 Formation

- mai 1988: Bachelor of Science (BS en Mététorologie), université de Northern Illinois, IL, EU (Outstanding Senior in Meteorology Award)
- mars 1992: Masters of Science (MS en Mététorologie), The Florida State University (thèse de MS: Clear Air Radar Analysis of the Convective Planetary Boundary Layer)
- 13 avril 2000: Thèse de l'université Paul Sabatier Toulouse III, directeur de thèse Joël Noilhan, spécialité Hydrologie "Modélisation des processes hydrologiques dans le schéma de surface ISBA: inclusion d'un réservoir hydrologique, du gel et modélisation de la neige". Specialité: météorologie et hydrologie.

7.2 Expérience professionnelle

- Depuis Octobre 2006: Chargé de recherche CR1 à l'UMR-3589 CNRM-GAME, Météo-France, Toulouse

- Septembre 1997-1998: Visiteur Scientifique, Octobre 1998-Mai 2000: Thèse, Juin 2000-2001; 2004-2005: Post Doc à l'UMR-3589 CNRM-GAME, Météo-France, Toulouse
- Janvier 2002-Mai 2003: Post Doc à Centre d'Etudes Spatiales de la Biosphère (CESBIO), Toulouse
- Mars 1992-Aout 1997: Research Support Scientist. NASA-GSFC (NASA Goodard Space Flight Center, Greenbelt, MD, USA) Mesoscale Atmospheric Processes (MAP) Branch.

7.3 Encadrement d'étudiants

7.3.1 Thèse

- Co-direction avec Sylvain Biancamaria de la thèse de Charlotte Emery sur le sujet "Contribution de la future mission altimétrique large fauchée SWOT à la modélisation hydrologique à l'échelle globale", financement CNES-Région Midi-Pyrenees, soutenance prévue octobre 2016.
- Co-direction avec Eric Martin de la thèse d'Adrien Naploy sur le sujet "Apport de paramétrisations avancées des processus liés à la végétation dans les modèles de surface pour la simulation des flux atmosphériques et hydrologiques", financement Météo-France, soutenance prévue octobre 2016.
- Co-direction avec Eric Martin de la thèse de Vincent Haefliger, sur le sujet "Assimilation de données de hauteurs d'eau SWOT dans un modèle hydrologique distribué régional", financement CNES-Météo-France, thèse soutenue le 23 novembre 2015.
- Co-direction avec Nelly Mognard de la thèse de Vanessa Pedinotti sur le sujet "Préparation à la mission SWOT (Surface Water Ocean Topography) : Apport de l'altimétrie à large fauchée à la modélisation grande échelle des processus hydrologiques et hydrodynamiques en Afrique de l'Ouest.", financement CNES-Région Midi-Pyrénées, thèse soutenue le 21 février 2014.
- Co-direction avec Jean-Louis Roujean de la thèse d'Armel Kaptué sur le sujet "Cartographie des écosystèmes et paramètres biophysiques satellitaires pour l'étude des flux hydriques sur le continent africain", thèse soutenue en 2010.

7.3.2 Post-Doc

- co-encadrement de Mamadou Dramé avec X. Cemanos, Jean-Louis Roujean et Jean-Philippe Lafore effectué au CNRM-GAME (2013-2014) Post-doc dans le cadre du projet LAND-SAF "Development and evaluation of dust aerosol corrections of DSSF and DSLF products over West Africa: Inter-comparison with in situ measurements, transport model outputs and remote sensing and validation with mesoscale modeling."
- encadrement d'Augusto Getirana. Post-doc CNES effectué au CNRM-GAME (2011-2012) "Towards a real time global discharge modeling system for SWOT."

- co-encadrement de Mélodie Mouffe avec S. Ricci et P. Rogel. Post-doc CNES effectué au CERFACS (2011-2012) "Towards SWOT data assimilation for hydrology: Automatic calibration of global flow routing model parameters."

- encadrement de Matthieu LeLay. Post-doc dans le cadre du projet ALMIP2 (AMMA) effectué au CNRM-GAME (2007) en collaboration avec LTHE. "Intercomparaison des simulations du bilan d'eau méso-échelle (au Benin) par les Land Surface Models et des modèles hydrologiques."

7.3.3 Comité du thèse

- G. Aouade (directeurs de thèse: A. Benkaddour, S. Er-Raki et G. Boulet), thèse effectuée à l'Univ. Cadi Ayyad, Marrakech, Maroc. (2013-présent).

- J. Eeckman (directeurs de thèse: P. Chevallier et L. Neppel), thèse effectuée au MSE, Montpellier (2014-2016).

- E. Redon (directeurs de thèse: A. Lemonsu et V. Masson), thèse effectuée au CNRM-GAME, Météo-France (2013-2017).

- C. Cassé (directeur du thèse: Marielle GOSSET), thèse effectuée au GET (2012-2015).

- E. Bozzi (directeurs de thèse: R. Vautard, F. Miglietta, et L. Genesio), thèse effectuée au LSCE et Istituto di Biometeorologia - Cnr, Italie (2012-2016).

- C. Velluet (directeurs de thèse: V. Guinot et B. Cappelaere, MSE), thèse effectuée au MSE. Soutenue le 6 mars, 2014.

- C. Demunck (directeurs de thèse: A. Lemonsu et V. Masson), thèse effectuée au CNRM-GAME, Météo-France. Soutenue le 8 novembre 2013.

7.3.4 Jury de thèse

- Membre du jury de thèse de Vincent Yin Zun (Directeurs - H. A. Dijkstra, B.J.J.M. van den Hurk, et S. C. Dekker) "Vegetation-climate interactions in arid and semi-arid regions" effectuée à l'université d'Utrecht, Pays Bas. Soutenue le 02 décembre, 2015, Pays Bas.

- Membre du jury de thèse de Vincent Haefliger (Directeurs - E. Martin et A. Boone) "Préparation à l'assimilation de hauteurs d'eau SWOT dans un modèl hydrologique distribué régional" effectuée à l'université Paul Sabatier, Toulouse. Soutenue le 23 novembre, 2015, CNRM, Météo-France.

- Membre du jury de thèse de C. Magand (Directrice A. Ducharme) "Influence de la représentation des processus nivaux sur l'hydrologie de la Durance et sa réponse au changement climatique" effectué à l'UMPC. Thèse Soutenue en mai, 2014.

- Membre du jury de thèse de T. Wang (Directeurs - C. Ottlé, S.L. Piao et P. Ciais) "Développement et évaluation du modèle de surface ORCHIDEE : apport pour la simulation des cycles du carbone aux hautes latitudes" effectuée au LSCE et à l'IPSL. Soutenue le 15 décembre, 2011.

- Membre du jury de thèse de S. Gascoin (Directeurs A. Ducharme, P. Ribstein) "Etude des paramétrisations hydrologiques d'un modèle de surface continentale : des aquifères jusqu'aux premiers centimètres du sol" effectuée à l'UMPC. Soutenue en 2009.

7.4 Divers

Co-Encadrement de F. Baali (avec S. Biancamari et V. Pedinotti), stage master sciences effectué au LEGOS, Toulouse. "Amélioration d'une modélisation hydrologique du bassin du Niger". Université Paul Sabatier. Soutenu en 2013.

Co-Encadrement de C. Canac (avec E. Brun et B. Decharme), stage master sciences, effectué au CNRM "Analyse, évolution et amélioration d'une paramétrisation du manteau neigeux en présence de végétation." Ecole Nationale de la Météorologie et l'Université Paul Sabatier. Soutenu en juin 2011.

Co-Encadrement de P. Peyrille (avec J.-P. Lafore), Stage d'approndissement réalisé au CNRM-GAME. "Analyse du couplage continent-atmosphère à partir d'un modèle bidimensionnel de mousson africaine". 2008. Promotion d'élève Ingénieurs de l'Ecole Nationale de la Météorologie, 21 janvier au 20 juin 2008.

Encadrement de P. Peyrille, V. Plante-Broqua et N. Pastuschak. "Simulation de la végétation sur l'Afrique de l'Ouest avec un modèle de surface". Projet de modélisation de l'Ecole Nationale de la Météorologie du 8 janvier au 16 février 2007.

Co-Encadrement de K. Kerrigan (avec N. Mognard), stage masters au LEGOS, Toulouse. "Estimation of snow depth over Siberia from SSM/I and land surface modeling". Soutenu en 2004.

7.5 Responsabilités

- co-coordinateur (avec J. Noilhan et F. Habets) du projet GEWEX international Rhône-AGGregation (Rhône-AGG) en association avec le projet international Global Soil Wetness Project phase 2 (GSWP2) de 2002 à 2004.

- coordinateur du Land Use-Cover Change Impacts sub-group dans le cadre du projet international West African Monsoon Modelling Experiment phase 2 (WAMME2) de 2012 à présent.

- membre de l'African Monsoon Modeling and Analysis (AMMA) International Scientific Steering Committee (AMMA ISSC).

- coordinateur du projet international AMMA Land surface Model Intercomparison Project (ALMIP) de 2006 à 2009.

- co-coordinateur (avec C. Peugeot, MSE) du projet international AMMA Land surface Model Intercomparison Project (ALMIP2) de 2009 à 2016.
- membre du Surface Water and Ocean Topography (SWOT) Science Definition Team (SDT) (mission du satellite CNES-NASA) de 2012 à 2015.
- membre du International Working Group on Numerical Experimentation (WGNE) de 2013 à 2016.
- membre du comité du pilotage du projet ANR AMETHYST (de 2015 à présent)
- membre du comité du pilotage du Surface EXternalisé (SURFEX)
- Co-Chair du Global Energy and Water Cycle Experiment (GEWEX) Global Land Atmosphere System Study (GLASS) Panel international de 2013 à 2016

7.6 Participation à l'organisation de conférences, ateliers

- Organisation du GEWEX-GLASS Annual Panel Meeting, mai 2014 (CIC, Météo-France, Toulouse).
- Scientific Organization Committee for the 7th International GEWEX Conference on the Global Water and Energy Cycle, Trending Now-Water, The Hague, Nehterlands, 14-17 July, 2014.
- Co-organization of the International ALMIP2 Workshop (CIC, Météo-France, Toulouse), 15-17 avril 2013.
- Co-organization of the International Rhône-AGGregation Workshop (CIC, Météo-France, Toulouse), 25-26, octobre 2001.

7.7 Liste de Publications

7.7.1 Revues à comité de lecture

1995

Wetzel, P. J. and A. Boone: A parameterization for Land-Atmosphere-Cloud-Exchange (PLACE): Documentation and testing of a detailed process model of the partly cloudy boundary layer over heterogeneous land. 1995, J. Climate, 8, 1810-1837.

1996

A. Boone, A., and P. J. Wetzel: Issues related to low resolution modeling of soil moisture: Experience with the PLACE model. 1996, Glob. Plan. Change, 13, 161-181.

Wetzel, P. J., X. Liang, P. Irannejad, A. Boone,J. Noilhan, Y. Shao, C. Skelly, Y. Xue and Z. L. Yang: Modeling vadose zone liquid water fluxes: Infiltration, runoff, drainage, interflow. 1996, Glob. Plan. Change, 13, 57-71.

Wetzel, P., S. Argentini and A. Boone: The role of the land surface in controlling daytime cloud amount: Two case studies in the GCIP-SW area. 1996, J. Geophys. Res., 101, 7359-7370.

1997

Chen, T. H., A. Henderson-Sellers, P. C. D. Milly, A. J. Pitman, A. C. M. Beljaars, J. Polcher, F. Abramopoulos, A. Boone, S. Chang, F. Chen, Y. Dai, C. E. Desborough, R. E. Dickinson, L. Duemenil, M. Ek, J. R. Garratt, N. Gedney, Y. M. Gusev, J. Kim, R. Koster, E. Kowalczyk, K. Laval, J. Lean, D. Lettenmaier, X. Liang, J.-F. Mahfouf, H.-T. Mengelkamp, K. Mitchell, O. N. Nasonova, J. Noilhan, A. Robock, C. Rosenweig, J. Schaake, C. A. Schlosser, J.-P. Schulz, Y. Shao, A. B. Shmakin, D. L. Verseghy, P. Wetzel, E. F. Wood, Y. Xue, Z.-L. Yang, and Q. Zeng: Cabauw experimental results from the project for intercomparison of landsurface schemes (PILPS). 1997, J. Climate, 10, 1194-1215.

Weiqing, Q., A. Henderson-Sellers, A. J. Pitman, T. H. Chen, F. Abramopoulos, A. C. M. Beljaars, A. Boone, S. Chang, F. Chen, Y. Dai, C. E. Desborough, R. E. Dickinson, L. Dumenil, M. Ek, J. R. Garratt, N. Gedney, Y. M. Gusev, J. Kim, R. Koster, E. A .Kowalczyk, K. Laval, J. Lean, D .Lettenmaier, X. Liang, J.-F. Mahfouf, H.-T. Mengelkamp, P. C. D. Milly, K. Mitchell, O. N. Nasonova, J. Noilhan, J. Polcher, A. Robock, C. Rosenzweig, J. Schaake, C. A. Schlosser, J.-P. Schulz, A. B. Shmakin, D. L. Verseghy, P. Wetzel, E. F. Wood, Y. Xue, Z.-L. Yan and Q. Zeng: Sensitivity of latent heat flux from PILPS land-surface schemes to perterbations of surface air temperature. 1997, J. Atmos. Sci., 55, 1909-1927.

1998

Liang, X., E. F. Wood, D. Lettenmaier, D. Lohmann, A. Boone, S. Chang, F. Chen, Y. Dai, C. Desborough, Q. Duan, M. Ek, Y. Gusev, F. Habets, P. Irannejad, R. Koster, O. Nasanova, J. Noilhan, J. Schaake, A. Schlosser, Y. Shao, A. Shmakin, D. Verseghy, J. Wang, K. Warrach, P. Wetzel, Y. Xue, Z.-L. Yang and Q. Zeng: The Porject for Intercomparison of Land-Surface Parameterization Schemes (PILPS) Phase-2c Red-Arkansas River Basin experiment: 2. spatial and temporal analysis of energy fluxes. 1998, Glob. Plan. Change, 19, 137-159.

Lohmann, D., X. Liang, E. F. Wood, D. Lettenmaier, A. Boone, S. Chang, F. Chen, Y. Dai, C. Desborough, Q. Duan, M. Ek, Y. Gusev, F. Habets, P. Irannejad, R. Koster, O. Nasanova, J. Noilhan, J. Schaake, A. Schlosser, Y. Shao, A. Shmakin, D. Verseghy, J. Wang, K. Warrach, P. Wetzel, Y. Xue, Z.-L. Yang and Q. Zeng: The Porject for Intercomparison of Land-Surface Parameterization Schemes (PILPS) Phase-2c Red-Arkansas River Basin experiment: 3. spatial and temporal analysis of water fluxes. 1998, Glob. Plan. Change, 19, 161-179.

Wood, E. F., D. Lettenmaier, X. Liang, D. Lohmann, A. Boone, S. Chang, F. Chen, Y. Dai, C. Desborough, Q. Duan, M. Ek, Y. Gusev, F. Habets, P. Irannejad, R. Koster, O. Nasanova, J. Noilhan, J. Schaake, A. Schlosser, Y. Shao, A. Shmakin, D. Verseghy, J. Wang, K. Warrach, P. Wetzel, Y. Xue, Z.-L. Yang and Q. Zeng: The Porject for Intercomparison of Land-Surface Parameterization Schemes (PILPS) Phase-2c Red-Arkansas River Basin experiment: 3. experiment description and summary intercomparisons. 1998, Glob. Plan. Change, 19, 115-139.

1999

Boone, A. and P. J. Wetzel: A simple scheme for modeling sub-grid soil texture variability for use in an atmospheric climate model. 1999, J. Met. Soc. Japan, 77(1B), 317-333.

Boone, J.-C. Calvet, and J. Noilhan: Inclusion of a Third Soil Layer in a Land-Surface Scheme using the Force-Restore method. 1999, J. Appl. Meteor., 38, 1611-1630.

Pitman, A. J., A. Henderson-Sellers, C. E. Desborough, F. Abramopoulos, A. Boone, R. E. Dickinson, N. Gedney, R. Koster, E. Kowalczyk, D. Lettenmaier, X. Liang, J-F. Mahfouf, J. Noilhan, J. Polcher, W. Qu, A. Robock, C. Rosenzweig, C. A. Schlosser, A. B. Shmakin, J. Smith, M. Suarez, D. Verseghy, P. Wetzel, E. Wood, Y. Xue: Key results and implications from phase 1(c) of the Project for Intercomparison of Land-Surface Parameterization Schemes. 1999, Clim. Dyn., 15, 673-684.

Schlosser, C. A., A. G. Slater, A. Robock, A. J. Pitman, K. Y. Vinnkov, A. Henderson-Sellers, N. A. Speranskaya, K. Mitchell, A. Boone, H. Braden, F. Chen, P. Cox, P. de Rosnay, C. E. Desborough, R. E. Dickinson, Y.-J. Dai, Q. Duan, J. Entin, P. Etchevers, N. Gedney, Y. M. Gusev, F. Habets, J. Kim, V. Koren, E. Kowalczyk, O. N. Nasonova, J. Noilhan, J. Schaake, A. B. Shmakin, T. G. Smirnova, D. Verseghy, P. Wetzel, Y. Xue, and Z.-L. Yang: Simulations of a boreal grassland hydrology at Valdai, Russia: PILPS Phase 2(d). 1999, Mon. Wea. Rev., 128, 301-321.

2000

Boone, A. V. Masson, T. Meyers, and J. Noilhan: The influence of the inclusion of soil freezing on simulations by a soil-vegetation-atmosphere transfer scheme. 2000, J. Appl. Meteor., 9, 1544-1569.

Mohr, K. I., J. Famiglietti, A. Boone, and P. Starks: Modeling soil moisture and surface flux variability with an untuned land surface scheme: A case study from the Southern Great Plains 1997 Hydrology Experiment. 2000, J. Hydrometeor., 1, 154-169.

2001

Baker, R. D., B. H. Lynn, A. Boone, W.-K. Tao, and J. Simpson: The influence of soil moisture, coastline curvature, and land-breeze circulations on sea-breeze-initiated precipitation. 2001, J. Hydrometeor., 2, 193-211.

Boone, A. and P. Etchevers: An intercomparison of three snow schemes of varying complexity coupled to the same land-surface model: Local scale evaluation at an Alpine site. 2001, J. Hydrometeor., 2, 374-394.

Lynn, B. H., D. Stauffer, P. Wetzel, W.-K. Tao, P. Alpert, N. Perlin, D. Baker, R. Munoz, A. Boone, and Y. Jia: Improved Simulation of Florida Summer Convection Using the PLACE Land Model and a 1.5-Order Turbulence Parameterization Coupled to the Penn State/NCAR Mesoscale Model. 2001, Mon. Wea. Rev., 129, 1441-1461.

Slater, A. G., C. A. Schlosser, C. E. Desborough, A. J. Pitman, A. Henderson-Sellers, A. Robock, K. Ya. Vinnikov, K. Mitchell, A. Boone, H. Braden, F. Chen, P. M. Cox, P. de Rosnay, R. E. Dickinson, Y.-J. Dai, Q. Duan, J. Entin, P. Etchevers, N. Gedney, Ye. M. Gusev, F. Habets, J. Kim, V. Koren, E. A. Kowalczyk, O. N. Nasonova, J. Noilhan, S. Schaake, A. B. Shmakin, T. G. Smirnova, D. Verseghy, P. Wetzel, Y. Xue, Z.-L. Yang, Q. Zeng: The Representation of Snow in Land Surface Schemes: Results from PILPS 2(d). 2001, J. Hydrometeor., 2, 7-25.

2003

Habets, F., A. Boone, and J. Noilhan: Simulation of a Scandinavian basin using the diffusion transfer version of ISBA. 2003, Glob. Plan. Change, 38, 137-149.

Luo, L., A. Robock, K. Y. Vinnikov, C. A. Schlosser, Slater, A. G., N. A. Speranskaya, A. Boone, H. Braden, F. Chen, P. M. Cox, P. de Rosnay, C. E. Desborough, R. E. Dickinson, Y.-J. Dai, Q. Duan, J. Entin, P. Etchevers, A. Henderson-Sellers, N. Gedney, Ye. M. Gusev, F. Habets, J. Kim, V. Koren, E. A. Kowalczyk, K. Mitchell, O. N. Nasonova, J. Noilhan, A. J. Pitman, S. Schaake, A. B. Shmakin, T. G. Smirnova, D. Verseghy, P. Wetzel, Y. Xue, Z.-L. Yang, Q. Zeng: Effects of frozen soil on soil temperature, spring infiltration, and runoff: Results from the PILPS 2(d) Experiment at Valdai, Russia. 2003, J. Hydrometeor., 4, 334-351.

2004

Boone, A. F. Habets, J. Noilhan, D. Clark, P. Dirmeyer, S. Fox, Y. Gusev, I. Haddeland, R. Koster, D. Lohmann, S. Mahanama, K. Mitchell, O. Nasonova, G.-Y. Niu, A. Pitman, J. Polcher, A. B. Shmakin, K. Tanaka, B. van den Hurk, S. Vérant, D. Verseghy, P. Viterbo and Z.-L. Yang: The Rhône-Aggregation Land Surface Scheme Intercomparison Project: An Overview. 2004, J. Climate, 17, 187-208.

Etchevers, P., E. Martin, R. Brown, C. Fierz, Y. Lejeune, E. Bazile, A. Boone, Y.-J. Dai, R. Essery, A. Fernandez, Y. Gusev, R. Jordan, V. Koren, E. Kowalczyk, N. O. Nasonova, R. D. Pyles, A. Schlosser, A. B. Shmakin, T. G. Smirnova, U. Strasser, D. Verseghy, T. Yamazaki and Z.-L. Yang, 2004: Validation of the energy budget of an alpine snowpack simulated by several snow models (SNOWMIP project). Annals of Glaciology, 38, 150-158.

2005

Coret, L., Ph. Maisongrande, A. Boone, A. Lobo, G. Dedieu, and P. Gouaux, 2005: Diagnosis of the 2003 drought impact with high resolution remote sensing time series over southÂwestern France. Int. J. remote Sensing, 26(11), 2461-2469.

2006

Boone, A., N. Mognard, B. Decharme, H. Douville, M. Grippa, and K. Kerrigan, 2006: Impact of simulated soil temperatures on the estimation of snow depth over Siberia from SSM/I compared to a multi-model climatology. Remote Sens. Env., 101, 482-494.

Decharme, B., H. Douville, A. Boone, F. Habets and J. Noilhan, 2006: Advantage of an exponential soil profile of saturated hydraulic conductivity within the IBA LSM: simulations over the Rhône basin. J. Hydrometeor., 7, 61-80.

Fox, S., A. Pitman, A. Boone and F. Habets, 2006: The relationship between inter-model differences and surface energy balance complexity in the Rhône Aggregation Intercomparison Project. J. Hydrometeor., 7, 81-100.

2007

Caballero, Y., P. Chevallier, A. Boone, F. Habets, and J. Noilhan, 2007: Calibration of the Interaction Soil Biosphere Atmosphere land-surface scheme on a small tropical high-mountain basin (Cordillera Real, Bolivia). Wat. Res. Research, 43, W07423, doi:10.1029/2005WR004490.

Caballero, Y., S. Voirin-Morel, F. Habets, J. Noilhan, P. LeMoigne, A. Lehenaff, and A. Boone, 2007: Hydrological sensitivity of the Adour-Garonne river basin to climate change. Wat. Res. Research, 43, W07448, doi:10.1029/2005WR004192.

Stockli, R., P. L. Vidale, A. Boone and C. Schar, 2007: Impact of scale and aggregation on the terrestrial water exchange: integrating land surface models and rhone catchment observations. J. Hydrometeorol., 8(5), 1002-1015.

2008

Biancamaria, S., N. Mognard, A. Boone, M. Grippa, and E. G. Josberger, 2008: A satellite snow depth multi-year average derived from SSM/I for high latitude regions. Remote Sens. Env., 112,

2557-2568, doi:10.1016/j.rse.2007.12.002.

Habets, F., A. Boone, J.L Champeaux, P. Etchevers, E. Leblois, E. Ledoux, P. Le Moigne, E. Martin, S. Morel, Q. Segui, F. Rousset-Regimbeau, P. Viennot, 2008: The SAFRAN-ISBA-MODCOU hydrometeorological model applied over France. J. Geophys. Res., 113, doi:10.1029/2007JD008548.

Tulet, P., M. Mallet, V. Pont, J. Pelon, and A. Boone, 2008: The 7-12 March dust storm over West Africa: Mineral dust generation and vertical layering in the atmosphere. J. Geophys. Res., 113, D00C08, doi:10.1029/2008JD009871.

2009

Biancamaria, S., P. Bates, A. Boone, and N. Mognard, 2009: Large-scale coupled hydrologic and hydraulic modelling of an arctic river: the Ob river in Siberia. J. of Hydrology, 379, 136-150.

Boone, A. P. de Rosnay, G. Basalmo, A. Beljaars, F. Chopin, B. Decharme, C. Delire, A. Ducharne, S. Gascoin, M. Grippa, F. Guichard, Y. Gusev, P. Harris, L. Jarlan, L. Kergoat, E. Mougin, O. Nasonova, A. Norgaard, T. Orgeval, C. Ottlé, I. Poccard-Leclercq, J. Polcher, I. Sandholt, S. Saux-Picart, C. Taylor, and Y. Xue, 2009: The AMMA Land Surface Model Intercomparison Project. Bull. Amer. Meteor. Soc., 90(12), 1865-1880, doi:10.1175/2009BAMS2786.1

Bouilloud, L., E. Martin, F. Habets, A. Boone, P. Le Moigne, J. Livet, M. Marchetti, A. Foidart, L. Franchisteguy, S. Morel, J.Noilhan, and P.Pettre, 2009: Road surface condition forecasting in France. J. App. Meteor., DOI: 10.1175/2009JAMC1900.1

de Rosnay, P., M. Drusch, A. Boone, G. Balsamo, B. Decharme, P. Harris, Y. Kerr, T. Pellarin, J. Polcher, and J.-P. Wigneron, 2009: AMMA Land Surface Model Intercomparison Experiment coupled to the Community Microwave Emission Model: ALMIP-MEM, J. Geophys. Res., 114, D05108, doi:10.1029/2008JD010724.

Rutteri, N., R. Essery, J. Pomeroy, N. Altimir, K. Andreadis, I. Baker, A. Barr, P. Bartlett, A. Boone, H. Deng, H. Douville, E. Dutra, K. Elder, C. Ellis, X. Feng, A. Gelfan, A. Goodbody, Y. Gusev, D. Gustafsson, R. Hellstrom, Y. Hirabayashi, T. Hirota, T. Jonas, V. Koren, A. Kuragina, D. Lettenmaier, W.-P. Li, C. Luce, E. Martin, O. Nasonova, J. Pumpanen, R. D. Pyles, P. Samuelsson, M. Sandells, G. Schadler, A. Shmakin, T. G. Smirnova, M. Stahli, R. Stockli, U. Strasser, H. Su, K. Suzuki, K. Takata, K. Tanaka, E. Thompson, T. Vesala, P. Viterbo, A. Wiltshire, K. Xia, Y. Xue, and T. Yamazaki, 2009: Evaluation of forest snow processes models (SnowMIP2). J. Geophys. Res., 114, D06111, doi:10.1029/2008JD011063.

Steiner, A., J. Pal, S. Rauscher, J. Bell, N. Diffenbaugh, A. Boone, L. Sloan and F. Giorgi, 2009: Land surface coupling in regional climate simulations of the West African monsoon. Clim. Dynamics, DOI 10.1007/s00382-009-0543-6.

2010

Biancamaria, S., M. Durand, K. M. Andreadis, P. D. Bates, A. Boone, N. M. Mognard, E. Rodriguez, D. E. Alsdorf, D. Lettenmaier, and E. Clark, 2010: Assimilation of virtual wide swath altimetry to improve Arctic river modeling. Rem. Sens. Environ., DOI 10.1016/j.rse.2010.09.008.

Bock, O., F. Guichard, R. Meynadier, S. Gervois, A. Agusta-Panareda, A. Beljaars, A. Boone, M. Nuret, J.-L. Redelsperger, P. Roucou, 2010: The large scale water cycle of the West African Monsoon. Atmos. Sci. Let., 12, 51-57, Doi : 10.1002/asl.288.

Boone, A., Y. Xue, I. Poccard-Leclerq, J. Feng, and P. deRosnay, 2010: Evaluation of the WAMME model surface fluxes using results from the AMMA land-surface model intercomparison project. Clim. Dynamics, 35(1), 127-142. DOI 10.1007/s00382-009-0653-1

Delon, C., C. Galy-Lacaux, A. Boone, C. Liousse, D. Serça, M. Adon, B. Diop, A. Akpo, F. Lavenu, E. Mougin, and F. Timouk, 2010: Atmospheric Nitrogen budget in Sahelian dry savannas. Atmos. Phys. and Chem., 10, 2691-2708.

Guichard, F., N. Asencio, C. Peugeot, O. Bock, J.-L. Redelsperger, X. Cui, M. Garvert, B. Lamptey, E. Orlandi, J. Sander, F. Fierli, M. A. Gaertner, S. Jones, J.-P. Lafore, A. Morse, M. Nuret, A. Boone, G. Balsamo, P. de Rosnay, B. Decharme, P. P. Harris and J.-C. Bergès, 2010 : An intercomparison of simulated rainfall and evapotranspiration associated with a mesoscale convective system over West Africa, Wea. and Forcasting, 25, 37-60. doi : 10.1175/2009WAF2222250.1

Hourdin, F., F. Guichard, F. Favot, P. Marquet, A. Boone, J.-P. Lafore and J.-L. Redelsperger, P. Ruti, A. Dell'Aquila, T. L. Doval, A. K. Traore, and H. Gallee, 2010: AMMA-Model Intercomparison Project. Bull. Amer. Meteor. Soc., 91(1), 95-104.

Meynadier, R., O. Bock, F. Guichard, A. Boone, P. Roucou, J.-L. Redelsperger, 2010: The West African Monsoon water cycle. Part I: a hybrid water budget dataset. J. Geophys. Res., 115, doi:10.1029/2010JD013917.

Xue, Y., K.-M. Lau, K. H. Cook, D. Rowell, A. Boone, J. Feng, T. Bruecher, F. De Sales, P. Dirmeyer, L. M. Druyan, A. Fink, M. Fulakeza, Z. Guo, S. M. Hagos, S. S. Ibrah, K.-M. Kim, A. Kitoh, A. Konare, V. Kumar, P. Lonergan, M. Pasqui, I. Poccard-Leclercq, N. Mahowald, W. Moufouma-Okia, P. Pegion, J. K. Schemm, S. D. Schubert, A. Sealy, W. M. Thiaw, A. Vintzileos, E. K. Vizy, S. Williams, M.-L. C. Wu, 2010: The West African Monsoon Modeling and Evaluation project (WAMME) and its First Model Intercomparison Experiment. Clim. Dyn., doi: 10.1007/s00382-010-0778-2.

2011

Brun, E., D. Six, G. Picard, V. Vionnet, L. Arnaud, E. Bazile, A. Boone, A. Bouchard, C. Genthon,V. Guidard, P. Le Moigne, F. Rabier, and Y. Seity, 2011: Snow-atmosphere coupled

simulation at Dome C, Antarctica. J. Glaciol., 52 (204), J. Glaciol., 52 (211), 721-736.

Decharme, B., A. Boone, C. Delire and J. Noilhan, 2011: Local evaluation of the ISBA soil multilayer diffusion scheme using four pedotransfer functions. J. Geophys. Res., doi:10.1029/2011JD016002.

Grippa, M., L. Kergoat, F. Frappart, Q. Araud, A. Boone, P. de Rosnay, J.M. Lemoine, S. Gascoin, G. Balsamo, C. Ottlé, B. Decharme, S. SauxPicart, and G. Ramillien, 2011: Land water storage changes over West Africa estimated by GRACE and land surface models. Water Res. Res., 47, W05549, doi:10.1029/2009WR008856.

Kaptue-Tchuente, A. T., A. Begue, J.-L. Roujean, S. O. Los, J. Morisette, A. Boone, J.-F. Mahfouf and B. Daouda, 2011: A new characterisation of the land surface heterogeneity of Africa for use in Land Surface Models. J. Hydrometeor., 12(6), 1321-1336. doi: 10.1175/JHM-D-11-020.1.

Peugeot, C., F. Guichard, O. Bock, D. Bouniol, M. Chong, A. Boone, B. Capplaere, S. Galle, M. Gosset, L. Séguis, A. Zannou, and J.-L. Redelsperger, 2011: Meso-scale water cycle within the West African monsoon. Atmos. Sci. Let., 12, 45-50. DOI: 10.1002/asl.309

Ruti, P. M., J. E. Williams, F. Hourdin, F. Guichard, A. Boone, P. Van Velthoven, F. Favot, I. Musat, M. Rumukkainen, M. Dominguez, M. A. Gaertner, J.-P. Lafore, T. Losada, M. B. Rodriguez de Fonseca, J. Polcher, F. Giorgi,Y. Xue, I. Bouarar, K. Law, B. Josse, B. Barret, X. Yang, C. Mari, and A. K. Traore, 2011: Modeling the West African climate system: systematic errors and future steps. Atmos. Sci. Let., 12, 116-122. DOI: 10.1002/asl.305

Taylor, C. M., D. J. Parker, N. Kalthoff, M. A. Gaertner, N. Philippon, S. Bastin, P. P. Harris, A. Boone, F. Guichard, C. Flamant, J.-Y. Grandpeix, P. Cerlini, M. Baldi, L. Descroix, H. Douville, J. Polcher, A. Agusti-Panareda, 2011: New perspectives on land-atmosphere feedbacks from the African monsoon multidisciplinary analysis (AMMA), Atmos. Sci. Let., 12, 38-44. DOI: 10.1002/asl.336

2012

Brun, E., V. Vionnet, S. Morin, A. Boone, E. Martin, S. Faroux, P. Le Moigne, and J.-M. Willemet, 2012: Le modèle de manteau neigeux Crocus et ses applications (The snow pack model CROCUS and it's applications). La Météorologie, 76, 44-54, 2012.

Getirana, A. C. V., A. Boone, D. Yamazaki, B. Decharme, F. Papa, and N. Mognard, 2012: The Hydrological Modeling and Analysis Platform (HyMAP): evaluation in the Amazon basin. J. Hydrometeor., 13, 1641-1665. doi: http://dx.doi.org/10.1175/JHM-D-12-021.1

Pedinotti, V., A. Boone, B. Decharme, J.-F. Crétaux, N. Mognard, G. Panthou, and F. Papa, 2012: Characterization of the hydrological functioning of the Niger basin using the ISBA-TRIP

model. Hydrol. and Earth Sys. Sci., 16, 1745-1773, doi:10.5194/hess-16-1745-2012

Peugeot, C., O. Bock, A. Boone, B. Cappelaere, M. Gosset, R. Meynadier, L. Séguis, T. Lebel, and J-L. Redelsperger, 2012: Le cycle de l'eau dans le système de mousson d'Afrique de l'Ouest. La Météorologie, 55-63 - http://hal.archives-ouvertes.fr/hal-00751518

Vionnet, V., E. Brun, S. Morin, A. Boone, S. Faroux, P. Le Moigne, E. Martin, and J.-M. Willemet, 2012: Crocus/SURFEX :Implementation of the detailed snowpack model Crocus in SURFEX v7. Geosci. Model Dev., 5, 773-791. doi:10.5194/gmd-5-773-2012

Xue, Y., A. Boone, and C. M. Taylor, 2012: Review and Prospective of Recent Development in West African Atmosphere/Land Interaction Studies. Int. J. Geophys., 2012, doi:10.1155/2012/748921.

2013

Brun, E., V. Vionnet, B. Decharme, Y. Peings, R. Valette, A. Boone, F. Karbou and S. Morin, 2013: Simulation of northern Eurasian local snow depth, mass and density using a detailed snowpack model and meteorological reanalyses. J. Hydrometeor., 14, 203-219.

Carrer, D., J.-L. Roujean, S. Lafont, J.-C. Calvet, A. Boone, B. Decharme, C. Delire and J.-P. Gastellu-Etchegorry, 2013: A canopy radiative transfer scheme with explicit FAPAR for the interactive vegetation model ISBA-A-gs: impact on carbon fluxes. J. Geophys. Res.-Biogeosciences, 118, doi:10.1002/jgrg.20070.

Getirana, A. C. V., A. Boone, D. Yamazaki and N. Mognard, 2013: Automatic calibration of global flow routing scheme parameters driven by spatial altimetry data: evaluation in the Amazon basin. Wat. Res. Res., 49, 1-16, doi:10.1002/wrcr.20077.

Masson, V., P. Le Moigne, E. Martin, S. Faroux, A. Alias, R. Alkama, S. Belamari, A. Barbu, A. Boone, F. Bouyssel, P. Brousseau, E. Brun, J.-C. Calvet, D. Carrer, B. Decharme, C. Delire, S. Donier, R. El Khatib, K. Essaouini2, A.-L. Gibelin, H. Giordani, F. Habets, M. Jidane, G. Kerdraon, E. Kourzeneva, S. Lafont, C. Lebeaupin, A. Lemonsu, J.-F. Mahfouf, P. Marguinaud, M. Moktari, S. Morin, G. Pigeon, R. Salgado, Y. Seity, F. Taillefer, G. Tanguy, P. Tulet, B. Vincendon, V. Vionnet and A. Voldoire, 2013: The SURFEXv7.2 externalized platform for the simulation of Earth surface variables and fluxes. Geosci. Model Dev., 6, 929-960, doi:10.5194/gmd-6-929-2013.

Wang, T., C. Ottlé, A. Boone, P. Ciais, E. Brun, S. Morin, G. Krinner and S. Piao, 2013: Evaluation of a new snow scheme in ORCHIDEE land surface model. J. Geophys. Res., 118, 6064–6079. doi: 6064Ž0136079, doi:10.1002/jgrd.50395

2014

Getirana, A. C. V., E. Dutra, M. Guimberteau, J. Kam, H.-Y. Li, B. Decharme, Z. Zhang, A. Ducharne, A. Boone, G. Balsamo, M. Rodell, A. M. Toure, Y. Xue, C. D. Peters-Lidard, S. V. Kumar, K. Arsenault, G. Drapeau, L. R. Leung, J. Ronchail, and J. Sheffield, 2014: Water Balance in the Amazon Basin from a Land Surface Model Ensemble. J. Hydrometeor., 15, pp. 2586-2614. doi: 10.1175/JHM-D-14-0068.1

Getirana, A. C. V., A. Boone, and C. Peugeot, 2014: Evaluating LSM-based water budgets over a West African basin assisted with a river routing scheme, J. Hydrometeor., 15, pp. 2331-2346, doi: 10.1175/JHM-D-14-0012.1

Hagos, S., L. R. Leung, Y. Xue, A. Boone, , F. de Sales, N. Neupane, M. Huang, and J.-H. Yoon, 2014: On the Response of the African Monsoon Precipitation to Land Use Change in Regional Model Simulations. Clim. Dyn., DOI: 10.1007/s00382-014-2092-x

Lohou, F., L. Kergoat, F. Guichard, A. Boone, B. Cappelaere, J.-M. Cohard, J. Demarty, S. Galle, C. Peugeot, D. Ramier, C. Taylor and F. Timouk, 2014: Surface response to rain events throughout the West African monsoon. Atmospheric Chemistry and Physics, 14, 3883–3898. doi:10.5194/acp-14-3883-2014

Pedinotti, V., A. Boone, S. Ricci, S. Biancamaria and N. Mognard, 2014: Assimilation of satellite data to optimize large scale hydrological model parameters : A case study for the SWOT mission. Hydrol. and Earth Sys. Sci., 18, 4485-4507. doi:10.5194/hess-18-4485-20

2015

Best, M.J., G. Abramowitz, H. Johnson, A.J. Pitman, A. Boone, M. Cuntz, B. Decharme, P.A. Dirmeyer, J. Dong, M. Ek, V. Haverd, B.J.J.M van den Hurk, G.S. Nearing, B. Pak, C. Peters-Lidard, J.A. Santanello Jr., L. Stevens, N. Vuichard, 2015: The plumbing of land surface models. J. Hydrometeor., 16, 1425-1442. doi:http://dx.doi.org/10.1175/JHM-D-14-0158.1

Boone, A., Y. Xue, F. De Sales, R. Comer, S. Hagos, S. Mahanama, K. Schiro, G. Song, G. Wang and C. R. Mechoso, 2015: The regional impact of Land-Use Land-cover Change (LULCC) over West Africa from an ensemble of global climate models under the auspices of the WAMME2 project. Clim. Dyns., (sous révision)

Casse, C., M. Gosset, V. Pedinotti, C. Peugeot, A. Boone, B. A. Tanimoun and B.Decharme, 2015: The potential of satellite rainfall products to predict Niger river flood events. Atmos. Res., doi:10.1016/j.atmosres.2015.01.010

Decharme, B., E. Brun, A. Boone, C. Delire, P. Le Moigne and S. Morin, 2015: Impacts of snowpack properties and soil organic carbon content on snow characteristics and soil temperature profiles simulated by the ISBA land surface model. The Cryosphere, (soumis)

Drame, M. S., X. Ceamanos, J.-L. Roujean, A. Boone, J.-P. Lafore, D. Carrer, and O. Geoffroy, 2015: On the importance of aerosol composition for estimating incoming solar radiation: Focus on the Western African stations of Dakar and Niamey during the dry season. Atmosphere, 6, 1608-1632; doi:10.3390/atmos6111608

Haefliger, V., E. Martin, A. Boone, F. Habets, C.H. David, P.A. Garambois, H. Roux, and S. Ricci, L. Berthon, and A. Thévenin, 2015: Evaluation of regional-scale water level simulations using various river routing schemes within a hydrometeorological modelling framework for the preparation of the SWOT mission. J. Hydrometeor., (in press) doi: http://dx.doi.org/10.1175/JHM-D-14-0107.1

Haughton, N., G. Abramowitz, A. J. Pitman, D. Or, M. J. Best, H. R. Johnson, G. Balsamo, A. Boone, M. Cuntz, B. Decharme, P. A. Dirmeyer, J. Dong, M. Ek, Z. Guo, V. Haverd, B. J. van den Hurk, G. S. Nearing, B. Pak, C. Peters-Lidard, J. A. Santanello Jr., L. Stevens, and N. Vuichard, 2015: The plumbing of land surface models: why are models performing so poorly? J. Hydrometeor., (soumis).

Peyrille, P., J.-P. Lafore and A. Boone, 2015: The annual cycle of the West African Monsoon in a two-dimensional model: Mechanisms of the rainband migration. Q. J. Roy. Met. Soc., (sous révision).

Xue, Y., F. De Sales, W. K.-M. Lau, A. Boone, K.-M. Kim, F. Kucharsk, G. Wang, M. Hosaka, M., S. Li, K. Schiro, R. Comer, S. Mahanama, G. Song, M. Chin, L. M. Druyan, P. A. Dirmeyer, Y. Gu, S. M. Hagos, E. Kalnay, A. Kito, R. D. Koster, R. Leung, N. M. Mahowald, C. R. Mechoso, D. Rowell, I. Seidou Sanda, W. Thiaw, Z. Zhang, and N. Zeng, 2015: West African monsoon decadal variability and surface-related forcings: Second West African Monsoon Modeling and Evaluation Project Experiment (WAMME II). Clim. Dyns., (sous révision).

7.7.2 Actes de colloques à comité de lecture

Boone, A. and P. deRosnay, 2007: AMMA forcing data for a better understanding of the West African monsoon surface-atmosphere interactions. Quantification and Reduction of Predictive Uncertainty for Sustainable Water Resource Management. IAHS Publ., 313, July 2007, 231-241.

7.7.3 Chapitres d'ouvrages

Mohr, K.I., J.S. Famiglietti, and A. Boone, 2001: The effect of sub-grid variability of soil moisture on the simulation of mesoscale watershed hydrology: A case study from the Southern Great Plains 1997 Hydrology Experiment. In Land Surface Hydrology, Meteorology, and Climate: Observations and Modeling, V. Lakshmi, J. Albertson, and J. Schaake, Eds., American Geophysical Union, 161-176.

Editeur du Chapitre 8: Land Atmosphere Interactions and the Water Cycle, dans *Seamless Prediction of the earth system: from minutes to months*. WMO publication 1156, 2015.

7.7.4 Publications dans des revues sans comité (depuis 2001)

Boone, A., F. Habets, J. Noilhan, 2001: The Rhône-AGGregation Experiment. GEWEX News, August, 11(3), 3-5.

Boone, A., 2002: Description du schema de neige ISBA-ES (ISBA-Explicit Snow) (Description of the ISBA-ES Snow Scheme). Technical Note 70, CNRM Météo-France, 53 pp.

Boone, A., F. Habets, and J. Noilhan, 2002: The Rhône-Aggregation Experiment. French Science and Technology, 42, 9.

Boone, A., F. Habets, J. Noilhan, B. Van den Hurk, M. Lange, J. Parodi, B. Ritter and E. Rodriguez, 2004: Intercomparison of the ELDAS models using the Rhône-AGGregation experimental design. European Land Data Assimilation System (ELDAS) Project report, 57pp.

Boone, A. and P. deRosnay, 2007: Towards the improved understanding of land-surface processes and coupling with the atmosphere over West Africa. iLEAPS Newletter, 3, 33-34.

Boone, A., A. C. V. Getirana, J. Demarty, B. Cappelaere, S. Galle, M. Grippa, T. Lebel, E. Mougin, C. Peugeot and T. Vischel, 2009: The African Monsoon Multidisciplinary Analyses (AMMA) Land surface Model Intercomparison Project Phase 2 (ALMIP2). GEWEX News, Novemeber, 19(4), 9-10.

Boone, A. and A. Beljaars, 2015: Summary of the ECMWF Annual Seminar. GEWEX News, 27(4).

Boone, A., 2015: Land surface model parameterization schemes: state of the art and future developments. Physical processes in present and future large scale models. Proceedings of the ECMWF Annual Seminar, Sept. 1-4, 2015, Reading UK.

Ek, M. and A. Boone, 2015: GLASS Panel Meeting Summary, 18-19 May, Toulouse. GEWEX News, 27(4).

Emery, C., S. Biancamaria, A. Boone, B. Decharme, S. Ricci and P.-A. Garambois, 2015: Toward the use of SWOT data to improve global scale hydrological modeling: A test case study over the Amazon basin. Proceedings of the Third Space for Hydrology Workshop, 15-17 September 2015, ESA-ESRIN, Frascati (Rome), Italy.

Haefliger, V., E. Martin, A. Boone, 2015: The use of satellite data for improving regional scale hydrological modeling. Annual Research Report, Météo-France, (sous presse)

Harding, R., J. Polcher, A. Boone, M. Ek, H. Wheater, and A. Nazemi, 2015: Anthropogenic Influences on the Global Water Cycle - Challenges for the GEWEX Community. GEWEX News, 27(4).

Janicot, S., M. Gaetani, F. Hourdin, A. Giannini, M. Biasutti, E. Mohino, Y. Xue, A. Boone, A. Gaye, S. Salack and C. Lavaysse, 2015: The recent partial recovery in Sahel rainfall: A fingerprint of greenhouse gases forcing? GEWEX News, 27(4).

Kumar, P., M. Jasinski, P. J. Wetzel, M. Karyampudi, A. Boone, and E. Engman, 1995: Implementation of PLACE Land Surface Hydrology in MM5. MM5 Mesoscale Modeling System Users' Workshop, NCAR, Boulder, Colorado, pp. 121-124.

Noilhan, J., A. Boone, and P. Etchevers, 2001: Application of Climate Change Scenarios to the Rhône basin. Proceeding of the ECLAT 2 Toulouse workshop, Report No. 4, 25-27 October, 58-74.

Pedinotti, V. and A. Boone, 2013: Using satellite data from the future satellite mission SWOT to improve the representation of the continental hydrological cycle in global earth system models. Annual Research Report, Météo-France.

Peyrillé, P., J.-P. Lafore and A. Boone, 2015: Role of rain evaporation, water recycling and atmospheric circulation on the African monsoon. Annual Research Report, Météo-France.

Pitman, A. J., A. Henderson-Sellers, F. Abramopoulos, R. Avvisar, G. Bonan, A. Boone, J. G. Cogley, R. E. Dickinson, M. Ek, D. Entekhabi, J. Famiglietti, J. R. Garratt, M. Frech, A. Hahmann, R. Koster, E. Kowalczyk, K. Laval, L. Lean, T. J. Lee, D. Lettenmaier, X. Liang, J-F. Mahfouf, L. Mahrt, C. Milly, K. Mitchell, N. de Noblet, J. Noilhan, H. Pan, R. Pielke, A. Robock, C. Rosenzwig, S. W. Running, A. Schlosser, R. Scott, M. Suarez, S. Thompson, D. Verseghy, P. Wetzel, E. Wood, Y. Xue, Z-L. Yang, L. Zhang, 1993: Results from the off-line Control Simulation Phase of the Project for Intercomparison of Landsurface Parameterization Schemes (PILPS), GEWEX Tech. Note, IGPO Publ. Series, 7, 47 pp.

Redelsperger J.L., C. Thorncroft, D. Parker, S. Janicot, E. Afiesimama, A. Boone, P. Brandt, S. Danuor, A. Dia, A. Diedhiou, A. Diongue, A. Fink, R. Folorunsho, M. Kadi, A. Konaré, S. Konaté, T. Lebel, B. Sultan, R. Washington, 2012: An update on AMMA activities in the CLIVAR framework. CLIVAR Exchanges, No. 60, 17 (3), October 2012, 14-15.

de Rosnay P., M. Drusch, A. Boone, G. Balsamo, B. Decharme, P. Harris, Y. Kerr, T. Pellarin, J. Polcher and J.P. Wigneron, 2008: The AMMA Land Surface Model Intercomparison Experiment coupled to the Community Microwave Emission Model: ALMIP-MEM. ECMWF Tech. Memorandum, 565, 28 pp.

de Rosnay, P., A. Boone, A. Beljaars, and J. Polcher, 2006: AMMA Land-Surface modeling

and intercomparison projects. GEWEX News, February, 16 (1), 10-11.

Santanello, J. and A. Boone, 2014: Global Land/Atmosphere System Study Panel Meeting. GEWEX News, November 2013, 23(4), 13-16.

Seneviratne, S. I., B. van den Hurk, D. Lawrence, G. Krinner, G. Hurtt, H. Kim, C. Derksen, T. Oki, A. Boone, M. Ek, V. Brovkin, P. Dirmeyer, H. Douville, P. Friedlingstein, S. Hagemann, R. Koster, N. de Noblet-Ducoudré and A. Pitman, 2014: Land processes, forcings, and feedbacks in climate change simulations: The CMIP6 LandMIPs. GEWEX News, 24(4), Nov., 2014.

7.7.5 Communications à des congrès, symposium

Araud Q., L. Kergoat, F. Frappart, M. Grippa, A. Boone, P. de Rosnay, J.-M. Lemoine and the ALMIP Working Group, 2008: Comparison between soil moisture estimations by GRACE satellite mission and by land surface models over West Africa. EGU General Assembly; Vienna, 13-18 April 2008.

Asencio, N., Lafore, J.-P., Boone, A., Guichard, F., Favot, F. and Redelsperger, J.-L. 2009. Land surface-atmosphere feedback analyze based on sensitivity experiments of cloud-resolving simulations on the 25-27 July 2006 convective period over Niamey. Work presented at Third International AMMA Conference, July 2004, at Ouagadougou, Burkina Faso.

Biancamaria, S., P. Bates, A. Boone, N. Mognard, and J.-F. Crétaux, 2007: Modelling the Ob river in Western Siberia using remotely sensed digital elevation models. 2nd Space for Hydrology Workshop Proceedings, Geneva, Switzerland, 12-14, November 2007.

Bock, O., R. Meynadier, F. Guichard, P. Roucou, A. Boone, J.L. Redelsperger, and S. Janicot, 2008: Assessment of water budgets computed from NWP models and observational datasets during AMMA-EOP, 28th Conference on Hurricanes and Tropical Meteorology, 28 April-02 May, 2008, Orlando, Florida.

Boone, A., P. de Rosnay, J.-P. Lafore, and ALMIP Working Group, 2006: Multiscale land surface model database and intercomparison within AMMA. Preprints from the AMMA 1st International Conference, Dakar, Senegal, 430-432. (présentation orale).

Boone, A. and P. deRosnay, 2007: AMMA Land Surface Model Intercomparison Project. Second AMMA International Conference, Karlsruhe, Germany, Nov. 26-30, 2007.(présentation orale).

Boone, A. and the ALMIP Working Group, 2008: Applications of ALMIP multi-model land surface model diagnostics for evaluating the surface component of the WAMME GCMs. 1st West African Monsoon Modeling and Evaluation (WAMME) Workshop, American Meteorological Society Annual Meeting, Jan. 20, 2008. (présentation orale).

Boone, A., I. Poccard-Leclercq and Y. K. Xue, 2008: Evaluation of GCM surface processes over West Africa using offline land surface models and observations. 22nd Conference on Hydrology, American Meteorological Society Annual Meeting, Jan. 20-24, 2008. (présentation orale).

Boone, A., Xue, Y., Poccard-Leclercq, I., Feng, J., de Rosnay, P. ALMIP Working Group. 2009. Evaluation of the WAMME model surface fluxes using results from the AMMA Landsurface Model Intercomparison Project (ALMIP). Work presented at Third International AMMA Conference, July 2009, at Ouagadougou, Burkina Faso. (présentation poster).

Boone, A. and the ALMIP Working Group, 2009: The AMMA land surface model intercomparison project: Summary of Phase 1 and Perspectives for Phase 2. 3rd International AMMA Conference, Ouagadougou, Burkina Fasso, July, 2009. (présentation orale).

Boone, A. and the ALMIP Working Group, 2010: The African Monsoon Multi-disciplinary Analysis land surface model inter-comparison project (ALMIP): Applications in coupled model studies. 90th American Meteorological Society Annual Meeting, joint Session between the 22nd Conference on Climate Variability and Change, and the 24th Conference on Hydrology, Atlanta, GA, USA, Jan. 17-21, 2010. (présentation orale).

Boone, A., 2010: Les modèles disponibles dans SURFEX. Rencontres Recherche et Développement 2010, Toulouse, 7-10 juin 2010.(présentation orale).

Boone, A. C. V. Getirana, J. Demarty, B. Cappelaere, S. Galle, M. Gosset, M. Grippa, T. Lebel, E. Mougin, C. Peugeot, G. Quantin, L. Seguis, J. Viarre and T. Vischel, and the ALMIP2 Working Group, 2010: Current Status of ALMIP Phase 2. 2nd Pan-GEWEX Science Meeting, Aug. 22-27, Seattle, WA, USA.(présentation orale).

Boone A., Peugeot C., Demarty J, Grippa M, Benarrosh N, Brender P, Cappelaere B, Chaffard V, Charvet G., Chazarin J-P, Cloché S, Cohard J-M, Ducharne A, Fleury L, Galle S, Getirana, A., Gosset M, Guichard F, Hiernaux P, Kaptué A., Kergoat L, Lebel T, Maignan F, Mougin E, Ottlé C, Polcher J, Quantin G., Ramage K, Robert D, Roujean, J.-L., Séguis, L., Timouk F, Velluet C., Viarre J, Vischel T., 2011: African Monsoon Multidisciplinary Analysis (AMMA) Land survae Model Intercomparison Project Phase 2 (ALMIP2). WCRP Open Science Conference, Denver, CO, USA, Oct 22-25. (présentation poster).

Boone, A., and the ALMIP2 Working Group, 2012: The AMMA Land surface Model Intercomparison Project Phase 2: Mesoscale to Local scale. 3rd International AMMA Conference, July 2012, Toulouse, France.(présentation orale).

Boone, A., Y. Xue, R. Comer, F. De Sales, S. Hagos, G. Song, G. Wang, Z. Guo, and S. P. Mahanama, 2013: The regional impact of Land-Use Land-cover Change using an ensemble of global climate models under the aupsices of WAMME-Phase 2. American Geophysical Union,

Fall Meeting, San Francisco, CA, USA. (présentation orale).

Boone, A., Y. Xue, R. Comer, F. De Sales, S. Hagos, S. P. Mahanama, K. Schiro, G. Song, G. Wang, R. Koster and C. R. Mechoso, 2014: Characterization of the impact of land degradation in the Sahel on the West African monsoon using an ensemble of climate models from the WAMME project. American Geophysical Union, Fall Meeting, San Francisco, CA, USA. (présentation orale).

Boone, A., Y. Xue, R. Comer, F. De Sales, S. Hagos, S. P. Mahanama, K. Schiro, G. Song, G. Wang, R. Koster and C. R. Mechoso, 2015: On the Impact of Land Use and Land Cover Change on the West African Monsoon: Approach and Results from the WAMME Inter-comparison Project. American Geophysical Union, Spring Meeting, Montreal, Canada. (présentation orale).

Bouet, C., Cautenet, G., Cautenet, S., Marticorena, B., Bergametti, G., Chatenet, B., Rajot, J.-L., Desboeufs, K., Formenti, P. and Boone, A. 2009. Are tropical mesoscale convective systems sources or sinks of desert dust in the Sahel? First insight from an AMMA case study. Work presented at Third International AMMA Conference, July, 2009, at Ouagadougou, Burkina Faso.

Carrer, D., J.-L. Roujean, S. Lafont, A. Boone, and J.-C. Calvet, 2012: A vegetation radiative transfer scheme in the ISBA A-gs interactive vegetation SVAT model. IGARSS 2012 Proceedings.

Casse, C.; Gosset, M.; Peugeot, C.; Boone, A.; Pedinotti, V., 2013: Propagation of Satelite Rainfall Products uncertainties in hydrological applications : Examples in West-Africa in the framework of the Megha-Tropiques Satellite Mission. American Geophysical Union, Fall Meeting, San Francisco, CA, USA.

Delon, C., Galy-Lacaux, C., Boone, A., Liousse, C., Serça, D., Adon, M., Diop, B., Akpo, A., Lavenu, F., Mougin, E. Timouk, F. 2009. Atmospheric nitrogen budget in Sahelian dry savannas. Work presented at Third International AMMA Conference, July 2009, at Ouagadougou, Burkina Faso.

Emery, C., S. Biancamaria, A. Boone, B. Decharme, S. Ricci and P.-A. Garambois, 2015: Toward the use of SWOT data to improve global scale hydrological modeling: A test case study over the Amazon basin. The Third Space for Hydrology Workshop, 15-17 September 2015, ESA-ESRIN, Frascati (Rome), Italy.

Etchevers P., E. Martin, R. Brown, C. Fierz ,Y. Lejeune, E. Bazile, A. Boone, Y.-J. Dai, R. Essery, A. Fernandez , Y. Gusev, R. Jordan, V. Koren, E. Kowalczyk, R. D. Pyles, A. Schlosser, A. B.Shmakin, T. G. Smirnova, U. Strasser, D. Verseghy, T. Yamazaki, Z.-L. Yang (2002) : SnowMIP, an intercomparison of snow models: first results. Proceedings of the International Snow Science Workshop (ISSW 2002), October 2002, Penticton, British Columbia, Canada.

Gounou, A., Couvreux, F., Guichard, F., Boone, A. and Kohler, M. 2009. Observation and modelling of continental diurnal cycles in West Africa. Work presented at Third International AMMA Conference, July 2009, at Ouagadougou, Burkina Faso.

Grippa, M., Kergoat, L., Frappart, F., Araud, Q., Boone, A., de Rosnay, P., Lemoine, J.-M. and ALMIP Working Group. 2009. Evaluation of land water storage changes over West Africa estimated by GRACE and by land surface models. Work presented at Third International AMMA Conference, July 2009, at Ouagadougou, Burkina Faso.

Grippa M, Demarty J, Boone A, Peugeot C, Ottlé C, Kergoat L, Mougin E, Pierre C, Cappelaere B, Cohard J-M, Galle S, Gosset M, Guichard F, Kaptué A, Lebel T, Quantin G, Séguis L, Timouk F, Vischel T, Benarrosh N, Brender P, Chaffard V, Charvet G, Chazarin J-P, Cloché S, Ducharne A, Fleury L, Gascoin S, Getirana M, Hiernaux P, Magand C, Maignan F, Polcher J, Ramage K, Robert D, Roujean J-L, Velluet C, Viarre J: Dynamic Vegetation Modeling over West Africa within the AMMA Land Surface Model Intercomparison Project (ALMIP-II), 2nd Terrabites Symposium, 6-8 Février 2012 (Frascati, Italy).

Guichard, F., F. Couvreux, A. Gounou, A. Boone, and M. Nuret, 2010: Role of low-level thermodynamics on surface-convection interactions over West-Africa. 90th American Meteorological Society Annual Meeting, 22nd Conference on Climate Variability and Change, Atlanta, GA, USA, Jan. 17-21, 2010.

Haefliger, V.; Martin, E.; Boone, A.; Habets, F.; David, C. H.; Garambois, P. A.; Roux, H.; Ricci, S.; Berthon, L. and Thévenin, A., 2014: Preparing for the SWOT mission: Evaluating the simulations of river water levels within a regional-scale hydrometeorological modelling framework EGU General assembly, Vienna, Austria.

Haefliger, V.; Martin, E.; Boone, A.; Habets, F.; David, C. H.; Garambois, P. A.; Roux, H.; Ricci, S.; Berthon, L. and Thévenin, A., 2014: Preparing for the SWOT mission: Evaluating the simulations of river water levels within a regional-scale hydrometeorological modelling framework 7th International Scientific Conference on the Global Energy and Water Cycle, The Hague, Netherlands.

Mouffe, M., A. Getirana, S. Ricci, C. Lion, S. Biancamaria, N. Mognard, A. Boone, and P. Rogel, 2012: Towards SWOT data assimilation for hydrologic:automatic caibration of global flow routing model parameters in the Amazon basin. SimHydro, 12-14 September 2012, Nice, France.

Pedinotti, V., A. Boone, N. Mognard, J.-F. Crétaux, and Bertrand Decharme, 2010: Towards a large scale modelling system over the Niger basin in preparation for the future SWOT satellite mission. AGU Meeting of the Americas, Foz do Iguassu, Aug. 8-13.

Pedinotti, V., A. Boone, N. Mognard, et al., 2012: Evaluation of the ISBA-TRIP continental

hydrologic system over the Niger basin using in situ and satellite derived dataset. ESA conference for 20 years of altimetry, Venice, Italie, 2012.

Pedinotti, V., A. Boone, N. Mognard, et al., 2013: The impact of the assimilation of SWOT satellite data into a large scale hydrological model parametrization over the Niger basin. EGU, Vienna, Austria, 2013.

Pedinotti, V., A. Boone, N. Mognard, et al., 2012: Evaluation of the ISBA-TRIP continental hydrologic system over the Niger basin using in situ and satellite derived datasets. 3rd International AMMA Conference, July 2012, Toulouse, France.

Peugeot, C., Zin, I., Gosset, M., Galle, S., Cohard, J.-M., Boone, A., de Rosnay, P., Mamadou, O., Séguis, L., Le Lay, M. and Zannou, A. 2009. Water cycle as simulated by a hydrologic model: evaluation of evapotranspiration and other terms with ALMIP data over the Ouémé watershed (Benin). Work presented at Third International AMMA Conference, July 2009, at Ouagadougou, Burkina Faso.

Peugeot C, Boone A, Kergoat L, Cappelaere B, Demarty J, Grippa M, Anderson M, Awessou B, Cohard JM, Ducharne A, Eswar R, Galle S, Getirana A, Hain C, Mamadou O, Muddu S, Ottlé C, Richard A, Seghieri J, Séguis L, and the ALMIP2 Working group. Model, satellite and ground-based estimates of evapotranspiration. A comparison in sub-humid tropical West Africa (ALMIP2 project). 94th Annual AMS Meeting, 2-6 February 2014, Atlanta, GA.

Peyrillé, P., Boone, A. Lafore, J.-P. 2009. Analysis of the land surface-atmosphere coupling in West Africa using a two-dimensional model. Work presented at Third International AMMA Conference, July 2009, at Ouagadougou, Burkina Faso.

de Rosnay, P., M. Drusch, J.-P. Wigneron, T. Holmes, G. Balsamo, A. Boone, C. Rudiger, J.-C. Calvet, Y. Kerr, 2008: Soil moisture remote sensing for numerical weather prediction: L-band and C-band emission modeling over land surfaces, the community microwave emission model (CMEM). IGARSS IEEE International Geoscience and Remote Sensing Symposium, 978-1-4244-2808-3/08, Boston, 6-11 July 2008, pp. 563-566.

de Rosnay P., A. Boone, M. Drusch, G. Balsamo, T. Pellarin, J.-P. Wigneron, 2008: ALMIP-MEM: AMMA Land surface Models Inter-comparison Project - Microwave Emission Model. EGU General Assembly, Vienna, 13-18 April 2008.

Van Oevelen, P. J., J. A. Santanello, M. Best, A. Boone, B. van den Hurk, 2013: GEWEX Land - Atmosphere Research: An Outlook. Climate and Land Surface Changes in Hydrology, IAHS-IAPSO-IASPEI Assembly Proceedings, Gothenburg, Sweden, July 2013.

Wetzel, P. J. and A. Boone, 1993: A 1-D model study of the sensitivity of the atmosphere to heterogeneous precipitation, including the effect of downdrafts. AMS Conference on Hydrocli-

matology, Anaheim, CA., January 17-22, Preprint 104-105.

Zin I., Peugeot C., Seguis L., Galle S., Gosset M., Le Lay M., Tillery S., Zannou A., Boone A., de Rosnay P., and the ALMIP group, 2009: Water balance sensitivity to the evapotranspiration term: issues from hydrological modelling on the sudanian site of AMMA (Benin). 3rd International AMMA Conference 20-24 July 2009, Ouagadougou, Burkina Faso.

7.7.6 Séminaires, Workshops

Boone, A., F. Habets, J. Noilhan, B. Van den Hurk, M. Lange, J. Parodi, B. Ritter and E. Rodriguez, 2004: Intercomparison of the ELDAS models using the Rhône-AGGregation experimental design. European Land Data Assimilation System (ELDAS). GEWEX-GLASS Workshop. (présentation orale).

Boone, A., 2006: The use of LAND SAF products in the AMMA project. LAND SAF 2nd Workshop, Lisbon, Portugal, March 8-10, 2006. (présentation orale sollicitée).

Boone, A., and C. Peters-Lidard, 2006: Land Data Assimilation Systems (LDAS). AMMA-US Workshop, Silver Spring, MD, USA, 4-5 May, 2006.(présentation orale).

Boone, A., 2007: Applications of the LAND-SAF downwelling radiative flux products within AMMA. Proceedings of the LAND-SAF 2nd Workshop, Lisbon, Portugal, March 8-9, 2006 (présentation orale).

Boone, A., 2008: SWOT measurements for improving hydrological parameterization in Regional and Global Climate Models. SWOT (joint CNES/NASA) Hydrology Workshop, September 15-17, 2008, The Ohio State University, Columbus Ohio. (présentation orale).

Boone, A., 2008: Science and Applications of Space-based Surface Water Observations .The International Workshop on Microwave Remote Sensing for Land Hydrology Research and Applications, October 20-22, 2008, Oxnard, California, USA.(présentation orale).

Boone, A. and the ALMIP Working Group, 2009: The ALMIP experience: Implications for NWP soil schemes, Land Surface Modelling, Data Assimilation and the implications for predictability GEWEX-GLASS Workshop , ECMWF, Reading UK, Nov. 8-11, 2009. (présentation orale).

Boone, A., 2010: SURFEX Snow schemes. Muscaten Workshop, March 23-25, Kuopio, Finland. (présentation orale).

Boone, A. C. V. Getirana, J. Demarty, B. Cappelaere, S. Galle, M. Gosset, M. Grippa, T. Lebel, E. Mougin, C. Peugeot, G. Quantin, L. Seguis, J. Viarre and T. Vischel, and the ALMIP2 Working Group, 2010: Current Status of ALMIP Phase 2. 2nd Pan-GEWEX Science Meeting,

Aug. 22-27, Seattle, WA, USA.(présentation orale).

Boone, A., and the ALMIP Working Group, 2010: The ALMIP Experience: Implications for land-atmosphere coupled systems. Land surface modelling and data assimilation and the implications for predictability, ECMWF-GLASS Workshop Proceedings, 9-12 Nov., ECMWF, August, 2010, 11-18. (présentation orale).

Boone, A., C. Peugeot, J. Demarty, M. Grippa, B. Cappelaere, L. Kergoat and the ALMIP2 Working Group, 2013: Preliminary Synthetic Site Inter-comparison. GEWEX ALMIP2 Workshop, 13-15/02/2013, CIC, Météo-France, Toulouse. (présentation orale).

Boone A., Peugeot C., Cappelaere B, Demarty J, Grippa M, Kergoat L, Benarrosh N, Brender P, Chaffard V, Charvet G., Chazarin J-P, Cloché S, Cohard J-M, Ducharne A, Fleury L, Galle S, Getirana, A., Gosset M, Guichard F, Hiernaux P, Kaptué A., Lebel T, Maignan F, Mougin E, Ottlé C, Polcher J, Quantin G., Ramage K, Robert D, Roujean, J.-L., Séguis, L., Timouk F, Velluet C., Viarre J, and Vischel T. and the International ALMIP2 Working Group, 2013: Land Surface model Scaling issues over West Africa: Perspectives from the AMMA Land surface Model Inter-comparison Project (ALMIP). LSM Workshop in support of NWP and Sub-Seasonal Climate Pred., George Mason Univ., Dec. 2013. (présentation orale).

Boone, A. and M. Ek, 2015: Global Energy and Water EXchanges project (GEWEX)Global Land Atmosphere System Study (GLASS). LandMIP Workshop. Swiss Federal Institute of Technology in Zurich (ETHZ). Switzerland, 26-28 October 2015 (présentation orale).

Boone, A., 2015: Land surface model parameterization schemes: state of the art and future developments. Physical processes in present and future large scale models. Proceedings of the ECMWF Annual Seminar, Sept. 1-4, 2015, Reading UK. (présentation orale).

Brun, E., Y. Peings, V. Vionnet, A. Boone, B. Decharme, F. Karbou and S. Morin, 2013: Using reanalyses for studying past Eurasian snow cover and its relationship with circulation variability. ECMWF-WWRP/THORPEX Workshop on Polar Prediction, 24-27 June 2013.

Demarty, J., B. Cappelaere, A. Boone, M. Grippa, L. Kergoat, C. Peugeot, and the ALMIP2 Working Group, 2013: Preliminary analysis of the ALMIP-2 mesoscale simulations over the SW Niger AMMA Catch site. GEWEX ALMIP2 Workshop, 13-15/02/2/2013, CIC, Météo-France, Toulouse.

Grippa, M., L. Kergoat, A. Boone, C. Peugeot, J. Demarty, B. Cappelaere and the ALMIP2 Working group, 2013: Preliminary Intercomparison over the Mali-meso site. GEWEX ALMIP2 Workshop, 13-15/02/2013, CIC, Météo-France, Toulouse.

Pedinotti, V., A. Boone, N. Mognard, et al., 2010: Evaluation of a river flooding scheme over the Niger basin in preparation for the future SWOT satellite mission. OSTST 2010, Ocean

and Hydrology Applications, Lisbon, Portugal.

Peugeot, C., A. Boone, V. Chaffard, S. Cloché, J.M. Cohard, A. Ducharne, S. Galle, T. Gascon, F. Favot, L. Fleury, M. Gosset, C. Magand, F. Maignan, O. Mamadou, C. Ottlé, G. Quantin, , T. Pellarin, J. Polcher, K. Ramage, A. Richard, L. Séguis, J. Viarre, T. Vischel, and I. Zin, 2013: Benin meso-scale site : first model evaluations. GEWEX ALMIP2 Workshop, 13-15/02/2013, CIC, Météo-France, Toulouse.

Chapter 8

Selected Publications

- Boone, A., N. Mognard, B. Decharme, H. Douville, M. Grippa, and K. Kerrigan, 2006: Impact of simulated soil temperatures on the estimation of snow depth over Siberia from SSM/I compared to a multi-model climatology. Remote Sens. Env., 101, 482-494.

- Boone, A., P. de Rosnay, G. Basalmo, A. Beljaars, F. Chopin, B. Decharme, C. Delire, A. Ducharne, S. Gascoin, M. Grippa, F. Guichard, Y. Gusev, P. Harris, L. Jarlan, L. Kergoat, E. Mougin, O. Nasonova, A. Norgaard, T. Orgeval, C. Ottlé, I. Poccard-Leclercq, J. Polcher, I. Sandholt, S. Saux-Picart, C. Taylor, and Y. Xue, 2009: The AMMA Land Surface Model Intercomparison Project. Bull. Amer. Meteor. Soc., 90(12), 1865-1880, doi:10.1175/2009BAMS2786.1

- Boone, A., Y. Xue, I. Poccard-Leclerq, J. Feng, and P. deRosnay, 2010: Evaluation of the WAMME model surface fluxes using results from the AMMA land-surface model intercomparison project. Clim. Dynamics, 35(1), 127-142. DOI 10.1007/s00382-009-0653-1

- Getirana, A. C. V., A. Boone, D. Yamazaki, B. Decharme, F. Papa, and N. Mognard, 2012: The Hydrological Modeling and Analysis Platform (HyMAP): evaluation in the Amazon basin. J. Hydrometeor., 13, 1641-1665.
doi: http://dx.doi.org/10.1175/JHM-D-12-021.1

- Pedinotti, V., A. Boone, S. Ricci, S. Biancamaria and N. Mognard, 2014: Assimilation of satellite data to optimize large scale hydrological model parameters : A case study for the SWOT mission. Hydrol. and Earth Sys. Sci., 18, 4485-4507. doi:10.5194/hess-18-4485-20

Available online at www.sciencedirect.com
SCIENCE DIRECT®
Remote Sensing of Environment 101 (2006) 482–494
Remote Sensing of Environment
www.elsevier.com/locate/rse

The impact of simulated soil temperatures on the estimation of snow depth over Siberia from SSM/I compared to a multi-model climatology

A. Boone [a,*], N. Mognard [b], B. Decharme [c], H. Douville [c], M. Grippa [d], K. Kerrigan [b]

[a] CNRM/GAME, Météo-France, CNRS, Toulouse, France
[b] Laboratoire d'Etudes en Géophysique et Océanographie Spatiales (LEGOS), Toulouse, France
[c] CNRM/GMGEC, Météo-France, Toulouse, France
[d] Centre d'Etudes Spatiales de la BIOsphère (CESBIO), Toulouse, France

Received 22 June 2005; received in revised form 4 January 2006; accepted 8 January 2006

Abstract

The snowpack is a key variable of the hydrological cycle. In recent years, numerous studies have demonstrated the importance of long-term monitoring of the Siberian snowpack on large spatial scales owing to evidence of increased river discharge, changes in snow fall amount and alterations with respect to the timing of ablation. This can currently only be accomplished using remote sensing methods. The main objective of this study is to take advantage of a new land surface forcing and simulation database in order to both improve and evaluate the snow depths retrieved using a dynamic snow depth retrieval algorithm. The dynamic algorithm attempts to account for the spatial and temporal internal properties of the snow cover. The passive microwave radiances used to derive snow depth were measured by the Special Sensor Microwave/Imager (SSM/I) data between July 1987 and July 1995.

The evaluation of remotely sensed algorithms is especially difficult over regions such as Siberia which are characterized by relatively sparse surface measurement networks. In addition, existing gridded climatological snow depth databases do not necessarily correspond to the same time period as the available satellite data. In order to evaluate the retrieval algorithm over Siberia for a recent multi-year period at a relatively large spatial scale, a land surface scheme reanalysis product from the Global Soil Wetness Project-Phase 2 (GSWP-2) is used in the current study. First, the high quality GSWP-2 input forcing data were used to drive a land surface scheme (LSS) in order to derive a climatological near-surface soil temperature. Four different snow depth retrieval methods are compared, two of which use the new soil temperature climatology as input. Second, a GSWP-2 snow water equivalent (SWE) climatology is computed from 12 state-of-the-art LSS over the same time period covered by the SSM/I data. This climatology was compared to the corresponding fields from the retrievals. This study reaffirmed the results of recent studies which showed that the inclusion of ancillary data into a satellite data-based snow retrieval algorithm, such as soil temperatures, can significantly improve the results. The current study also goes a step further and reveals the importance of including the monthly soil temperature variation into the retrieval, which improves results in terms of the spatial distribution of the snowpack. Finally, it is shown that further improved predictions of SWE are obtained when spatial and temporal variations in snow density are accounted for.

Keywords: SSM/I; Global Soil Wetness Project 2; Snow water equivalent; Snow depth; Snow density; ISBA; Soil temperature; Land surface scheme

1. Introduction

The snowpack is a key variable of the hydrological cycle. In recent years, there has been an increased emphasis on long-term monitoring of the snowpack at large scales. One reason is that climate studies have shown evidence that the climate system is highly sensitive to the snow cover and that its depletion could have a positive feedback with the atmosphere thereby further enhancing theorized global warming (Hall, 2004). Siberian water resources are highly sensitive to climate change due to the extensive winter snow cover and large areas of permafrost. Ye and Ellison (2003) suggest that there is an increase in the transitional snow cover (earlier snow cover in autumn in central Siberia) owing to the increased frequency of anomalous weather

* Corresponding author. CNRM/GAME, 42 av. G. Coriolis, 31057 Toulouse Cedex, France.
E-mail addresses: aaron.boone@cnrm.meteo.fr (A. Boone), nelly.mognard@cnes.fr (N. Mognard), bertrand.decharme@cnrm.meteo.fr (B. Decharme), herve.douville@meteo.fr (H. Douville), manuela.grippa@cesbio.cnes.fr (M. Grippa).

0034-4257/$ - see front matter © 2006 Elsevier Inc. All rights reserved.
doi:10.1016/j.rse.2006.01.014

conditions and a warmer climate in recent years. It has been observed that the surface area covered by permafrost in northern Siberia is shrinking (Pavlov, 1994), and this soil warming is probably related to both increased air temperature and changes in the snow cover. In accordance with the aforementioned studies, there is also observational evidence of increased discharge from Arctic Siberian rivers during the winter and spring (Peterson et al., 2002; Serreze et al., 2003).

These studies demonstrate the importance of long-term monitoring of the Siberian snowpack on large spatial scales, which can currently only be accomplished using remote sensing methods. Algorithms have been developed for snow cover monitoring from space over the last few decades, with a particular effort over the last two on estimating the snow depth or liquid water equivalent. One factor limiting the development of such large-scale algorithms, however, has been the lack of validation data over large spatio-temporal scales (Chang et al., 2005).

The main objective of this study is to take advantage of a new land surface forcing and model simulation database in order to both improve and evaluate the retrieved snow depth spatial distribution using the dynamic portion of the snow depth retrieval algorithm described in Grippa et al. (2004: hereafter referred to as GEA04). The original snow depth retrieval dynamic algorithm (Josberger & Mognard, 2002; Mognard & Josberger, 2002) was recently improved by GEA04 in order to permit application of the algorithm over an entire snow season and to generalize it for application in other geographical regions such as Siberia. In addition, GEA04 showed that the incorporation of soil temperatures from a Russian climatology further improved their results based on evaluations using a long-term snow depth climatological database.

In addition to evaluation limitations owing to relatively sparse observational networks over Siberia, existing gridded climatological snow depth databases (such as the widely used United States Air Force/Environmental Technical Applications Center USAF/ETAC climatology: Foster and Davy, 1988) do not necessarily correspond to the same time period as the available satellite data. In order to evaluate the retrieval algorithm over Siberia for a recent multi-year period at a relatively large spatial scale, a land surface scheme (LSS) reanalysis product from the Global Soil Wetness Project Phase 2 (GSWP2) is used in the current study. GSWP2 is an ongoing environmental modeling research activity of the Global Land-Atmosphere System Study (GLASS) and the International Satellite Land-Surface Climatology Project (ISLSCP). These projects are a part of the Global Energy and Water Cycle Experiment (GEWEX). The current study is based on the phase-2 results of this project (Dirmeyer et al., in press). One of the main goals of GSWP2 is to foster a stronger connection to remote sensing applications. This goal is addressed in the current study in two ways. First, the high quality input forcing data are used as input into a LSS to derive the soil temperature which is needed by a remote sensing based snow depth retrieval algorithm. Second, three GSWP2 snow water equivalent (SWE) climatologies (corresponding to different input atmospheric model re-analysis products) were computed from an ensemble of state-of-the-art LSSs over the same time period covered by the SSM/I data, and then compared to the corresponding fields from the retrievals.

This paper is organized into 5 sections. The input data, study domain, and algorithm evaluation data are described in Section 2. The snow retrieval algorithm, the methods used to obtain a new near-surface soil temperature database, and the construction of the snow depth climatologies for evaluation of the algorithm are described in Section 3. Comparisons of the results using two snow depth retrieval algorithms, different input soil temperature data sets, and a variable snow density to estimate SWE are described in Section 4. Conclusions and perspectives for future work are given in Section 5.

2. Data and study area

The snow depth retrieval algorithm, satellite-based input, ancillary input data and evaluation metrics are described in this section, along with the main domain characteristics. In addition, the new remote-sensing model evaluation data set used in this study is described in detail.

2.1. Domain

The domain considered in this study is enclosed within the boxed region centered over Asia shown in Fig. 1. The region extends from west of the Ural mountains to the east of lake Baikal, including the Ob and the Yenisei river basins. The main vegetation zones consist in steppe and agricultural areas in the southwest, forests (mainly coniferous and larch) centered along a latitude of approximately 60N and in the south-east, and tundra in the north (where shrubs, sedge grasses, lichens and mosses dominate). In terms of winter climate, there is a general east-west precipitation gradient (decreasing eastward), and air temperatures are increasingly colder moving from southwest to northeast. For more details on the study zone, see GEA04.

2.2. Input satellite data

The passive microwave radiances used to derive snow depth have been measured by the Special Sensor Microwave/ Imager (SSM/I) on a sun-synchronous orbit with a 1349 km wide swath, on board the Defense Meteorological Satellite Program satellite series since July 1987 (DMSP F-8, F-11 and F-13 platforms). For this analysis, daily data between July 1987 and July 1995 are used. SSM/I is a multi-spectral radiometer with horizontally and vertically polarized channels at 19.35, 37 and 85.5 GHz and a vertically polarized channel at 22.235 GHz. The radiometer sensitivity or noise equivalent temperature differential is 0.41 K in the 19 GHz and 0.37 K in the 37 GHz horizontally polarized channels (Hollinger et al., 1990). The National Snow and Ice Data Center (NSIDC) provided the SSM/I data mapped to the Equal Area SSM/I Earth Grid (EASE-Grid) using a $25 \times 25\,km^2$ resolution (Armstrong et al., 1994). To minimise the spatial gaps resulting from the swath width, the daily data were averaged over pentads (5-day periods).

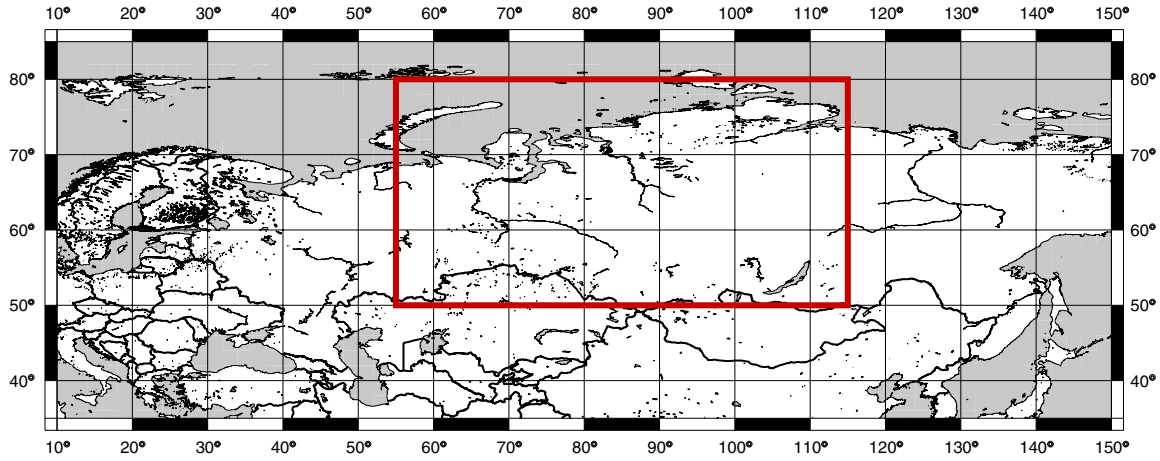

Fig. 1. The Siberian study domain is enclosed within the boxed region.

2.3. Ancillary input data: snow and soil temperatures

The dynamic algorithm based on SSM/I data requires information on the thermal gradient in the snowpack, which is represented by the difference between the atmosphere–snow interface (referred to here as "surface") and the ground temperatures. The NCEP global air temperature reanalysis from the Joint Institute for the Study of Atmosphere and Ocean (JISAO) (Kalnay et al., 1996) is used in this study. The NCEP data were interpolated to the EASE-Grid, averaged into pentads and finally smoothed using a five-pentad running average in order to dampen abrupt air temperature variations that generate the computation of erroneous crystal grain growth in the algorithm.

In addition to the air temperature, a near surface (soil) temperature estimate is required which is used to represent the temperature at the base of the snowpack. GEA04 used the climatological ground permafrost temperature data from the International Institute for Applied System Analysis (IIASA) (Stolbovoi & McCallum, 2002). It is important to note that these climatological temperatures only vary in space. In the current study, a new soil temperature data set is presented (see Section 3.1).

2.4. Evaluation data: snow cover depth

GEA04 used the gridded snow depth estimates from the USAF/ETAC climatology (Foster & Davy, 1988) and the IIASA data set in order to evaluate the retrieval algorithm performance. These data cover an approximately 30 year period ending in the 1980s. The manually edited depths are derived from many sources from all over the world based on an extensive literature search. In the current study, a more recent model-based analysis snow water equivalent product from the GSWP2 is used to evaluate the retrieval algorithm. One of the advantages of using this product is that it corresponds to the same period as the SSM/I data.

In a nutshell, GSWP consists in driving state-of-the-art LSSs by the best quality atmospheric and land surface databases currently available in order to produce multi-year global fields of land-surface state variables and fluxes. The LSS simulations at a 1 degree spatial resolution encompass the same core 10-year period as the ISLSCP Initiative II (1986–1995), and they can be considered as an analogue of atmospheric reanalyses. The LSSs participating in GSWP2 are used in operational numerical weather prediction (NWP) systems, atmospheric global climate models (GCMs), regional scale hydrological applications, and other land-surface modeling research activities (see Dirmeyer et al., in press).

3. Methods

The static algorithm for estimating the snow depth is given by the equation (Chang et al., 1987)

$$D = a\mathrm{SG} \tag{1}$$

$$\mathrm{SG} = T_{\mathrm{b}\,19\mathrm{H}} - T_{\mathrm{b}\,37\mathrm{H}} \tag{2}$$

where D corresponds to the snow depth (m), $T_{\mathrm{b}x\mathrm{H}}$ represents the horizontally polarized brightness temperature from SSM/I at a frequency of x GHz, and $a = 1.59\,(\mathrm{m\ K^{-1}})$. This value corresponds to a snow grain size (radius) of 3×10^{-4} m and a snow density of 300 kg m^{-3}. This model has been widely employed for nearly the last 20 years to obtain global estimations of the snow depth and liquid water equivalent at continental to hemispheric scales (Chang et al., 1990) in climate (Bamzai & Shukla, 1999) and global snow depth monitoring studies (Foster et al., 1997).

The emissivity of the earth's surface is affected by variations in surface roughness and in the type of land cover which provide a signal that includes a mixture of emissions from trees and the snow canopy, as well as the underlying surface. This may result in estimates of mean snow depth that are too low

compared to retrievals over flat, homogeneous terrain. Also, lower confidence in SWE reliability is due to over-measure that occurs in areas with significant depth hoar formation. The conditions for depth hoar formation involve the combination of shallow snow exposed to strong temperature gradients driven by cold overlying air. This results in a snow cover with large grains that enhance scattering of the microwave signal and causes over-measure when a particular algorithm has been tuned to a smaller mean grain size. In order to take the effect of depth hoar into account, dynamic algorithms have been developed (Josberger & Mognard, 2002; Kelly & Chang, 2003; Kelly et al., 2003).

The dynamic algorithm used in this study (Josberger & Mognard, 2002; Mognard & Josberger, 2002) differs from the static method primarily in that it attempts to account for the spatial and temporal internal properties of the snow cover, in particular, the snow grain size. Mognard and Josberger (2002) defined the thermal gradient index (TGI) to represent the effects of the bulk temperature gradient through the snowpack, as a proxy for snow grain growth:

$$\mathrm{TGI} = \frac{1}{C}\int \frac{T_g - T_a}{D(t)} \tag{3}$$

where C is a scaling constant which represents the critical temperature gradient of 20°C m^{-1}. They showed using the snow depth measurements from the National Weather Stations in the Northern Great Plains of North America, that a linear relationship exists between the spectral gradient SG and TGI:

$$\mathrm{SG} = \alpha \mathrm{TGI} + \beta \tag{4}$$

By differentiating the equations above, the snow depth is calculated as:

$$D = \frac{\alpha(T_g - T_a)}{\mathrm{dSG}/\mathrm{d}t} \tag{5}$$

where T_g and T_a represent the soil and 2 m air temperatures (K), respectively, and dSG/dt is the time tendency of the spectral gradient. α represents the slope of the linear relationship between SG and TGI which was determined using the ETAC climatology in GEA04. In their study and the current one, this coefficient has a constant (in time and space) value of 3.5. The air temperature from the NCEP reanalysis is used for T_a as in GEA04. The soil temperature, T_g, in Eq. (5) represents the temperature of the uppermost soil layer at the snowsoil interface. Mognard and Josberger (2002) assumed that $T_g = 0$ K, which gave reasonable results for the northern plains of the United States. GEA04 found that this assumption was unacceptable for Siberia, and therefore used a climatological permafrost temperature as a proxy from the IIASA database.

The snow depth relationship in Eq. (5) is applicable early in the snow season when the snow grain size and/or depth is evolving at an appreciable rate. Late in the season, these processes slow and cause the dSG/dt term to become small, so that GEA04 used a static method with a spatially variable coefficient (a in Eq. (1)) when the time-varying spectral gradient fell below a pre-defined a threshold (which was also applied in the current study). The threshold is usually reached in late March or April, depending on the location and on the climatic conditions (see GEA04 for further details).

As a final note, the conversion to SWE (the more meaningful hydrological quantity) is usually done by multiplying D by a constant snow density (generally 300 kg m^{-3}). Therefore, papers describing satellite-based snow retrieval algorithms often refer to D or SWE interchangeably. However, the neglect of the variations in snow density comprises an additional error source in determining SWE from D: this is discussed further in Section 4.2.

3.1. Simulated soil temperature

GEA04 showed that specification of T_g is quite important in the determination of D from the dynamic algorithm (Eq. (5)). At the time of that study, the only existing gridded estimate of ground temperature for Siberia was that of the IIASA (see Section 2.3) database. There are mainly three limitations to this database for use with the dynamic algorithm. First, the $T_{g\,\mathrm{IIASA}}$ represents the permafrost temperature, and is therefore not necessarily indicative of the temperature at the snow–soil interface (which is needed to more accurately represent the snowpack thermal gradient). Second, the temperature data is constant in time so that seasonal variations in T_g are not accounted for (while T_a does vary in time). Finally, the climatological values do not necessarily correspond to the time period encompassed by the SSM/I data.

In order to address these limitations, the GSWP2 LSS forcing database has been used to drive the Interactions between the Soil–Biosphere–Atmosphere (ISBA) LSS in order to derive a T_g climatology. ISBA (Noilhan & Mahfouf, 1996) is a state-of-the-art LSS which is currently used in numerical weather prediction (Giard & Bazile , 2000), global climate model (Douville, 2004), mesoscale meteorological and operational hydrological forecast modeling systems (Rousset et al., 2004) at Météo-France. The cold-season physics options used in this study (discussed below) have been evaluated in numerous local (Boone & Etchevers, 2001; Etchevers et al., 2005), and regional (Boone et al., 2004; Bowling et al., 2002; Habets et al., 2003) scale experiments.

A special multi-year simulation has been performed for this study using the GSWP2 database. ISBA has several options, and two which are the most relevant to the current study are briefly discussed here. The ISBA explicit soil diffusion option (Boone et al., 2000; Habets et al., 2003) using a six-layer soil layer configuration with the highest vertical resolution at the surface is used for the current study in order to facilitate a "realistic" simulation of the near-surface soil temperature gradient and freeze–thaw cycles. The soil layer thicknesses are fixed in space (from the surface downward: 0.03, 0.09, 0.27, 0.81, 2.43 and 7.29 m). The uppermost soil temperature (centered at 0.015 m) is assumed to represent the temperature at the soil–snow interface (i.e. at $z = 0$). This approximation has a negligible impact, especially considering the use of monthly

averages in the current study. It should be noted that the simple available energy method for phase changes (i.e. all liquid water can freeze given sufficiently cold temperatures) in the aforementioned publications has since been replaced by a more physically realistic method in which phases changes are governed by a relation between the maximum liquid water content and temperature (Cherkauer & Lettenmaier, 1999).

Soil and vegetation parameters are taken from the default ISBA land-surface parameter database ECOCLIMAP (Masson et al., 2003). In addition, the three-layer explicit snow scheme option (Boone & Etchevers, 2001) is used. The only change made to the model was a replacement of the relationship governing the Fractional Snow Covered Area (FSCA). In this study, FSCA linearly approaches 100% as the grid box average SWE approaches 10 kg m^{-2} (which generally corresponds to snow depths of 2–5 cm). This causes the simulated T_g to be more representative of the temperature below the snowpack than the default parameterization which can incorporate extensive snow-free areas.

The model was spun-up by repeating the first year (1982–1983) 10 times in order to obtain initial soil moisture and thermal states. After 10 years, deeper soil layer temperatures were still slowly evolving, however, temperatures in the uppermost meter of the soil were changing negligibly at this point (and only the uppermost T_g is used in the snow depth retrieval algorithm). The model was then run continuously until August, 1995. The ISBA climatology was then computed by averaging T_g over a 10 year period (1986–1995) for each month and at each grid point.

The annual domain average IIASA and ISBA T_g values are shown in Fig. 2, along with the monthly varying domain average ISBA T_g. The point of this figure is to illustrate that the monthly varying ISBA T_g ($T_{g\,ISBA}$) has a large amplitude annual

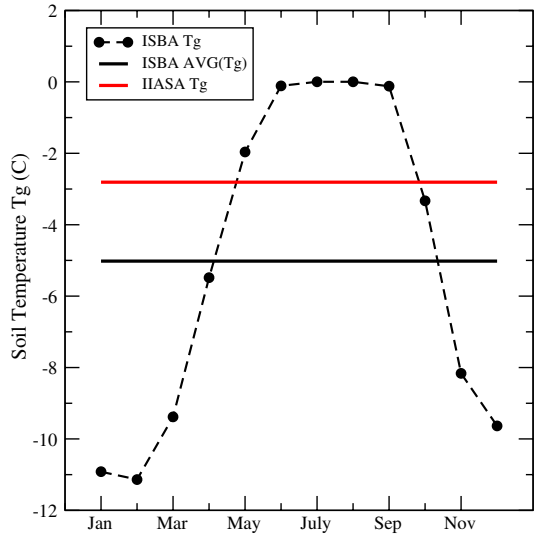

Fig. 2. The domain average soil temperatures, T_g: the 10-year average monthly ISBA values are represented by the dashed line, and the annual average is indicated using the solid black line.

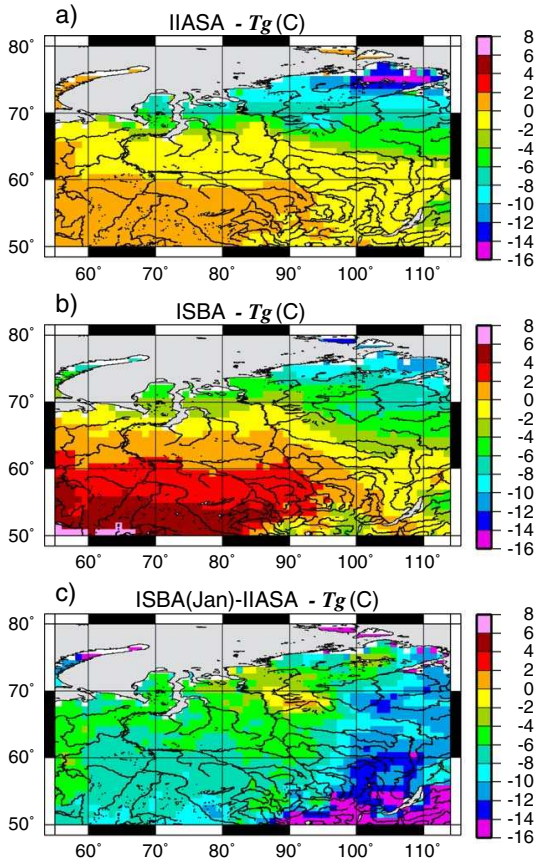

Fig. 3. The soil temperature, T_g, from the IIASA climatology (panel a), the annual average over 10 years from ISBA (panel b) simulated using the GSWP2 forcing, and the difference between ISBA (January) and IIASA (panel c).

cycle (which is obviously neglected when using the IIASA data set). The time-averaged uppermost soil temperature from ISBA is shown in Fig. 3b, together with $T_{g\,IIASA}$ (Fig. 3a). The spatial patterns are coherent, although the ISBA 0° (C) isotherm is slightly further to the north. Note that when the annually averaged $T_{g\ ISBA}$ is used within the retrieval algorithm, it is constrained to be less than or equal to the freezing point (as it represents the temperature at the base of the snowpack). However, this constraint is not required for the monthly $T_{g\,ISBA}$ because the values at all of the grid points are less than the freezing point from January through March.

Note that it is very important to bear in mind that $T_{g\,IIASA}$ represents the permafrost temperature, therefore it does not exceed the freezing point in Fig. 3a and it does not correspond to a fixed depth. In contrast, $T_{g\ ISBA}$ corresponds to a near surface value centered at a fixed depth (0.015 m), so some differences between the two fields are to be expected, especially in terms of the actual values. But in terms of the snow retrieval algorithm used in the current study, the $T_{g\ ISBA}$ is much more consistent with the snow–soil interface temperature than a permafrost temperature.

The difference between the January average $T_{g\ ISBA}$ and the time-invariant $T_{g\ IIASA}$ is shown in Fig. 3c. This shows that the wintertime $T_{g\ ISBA}$ values are generally cooler than the corresponding $T_{g\ IIASA}$ values, but in addition there is significant spatial variability in this difference. For example, the differences are relatively small over the Central Siberian plateau (several K at most), while they are quite large in the extreme eastern part of the domain (over 10 K). The differences in T_g shown in Fig. 3c should then result in significant differences in estimated snow thermal gradient (between ISBA and IIASA T_g) and therefore the snow depth (see Eq. (5)). Finally, it should be noted that there is very little in the way of validation data during the period covered by SSM/I measurements. In addition, the limited available data are at the point scale so that a quantitative T_g validation has not been undertaken for the current study: only a comparison with the spatial soil temperature distribution from IIASA has been done.

3.2. Snow climatology

3.2.1. Historical data

One of the main challenges for developing remote sensing based algorithms is validation, especially for relatively observation-sparse zones such as Siberia. Indeed, Chang et al. (2005) performed a statistical analysis which showed that one in-situ measurement within a 100 by 100 km region provides a comparison with an uncertainty of approximately 0.20 m (for a range of snow depth values between 0.015 and 0.454 m). In particular, GEA04 discussed the problem that local scale data is difficult to compare with large scale averages over Siberia for the time period considered herein, so that no comparison with local scale data is performed in the current study.

ETAC is a gridded data set comprised of snow depths averaged over an approximately 30-year window ending in the 1980s. The data comes from a myriad of sources with varying degrees of accuracy, and was manually edited and interpolated using relatively simple methods. As mentioned in Introduction, the ETAC data do not correspond to the period covered by the SSM/I data. In addition, the spatial distribution of the corresponding observation network sites is rather irregular and has a low density over this region.

3.2.2. GSWP2 climatologies

The GSWP2 offers the possibility of constructing a new gridded snow depth data set. The simulated SWE fields from multiple LSSs for the period from 1986 to 1995 were used to derive a SWE monthly climatology over Siberia (the domain is shown in Fig. 1). The LSS acronyms and the corresponding institutions responsible for the simulations are shown in Table 1. More information on the LSSs can be found in Dirmeyer et al. (in press). The obvious advantage of using a multi-model SWE is to reduce the influence of any one LSS, as differences between LSS simulated snow cover can be considerable for such climates (Schlosser et al., 1999).

A critical aspect of the simulated SWE is the input atmospheric forcing database. The GSWP2 provided forcing data for a series of sensitivity experiments in order to explore LSS sensitivity to different data sources. In this paper, SWE climatologies from three different experiments are used: the basic distinguishing features of the forcing data are shown in Table 2. The "B0" experiment corresponds to the GSWP2 default or control simulation. At the time of the writing of this paper, SWE results from 12 models were available.

Table 1
LSS acronyms and the corresponding names of the institutions which had submitted results to GSWP2 at the time of this study

LSS	Institution
BUCKET	Univ. of Tokyo, Japan
CLM-2	Univ. of Texas, Austin, USA
ISBA	Centre National de Recherches Météorologiques, Toulouse, France
LaD	Geophysical Fluid Dynamics Lab., Princeton, USA
MOSES	U.K. Met. Office, Exeter, UK
NOAH*	National Center for Env. Pred., Camp Springs, USA
NSIPP*	NASA Goddard, Greenbelt, USA
ORCHIDEE	Laboratoire de Météorologie Dynamique, Paris, France
SiBUCK	Univ. of Kyoto, Japan
SSiB*	Center for Ocean Land Atmosphere studies, Calverton, USA
SWAP*	Inst. of Water Problems, Moscow, Russia
VISA	Univ. of AZ, Tucson, USA

All 12 were used to construct the B0 SWE climatology. The LSS results used to construct the P1 and P3 climatologies are indicated using an *. Note that this list is not final: more LSSs have been added since the time of this study. See Dirmeyer et al. (in press) for more information on the LSSs and GSWP2.

Data from the NCEP-DOE reanalysis (Kanamitsu et al., 2002) were "hybridized" (corrected using observed and satellite based precipitation data) and "corrected" for gauge under-catch, which can be significant at high latitudes (see Dirmeyer et al., in press for further details). The "P1" experiment uses the ERA40 (Betts & Beljaars, 2003) data set from the European Centre for Medium Range Weather Forecasts (ECMWF). This experiment was selected for the current study due to the widespread use of ERA40 within the hydrological and land surface modeling communities: no corrections were applied. The final data set used herein comes from the "P3" experiment. This resembles the B0 experiment, except that the gauge corrections have not been applied. Indeed, the corrections in B0 result in a significant augmentation of precipitation, notably in northern latitudes, so it is of interest to explore the impact of their removal. At the time of the writing of this paper, SWE data from four LSSs were available for experiments P1 and P3, and the corresponding LSSs are indicated in Table 1 (using an asterisk).

The annual average SWE for the three SWE climatologies are shown over the domain in Fig. 4. General agreement in terms of the spatial distribution is seen, although the SWE values are considerably larger in the B0 experiment than for P1 and P3. In terms of common features, there is a very large spatial gradient in snow cover depth, with the largest depths being associated with the Ural mountain range in the north-eastern part of the domain, and a second maximum which is located along the western part of the Central Siberian Plateau near the center of the domain. Considerably lower SWE values

Table 2
Acronyms for the GSWP2 experiments used to compute the three 10-year monthly SWE climatologies which are used for the evaluation of the various retrievals in the current study

GSWP2 experiment	Reanalysis	Hybridization	Gauge corrections
B0	NCEP-DOE	Yes	Yes
P1	ERA40	No	No
P3	NCEP-DOE	Yes	No

The sources and corrections for the input atmospheric forcing data are shown.

are located in the eastern and especially southern parts of the domain.

The 10-year domain-averaged monthly SWE time series for the each of the LSSs are shown in Fig. 5 for each of the three climatologies. The multi-model averages are highlighted using thick lines, and these three multi-model averages are used as proxies to evaluate the snow depth retrievals. The ratio of the square root of the inter-model variance to the model-average SWE shown in Fig. 5 ranges from 9% in January and February, to 12% in March for the B0 experiment, so that the LSSs have a fairly reasonable agreement through this time period (there is also similar good agreement among the LSSs used in the P1 and

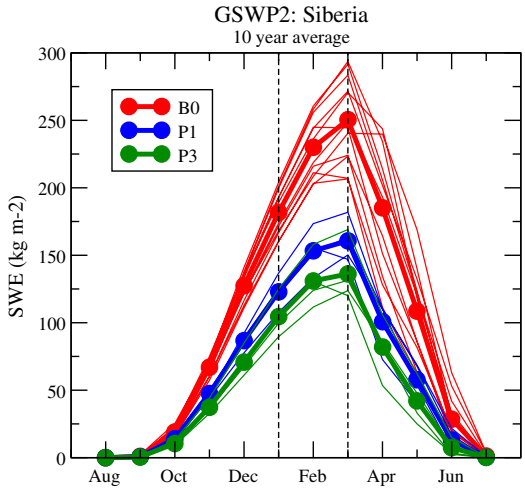

Fig. 5. The GSWP2 10-year average monthly SWE averaged over the domain. Each thin curve corresponds to a single LSS, while the heavy lines correspond to the three multi-model averages (referred to as the GSWP2 B0, P1 and P3 SWE climatologies in the text). The vertical dashed lines enclose the time period covered in the current study.

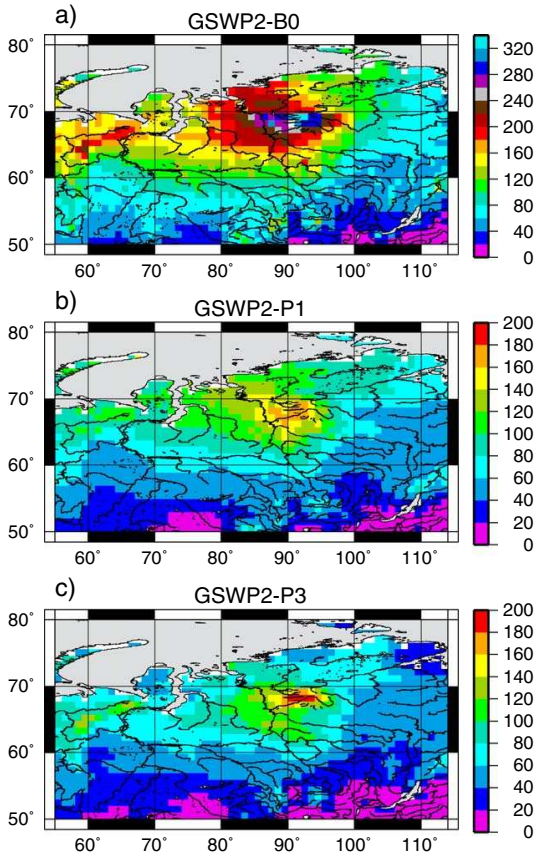

Fig. 4. The 10-year multi-model GSWP2 average SWE (kg m^{-2}) for experiments B0, P1 and P3 (panels a, b, and c, respectively) over central Siberia.

P3 climatologies). After March, the model differences are enhanced owing to the strong dependence of simulated snow melt processes on the differing parameterizations for turbulence (and surface roughness), snow albedo and FSCA (see Slater et al., 2001 for a discussion on LSS snow parameterizations). In the current study, only the period from January through March is examined.

4. Results

Four snow depth retrievals were done for the current study (Fig. 6). The acronyms corresponding to each retrieval are given in Table 3. The snow depth was retrieved for all four methods over the time period from 1987 to 1995 using the same SSM/I data set. The first experiment (denoted ST) consisted in computing the snow depth using the static algorithm (Chang et al., 1987), which only uses the spectral gradient from SSM/I as input (Eq. (1)). The remaining three retrievals were done using the dynamic algorithm from GEA04 (Eq. (5)) using the NCEP 2m air temperature (T_a) and SSM/I data as standard inputs, but three different soil temperature (T_g) data sets.

The first of the dynamic retrievals used the Russian IIASA time-invariant soil permafrost temperature data set (DR), the second used the ISBA time-invariant simulated surface soil temperature data (DI), and the third used the monthly varying ISBA temperatures (DIM). Note that for the current study, the DIM soil temperature annual cycle represents a climatological average for the entire 10 year simulation period. It is important to reiterate here that the IIASA climatology is constant in time, whereas the DIM soil–snow interface temperatures have a significant month-to-month variability (the TGI in the retrieval algorithm directly impacts the snow depth retrieval, and it is

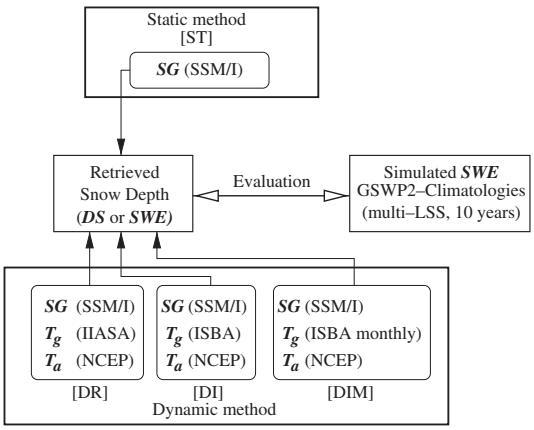

Fig. 6. A schematic illustrating the four snow depth retrievals described in this study and the corresponding input data sets. See Table 3 for a definition of the retrieval acronyms. The retrieved snow depths are evaluated using three multi-LSS snow depth climatologies from GSWP2. The inputs are the 2 m air temperature (T_a), the soil–snow interface temperature (T_g), and the spectral gradient from SSM/I (SG). See the text for further definitions.

significantly modified using a monthly varying T_g verses a constant value). Because of the ambiguity in distinguishing between snow depth and SWE in the aforementioned snow retrieval algorithms, the current study focuses on the ability of the algorithms to reproduce the spatial variability of the snow (as opposed to the actual snow depth or SWE values).

Previous studies using the dynamic algorithm converted the retrieved snow depth, D, to SWE using

$$\mathrm{SWE_r}(x,t) = \overline{\rho}_s D_r(x,t) \quad (6)$$

where the subscript r represents a retrieval (ST, DR, DI or DIM), and $\overline{\rho}_s$ corresponds to a nominal constant (space and time) snow density of 300 kg m^{-3}. It would be more realistic to consider (if possible) the spatial and temporal variations in ρ_s, which can obviously have a significant impact on the estimated SWE. The remaining part of this section is split into two sub-sections: in Section 4.1, the comparison between the GSWP2 SWE climatologies and the corresponding values using the retrieved D and constant density (Eq. (6)) is presented (representing the standard approach). In Section 4.2, some of the same results are presented, but the constant snow density value is replaced by GSWP2 snow density (which varies in space for each month) when computing the retrieved SWE.

4.1. Constant density

The SWE January climatologies estimated from the four retrieval algorithms are shown in Fig. 7e–h, along with the GSWP2 SWE climatologies for January in (Fig. 7b–d). The GSWP2 1 × 1° gridded elevation is also shown as a reference in Fig. 7a. Note that as discussed in Section 3.2.2, the B0 SWE values are considerably larger than those from the P1 and P3 experiments (and the retrieved values) even though the spatial distribution is similar. In the following discussion, the comparison therefore focuses on the P1 and P3 SWE values.

Comparison between the static (ST) algorithm SWE (Fig. 7e) and the GSWP2 P1 and P3 climatologies (Fig. 7c–d) reveals a great deal of inconsistency. The regions of ST maximum SWE are generally located in the eastern, coldest part of the domain. The baseline dynamic retrieval (DR: Fig. 7f) shows a significant improvement in the spatial distribution of SWE relative to the GSWP2 climatology compared to the ST retrieval, as areas with the largest SWE values (notably the Central Siberian Plateau) are more consistent. However, in contrast to the GSWP2 climatology, DR has SWE maxima located in the northeastern, east-central, and in southeastern parts of the domain.

The DI SWE values are shown in Fig. 7g. Not surprisingly, the retrieved SWE values have a very similar spatial distribution to the DR values since the annually averaged ISBA soil temperature spatial distribution is very similar to that of IIASA (see Fig. 3a–b). The DI SWE generally tends to be slightly larger since the ISBA T_g values tend to be slightly warmer which enhances the predicted snow depth owing to the larger thermal gradient (Eq. (5)).

The DIM SWE field is shown in Fig. 7h, and the spatial distribution of this retrieval compares best with the GSWP2 P1 and P3 SWE climatologies: the two SWE maximum have a more consistent location and spatial coverage, and the lowered SWE values in the southeastern part of the domain are in better agreement than those for the other three retrievals.

A simple statistical comparison is shown in Fig. 8 where each row of the array of scatter plots corresponds to a winter month (January through March), and each column corresponds to a retrieval method. In each scatter plot, the GSWP2 P3 climatological values are shown along the abscissa, while the retrieved values are located along the ordinate. The corresponding correlation coefficients are shown in the lower right corner of each panel in Fig. 8, and the corresponding root mean square (RMS) error, bias, and average SWE are provided in Table 4. Clearly, the static, ST, retrieval performs poorly over this region for the considered time period. The DR and DI (dynamic) retrievals give improved results, in agreement with the results of GEA04 which show the value of using ancillary information (such as T_a and T_g) in the retrievals. But, it is evident that there is relatively little value in using the annually averaged ISBA T_g values compared to the Russian climatology (indeed, the differences between $T_{g\ \mathrm{IIASA}}$ and the annual average $T_{g\ \mathrm{ISBA}}$ shown in Figs. 2 and 3a–b have little impact). However, there is significant improvement when the monthly T_g

Table 3
Acronyms used to designate each snow depth retrieval algorithm used in the current study

Retrieval	Definition
ST	Static
DR	Dynamic using IIASA T_g climatology
DI	Dynamic using ISBA T_g climatology
DIM	Dynamic using ISBA monthly varying T_g climatology

See Fig. 6 for a schematic describing the inputs and outputs of the algorithms.

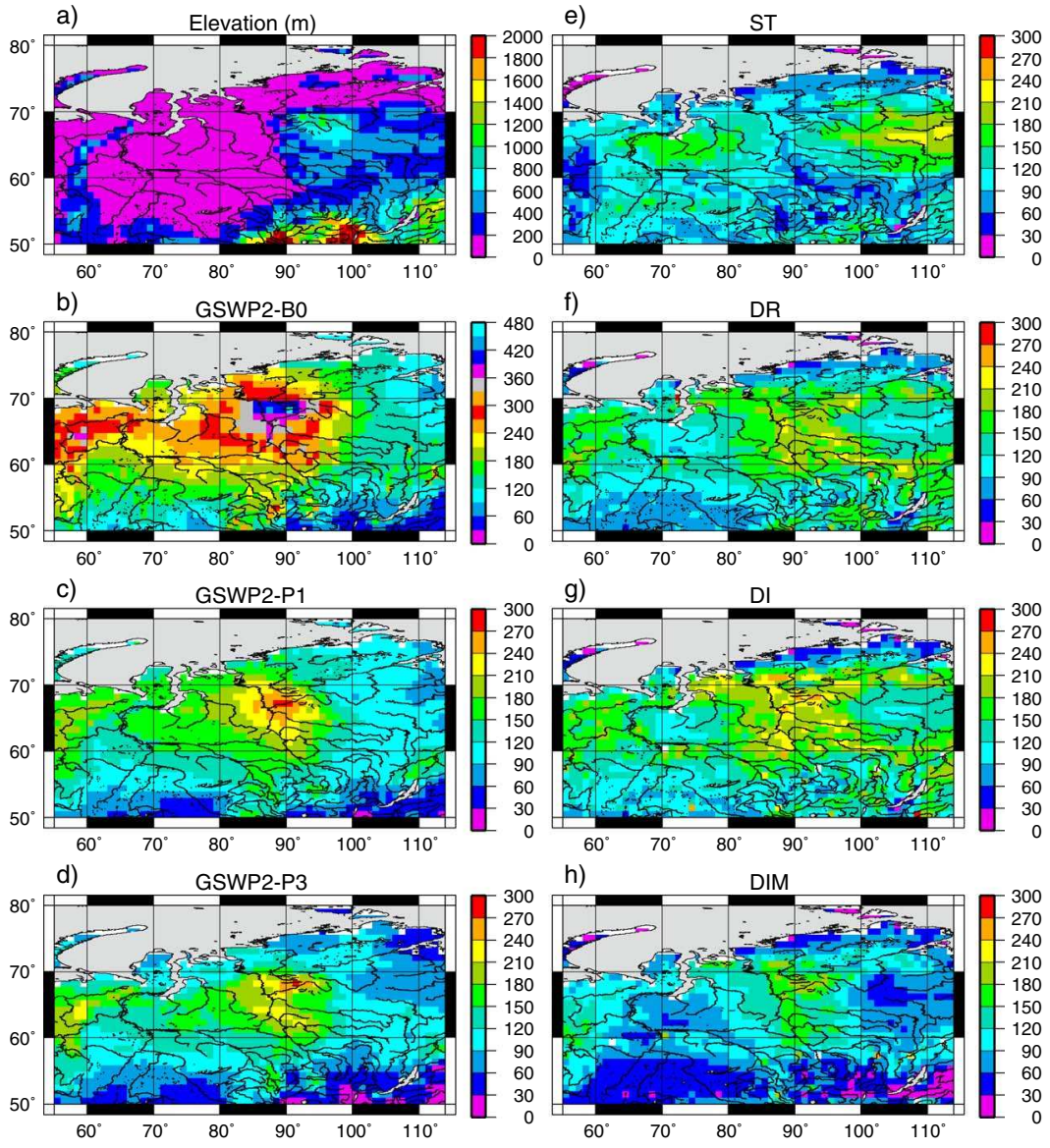

Fig. 7. The SWE (kg m^{-2}) climatology comparison for January. The GSWP2 average elevation (m) is shown in panel a as a reference (all elevations exceeding 2000 m are indicated by dark red). The SWE for GSWP2 experiments B0, P1 and P3 are shown in panels b, c and d, respectively. The SWE for the ST, DR, DI, and DIM retrievals are shown in panels e, f, g and h, respectively (see Table 3 for the retrieval acronym definitions). The corresponding color scales are to the right of each panel.

variability is considered (DIM retrieval), especially in terms of the correlation.

For all of the retrievals, the quality of the statistical relationships degrade in time. This degradation is mainly related to two factors. First, the relatively simple retrieval algorithm is compromised late in the season owing to ice layer formation, the presence of snow melt (liquid water), and the reduction in snow grain growth (arising from thermal gradients). Second, there is an increasing inter-model spread in the GSWP2 SWE climatology in time owing to scheme differences which are enhanced as the snow begins to melt (see Fig. 5).

Finally, it is of interest to compare the statistics between the DIM retrieval and the three GSWP2 SWE climatologies: a summary is shown in Table 5. The correlation coefficients for each month are quite similar between the schemes, although a slightly better agreement is seen for the P1 and P3 climatologies. This means that the overall spatial distributions

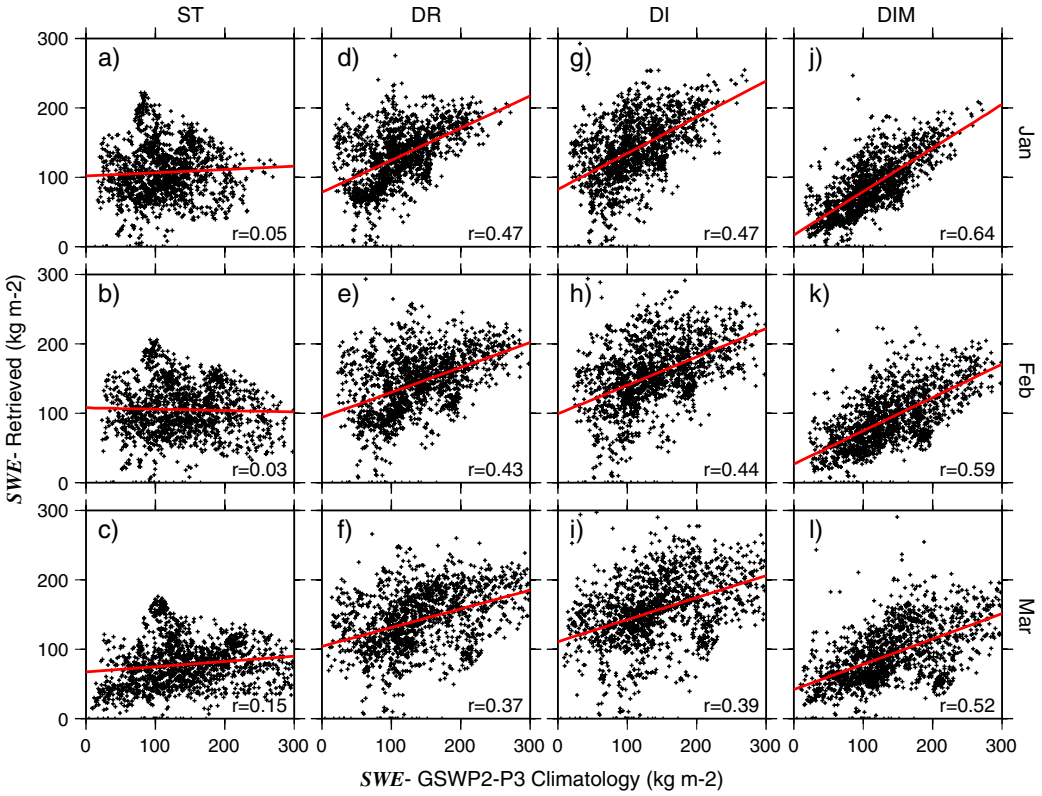

Fig. 8. Scatter plots (corresponding to the data shown in Fig. 7. The relation between the retrieved (abscissa) and the GSWP2 P3 climatological (ordinate) SWE are shown. Each row corresponds to a month, and each column corresponds to a retrieval (see Table 3 for the acronym definitions). The linear regression fits (solid lines) are shown. The correlation coefficients (denoted by r) are shown in the lower right-hand corner of each panel.

are similar. However, the bias and RMS errors considerably larger for the B0 experiment, and are the lowest for P3. This implies that the P3 climatology has typical SWE magnitudes which are the most similar to those from the ETAC climatology (again, assuming a constant snow density) since the dynamic algorithm was calibrated by GEA04 using ETAC.

Table 4
Statistical results of the retrievals compared to the GSWP2-P3 SWE climatology (see Fig. 8). The RMS, bias and average snow water equivalent ($\overline{\mathrm{SWE}}$) are in units of kg m^{-2}

Retrieval	Month	Corl.	RMS	Bias	SWE
ST	Jan	0.05	60.06	3.44	107.05
ST	Feb	−0.03	78.51	33.17	105.15
ST	Mar	0.15	97.91	66.03	78.17
DR	Jan	0.47	51.23	−19.02	129.51
DR	Feb	0.43	58.02	−5.53	143.86
DR	Mar	0.37	68.31	1.08	143.12
DI	Jan	0.47	58.17	−29.58	140.07
DI	Feb	0.44	62.69	−17.62	155.95
DI	Mar	0.39	71.24	−12.44	156.63
DIM	Jan	0.64	45.50	24.37	86.12
DIM	Feb	0.59	66.84	45.19	93.13
DIM	Mar	0.52	78.28	49.79	94.41

See Table 3 for a description of the retrieval methods.

4.2. Variable density

The GSWP2 SWE is given by

$$\mathrm{SWE}_{\mathrm{G}}(x,t) = \rho_{\mathrm{G}}(x,t) D_{\mathrm{G}}(x,t) \tag{7}$$

where the subscript G indicates a GSWP2 climatology (B0, P1 or P3). The impact of using a constant snow density on the retrieved SWE values is investigated in this section by replacing

Table 5
Statistical results of the DIM retrieval compared to the three GSWP2 SWE climatologies

GSWP2-climatology	Month	Corl.	RMS	Bias
B0	Jan	0.61	114.89	97.53
B0	Feb	0.55	161.53	139.28
B0	Mar	0.50	189.38	158.09
P1	Jan	0.65	58.21	43.90
P1	Feb	0.58	84.13	68.90
P1	Mar	0.50	97.85	76.12
P3	Jan	0.64	45.50	24.37
P3	Feb	0.59	66.84	45.19
P3	Mar	0.52	78.28	49.79

The correlation, RMS, and bias are in units of kg m^{-2}. The monthly average snow water equivalents ($\overline{\mathrm{SWE}}$) (for the DIM retrieval) can be found in Table 4.

$\bar{\rho}_s$ in Eq. (6) by $\rho_G(x,t)$. It is important to note that this is analogous to comparing the directly retrieved snow depths, D_r, to D_G. This allows the examination of the impact of using a spatially and temporally varying snow density.

The scatter plots of the retrieved verses GSWP2 P3 climatological SWE values are shown in Fig. 9 (the corresponding correlation coefficients are shown in the lower right hand corner of each panel). Thus, the only difference between these results and those shown in Fig. 8 is the use of a spatially and temporally varying snow density. The correlations for the DI, DR and DIM retrievals are all in much better agreement with the climatological values in January and February, while in March there is almost no improvement. This underscores the difficulties in using such an algorithm during months when snow melt begins, which is the subject of ongoing research.

The bias and RMS errors (not shown) are slightly larger, primarily owing to the fact that the spatial averages of ρ_G vary between approximately 191 (January) and 231 (March) kg m^{-3} for the months considered (lower than the constant value $\bar{\rho}_s$, therefore leading to lower SWE values for the same retrieved snow depths). But again, the goal of this study is to better resolve the spatial distribution of the retrieved D or SWE, so the focus is on the improvement in the correlation. The RMS and bias errors will be reduced once a calibration of α (in Eq. (4)) has been undertaken. From these results, it is obvious that information on the spatial distribution and the temporal evolution of temperature and density add value to the quality of the final product.

5. Conclusions and perspectives

This study has reaffirmed one of the main results of GEA04, which was that the inclusion of ancillary data, such as soil temperatures, into a satellite data-based snow retrieval algorithm can significantly improve the results. The current study went a step further and revealed the importance of including the monthly soil temperature variation into the retrieval, which improved results compared to a series of model-based climatologies. The GSWP2 experiment provided the atmospheric forcing data which facilitated the simulation of a new soil temperature climatology using the ISBA LSS. The ISBA T_g simulation in the current study differs from the GSWP2 default ISBA simulation (which comprises one of the 12 LSS data sets used in the climatological B0 SWE) in that it was done using the multi-level soil and snow scheme options, along with a modification to the fractional snow covered area parameterization in order to better represent the temperature at the base of the snowpack.

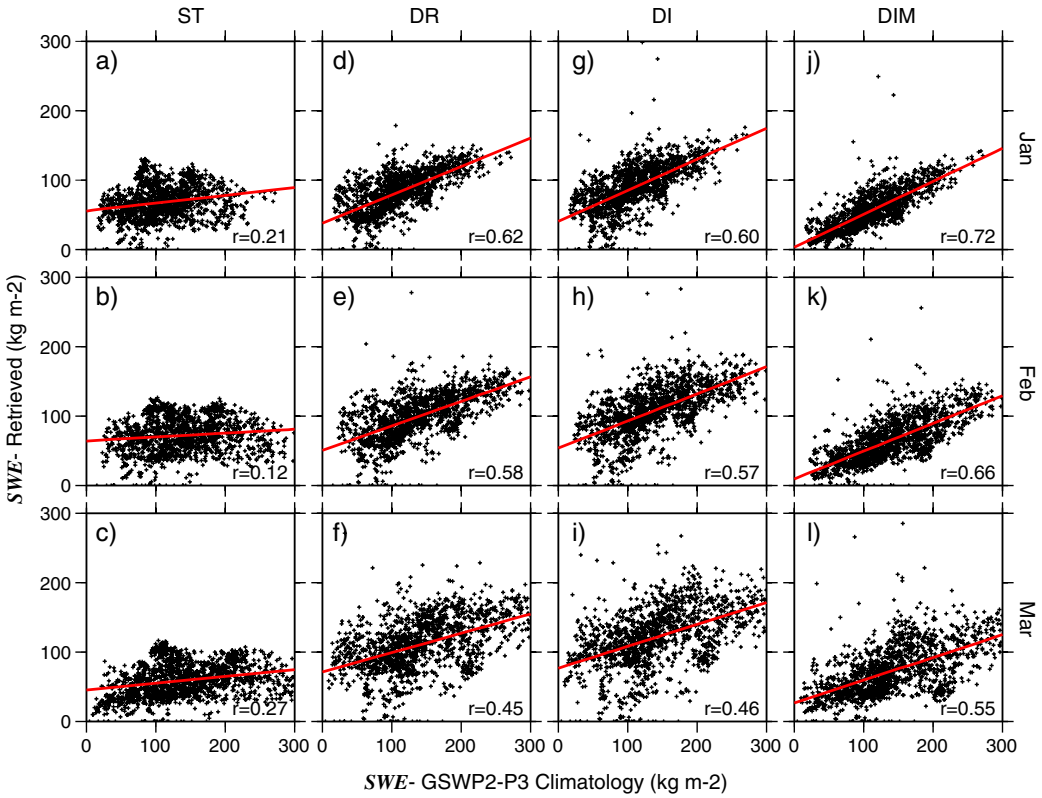

Fig. 9. As in Fig. 8, but with the retrieved SWE values computed using a snow density climatology computed from GSWP2 P3 (as opposed to using a constant density value of 300 kg m^{-3}). Note that the correlations are equivalent to a direct comparison between the retrieved and the GSWP2 P3 snow depths.

Three SWE climatologies were constructed using an ensemble of results from between 4 and 12 state-of-the-art LSSs. The models were forced using the best available land surface and atmospheric forcing data (based on reanalysis data, and also hybridized using observational data), so that the resulting simulations can be considered as a land-surface analogue of atmospheric reanalyses. These simulations at a 1° spatial resolution encompass the same time period as the SSM/I data, so that the data used to evaluate the retrieval algorithm are coherent with the satellite data input. This is important as climatological data such as ETAC covers a long-term period ending before the satellite data used in this study was recorded, and it is possible that it is not representative of the time period covered in this study owing to recent trends in terms of atmospheric conditions, notably the snowfall spatial and temporal distributions.

The SWE fields are much more significant to hydrologists and hydrometeorologists than the D fields. However, the limits in assuming a simple constant density, which is the general assumption used in many such algorithms, were shown. Here it is proposed that similar such algorithms can be evaluated by comparing the retrieved snow depths with the observed or simulated snow depth information, and then conversion to SWE can be made using observed or simulated snow density values from a climatology.

No calibration of the SWE or D amounts (in terms of the parameter α: see Eq. (5)) has been attempted using the GSWP2 climatologies for the current study. The P3 experiment SWE values compare the best with the retrieval algorithm, which has been calibrated using the ETAC climatology, however it is difficult at this stage to determine which GSWP2 climatology best represents "reality" over this region and time period. Several other experiments have been performed by the LSSs within GSWP2 which represent additional perturbations to the forcing data (applying different hybridization methods, correction factors, and model reanalysis products). An even more robust climatologically based SWE could be computed by incorporating these simulations and taking an average of the ensemble. In addition, if the GSWP2 is able to establish a single forcing database as the best over this region, then the corresponding climatology will be given preference in our analysis and might then be used to tune the magnitudes of the retrieved SWE or D values.

There are two ongoing research problems which are currently being addressed related to this study. First, the inter-annual variability of the DR snow depth retrieval has recently been examined, and it was found to be correlated with the observed discharge data for the Ob basin (Grippa et al., 2005). The next step is to explore the impact of the monthly and yearly varying soil temperatures on the retrieved snow depths compared to the discharge. Second, because of the promising results in terms of the improvement in the SWE retrieval in the current study owing to the T_g monthly climatology, work is currently underway to examine the impact of monthly varying model-derived T_g on SWE retrieved over other regions in the northern hemisphere (notably North America, where there is a more dense network of snow observation and soil temperature sites).

Acknowledgements

This work has been supported by the SIBERIA-II project within the EC 5th framework. We are thankful to A.V. Koureav for extracting the NCEP and SSM/I data, and to M. Aubin-Lecomte for assisting with running the algorithm and post-processing t'he data. Thanks to Dr. Paul Dirmeyer and Dr. Naota Hanasaki for making the GSWP2 model results available for this study, and to all of the GSWP2 participants for taking considerable time and energy to perform the simulations. Finally, we wish to thank three reviewers for their comments, and in particular one reviewer who made proposals which significantly improved this paper. Kevin Kerrigan was supported through a CNES grant during his stay at LEGOS. All of the figures in this paper using maps were created using the free GMT software package.

References

Armstrong, R. L., Knowles, K. W., Brodzik, M. J. & Hardman, M. A. (1994, updated 2003). *DMSP SSM/I Pathfinder daily EASE-Grid brightness temperatures*. Boulder, CO, National Snow and Ice Data Center (Digital media and CD-ROM).

Bamzai, A. S., & Shukla, J. (1999). Relation between Eurasian snow cover, snow depth, and the Indian summer monsoon: An observational study. *Journal of Climate*, *12*, 3117−3132.

Betts, A. K., & Beljaars, A. C. M. (2003). ECMWF ISLSCP-II near surface data set from ERA-40. ERA-40 Project Report Series 8, [Available from the European Centre for Medium Range Weather Forecasts, Shinfield Park, Reading, Berkshire RG2 9AX, England], 31 pp.

Boone, A., & Etchevers, P. (2001). An intercomparison of three snow schemes of varying complexity coupled to the same land-surface model: Local scale evaluation at an Alpine site. *Journal of Hydrometeorology*, *2*, 374−394.

Boone, A., Masson, V., Meyers, T., & Noilhan, J. (2000). The influence of the inclusion of soil freezing on simulations by a soil–vegetation–atmosphere transfer scheme. *Journal of Applied Meteorology*, *9*, 1544−1569.

Boone, A., et al. (2004). The Rhone-aggregation land surface scheme intercomparison project: An overview. *Journal of Climate*, *17*, 187−208.

Bowling, L. C., et al. (2002). Simulation of high latitude hydrological processes in the Torne-Kalix basin: PILPS Phase-2(e): 1. Experiment description and summary intercomparisons. *Global and Planetary Change*, *38*, 1−30.

Chang, A. T. C., Foster, J. L., & Hall, D. K. (1987). Nimbus-7 SMMR derived global snow cover parameters. *Annals of Glaciology*, *9*, 39−44.

Chang, A. T. C., Foster, J. L., & Hall, D. K. (1990). Satellite sensor estimates of Northern Hemisphere snow volume. *International Journal of Remote Sensing*, *11*, 167−171.

Chang, A. T. C., Josb erger, E. G., Armstrong, R. L., Kelly, R., Foster, J. L., Hall, D. K., et al. (2005). Analysis of ground-measured and passive microwave derived snow depth variations in mid-winter across the Northern Great Plains. *Journal of Hydrometeorology*, *6*, 20−33.

Cherkauer, K. A., & Lettenmaier, D. P. (1999). Hydrologic effects of frozen soils in the upper Mississippi River basin. *Journal of Geophysical Research*, *104* (D16), 19599−19610.

Dirmeyer, P. A., Gao, X., Zhao, M., Guo, Z., Oki, T., Hanasaki, N., et al. (in press). The Second Global Soil Wetness Project (GSWP2): Multi-model analysis and implications for our perception of the land surface. *Bull. Amer. Meteor. Soc.*

Douville, H. (2004). Relevance of soil moisture for seasonal atmospheric predictions: Is it an initial value problem? *Climate Dynamics*, *22*, 429−446.

Etchevers, P., et al. (2005). Validation of the energy budget of an alpine snowpack simulated by several snow models (SNOWMIP project). *Annals of Glaciology*, *38*, 150−158.

Foster, J. L., Chang, A. T. C., & Hall, D. K. (1997). Comparison of snow mass estimates from a prototype passive microwave snow algorithm, a revised algorithm and snow depth climatology. *Remote Sensing of Environment*, *62*, 132−142.

Foster, D. J., & Davy, R. D. (1988). *Global snow depth climatology, USAFETAC/TN-88/006.* Illinois: Scott Air Force Base, 48 pp.

Giard, D., & Bazile, E. (2000). Implementation of a new assimilation scheme for soil and surface variables in a global NWP model. *Monthly Weather Review*, *128*, 997−1015.

Grippa, M., Mognard, N. M., & Le Toan, T. (2005). Comparison between the interannual variability of snow parameters derived from SSM/I and the Ob river discharge. *Remote Sensing of Environment*, *98*(1), 35−44.

Grippa, M., Mognard, N., Le Toan, T., & Josberger, E. (2004). Siberia snow depth climatology derived from SSM/I data using a combined dynamic and static algorithm. *Remote Sensing of Environment*, *93*, 30−41.

Habets, F., Boone, A., & Noilhan, J. (2003). Simulation of a Scandinavian basin using the diffusion transfer version of ISBA. *Global and Planet Change*, *38*, 137−149.

Hall, A. (2004). The role of surface albedo feedback in climate. *Journal of Climate*, *17*, 1150−1568.

Hollinger, J. P., Peirce, J. L., & Poe, G. A. (1990). SSM/I instrument evaluation. *IEEE Transactions on Geoscience and Remote Sensing*, *28*(5), 781−790.

Josberger, E. G., & Mognard, N. (2002). A passive snow depth algorithm with a proxy for snow depth metamorphism. *Hydrological Processes*, *16*, 1557−1568.

Kalnay, E., et al. (1996). The NCEP/NCAR 40-year reanalysis project. *Bulletin of the American Meteorological Society*, *77*(3), 437−471.

Kanamitsu, M., Ebisuzaki, W., Woollen, J., & Yang, S. -K. (2002). NCEP/DOE AMIP-II reanalysis (R-2). Bull. *Bulletin of the American Meteorological Society*, *83*, 1631−1643.

Kelly, R. E. J., & Chang, A. T. C. (2003). Development of a passive microwave global snow depth retrieval algorithm for Special Sensor Microwave Imagery (SSM/I) and Advanced Microwave Scanning Radiometer-EOS (AMSR-E) data. *Radio Science*, *38*(4), 1−11.

Kelly, R. E. J., Chang, A. T., Tsang, L., & Foster, J. L. (2003). A prototype AMSR-E global snow area and snow depth algorithm. *IEEE Transactions 29 on Geoscience and Remote Sensing*, *41*(2), 1−13.

Masson, V., Champeaux, J. -L., Chauvin, F., Meriguet, C., & Lacaze, R. (2003). A global database of land surface parameters at 1-km resolution in meteorological and climate models. *Journal of Climate*, *16*, 1261−1282.

Mognard, N., & Josberger, E. G. (2002). Northern Great Plains 1996/97 seasonal evolution of snowpack parameters from satellite passive microwave measurements. *Annals of Glaciology*, *34*, 15−23.

Noilhan, J., & Mahfouf, J. -F. (1996). The ISBA land surface parameterization scheme. *Global and Planet Change*, *13*, 145−159.

Pavlov, A. V. (1994). Current change of climate and permafrost in the Arctic and subarctic of Russia. *Permafrost Periglacial Processes*, *5*, 101−110.

Peterson, B. J., Holmes, R. M., McClelland, J. W., Vorosmarty, C. J., Lammers, R. B., Shiklomanov, A. I., et al. (2002). Increasing river discharge to the Arctic Ocean. *Science*, *298*, 2171−2173.

Rousset, F., Habets, F., Gomez, E., Le Moigne, P., Morel, S., Noilhan, J., et al. (2004). Hydrometeorological modeling of the Seine basin using the SAFRAN–ISBA–MODCOU system. *Journal of Geophysical Research*, *109*, D14105, doi:10.1029/2003 JD004 403.

Serreze, M. C., Bromwich, D. H., Clark, M. P., Etringer, A. J., Zhang, T., & Lammers, R. B. (2003). The large-scale hydro-climatology of the terrestrial Arctic drainage system. *Journal of Geophysical Research*, *108*, 8160, doi:10.1029/2001JD000919.

Slater, A. G., et al. (2001). The representation of snow in land surface schemes: Results from PILPS 2(d). *Journal of Hydrometeorology*, *2*, 7−25.

Schlosser, C. A., et al. (1999). Simulations of a boreal grassland hydrology at Valdai, Russia: PILPS phase 2(d). *Monthly Weather Review*, *128*, 301−321.

Stolbovoi, V., & McCallum, I. (2002). *CD-ROM Land resources of Russia*. Laxenburg, Austria: International Institute for Applied System Analysis and the Russian Academy of Science.

Ye, H., & Ellison, M. (2003). Changes in transitional snowfall season length in northern Eurasia. *Geophysical Research Letters*, *30*(5), 1252, doi:10.1029/2003GL016873.

THE AMMA LAND SURFACE MODEL INTERCOMPARISON PROJECT (ALMIP)

BY AARON BOONE, PATRICIA DE ROSNAY, GIANPAOLO BALSAMO, ANTON BELJAARS, FRANCK CHOPIN, BERTRAND DECHARME, CHRISTINE DELIRE, AGNES DUCHARNE, SIMON GASCOIN, MANUELA GRIPPA, FRANÇOISE GUICHARD, YEUGENIY GUSEV, PHIL HARRIS, LIONEL JARLAN, LAURENT KERGOAT, ERIC MOUGIN, OLGA NASONOVA, ANETTE NORGAARD, TRISTAN ORGEVAL, CATHERINE OTTLÉ, ISABELLE POCCARD-LECLERCQ, JAN POLCHER, INGE SANDHOLT, STEPHANE SAUX-PICART, CHRISTOPHER TAYLOR, AND YONGKANG XUE

A multimodel comparison of the performance of land surface parameterization schemes increases understanding of the land–atmosphere feedback mechanisms over West Africa.

The West African monsoon (WAM) circulation modulates the seasonal northward displacement of the intertropical convergence zone (ITCZ). It is the main source of precipitation over a large part of West Africa. However, predominantly relatively wet years during the 1950s and 1960s were followed by a much drier period during the 1970s and 1990s. This extreme rainfall variability corresponds to one of the strongest interdecadal signals on the planet over the last half-century. There is an urgent need to better understand and predict the WAM, because social stability in this region depends to a large degree on water resources. The economies are primarily agrarian, and there are issues related to food security and health. In addition, there is increasing pressure on the already limited water resources in this region, owing to one of the most rapidly increasing populations on the planet.

Numerous researchers over the last three decades have investigated the nature of the extreme rainfall variability (e.g., Nicholson 1980; Le Barbé et al. 2002). It has been shown that a significant part of the interannual variability can be linked to sea surface (sfc) temperature anomalies (e.g., Folland et al. 1986; Fontaine and Janicot 1996), but there is also evidence that land surface conditions over West Africa make a significant contribution to this variability (e.g., Nicholson 2000; Philippon et al. 2005).

Importance of the land–atmosphere interactions on the WAM. The monsoon flow is driven by land–sea thermal contrast. The atmosphere–land surface interactions are modulated by the magnitude of the associated north–south gradient of heat and moisture in the lower atmosphere (Eltahir and Gong 1996). The links between land surface processes and the WAM have been demonstrated in numerous numerical studies using global climate models (GCMs) and regional-scale atmospheric climate models (RCMs) over the last several decades. Charney (1975) were one of the first set of researchers to use a coupled land surface–atmosphere model to demonstrate a proposed positive feedback mechanism between decreasing vegetation cover and the increase in drought conditions across the Sahel region of western Africa. Numerous modeling studies since have examined the influence of the land surface on the WAM in terms of surface albedo (e.g., Sud and Fennessy 1982; Laval and Picon 1986), the vegetation spatial distribution (e.g.,

Xue and Shukla 1996; Xue et al. 2004; Li et al. 2007), and the soil moisture (e.g., Walker and Rowntree 1977; Cunnington and Rowntree 1986; Douville et al. 2001). However, interpretation of the results, from any one of such studies, must be tempered by the fact that there are substantial discrepancies in African land–atmosphere coupling strength among current state-of-the-art GCMs (Koster et al. 2002).

There is also a need to study and provide estimates of changes in rainfall variability resulting from predicted global climate change. Indeed, studies using GCMs have indicated that the impact in this region could be further amplified, owing to surface anthropogenic factors such as clearing the land of natural vegetation for crops and overgrazing (e.g., Xue et al. 2004). The above-mentioned factors will not only affect the atmosphere but also the regional-scale hydrology in terms of changes in runoff regimes. This, in turn, would impact the quantity of water stored in surface reservoirs and the recharge of local and regional water tables. However, it should be noted that considerable progress is needed in order to develop reliable estimations of land–atmosphere impacts for GCM climate scenarios. A recent study examining the performance of GCMs within the Intergovernmental Panel on Climate Change (IPCC) framework showed that models have significant problems simulating key aspects of the WAM for the present climate. Even the GCMs that show some skill produce considerably different West African climatologies at the end of this century (Cook and Vizey 2006).

Improving models in order to better understand and predict the WAM. The deficiencies, with respect to modeling the African monsoon, arise from both the paucity of observations at sufficient space–time resolutions, and because of the complex interactions of the relevant processes between the biosphere, atmosphere, and hydrosphere over this region. The African Monsoon Multidisciplinary Analysis (AMMA) has organized comprehensive activities in data collection and modeling to further increase our understanding of the relevant processes, in order to improve prediction of the WAM (Redelsperger et al. 2006). In terms of large-scale atmospheric multimodel initiatives, the AMMA Model Intercomparison Project (MIP; Hourdin et al. 2010) intercompares GCMs and RCMs over a meridional transect in West Africa, focusing on seasonal prediction. The West African Monsoon Modeling and Evaluation (WAMME) project utilizes such models to address issues regarding the role of ocean–land–aerosol–atmosphere interactions on WAM development (Xue et al. 2009, manuscript submitted to *Climate Dyn.*). The modeling of the land surface component of the WAM is being addressed by the AMMA Land Surface Model (LSM) Intercomparison Project (ALMIP), which is the focus of this paper.

Land surface modeling initiatives. In recent years, there have been a number of LSM intercomparison projects on an international level. In particular, the Project for the Intercomparison of Land-Surface Parameterization Schemes (PILPS) has increased the understanding of LSMs, and it has lead to many model improvements. In phase 2 of PILPS (Henderson-Sellers et al. 1995), LSMs were used in so-called offline mode (i.e., the LSM is uncoupled from an atmospheric model and is therefore driven using prescribed atmospheric forcing either from observations, satellite products, atmospheric model data, or some combination of those three sources), and the resulting simulations were compared to observational data. The first attempt by PILPS to address LSM behavior at a regional scale was undertaken in PILPS-2c (Wood et al. 1998). The Global

AFFILIATIONS: Boone, Decharme, and Guichard—GAME-Centre National de Recherche Météorologique, Toulouse, France; De Rosnay, Balsamo, and Beljaars—European Centre for Medium-Range Weather Forecasts, Reading, United Kingdom; Chopin, Orgeval, and Polcher—IPSL, Laboratoire de Météorologie Dynamique, Paris, France; Delire—ISE-Montpellier, Université Montpellier 2, Montpellier, France; Ducharne and Gascoin—Sisyphe, Université Pierre et Marie Curie (UMPC/CNRS), Paris, France; Grippa, Jarlan, Kergoat, and Mougin—Centres d'Etudes Spatiales de la Biosphère, Toulouse, France; Gusev and Nasonova—Institute of Water Problems, Russian Academy of Sciences, Moscow, Russia; Harris and Taylor—Centre for Ecology and Hydrology, Wallingford, United Kingdom; Norgaard and Sandholt—Institute of Geography, University of Copenhagen, Copenhagen, Denmark; Ottlé—IPSL-Laboratoire des Sciences du Climat et de l'Environnement, Gif-sur-Yvette, France; Poccard-Leclercq—LETG-Géolittomer, Université de Nantes, Nantes, France; Saux-Picart—IFREMER, Laboratoire d'Océanographie Spatiale, Plouzané, France; Xue—University of California, Los Angeles, Los Angeles, California
CORRESPONDING AUTHOR: Aaron Boone, GAME-CNRM Météo-France, 42 ave G. Coriolis, Toulouse, France 31057
E-mail: aaron.boone@meteo.fr

The abstract for this article can be found in this issue, following the table of contents.
DOI:10.1175/2009BAMS2786.1

In final form 15 June 2009

Soil Wetness Project, Phase 2 (GSWP-2; Dirmeyer et al. 2006a) was an offline global-scale LSM intercomparison study that produced the equivalent of a land surface reanalysis consisting in 10-yr global datasets of soil moisture, surface fluxes, and related hydrological quantites. The Rhône aggregation LSM intercomparison project (Boone et al. 2004) differed from the above-mentioned studies because the impact of changing the spatial scale on the LSM simulations was investigated. The main idea behind ALMIP is to take advantage of the significant international effort of the intensive field campaign and the various modeling efforts in order to better understand the role of land surface processes in the WAM.

ALMIP SCIENTIFIC OBJECTIVES. The strategy proposed in AMMA is to break the various components of the fully coupled system into more manageable portions. The first step is to begin with the LSM in offline mode. The multimodel offline technique has been used by numerous intercomparison projects (see appendix B). It is also used in operational land data assimilation systems (LDASs), such as the North American LDAS (NLDAS; Mitchell et al. 2004) and the Global LDAS (GLDAS; Rodell et al. 2004) for potential operational NWP applications. In addition, Douville et al. (2001) assimilated offline soil moisture into a GCM, as a proxy for reality, to study WAM surface–atmosphere feedback mechanisms.

Offline results have also been used for improved atmospheric model initialization. For example, ALMIP results are currently being used for numerous mesoscale case studies within AMMA [such as a study of feedbacks between dust emissions and the atmosphere in Tulet et al. (2008)], and to examine the influence of initial soil moisture on NWP at the European Centre for Medium-Range Weather Forecasts (ECMWF; A. Agusti-Panareda 2009, personal communication). In addition, ALMIP results have also been recently used for evaluating the land surface component of GCM and RCM (e.g., Steiner et al. 2009; Hourdin et al. 2010; Boone et al. 2009; Xue et al. 2009, manuscript submitted to *Climate Dyn.*).

The idea is to force state-of-the-art land surface models with the best quality and highest (space and time) resolution data available to better understand the key processes and their corresponding scales. The ALMIP therefore has the following main objectives:

1) intercompare results from an ensemble of state-of-the-art models and study model sensitivity to different parameterizations and forcing inputs;
2) determine which processes are missing, or are not adequately modeled, by the current generation of LSMs over this region;
3) examine how the various LSM respond to changing the spatial scale (three scales will be analyzed: local, mesoscale, and regional);
4) Develop a multimodel climatology of "realistic" high-resolution (multiscale) soil moisture, surface fluxes, and water and energy budget diagnostics at the surface (which can then be used for coupled land–atmosphere model evaluation, case studies, etc.); and
5) evaluate how relatively simple LSMs simulate the vegetation response to the atmospheric forcing on seasonal and interannual time scales.

ALMIP is an ongoing project, and phase 1 (regional-scale studies), which addresses items 1 and 4, has recently been completed; highlights from these items will be presented in this paper. In terms of item 1, the LSMs have run three multiyear experiments to explore LSM sensitivity to different input meteorological forcings. We present a brief overview of intercomparison results, along with some examples of evaluation efforts, which are under way (item 4). The next phase of ALMIP (phase 2) will begin this year, and it will address the remaining items (2, 3, and 5) by focusing on the meso- and local scales. We will also give general conclusions from phase 1 and perspectives for the next phase of ALMIP.

LAND SURFACE MODEL FORCING AND EXPERIMENTS. The creation of a multiscale low-level atmospheric forcing database over land is essential for a coherent multidisciplinary study with diverse LSMs. The forcing database is composed of land surface parameters, atmospheric state variables, precipitation, and downwelling radiative fluxes. The database has three scales (regional, mesoscale, and local), but we only used the regional-scale data for ALMIP phase 1 described here. All of the models use the same computational grid at a 0.50° spatial resolution (see domain in Fig. 1). The same soil–vegetation database is used for all experiments (see appendix A). Three experiments explored the LSM sensitivity to different input meteorological forcings (notably precipitation, which is the most critical field).

Control atmospheric forcing. The atmospheric forcing is based on the ECMWF NWP model forecasts for the years 2002–07. The forcing variables consist in the air temperature, specific humidity, and wind components at 10 m, the surface pressure, the total and

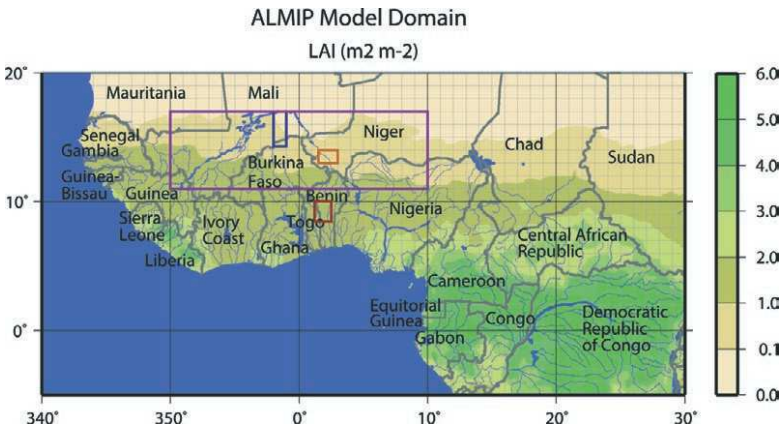

FIG. 1. The ALMIP regional-scale (phase 1) model domain. The three mesoscale supersites are indicated by boxes: Mali (blue), Niger (orange), and Benin (red). The Sahel box (referred to herein) is represented also (violet). The color shading corresponds to the annual average leaf area index (LAI; m^2 m^{-2}) from the Ecoclimap database.

convective rain rates, and the downwelling longwave and shortwave radiative fluxes (see appendix A for more details). There are, of course, several operational global-scale NWP models to choose from for forcing data. When ALMIP began (in 2003), ECMWF data were selected because the forecast data were available at approximately 50-km spatial resolution over West Africa, and this model simulated the regional-scale circulation over West Africa (e.g., Nuret et al. 2007) relatively well. These data comprise the experiment 1 or control forcing.

Merged atmospheric forcing. Because of the scarcity of surface observations over most of western Africa, remotely sensed data are needed for creating large-scale LSM forcing. The corresponding algorithms are generally calibrated, or supplemented, by any available local-scale data. Satellite-based data are most commonly available for the downwelling solar and atmospheric radiative fluxes and the rainfall. The radiative fluxes from the Ocean and Sea Ice Satellite Application Facility (OSI SAF; online at www.osi-saf.org) for 2004 and the Land Surface Analysis Satellite Application Facility (LSA SAF; Geiger et al. 2008) fluxes for 2005–07 are substituted for the corresponding NWP fluxes in experiments 2 and 3. They have been evaluated over this region (and this work is ongoing as more observational data become available).

Rainfall is the most problematic variable produced by NWP models, especially over West Africa. In ALMIP, however, we are limited to rainfall products with maximum time steps on the order of a few hours, because the LSMs in ALMIP resolve the diurnal cycle. Most of the precipitation events are convective, and thus relatively short lived for a given point. The Estimation des Pluies par Satellite Seconde Géneration (EPSAT-SG; Chopin et al. 2004) precipitation product from the AMMA satellite componet (AMMA-SAT; online at ammasat.ipsl.polytechnique.fr) offers the appropriate resolution and was developed especially to merge satellite and ground observations. This rainfall data were used for experiment 2.

The research community has increasingly demanded a longer-term record of surface fluxes and soil moisture. However, the experiment 2 precipitation data are only available during the core monsoon period (May–June) from 2004 to 2006. For this reason, we ran an additional experiment (experiment 3) with the Tropical Rainfall Measuring Mission (TRMM) precipitation product 3B-42 (Huffman et al. 2007) from 2002 to 2007 (hereafter this product is referred to as TRMM in this paper). The TRMM rainfall estimates combine calibrated microwave and infrared precipitation estimates, rescaled to monthly gauge data, and have a 3-h time step. Nicholson et al. (2003) showed that TRMM-combined products performed well on a monthly time scale over West Africa compared to other available products.[1]

The ECMWF model captures most of the main dynamical features of the WAM, but the simulated monsoon precipitation does not extend far enough to the north (Fig. 2a). Clearly, experiment 2 precipitation shows a northward displacement of the monsoon characterized by both increased precipitation to the north (roughly north of 8°N) and decreased values along the southern coast. In particular, the experiment 2 rainfall is approximately 9% higher over the Sahel region (indicated in Fig. 1) where the experiment 1 2006 June–September (JJAS) average rainfall is 3.8 kg m^{-2} day^{-1}, with the largest local relative increases over the northern part of this region. Further evidence of this problem will be given in the "Simulation evaluation methodology" section using satellite-based information. Downwelling shortwave radiation shows the same difference (Fig. 2b). The experiment 2 values are generally lower where pre-

[1] Note that the TRMM product has evolved since the above-mentioned study, but studies within AMMA have more recently come to the same conclusion.

cipitation and clouds have increased (the difference correspondes to about a 1% Sahel-average decrease for JJAS in experiment 2, although local decreases approach approximately 10%). This comparison emphasizes the importance of ancillary information to derive LSM forcings to reduce NWP model defaults or biases. The ultimate goal of ALMIP is to obtain more realistic estimates of surface processes.

SIMULATED SURFACE PROCESSES. Previous intercomparison studies have highlighted the necessity to use an ensemble of LSMs. Each individual model has its own biases and errors. Eleven LSMs participated in ALMIP phase 1 (see Table 2 and appendix B). Nine of the models used the provided Ecoclimap database soil and monthly varying vegetation parameter information; two LSMs used their native set of parameters. This implies that most of the model differences should be related to physics as opposed to parameters.

Intercomparison overview. One of the most critical land surface fields is evapotranspiration (Evap). This flux forms the critical link between land surface hydrology and the atmosphere. Despite the fact that the LSMs are using the same input atmospheric forcing, they show differences in the Evap spatial distribution in experiment 2 (Fig. 3). Of particular importance for the WAM are intermodel differences over the Sahel (essentially north of approximately 10°N). The meridional gradient of Evap is a maximum in this region during the monsoon season. When averaged over –10° to 10°E longitude, the gradient varies among the LSMs by up to approximately a factor of 2 (with the LSMs fairly equally distributed within this range). Because this gradient is coupled with the WAM circulation and intensity (Eltahir and Gong 1996), the strength of the feedbacks in different fully coupled land–atmosphere models could vary considerably, because of surface Evap parameterization differences (Dirmeyer et al. 2006b).

The difference between the multimodel average Evap in experiments 2 and 1 (Fig. 3p) shows that the impact of using the satellite-merged forcing is quite significant. Evap increases over 1 kg m^{-2} day^{-1} (with local increases of well over 2 kg m^{-2} day^{-1}) covering a large region north of approximately 8°N, with decreases along the southern West African coast. This response is consistent with the experiments 2 and 1 precipitation and radiation forcing differences shown in Fig. 2.

Even though different satellite-based precipitation products are merged with observational data, they can still have significant differences. Therefore, we compared ALMIP results for the three different forcing datasets. For each LSM and year from 2004 to 2006 in Fig. 4, the JJAS runoff ratio (the ratio of the total runoff to the rainfall) for the Sahel is plotted as a function of the latent heat ratio (here defined as the ratio of the latent to the net radiative flux). A low runoff ratio implies that much of the rainfall is going into evaporation or soil water storage (and therefore little is left for river flow). The latent heat ratio gives an estimate of the fraction of

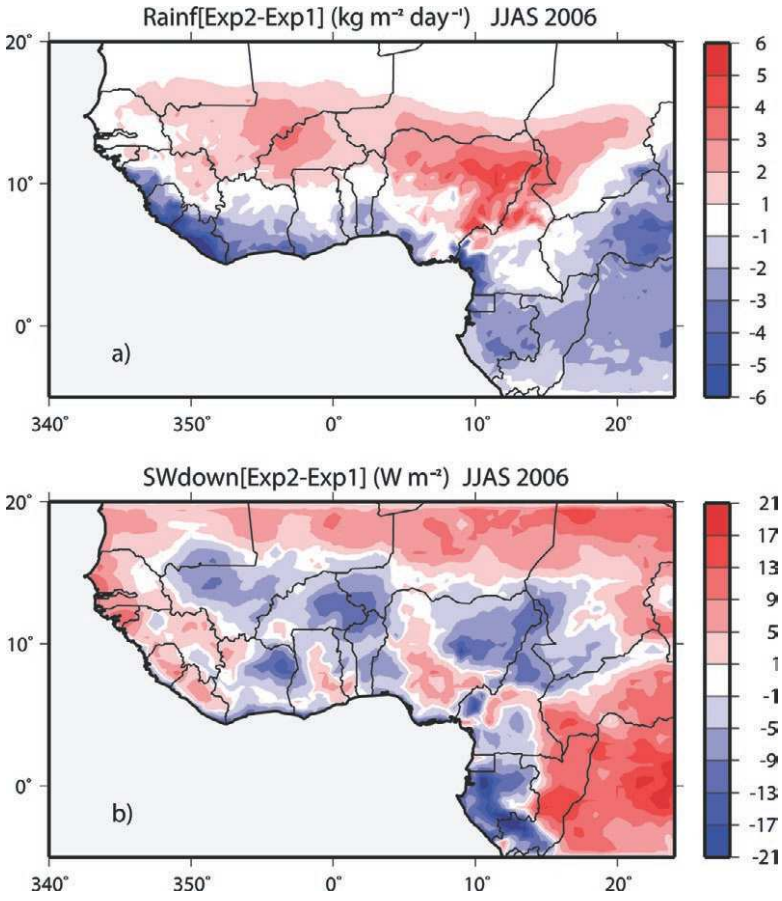

FIG. 2. (a) The JJAS average rainfall rate (Rainf) for 2006 from experiment 2 (EPSAT ECMWF forcing) less that from experiment 1 (pure ECMWF forcing) is shown. (b) The corresponding difference for the downwelling shortwave radiation (SWdown) is shown also, for which experiment 2 forcing consists in LSA SAF ECMWF data.

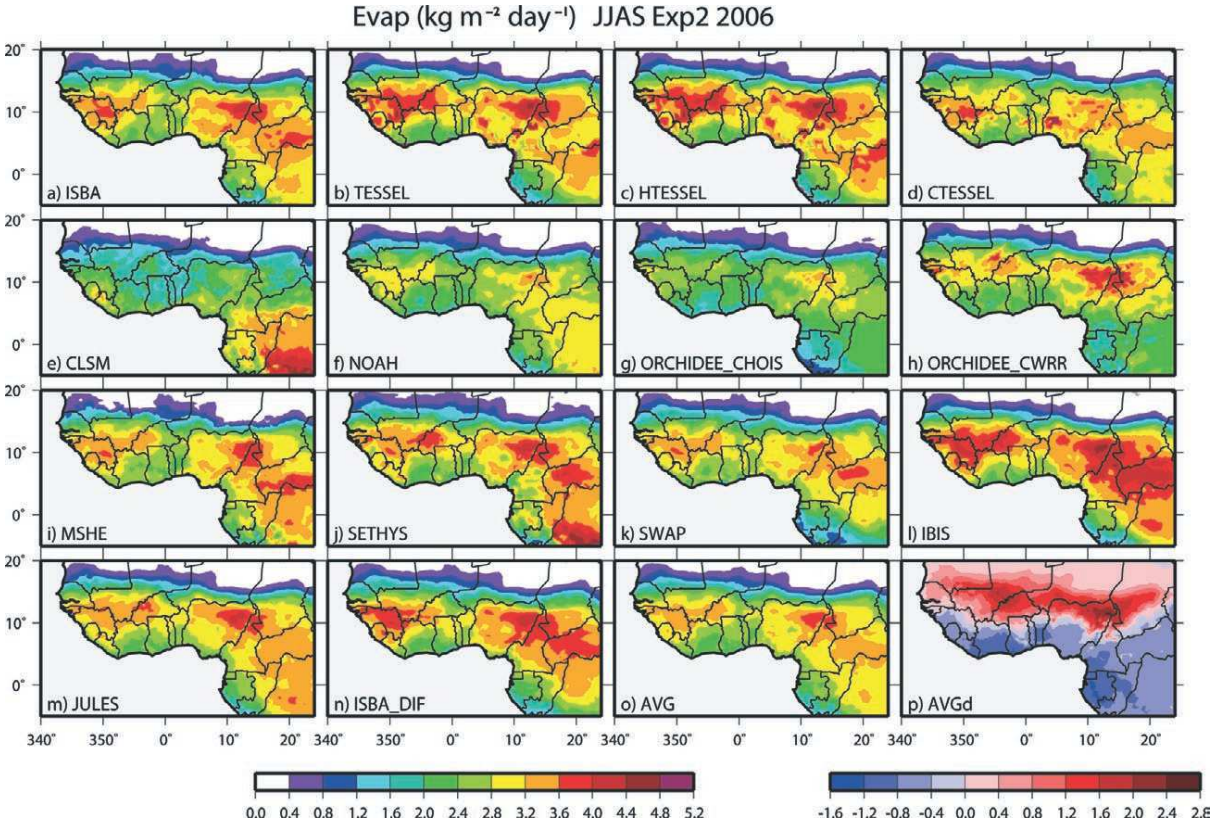

FIG. 3. The average Evap (mm day⁻¹) from experiment 2 for 2006 for 14 LSMs (see Table 2 for a list of model acronyms). (o) The multimodel AVG is shown. (p) The difference of the multimodel average Evap (experiment 2 minus experiment 1) for the same time period is shown.

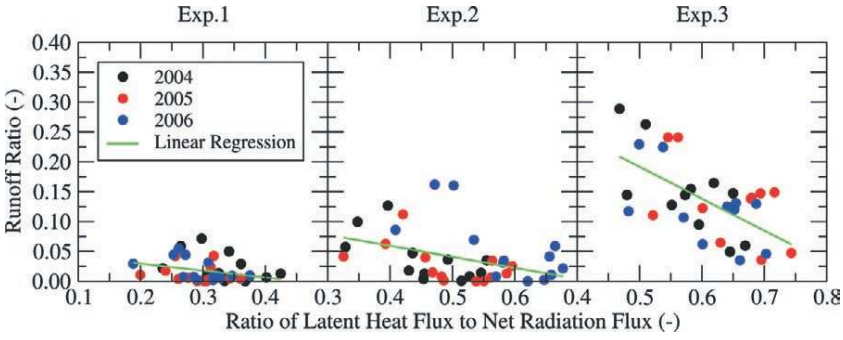

FIG. 4. Comparison of the runoff ratio (ratio of total runoff to rainfall) to the ratio of latent heat to net radiation flux. Each dot represents an LSM simulation averaged over the Sahel for the period from JJAS, inclusive. The green line represents a linear regression of the points for all years (2004–06). Results are shown using different forcing inputs for each panel: the rainfall amounts increased with each successive experiment.

the available energy at the surface used to evaporate water. The remaining fraction goes into heating the atmosphere.

It can be seen from Fig. 4 that the NWP forcing rainfall (experiment 1) results in an LSM average runoff ratio of 0.012. Nearly all of the rainfall is evaporated, but this still leaves most of the surface energy for sensible heating of the atmosphere (the LSM average latent heat ratio is 0.31). There is essentially no statistical relationship between the two ratios. There is 60% less rainfall and 50% less evaporation in experiment 1 than in experiment 2 over the Sahel (see Fig. 2). The larger experiment 2 rainfall increases both the runoff and latent heat ratios (the average latent heat ratio has increased to 0.51 in Fig. 4). The experiment 3 rainfall (TRMM) is even larger, resulting in 25% more rainfall and 18% more evaporation than that in experiment 2. There are much larger runoff ratios, and there is a greater statistical relationship between the latent heat and runoff ratios (the cor-

relation is −0.61); for the same input rainfall, increased runoff results in lower evaporation. In terms of physical processes, the models with the least surface runoff in experiments 2 and 3 tend to have the largest latent heat ratios, but for the remaining models there is no obvious relationship. In experiment 3, the rainfall exceeds the evaporative demand in many of the models, at times, resulting in considerably more runoff (therefore more water is available for river flow). The LSM simulation of river flow is currently being investigated, and it will be addressed in more detail in ALMIP phase 2. Finally, in the Sahel, the average interexperiment differences are far larger than the average of the intermodel differences for each experiment. This highlights the need to use satellite-based forcing data, whenever possible, to correct NWP model systematic biases.

TABLE 1. Summary of ALMIP phase 1 forcing inputs for each of three experiments. Here NWP data refer to those from the ECMWF forecast model. SAF refers to data from the OSI SAF (for 2004) and the LSA SAF (2005–07). EPSAT and TRMM 3B42 correspond to precipitation products consisting of merging satellite-based and rain-gauge estimates. See text for more details.

Experiment: Time period	Meteorological state variable source	Incoming radiative flux source	Precipitation source
1: 2002–06	NWP	NWP	NWP
2: 2004–06	NWP	Merged NWP and SAF	Merged NWP and EPSAT
3: 2002–07	NWP	SAF	TRMM 3B42

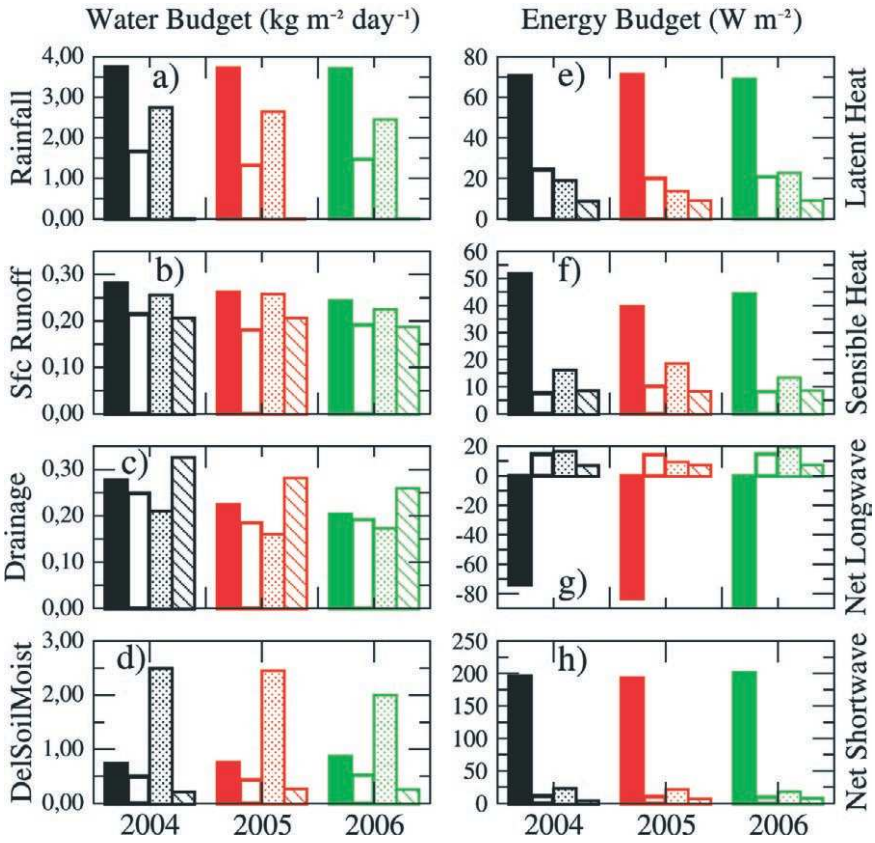

FIG. 5. A comparison of the mean (solid bars) water and energy budget components simulated by the LSMs for three years using TRMM rainfall (experiment 3). The means correspond to the average over the Sahel zone (Fig. 1), the 4-month period of JJAS (using daily values), and more than nine LSMs. The spatial, temporal, and intramodel variances are represented by the white-filled, stripped, and cross-hatched bars, respectively.

Characterization of the water and energy budgets by the LSM ensemble. Gao and Dirmeyer (2006) showed the advantages and improved realism of using a multi-LSM model average to study simulated surface properties. They presented several different weighting techniques from the simple average to one using optimized weights that minimized errors based on observations. The low spatial density of surface observations over West Africa precluded such optimization techniques, so we used the simple ensemble mean of the ALMIP-simulated surface fluxes (see appendix B for further details).

Figure 5 presents a summary of the water and energy budgets simulated by the LSMs and the ensemble LSM mean during JJAS for experiment 3 from 2004 to 2006 over the Sahel. These are respectively defined as

$$\text{Rainfall} = \text{SfcRunoff} + \text{Drainage} + \text{DelSoilMoist} + \text{Evap},$$

$$\text{SWnet} + \text{LWnet} \sim= \text{Sensible Heat Flux} + \text{Latent Heat Flux},$$

where DelSoilMoist represents the soil water storage change. Note that over the averaging period, the surface heat storage and the ground heat flux are much smaller than the other terms, and are negected here.

The Sahel has a prolonged dry season (lasting approximately five months), followed by a steady increase in rainfall starting in about April with a peak during late July or August. Finally, there is a more rapid decrease until about the end of October. The rainfall in 2006 lagged approximately two weeks compared to that in 2004. The rainfall began early in 2005, but there was a lull (and a suppression of rainfall in the southern Sahel) until mid- to late July. Then, rainfall rapidly increased northward. Despite these differences, the average rainfall from TRMM varies by just a few percent between the three years (Fig. 5a), as do the temporal and spatial variances.

The surface overland runoff (Fig. 5b) is slightly larger than the drainage (Fig. 5c). These two terms have the largest relative variability, as well as the least agreement between the LSMs, because the intramodel variance is comparable to the average. The drainage has the largest intra-LSM variance, but this is not surprising, because this variable is modulated by the surface runoff, the storage dynamics, vertical transfer, and finally, the evaporative uptake (in a sense, drainage is like a residual after the other above-mentioned processes have acted).

The soil water storage change (Fig. 5d) average is comparable in magnitude to the total runoff. Of note, it has an extremely large temporal variance. This is directly related and similar in magnitude to the temporal variance of the rainfall. The average soil water content (not shown) simulated by the LSMs is quite different. This is usually the case among LSMs (e.g., Dirmeyer et al. 2006a). Nonetheless, the relative intramodel agreement of the soil water storage change among the LSMs is quite good. The soil water dynamics are simulated in a fairly consistent manner in this region.

The remaining water budget variable is the evapotranspiration. This variable is the largest sink term (it corresponds to slightly more than 60% of the rainfall for each of the three years). The relative variances are fairly low, and the LSMs generally agree. The sensible heat flux (Fig. 5f) is slightly lower than the latent heat flux, on average; but again, the relative variances are

TABLE 2. Listing of model groups participating in ALMIP. The institute indicates where the ALMIP model simulation was performed. A recent model reference is given. The structure used for ALMIP is shown in the rightmost column where "L" represents the number of vertical soil layers, "E" represents the number of energy budgets per tile (a separate budget for snow cover is not considered here), and SV corresponds to the soil–vegetation parameters used. Tile refers to the maximum number of completely independent land surface types permitted within each grid box.

Model acronym	Institute	Recent reference	ALMIP structure
a) TESSEL, b) CTESSEL, c) HTESSEL	ECMWF, Reading, United Kingdom	a) Van den Hurk and Viterbo (2003), b) Lafont et al. (2006), c) Balsamo et al. (2009)	4L, 6 tiles, 1E SV: ECMWF
a) ORCHIDEE-CHOIS, b) ORCHIDEE-CWRR	IPSL, Paris, France	a) Krinner et al. (2005), b) d'Orgeval et al. (2008)	a) 2L, b) 11L, 13 tiles, 1E SV: Ecoclimap
a) ISBA, b) ISBA-DF	CNRM, Météo-France, Toulouse, France	a) Noilhan and Mahfouf (1996), b) Boone et al. (2000)	a) 3L, b) 5L, 1 tile, 1E SV: Ecoclimap
JULES	CEH, Wallingford, United Kingdom	Essery et al. (2003)	4L, 9 tiles, 1E SV: Ecoclimap
SETHYS	CETP/LSCE, Vélizy, France/ Gif-sur-Yvette, France	Coudert et al. (2006)	2L, 12 tiles, 2E SV: Ecoclimap
IBIS	ISE-Montpellier, France; SAGE, UW Madison—Madison, WI	Kucharik et al. (2000)	6L, 1 tile, 8E SV: Ecoclimap
NOAH	CETP/LSCE (NCEP)	Chen and Dudhia (2001), Decharme (2007)	7L, 12 tiles, 1E SV: Ecoclimap
CLSM	UPMC, Paris, France	Koster et al. (2000)	3L, 5 tiles, 3E SV: Ecoclimap
M SHE	University of Copenhagen, Copenhagen, Denmark	Graham and Butts (2006)	42L, 1 tile, 1E SV: Ecoclimap
SSiB	LETG, Nantes, France; UCLA, Los Angeles, CA	Xue et al. (1991)	3L, 1 tile, 2E SV: SSiB
SWAP	IWP, Moscow, Russia	Gusev et al. (2006)	3L, 1 tile, 1E SV: Ecoclimap

fairly low. This implies that for a given rainfall over this region, the various LSMs simulate the surface–atmosphere transfer of heat and moisture fairly consistently.

The net longwave and shortwave radiation fluxes (Figs. 5g,h, respectively) have the lowest variances in the energy budget, especially the intramodel variance, as expected. The prescribed downwelling fluxes dominate the forcing input, and the vast majority of the LSMs used the prescribed surface characteristics (albedo and emissivity). The spatial and temporal net longwave variances are a bit larger than those for the shortwave radiation, and they vary more from year to year. This results because there is a significant contribution from the simulated surface temperature (which is the result of the computation of the surface energy budget).

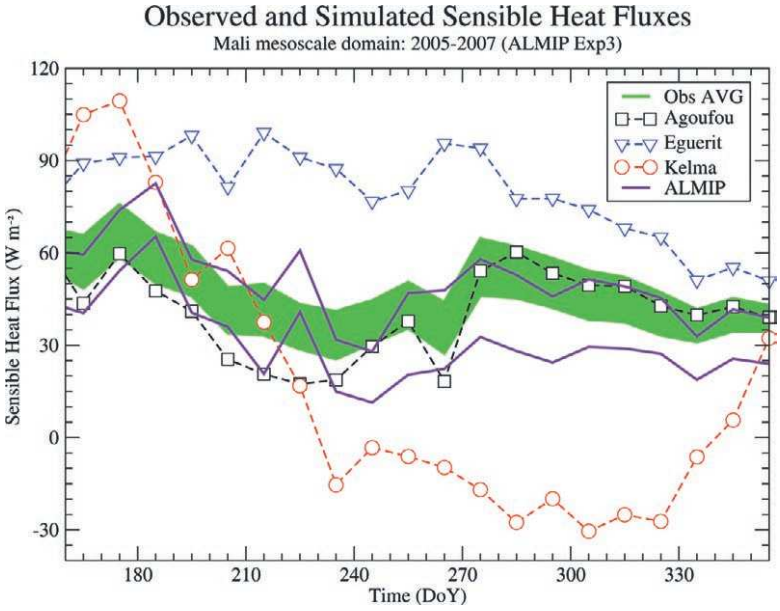

FIG. 6. The 3-yr average (2005–07) observed *Qh* for the three local sites are indicated by the nonfilled symbols, and the shaded green area corresponds to the spread of the spatially aggregated fluxes (representing the 60 × 60 km² mesoscale domain). The solid purple curves enclose a region bounded by ± one standard deviation about the ALMIP LSM average *Qh* averaged over 2005–07. Note that experiment 3 results are used here because they extend to 2007. The observed flux data for this figure were taken from Timouk et al. (2009).

SIMULATION EVALUATION METHODOLOGY. The obvious problem, in doing simulations over western Africa (and, in fact, for many large domain area applications), is the lack of appropriate evaluation data. However, in AMMA, considerable effort has been put into addressing such issues by processing remote sensing datasets and by establishing several dense surface observational networks along a meridional transect (Fig. 1; see also Redelsperger et al. 2006). In this paper, we give examples of ALMIP LSM evaluation methods at the gridbox scale and over a large-scale region.

Gridbox evaluation. Comparing local flux data with model output over a grid square is a scale problem. It is generally only useful if the grid-square surface parameters and forcing data are consistent with those observed at the local scale. There can be significant subgrid heterogeneity on the grid-square scale. This problem is being addressed in ALMIP using spatially aggregated surface flux data. We give an example for the Mali supersite square (an approximately 60 × 60 km² area; see Fig. 1), which is typical of the grid size of global-scale NWP models and relatively high-resolution GCMs.

Figure 6 compares the observed upscaled surface sensible heat flux *Qh* with the multimodel ALMIP spread (both averaged here over 10-day periods) for a single grid box. The spread of spatially aggregated surface fluxes is computed as the range in aggregated *Qh*. The different aggregated values were computed using different weighting schemes based on the spatial coverage of the dominant vegetation type at each site, and the ranges in the soil types, the surface albedo, and the coverage of standing water using remotely sensed data (see Timouk et al. 2009 for further details).

Each of the three observation sites in Fig. 6 represents a very different land cover type: Kelma is a low-lying marsh during the wet season and ensuing months (hence,the negative *Qh* values); Eguerit is very dry and rocky (soils quickly drain, thus *Qh* remains relatively high all year); and Agoufou has sparse, low vegetation. This is the dominant vegetation coverage over the mesoscale area, and the ALMIP land cover for this grid box from Ecoclimap (87% bare soil and 13% tropical grassland) is most consistent with the characteristics of this site.

ALMIP LSM average *Qh* values are approximately 70 W m^{-2} just before the onset of the summer rains (prior to yearday 180 in Fig. 6). They are approximately 2 times lower during the core monsoon period (yeardays 200–260). After yearday 260, *Qh* rapidly increases as the rains cease. However, *Qh* begins to

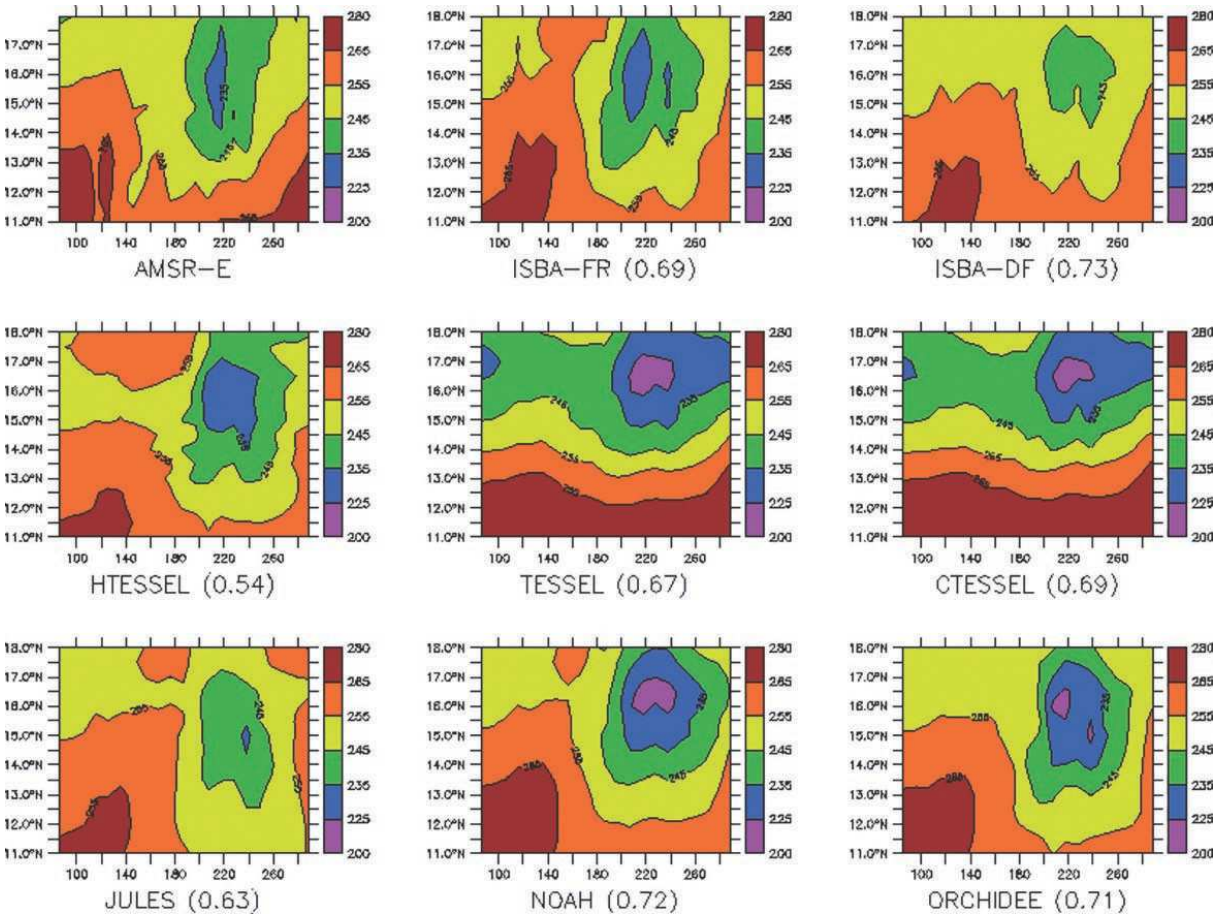

FIG. 7. (top left) The surface brightness temperature (T_B) observed from AMSR-E is shown (top left), while the T_B values simulated by several ALMIP models are shown in the remaining panels. The spatial correlation coefficient is indicated in parentheses. Data for this figure were taken from de Rosnay et al. (2009).

decline again after yearday 280 in response to reduced incoming radiation. The LSM average simulated *Qh* response to the wet season and the subsequent dry down are similar to the dynamic of the observed average *Qh*. There was far less year-to-year variability (not shown in Fig. 6) than intersite variability.

Large-scale surface evaluation. Within the joint framework of the Soil Moisture and Ocean Salinity (SMOS) satellite mission and AMMA, we evaluated ALMIP soil moisture for 2006 for eight LSMs from experiment 2 (whose results had already been processed). The ALMIP Microwave Emission Model (MEM) couples ALMIP soil moisture and temperature outputs to the Community Microwave Emission Model (CMEM; de Rosnay et al. 2009). It permits a quantification of the relative impact of land surface modeling and radiative transfer modeling on the simulated brightness temperature background errors. We evaluated ALMIP MEM brightness temperatures for 2006 against Advanced Microwave Scanning Radiometer for Earth Observing System (AMSR-E) C-band data provided by the National Snow and Ice Data Center (NSIDC). This work (Fig. 7) has been a part of the effort to test different forward models for data assimilation in the ECMWF model.

For each LSM, a simple correction has been applied to the simulated brightness temperatures based on the annual mean bias. LSMs need to reproduce features such as the observed wet patch centered at yearday 210 and 15.5°N, which can induce mesoscale circulations (Taylor et al. 2007). All of the LSMs capture this wet patch, but they either overestimate or underestimate the amplitude. However, Fig. 7 and the Taylor diagram in Fig. 8 emphasize the general good agreement between the forward approach and the AMSR-E.

In this study, CMEM has been used with the Kirdyashev vegetation opacity model (Kirdyashev et al. 1979) and the Wang and Schmugge dielectric model (Wang and Schmugge 1980) satellite data.

Exceptions are the ECMWF LSMs using the old hydrology (TESSEL and CTESSEL), which overestimated the variance. The newer (now operational) scheme has excellent agreement (HTESSEL), although the correlation has decreased.

This analysis also indirectly evaluates the ALMIP experiment 2 precipitation forcing. The LSMs were forced by pure NWP-based forcing data (meaning no satellite or observational data were used, see experiment 1), and the CMEM results were poor compared to the AMSR-E data (not shown here). In the future, we plan to rerun these tests using experiment 3 outputs. For a more in-depth analysis of these results, see de Rosnay et al. (2009).

Large-scale subsurface evaluation. Knowledge of the land surface water storage is important for estimating vegetation growth, and it may hold a key to increasing long-range atmospheric predictability over West Africa. However, even though numerous local-scale site measurements are now available within AMMA, measurements of the land water storage are not available at the regional scale. The Gravity Recovery and Climate Experiment (GRACE) satellite mission accurately measures gravity field variations, which are inverted to retrieve terrestrial water storage variations. Various products, based on different retrieval methods, are available. Here we present results using one of the most recent methods (Lemoine et al. 2007). GRACE has already been used with success to estimate regional-scale water storage in LSM studies (e.g., Zaitchik et al. 2008).

For 2005–06, GRACE soil moisture seasonal amplitudes are larger than those simulated by the ALMIP models, although the experiment 3 results are much closer than the experiment 1 results using NWP forcing. Indeed, this is further evidence that satellite-based remote sensing offers an improvement to NWP forcing data. The experiment 3 temporal correlation for the two years is quite good (0.90). The differences in the amplitudes (the temporal variance for the mean of the ALMIP LSM is 29 kg m^{-2}, while it is 45 kg m^{-2} for GRACE) can be due to a deficit in the precipitation forcing, or to an overestimation of the water storage anomalies derived from GRACE during the dry season. It is also possible that the ALMIP LSMs do not use sufficiently deep soil depths (in most LSMs, drained water is not retained in the vertical column, but rather it is assumed to be lost to the nearest river). Note that results from experiment 2 are not shown in Fig. 9, but in fact the water variation amplitude is smaller than that in experiment 3. This is consistent with the lower rainfall (used in experiment 2). A study is currently under way that shows that the satellite data reproduce the ALMIP experiment 3 LSM-modeled interannual variability over the Sahel during the study time period (2002–07). The next step is to use discharge to estimate the regional-scale evaporation.

CONCLUSIONS. There is a need to better understand land–atmosphere and hydrological processes over western Africa because of their potential feedbacks with the WAM circulation. This is being addressed through a multiscale modeling approach using an ensemble of LSMs that relies on dedicated, satellite-based forcing and land surface parameter products, and data from the AMMA observational field campaigns. The idea is to have the best estimate of surface processes for initializing and evaluating the surface component of atmospheric models, and to determine which LSM processes agree the least (in order to eventually improve the corresponding physics). The far-reaching goal of this effort is to obtain better understanding and prediction of the WAM to improve water management and agricultural practices.

Offline, multi-LSM simulations using a mix of NWP and satellite-based forcing data comprise the equivalent of a multimodel reanalysis product. This represents the best estimate of the land surface processes over large-scale regions (Dirmeyer et al. 2006a), and ALMIP has produced such an analysis for West Africa from 2004 to 2007. The use of using satellite-based forcings to correct systematic biases in NWP meteorological forcing significantly improves

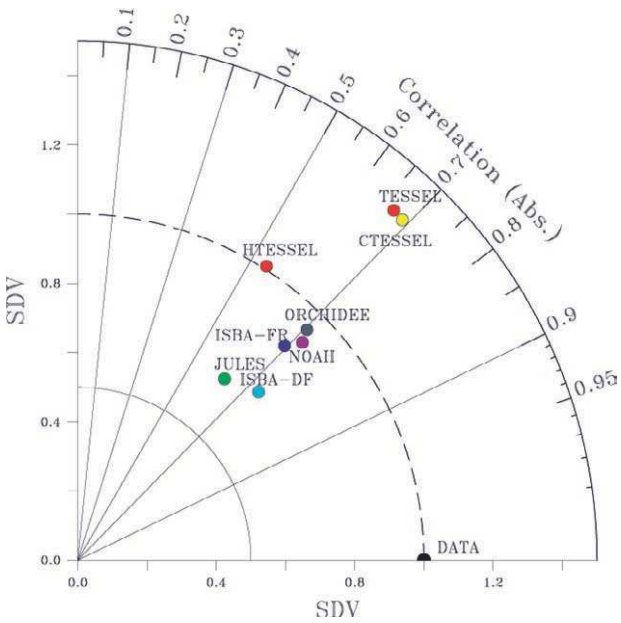

Fig. 8. Taylor diagram of the statistical evaluation of the simulated ALMIP T_B values. Data for this figure were taken from de Rosnay et al. (2009).

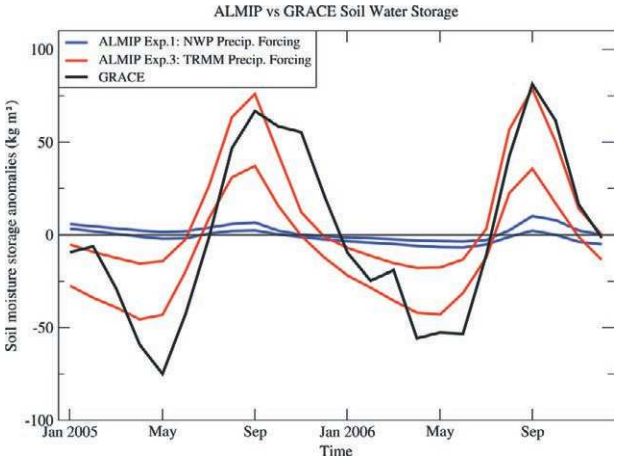

FIG. 9. Comparison of the soil moisture storage change anomaly derived from the GRACE satellite product (black curve) to two simulations by the ALMIP LSMs over the Sahel from 2005 to 2006. The blue lines enclosed the mean plus the root-mean-square difference for results from experiment 1 (using NWP rainfall forcing). The red lines correspond to results from experiment 3 (using TRMM rainfall input).

LSM-simulated evapotranspiration, especially over the Sahel and areas slightly southward [which is theorized to be the zone with considerable coupling with the atmosphere; e.g., Koster et al. (2004)]. In terms of ECMWF forcing data, this corresponds to a several hundred kilometer shift in precipitation compared to satellite-based data (and 60% less precipitation over the Sahel than in the TRMM-merged satellite–rain gauge product from 2004 to 2006 during JJAS). This implies that special care should be used when using NWP, or reanalysis data, to force LSMs over West Africa for hydrological or meteorological studies.

The ALMIP LSM simulations have moderate intermodel variability. It is considerably less than found in fully coupled land–atmosphere models. The surface fields from ALMIP are a good proxy for evaluating the surface flux components in terms of model improvements (Steiner et al. 2009) or in GCM–RCM intercomparison exercises, such as the AMMA MIP (Hourdin et al. 2010) and WAMME (Xue et al. 2010, submitted to *Climate Dyn.*; Boone et al. 2009). The ALMIP fields are also being used in numerous ongoing atmospheric case studies within AMMA (e.g., in terms of convective initiation, dust storm simulations, and chemical deposition) and in operational NWP (e.g., at ECMWF). Finally, ALMIP outputs are also being used within AMMA to estimate the surface contribution for atmospheric water budget studies and to estimate the production functions (evapotranspiration) for hydrological models.

There are considerable differences in terms of the partitioning of the surface (fast response: on the scale of a rainfall event) and drainage (slow response: on the scale of days up to approximately one week) runoff components. This partitioning is important because it modulates the amount of water that is evaporated, stored in lakes, transferred to rivers, or stored in the soil (which in turn impacts the partitioning of net radiation at the surface into latent and sensible heat fluxes). In addition, the intramodel variability is the largest of all of the land surface variables. These output fields have a very high degree of uncertainty. This component of the water budget is also the most sensitive to the precipitation input forcing. This aspect of LSMs must be refined if such models are to be used for regional-scale water management over West Africa, or in order for the popular soil moisture memory question to be properly addressed using coupled models (e.g., Douville et al. 2007). Increased surface runoff corresponds to reduced water recycling with the atmosphere, and it can impact the time scale and magnitude of this memory.

It is difficult to evaluate the realism of the simulated turbulent fluxes at regional scales. Indirect methods are being used for large-scale evaluation, which were all based on using remotely sensed data. A sample of such work was presented herein. The ALMIP LSMs compared favorably with aggregated surface flux data in the Sahel during the monsoon season over a 3-yr period for a given grid box. They are able to reasonably capture both the amplitude and the phase of the observed changes. At the regional scale, the simulated surface brightness temperature compared well with data from the satellite (which is a first step for assimilating such data into LSMs for operational NWP). Finally, estimates of water storage from GRACE show that the TRMM satellite-based precipitation product is more realistic than NWP-based forcing on the regional scale. This is currently the only method available to obtain reasonable estimates of the subsurface water storage over the entire West African region aside from using LSM models (in an offline mode or using some form of land data assimilation scheme).

PERSPECTIVES. ALMIP is an ongoing project, and phase 1 at the regional scale is nearing completion. However, further regional-scale simulations, experiments, and model evaluation will also be made as improved input data are made available. ALMIP phase 2 is scheduled to begin in 2009. This will focus on simulations for the three mesoscale supersites, in addition to several other local-scale sites (in Senegal, Ghana, etc.). There will be a special focus on semarid land surface process parameterizations. Indeed, they are quite

diverse among LSMs and generally lack consideration of some fundamental processes specific to this region (reduced infiltration over dry, crusty soils, drought-resistant plant species, lateral transfer of surface runoff from bare soil to vegetated surface areas, etc.). In addition, input rainfall will be based on dense observational networks, which should improve the realism of the land surface and hydrological simulations.

Météo-France is developing a new high-resolution version of Ecoclimap over West Africa. The main drawback of the current version of Ecoclimap is that there is no vegetation interannual variability (which, in fact, is fairly typical of such datasets used currently in GCM and NWP applications). However, this variability is known to be particularly large over this region (Philippon et al. 2007). The new Ecoclimap should further improve surface flux estimates. This is important from a modeling standpoint because the observed vegetation interannual variability is correlated with the precipitation over this region, notably, for the Sahel (Philippon et al. 2005). It will also be available for atmospheric model studies.

LSMs, which are able to simulate the life cycle of the vegetation, are increasingly used in GCMs. They will theoretically enable a more realistic feedback between the vegetation and potential increases in greenhouse gases in climate scenario studies. There will be a coordinated effort in ALMIP phase 2 to intercompare such LSMs on the mesoscale, which will be a first. ALMIP phase 1 focused on making a robust multimodel representation of surface processes. ALMIP phase 2 will also focus on improving the representation of such processes (for atmospheric and hydrological models). ALMIP phase 2 will be open to the general scientific community. Interested parties will be encouraged to participate.

ACKNOWLEDGMENTS. The authors would like to acknowledge the support of J.-P. Lafore at CNRM and the data providers, notably R. Lacaze, B. Geiger, D. Carrer, and J.-L. Roujean, who have offered considerable assistance with respect to using the LSA SAF downwelling radiative flux products. A. Marsouin provided guidance on the OSI SAF radiation product. We wish to extend our gratitude to the POSTEL Service Centre (http://postel.mediasfrance.org) at MEDIAS-France for customizing and providing the LSA SAF products, and to the people working on the AMMA-SAT database (http://ammasat.ipsl.polytechnique.fr) who have generated the EPSAT precipitation product developed by the Precip-AMMA group at IPSL/LMD (notably, K. Ramage). Thanks go to R. Meynadier who processed the TRMM data. Based on a French initiative, AMMA has been established by an international group and is currently funded by a large number of agencies, especially from France, the United Kingdom, and Africa. It has been the beneficiary of a major financial contribution from the European Community's Sixth Framework Research Programme. Detailed information on scientific coordination and funding is available on the AMMA international Web site (www.amma-eu.org/). Finally, we would like to acknowledge the efforts of three reviewers and the editor in improving this manuscript.

APPENDIX A: INPUT DATA. Additional details related to the input forcing data are presented herein.

Soil and vegetation model parameters. The Ecoclimap database (Masson et al. 2003) provides land surface parameters (albedo, vegetation cover fraction, surface roughness, leaf area index, soil texture, etc.) over the entire globe at a maximum spatial resolution of 1 km. It is intended for use by LSMs that are coupled to GCMs, numerical weather prediction (NWP) models, mesoscale meteorological research models, or hydrological models. The vegetation phenology for a single representative annual cycle, at a 10-day time step, is derived from the International Geosphere–Biosphere Programme (IGBP) 1-km Advanced Very High Resolution Radiometer (AVHRR) monthly normalized difference vegetation index (NDVI).

Atmospheric forcing. The forcing variables have been interpolated to a 0.5° cylindrical, equidistant projection at a 3-h time step. There is a well-known spin-down problem in terms of the simulated precipitation for the ECMWF model. The ALMIP forcing consists of a series of 36-h forecasts at 1200 UTC every 24 h, and the first 12 h are not used. In experiment 2, EPSAT rainfall replaced NWP data for the monsoon months. When either satellite-based radiative flux or precipitation data were missing, they were replaced by NWP data. In experiment 3, TRMM rainfall was used for all years (including spinup), and SAF fluxes were used from 2004 onward (refer to Table 1).

APPENDIX B: MODEL SETUP. This section describes the LSM configurations for ALMIP. Please refer to Table B1 for model references and scheme details referred to herein.

LSM initialization and output diagnostics. All of the models performed spinup for 2002 because initial conditions for each of the LSMs were not available. A single pass through 2003 was done as an adjustment year. The values of the prognostic variables at the end

of 2003 were then used as initial values for experiments 1 and 2. Nine of the 11 models (except for IBIS and MSHE) performed experiment 3. Model results were reported for all years, however, analysis focuses on 2004–07 because satellite-based radiative flux data and the EPSAT product were available (2004–06). This period also encompasses the special observation perdio in AMMA. A number of water and energy budget variables and diagnostics were reported at a 3-h time step. The output variables and conventions are essentially the same as those outlined in Dirmeyer et al. (2006a): the outputs consist in energy budget diagnostics (such as surface heat, mass, momentum, and radiative fluxes), water budget components (runoff, evapotranspiration, and soil water storage changes), and prognostic variables (soil temperature and moisture for ALMIP; see www.cnrm.meteo.fr/amma-moana/amma_surf/almip/index.html for a complete listing of LSM outputs).

LSM options. Two models did simulations using two different options. ISBA used the force–restore and the multilayer diffusion (DIF) soil options ORCHIDEE replaced its two-layer soil approach (CHOIS) by an explicit, multilayer model. HTESSEL uses the newly implemented hydrological updates (TESSEL was operational until recently), and CTESSEL contains a new photosynthesis option. All of the LSMs used the same computational grid and atmospheric forcing.

Several of the models used multiple tile options for these experiments because it is their default setting. This essentially amounts to an explicit treatment of each surface land cover type and aggregating the fluxes using weights based on spatial coverage within each grid box (in order to theoretically better represent the nonlinearity of the surface processes). Most of the LSMs use either a single composite or a double-energy budget representation (explicit treatment of canopy and soil). However, a few schemes have unique treatments. CLSM computes three energy budgets based on soil wetness, while ORCHIDEE computes evaporation for different surface types overlying the same soil. IBIS also uses a similar approach with four distinct plant functional types, and it has the most detailed representation of the canopy containing multiple energy budgets. Finally, the MSHE model was designed for hydrological applications, and it uses a very detailed treatment of vertical, subsurface fluxes of mass and energy (utilizing 42 layers).

LSM ensemble mean. Multiple simulations from the same model were first averaged to obtain a single representative result for a given model (e.g., ISBA and ISBA-DIF results were averaged to obtain a single ISBA representative result). This was done because the differences between multiple simulations by a single model were generally far less than the intra-LSM differences: we did not want to bias the ensemble average by weighting one model more than another.

REFERENCES

Balsamo, G., P. Viterbo, A. Beljaars, B. van den Hurk, M. Hirsch, A. Betts, and K. Scipal, 2009: A revised hydrology for the ECMWF model: Verification from field site to terrestrial water storage and impact in the Integrated Forecast System. *J. Hydrometeor.,* **10,** 623–643.

Boone, A., V. Masson, T. Meyers, and J. Noilhan, 2000: The influence of the inclusion of soil freezing on simulations by a soil–vegetation–atmosphere transfer scheme. *J. Appl. Meteor.,* **39,** 1544–1569.

——, and Coauthors, 2004: The Rhone-Aggregation Land Surface Scheme Intercomparison Project: An overview. *J. Climate,* **17,** 187–208.

——, Y. Xue, I. Poccard-Leclerq, J. Feng, and P. deRosnay, 2009: Evaluation of the WAMME model surface fluxes using results from the AMMA land-surface model intercomparison project. *Climate Dyn.,* in press, doi:10.1007/s00382-009-0653-1.

Charney, J. G., 1975: Dynamics of desert and drought in the Sahel. *Quart. J. Roy. Meteor. Soc.,* **101,** 193–202.

——, P. H. Stone, and W. J. Quirk, 1975: Drought in the Sahara: A biogeophysical feedback mechanism. *Science,* **187,** 434–435.

Chen, F., and J. Dudhia, 2001: Coupling an advanced land surface–hydrology model with the Penn State–NCAR MM5 modeling system. Part I: Model implementation and sensitivity. *Mon. Wea. Rev.,* **129,** 569–585.

Chopin, F., J. Berges, M. Desbois, I. Jobard, and T. Lebel, 2004: Multi-scale precipitation retrieval and validation in African monsoon systems. *Second Int. TRMM Science Conf.,* Nara, Japan, TRMM, 40 pp.

Cook, K. H., and E. K. Vizy, 2006: Coupled model simulations of the West African monsoon system: Twentieth and twenty-first-century simulations. *J. Climate,* **19,** 3681–3703.

Coudert, B., C. Ottlé, B. Boudevillain, P. Guillevic, and J. Demarty, 2006: Contribution of thermal infrared remote sensing data in multiobjective calibration of a dual source SVAT model. *J. Hydrometeor.,* **7,** 404–420.

Cunnington, W. M., and P. R. Rowntree, 1986: Simulations of the Saharan atmosphere dependence on moisture and albedo. *Quart. J. Roy. Meteor. Soc.,* **112,** 971–999.

Decharme, B., 2007: Influence of runoff parameterization on continental hydrology: Comparison between the Noah and the ISBA land surface models. *J. Geophys. Res.,* **112,** D19108, doi:10.1029/2007JD008463.

de Rosnay, P., and Coauthors, 2009: AMMA Land Surface Model Intercomparison Experiment coupled to the Community Microwave Emission Model: ALMIP-MEM. *J. Geophys. Res.,* **114,** D05108, doi:10.1029/2008JD010724.

Dirmeyer, P. A., X. Gao, M. Zhao, Z. Guo, T. Oki, and N. Hanasaki, 2006a: GSWP-2: Multimodel analysis and implications for our perception of the land surface. *Bull. Amer. Meteor. Soc.,* **87,** 1381–1397.

——, R. D. Koster, and Z. Guo, 2006b: Do global models properly represent the feedback between land and atmosphere? *J. Hydrometeor.,* **7,** 1177–1198.

d'Orgeval, T., J. Polcher, and P. de Rosnay, 2008: Sensitivity of the West African hydrological cycle in ORCHIDEE to infiltration processes. *Hydrol. Earth Syst. Sci. Discuss.,* **5,** 2251–2292.

Douville, H., F. Chauvin, and H. Broqua, 2001: Influence of soil moisture on the Asian and African monsoons. Part I: Mean monsoon and daily precipitation. *J. Climate,* **14,** 2381–2403.

——, S. Conil. S. Tyteca, and A. Voldoire, 2007: Soil moisture memory and West African monsoon predictability: Artefact or reality? *Climate Dyn.,* **28,** 723–742.

Eltahir, E. A. B., and C. Gong, 1996: Dynamics of wet and dry years in West Africa. *J. Climate,* **9,** 1030–1042.

Essery, R. L. H., M. Best, R. Betts, P. Cox, and C. M. Taylor, 2003: Explicit representation of subgrid heterogeneity in a GCM land surface scheme. *J. Hydrometeor.,* **4,** 530–543.

Folland, C. K., T. N. Palmer, and D. E. Parker, 1986: Sahel rainfall and worldwide sea temperature 1901–1985. *Nature,* **320,** 602–607.

Fontaine, B., and S. Janicot, 1996: Sea surface temperature fields associated with West African rainfall anomaly types. *J. Climate,* **9,** 2935–2940.

Gao, X., and P. A. Dirmeyer, 2006: A multimodel analysis, validation, and transferability study of global soil wetness products. *J. Hydrometeor,* **7,** 1218–1236.

Geiger, B., C. Meurey, D. Lajas, L. Franchistéguy, D. Carrer, and J.-L. Roujean, 2008: Near real-time provision of downwelling shortwave radiation estimates derived from satellite observations. *Meteor. Appl.,* **15,** 411–420.

Graham, D. N., and M. B. Butts, 2006: Flexible integrated watershed modeling with MIKE SHE. *Watershed Models,* V. P. Singh and D. K. Frevert, Eds., Taylor and Francis Group, 245–272.

Gusev, E. M., O. N. Nasonova, and E. E. Kovalev, 2006: Modeling the components of heat and water balance for the land surface of the globe. *Water Resour.,* **33,** 616–627.

Henderson-Sellers, A., A. J. Pitman, P. K. Love, P. Irannejad, and T. Chen, 1995: The Project for Intercomparison of Land-Surface Parameterization Schemes (PILPS): Phases 2 and 3. *Bull. Amer. Meteor. Soc.,* **76,** 489–503.

Hourdin, F., and Coauthors, 2010: AMMA Model Intercomparison Project. *Bull. Amer. Meteor. Soc.,* in press.

Huffman, G. J., and Coauthors, 2007: The TRMM Multisatellite Precipitation Analysis (TMPA): Quasi-global, multiyear, combined-sensor precipitation estimates at fine scales. *J. Hydrometeor.,* **8,** 38–55.

Kirdyashev, K., A. Chukhlantsev, and A. Shutko, 1979: Microwave radiation of the earth's surface in the presence of vegetation cover. *Radio Eng. Electron.,* **24,** 256–264.

Koster, R. D., M. J. Suarez, A. Ducharne, P. Kumar, and M. Stieglitz, 2000: A catchment based approach to modeling land surface processes in a GCM—Part 1: Model structure. *J. Geophys. Res.,* **105,** 24 809–24 822.

——, P. A. Dirmeyer, A. N. Hahmann, R. Ijpelaar, L. Tyahla, P. Cox, and M. J. Suarez, 2002: Comparing the degree of land–atmosphere interaction in four atmospheric general circulation models. *J. Hydrometeor.,* **3,** 363–375.

——, and Coauthors, 2004: Regions of strong coupling between soil moisture and precipitation. *Science,* **305,** 1138–1140.

Krinner, G., and Coauthors, 2005: A dynamic global vegetation model for studies of the coupled atmosphere-biosphere system. *Global Biogeochem. Cycles,* **19,** GB1015, doi:10.1029/2003GB002199.

Kucharik, C. J., and Coauthors, 2000: Testing the performance of a dynamic global ecosystem model: Water balance, carbon balance and vegetation structure. *Global Biogeochem. Cycles,* **14,** 795–825.

Lafont, S., A. Beljaars, M. Voogt, L. Jarlan, P. Viterbo, B. van den Hurk, and J.-C. Calvet, 2006: Comparison of C-TESSEL CO_2 fluxes with TransCom CO_2 fluxes. *Proc. Second Recent Advances in Quantitative Remote Sensing II,* Torrent, Spain, University of Valencia, 474–477.

Laval, K., and L. Picon, 1986: Effect of a change of the surface albedo of the Sahel on climate. *J. Atmos. Sci.,* **43,** 2418–2429.

Le Barbé, L., T. Lebel, and D. Tapsoba, 2002: Rainfall variability in West Africa during the years 1950–90. *J. Climate,* **15,** 187–202.

Lemoine, J.-M., S. Bruinsma, S. Loyer, R. Biancale, J.-C. Marty, F. Perosanz, and G. Balmino, 2007: Temporal gravity field models inferred from GRACE data. *Adv. Space Res.,* **39,** 1620–1629, doi:10.1016/j.asr.2007.03.062.

Li, W., Y. Xue, and I. Poccard, 2007: Numerical investigation of the impact of vegetation indices on the variability of West African summer monsoon. *J. Meteor. Soc. Japan,* **85A,** 363–383.

Masson, V., J.-L. Champeaux, F. Chauvin, C. Meriguet, and R. Lacaze, 2003: A global database of land surface parameters at 1-km resolution in meteorological and climate models. *J. Climate,* **16,** 1261–1282.

Mitchell, K. E., and Coauthors, 2004: The multi-institution North American Land Data Assimilation System (NLDAS): Utilizing multiple GCIP products and partners in a continental distributed hydrological modeling system. *J. Geophys. Res.,* **109,** D07590, doi:10.1029/2003JD003823.

Nicholson, S. E., 1980: The nature of rainfall fluctuations in subtropical West Africa. *Mon. Wea. Rev.,* **108,** 473–487.

——, 2000: Land surface processes and Sahel climate. *Rev. Geophys.,* **38,** 117–139.

——, and Coauthors, 2003: Validation of TRMM and other rainfall estimates with a high-density gauge dataset for West Africa. Part II: Validation of TRMM rainfall products. *J. Appl. Meteor.,* **42,** 1355–1368.

Noilhan, J., and J.-F. Mahfouf, 1996: The ISBA land surface parameterization scheme. *Global Planet. Change,* **13,** 145–159.

Nuret, M., J.-P. Lafore, N. Asencio, H. Bénichou, O. Bock, F. Favot, T. Montmerle, and Y. Seity, 2007: Evaluation of METEO-FRANCE NWP models during AMMA 2006-SOP. [Available online at www.cnrm.meteo.fr/aladin/newsletters/news32/news32.pdf.]

Philippon, N., E. Mougin, L. Jarlan, and P.-L. Frison, 2005: Analysis of the linkages between rainfall and land surface conditions in the West African monsoon through CMAP, ERS-WSC, and NOAA-AVHRR data. *J. Geophys. Res.,* **110,** D24115, doi:10.1029/2005JD006394.

——, L. Jarlan, N. Martiny, P. Camberlin, and E. Mougin, 2007: Characterization of the interannual and intraseasonal variability of West African vegetation between 1982 and 2002 by means of NOAA AVHRR NDVI data. *J. Climate,* **20,** 1202–1218.

Redelsperger, J.-L., C. D. Thorncroft, A. Diedhiou, T. Lebel, D. J. Parker, and J. Polcher, 2006: African Monsoon Multidisciplinary Analysis: An international research project and field campaign. *Bull. Amer. Meteor. Soc.,* **87,** 1739–1746.

Rodell, M., and Coauthors, 2004: The global land data assimilation system. *Bull. Amer. Meteor. Soc.,* **85,** 381–394.

Steiner, A., J. Pal, S. Rauscher, J. Bell, N. Diffenbaugh, A. Boone, L. Sloan, and F. Giorgi, 2009: Land surface coupling in regional climate simulations of the West African monsoon. *Climate Dyn.,* **33,** 869–892.

Sud, Y. C., and M. Fennessy, 1982: A study of the influence of surface albedo on July circulation in semi-arid regions using the GLAS GCM. *J. Climatol.,* **2,** 105–125.

Taylor, C. M., D. J. Parker, and P. Harris, 2007: An observational case study of mesoscale atmospheric circulations induced by soil moisture. *Geophys. Res. Lett.,* **34,** L15801, doi:10.1029/2007GL030572.

Timouk, F., and Coauthors, 2009: Response of sensible heat flux to water regime and vegetation development in a central Sahelian landscape. *J. Hydrol.,* **375,** 178–189.

Tulet, P., M. Mallet, V. Pont, J. Pelon, and A. Boone, 2008: The 7–13 March dust storm over West Africa: Generation, transport, and vertical stratification. *J. Geophys. Res.,* **113,** D00C08, doi:10.1029/2008JD009871.

Van den Hurk, B., and P. Viterbo, 2003: The Torne-Kalix PILPS 2(e) experiment as a test bed for modifications to the ECMWF land surface scheme. *Global Planet. Change,* **38,** 165–173.

Walker, J., and P. R. Rowntree, 1977: The effect of soil moisture on circulation and rainfall in a tropical model. *Quart. J. Roy. Meteor. Soc.,* **103,** 29–46.

Wang, J. R., and T. Schmugge, 1980: An empirical model for the complex dielectric permittivity of soils as a function of water content. *IEEE Trans. Geosci. Remote Sens.,* **18,** 288–295.

Wood, E. F., and Coauthors, 1998: The Project for Intercomparison of Land-Surface Parameterization Schemes (PILPS) Phase-2c Red–Arkansas River Basin experiment: 3. Experiment description and summary intercomparisons. *Global Planet. Change,* **19,** 115–139.

Xue, Y., and J. Shukla, 1996: The influence of land surface properties on Sahel climate. Part II: Afforestation. *J. Climate,* **9,** 3260–3275.

——, P. J. Sellers, J. L. Kinter III, and J. Shukla, 1991: A simplified biosphere model for global climate studies. *J. Climate,* **4,** 345–364.

——, and Coauthors, 2004: The Sahelian climate. *Vegetation, Water, Humans, and the Climate: A New Perspective on an Interactive System,* P. Kabat et al., Eds., Springer Verlag, 59–78.

Zaitchik, B. F., M. Rodell, and R. H. Reichle, 2008: Assimilation of GRACE terrestrial water storage data into a land surface model: Results for the Mississippi River basin. *J. Hydrometeor.,* **9,** 535–548.

Clim Dyn
DOI 10.1007/s00382-009-0653-1

Evaluation of the WAMME model surface fluxes using results from the AMMA land-surface model intercomparison project

Aaron Anthony Boone · Isabelle Poccard-Leclercq · Yongkang Xue · Jinming Feng · Patricia de Rosnay

Received: 13 March 2009 / Accepted: 13 August 2009

Abstract The West African monsoon (WAM) circulation and intensity have been shown to be influenced by the land surface in numerous numerical studies using regional scale and global scale atmospheric climate models (RCMs and GCMs, respectively) over the last several decades. The atmosphere–land surface interactions are modulated by the magnitude of the north–south gradient of the low level moist static energy, which is highly correlated with the steep latitudinal gradients of the vegetation characteristics and coverage, land use, and soil properties over this zone. The African Multidisciplinary Monsoon Analysis (AMMA) has organised comprehensive activities in data collection and modelling to further investigate the significance land–atmosphere feedbacks. Surface energy fluxes simulated by an ensemble of land surface models from AMMA Land-surface Model Intercomparison Project (ALMIP) have been used as a proxy for the best estimate of the "real world" values in order to evaluate GCM and RCM simulations under the auspices of the West African Monsoon Modelling Experiment (WAMME) project, since such large-scale observations do not exist. The ALMIP models have been forced in off-line mode using forcing based on a mixture of satellite, observational, and numerical weather prediction data. The ALMIP models were found to agree well over the region where land–atmosphere coupling is deemed to be most important (notably the Sahel), with a high signal to noise ratio (generally from 0.7 to 0.9) in the ensemble and a inter-model coefficient of variation between 5 and 15%. Most of the WAMME models simulated spatially averaged net radiation values over West Africa which were consistent with the ALMIP estimates, however, the partitioning of this energy between sensible and latent heat fluxes was significantly different: WAMME models tended to simulate larger (by nearly a factor of two) monthly latent heat fluxes than ALMIP. This results due to a positive precipitation bias in the WAMME models and a northward displacement of the monsoon in most of the GCMs and RCMs. Another key feature not found in the WAMME models is peak seasonal latent heat fluxes during the monsoon retreat (approximately a month after the peak precipitation rates) from soil water stores. This is likely related to the WAMME northward bias of the latent heat flux gradient during the WAM onset.

Keywords WAM · ALMIP · AMMA · WAMME · Monsoon · Surface fluxes

This paper is a contribution to the special issue on West African Climate, consisting of papers from the African Multidisciplinary Monsoon Analysis (AMMA) and West African Monsoon Modeling and Evaluation (WAMME) projects, and coordinated by Y. Xue and P. M. Ruti.

A. A. Boone (✉)
GAME-CNRM, Météo-France, Toulouse, France
e-mail: aaron.boone@meteo.fr; aaron.a.boone@gmail.com

I. Poccard-Leclercq
LETG-Géolittomer, Université de Nantes, Nantes, France

Y. Xue · J. Feng
University of California at Los Angeles, Los Angeles, CA, USA

P. de Rosnay
European Centre for Medium Range Weather Forecasting, Reading, UK

1 Introduction

The West African Monsoon (WAM) circulation intensity and extent are theorised to be significantly interconnected with the land surface. The overall circulation is driven by

Published online: 16 September 2009

land–sea thermal contrast, and the atmosphere–land surface interactions are modulated by the magnitude of the associated north–south gradient of the low level moist static energy (MSE: Eltahir and Gong 1996). The boundary layer MSE gradient exerts a strong influence on the position of the tropical front and the African Easterly Jet (Parker et al. 2005), and therefore the northward penetration of precipitation and it's intensity (Philippon and Fontaine 2002). The MSE distribution is a reflection of the surface turbulent fluxes which are highly correlated with the steep latitudinal gradients of the vegetation characteristics and coverage, land use, and soil properties over this zone.

Land surface processes have been shown to have an influence on the West African monsoon (WAM) circulation in numerous numerical studies using regional scale and global scale atmospheric climate models (RCMs and GCMs, respectively) over the last several decades. Charney et al. (1975) was one of the first researchers to use a coupled land-surface atmosphere model to demonstrate a proposed positive feedback mechanism between decreasing vegetation cover and the increase in drought conditions across the Sahel region of Western Africa. Numerous modelling studies since have examined the influence of the land surface on the WAM in terms of surface albedo (e.g. Sud and Fennessy 1982; Laval and Picon 1986), and the vegetation spatial distribution (e.g. Xue and Shukla 1996; Xue et al. 2004; Kang et al. 2007; Li et al. 2007). In addition, Zeng et al. (1999) used an idealised GCM configuration to show a significant contribution of vegetation dynamics to the WAM inter-annual precipitation variability.

The influence of soil moisture (which controls the partitioning of energy between the surface latent and sensible heat fluxes) on the WAM has also been examined using GCMs (e.g. Walker and Rowntree 1977; Cunnington and Rowntree 1986; Rowell and Blondin 1990; Douville et al. 2001). The emphasis on the role of soil moisture is related to the fact that this relatively slow temporally varying component of the coupled land–atmosphere monsoon system theoretically holds promise for improving long range predictability of the WAM. However, this long-term memory effect was recently put into question using a GCM and observational data (Douville et al. 2007), so further study is needed. Indeed there are significant differences with respect to the strength of this coupling simulated by state-of-the-art GCMs over western Africa and elsewhere (Koster et al. 2006; Guo et al. 2006), so the exploration of coupling should be done using a multi-model approach when possible. Part of this discrepancy is probably related to differences in the parameterisations of the surface fluxes and near-surface hydrology in land surface models (LSMs).

The African Multidisciplinary Monsoon Analysis (AMMA) has organised comprehensive activities in data collection and modelling to further investigate land–atmosphere feedbacks (Redelsperger et al. 2006). In terms of large scale atmospheric multi-model initiatives, the AMMA-Model Intercomparison Project (AMMA-MIP: Hourdin et al. 2009) inter-compares GCMs and RCMs over a meridional transect in West Africa focusing on seasonal prediction. The West African Monsoon Modelling Experiment (WAMME) project utilises such models to address issues regarding the role of ocean–land–aerosol–atmosphere interactions on WAM development (see Xue et al., this issue). The modelling of the land surface component of the WAM is being addressed by the AMMA Land-surface Model Intercomparison Project (ALMIP: Boone et al. 2009). The main idea behind ALMIP is to force a number of state-of-the-art LSMs off-line (i.e. de-coupled from atmospheric models) with the best quality and highest (space and time) resolution data available in order to better understand the key processes and their corresponding scales.

In recent years, there have been a number of offline multi-model intercomparison projects on an international level. Of note is the Project for the Intercomparison of Land-surface Parameterisation Schemes (PILPS: Henderson-Sellers et al. 1995). It dealt with land surface processes at the local to the regional scale and lead to significant improvements in LSM parameterisations. The Global Soil Wetness Project Phase 2 (GSWP-2: Dirmeyer et al. 2006) was an "off-line" global-scale LSM inter-comparison study which produced the equivalent of a land-surface reanalysis consisting in 10-year global data sets of soil moisture, surface fluxes, and related hydrological quantities. The advantage of such offline products is that biases in fully coupled models, notably in terms of precipitation and downwelling radiative fluxes, can be reduced by merging LSM forcing with observational and satellite-based data. The output data sets (notably soil moisture and surface fluxes) have been used as the best estimate of "truth" in numerous recent GCM and RCM studies at the global and regional scales. For example over Africa, Douville et al. (2001) assimilated offline-simulated soil moisture from GSWP-1 (Dirmeyer et al. 1999) into a GCM to study WAM surface–atmosphere feedback mechanisms.

ALMIP is similar to the aforementioned projects, but focuses on the west-African region and it covers the AMMA field campaign time period (the intensive observational phase or IOP was from 2004 to 2006). For example, ALMIP model outputs have recently been used to evaluate the impact of improved land surface physics on the simulation of the WAM by an RCM (Steiner et al. 2009). The main objective of this paper, therefore, is to utilise the off-line simulations of the surface energy fluxes from ALMIP as a proxy for the best estimate of observations in order to evaluate the corresponding fluxes simulated by the fully coupled (land–atmosphere) WAMME models. In this

paper, Sect. 2 describes the ALMIP input data and gives details about the LSM ensemble average, the WAMME-ALMIP surface flux comparison is given in Sect. 3, and conclusions and perspectives are given in Sect. 4.

2 Creation of the ALMIP surface flux dataset

2.1 ALMIP input forcing and parameters

The land surface model forcing database is comprised of two components, one for the land surface parameters, and the other for the LSM upper boundary conditions consisting in the atmospheric state variables, precipitation and downwelling radiative fluxes from multiple sources. The ECOCLIMAP global database (Masson et al. 2003) provides land surface parameters (albedo, vegetation cover fraction, surface roughness, leaf area index, soil texture, etc.). The vegetation phenology corresponds to a single representative annual at a 10-day time step. The default spatial resolution is 1 km, and included software up-scales and interpolates the data to the desired grid projection and spatial resolution. It is intended for use by LSMs in offline mode or which are coupled to GCM, numerical weather prediction (NWP), mesoscale meteorological research or hydrological models.

The low level atmospheric state variables are derived from the European Centre for Medium Range Weather Forecasts (ECMWF) forecasts from 2001 to 2007 at a 3 h time step. Downwelling radiative fluxes from OSI-SAF (Oceans and Ice Satellite Applications Facility: http://www.osi-saf.org) for 2004 and the LAND-SAF fluxes (Land Satellite Applications Facility: Geiger et al. 2008) for 2005–2007 are substituted for the corresponding NWP fluxes. The Tropical Rainfall Measurement Mission (TRMM) precipitation product 3B-42 (Huffman et al. 2007) is used from 2002 to 2007 (hereafter this product is simply referred to as TRMM in this paper). The TRMM rainfall estimates are based on combined calibrated microwave and infrared precipitation estimates with a rescaling to monthly gauge data where applicable. Note that there are many precipitation products available, but only TRMM met the main requirements of ALMIP-Exp3: (1) the spatial resolution (0.25°) was at or higher than that of the simulation grid, (2) the diurnal cycle is resolved (a 3 h time step is used by TRMM), (3) the entire annual cycle over the full LSM integration period is covered, (4) and TRMM was found to give relatively good rainfall estimates over this region in an AMMA-sponsored rainfall product intercomparison study (Jobard et al. 2007), and the best of the products meeting criteria 1–3. It should be noted that the goal of ALMIP is not to create new precipitation products, but rather to test existing datasets.

2.2 ALMIP experimental setup

The ALMIP model domain consists in the continental land surface bounded in the region from −5° to 20°N longitude, and −20° to 30°E latitude at a 0.50° spatial resolution (see Fig. 1). The ALMIP results presented in this paper are from Experiment 3 (hereafter these results are simply referred to as ALMIP in this paper) which uses a merged forcing which was described in the previous section (see Boone et al. 2009, for details on the other ALMIP experiments). Nine LSMs ran this experiment which covered the time period from 2002 to 2007, and they are listed along with a recent reference in Table 1. There were a total of 11 LSM simulations (two models did simulations using two different options: ISBA used the force-restore and the multi-layer diffusion soil options, while ORCHIDEE lowered the minimum allowable soil moisture from the default value). All of the LSMs used the same grid and atmospheric forcing, and the majority of the LSMs used either the provided soil and vegetation parameters or the closest equivalents, while a few used their own set of parameters (e.g. the ECMWF model used ALMIP results to test the influence of soil moisture initialisation in their operational forecast system, so they used their own set of parameters).

2.3 ALMIP ensemble average

Gao and Dirmeyer (2006) showed the advantages and improved realism of using a multi-LSM model average of simulated surface properties. They presented several different weighting techniques, ranging from a simple average to one using optimised weights which minimised errors based on observations. The low spatial density of surface observations over West Africa precluded the use of optimised weights, so the simple ensemble-mean of the ALMIP simulated surface fluxes are used in this study (which was also shown by Gao and Dirmeyer 2006, to be preferable to any single model realisation).

The evapotranspiration, *Evap*, for each LSM averaged over the core WAM season (June–September: JJAS) for 2005 is shown in Fig. 1. The northward extent and gradient of *Evap* is quite similar among the LSMs and is controlled to a large extent by the precipitation in this water-stressed region (north of about 15°N). While there are some differences around 10°N, the most significant differences are located over the equatorial forest region (east of 10°E, and south of 5°N). Because the inter-LSM differences in surface fluxes for the two ISBA and ORCHIDEE sensitivity runs were considerably smaller than the overall inter-LSM scatter (compare Fig. 1a, b, g, h, respectively), their results were simply averaged to give single realisation for these two models resulting in a 9-member ensemble average (denoted as AVG in Fig. 1l).

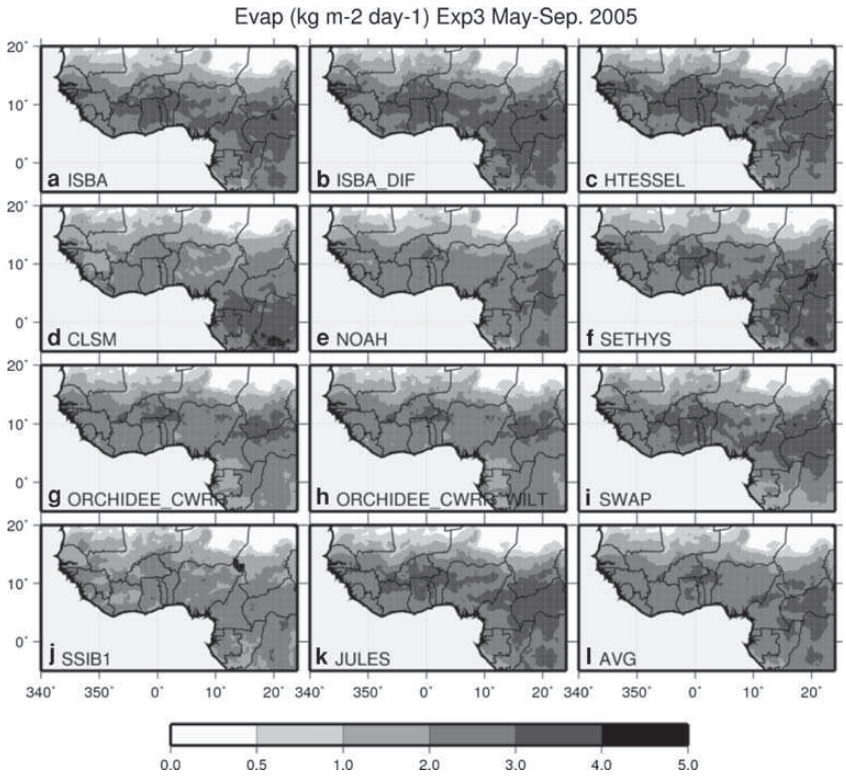

Fig. 1 ALMIP model evapotranspiration (*Evap*) averaged from May through October (the period covered by the WAMME model outputs) for 2005. The ALMIP ensemble average is shown in panel l

Table 1 ALMIP Exp.3 models

Model Acronym	Institute	Recent references	ALMIP model configuration
HTESSEL	ECMWF, Reading, UK *G. Balsamo*	Balsamo et al. (2009)	4L, 6 tiles, 1E, SV: ECMWF
ORCHIDEE-CWRR	IPSL, Paris, France T. *Orgeval and P. deRosnay*	d'Orgeval et al. (2008), de Rosnay et al. (2002)	11L, 13 tiles, 1E, SV: ECOCLIMAP
ISBA[a] ISBA-DIF[b]	CNRM, Météo-France, Toulouse *A. Boone*	(a) Noilhan and Mahfouf (1996), (b) Boone et al. (2000)	3L[a], 5L[b], 1 tile, 1E, SV: ECOCLIMAP
JULES	CEH, Wallingford, UK *P. Harris*	Essery et al. (2003)	4L, 9 tiles, 1E, SV:ECOCLIMAP
SETHYS	CETP/LSCE, France *S. Saux-Piccard and C. Ottlé*	Coudert et al. (2006)	2L, 12 tiles, 2E, SV: ECOCLIMAP
NOAH	CETP/LSCE (NCEP) *B. Decharme and C. Ottlé*	Chen and Dudhia (2001), Decharme (2007)	7L, 12 tiles, 1E, SV: ECOCLIMAP
CLSM	UPMC, Paris, France *S. Gascoin and A. Ducharne*	Koster et al. (2000)	5L, 5 tiles, 3E, SV: ECOCLIMAP
SSiB	LETG, Nantes, France; UCLA, Los Angeles, USA *I. Poccard-Leclercq*	Xue et al. (1991)	3L, 1 tile, 2E, SV: SSiB
SWAP	IWP, Moscow, Russia *Y. Gusev and O. Nasonova*	Gusev et al. (2006)	3L, 1 tile, 1E, SV: ECOCLIMAP

A recent model reference is given. The names of the people who performed the simulations are in italics. The model configuration used for ALMIP is shown in the rightmost column where L represents the number of vertical soil layers, E represents the number of energy budgets per tile (a separate budget for snow cover is not considered here), and SV corresponds to the soil–vegetation parameters used. Tile refers to the maximum number of completely independent land surface types permitted within each grid box

Quantitative estimates of the inter-LSM variability are shown in Fig. 2. The so called "omega" statistic (Koster et al. 2002) is used to give an estimate of the signal to noise ratio: it was computed using daily average *Evap* values over the entire annual cycle for 2005 and is shown in Fig. 2a. Large values (approaching unity) indicate areas were the model time series are well correlated, which corresponds to a more significant impact of the forcing (notably the precipitation). The best agreement occurs over the Sahel region (north of about 10°N), which is of interest as this is the region where precipitation recycling should be significant. Areas with lesser LSM agreement (lower values) are located where soils are generally deeper and the vegetation coverage is more dense (especially in forested areas). Several factors lead to greater LSM disagreement here: deeper soils coupled with parameterisation differences in sub-surface hydrology and water uptake by vegetation cause model dispersion, and there is considerable spread in terms of the time evolution of soil evaporation beneath forest canopies.

The coefficient of variation (ratio of the inter-LSM variability to the LSM average) for the same time interval is shown in Fig. 2b. Values are not surprisingly highest along the northern fringe of the domain owing to very low precipitation rates coupled with a very high atmospheric demand, however, elsewhere the inter-LSM variability is about 5–15% of the average which indicates a fairly good agreement. The values are slightly larger (exceeding 15%) over the equatorial forest region. In this paper, however, the lower agreement over the aforementioned zone is not very important as the focus is on the region from −10° to 10°E, where the LSMs have a fairly good agreement.

The monthly LSM-average (±1 SD) water and energy budget components averaged over the Sahel are shown in Figs. 3a and b, respectively. Note that hereafter in this paper, the Sahel is somewhat arbitrarily defined from −10° to 10°E longitude, and from 11° to 17°N latitude. Although the onset of heavier precipitation is earlier in 2005 than in 2004, some general observations can be made for both years. Peak *Evap* occurs approximately 2 months after peak rains (in July), and the timing of this peak corresponds with the change in sign of soil moisture storage (the peak is mostly storage driven). Also, the LSM-average runoff ratio (runoff to precipitation) is rather low (less than approximately 10% over the Sahel) and total annual soil water storage is also a relatively small, so much of the rainfall is recycled (evaporated).

The corresponding LSM surface flux components (net radiation, *Rnet*, sensible, *Qh*, and latent, *Qle*, heat fluxes) are shown in Fig. 3b. The inter-LSM *Rnet* scatter is lower

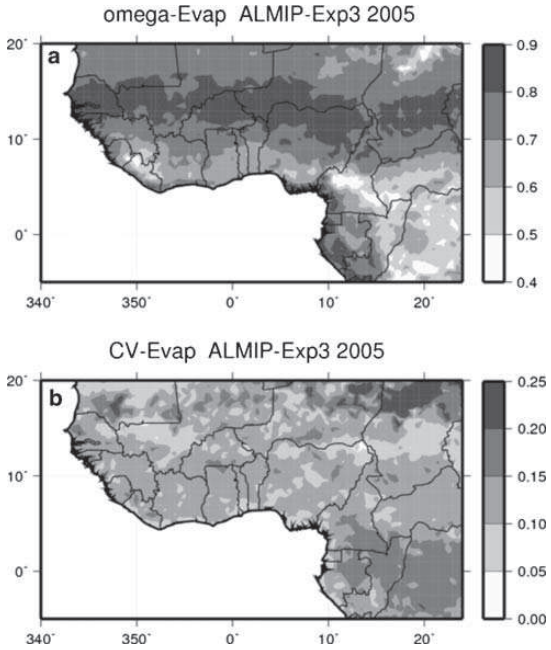

Fig. 2 The "omega" coefficient, which represents the signal to noise ratio in the ensemble, for the ALMIP *Evap* is shown in panel **a**, and the coefficient of variation is shown in panel **b**. Both statistics were computed using daily values for all of 2005

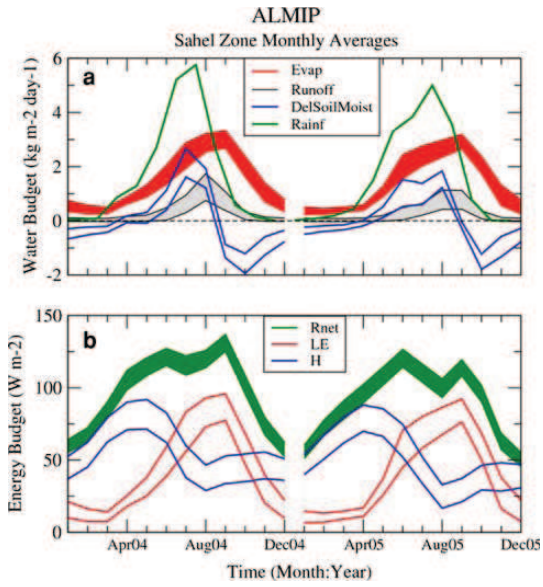

Fig. 3 The mean and spread (±1 SD) for the ALMIP ensemble computed over the Sahel (see the text for the definition of the Sahel used herein). The water budget components are shown in panel **a**, and the energy budget components are shown in panel **b**

than for the surface turbulent fluxes, which results because most of this flux is constrained by the forcing (incoming shortwave and longwave fluxes are the same for all models, and in addition the emissivity and albedo are prescribed). In both years, there is a double-peak (maxima in June and September), which result primarily due to high incoming shortwave radiation prior to monsoon onset and just after it's retreat. The sensible and latent heat flux peaks are approximately 5 months apart, with the *Qle* becoming dominant during the onset month, and the *Qh* becoming larger at the end of each year once the soil moisture reserve has been sufficiently depleted.

In terms of ALMIP evaluation, it was found that the LSMs performed well on the large scale in terms of capturing the seasonal cycle of the near surface soil moisture using remotely sensed data (see de Rosnay et al. 2009, for details). Many land surface flux stations were installed during the AMMA field campaign (Redelsperger et al. 2006), but it is difficult to compare ALMIP output fluxes directly with local scale values due to the ALMIP grid resolution. However, spatially up-scaled surface fluxes are available for the Mali mesoscale site which corresponds to the ALMIP grid box at −1.5°E 15.5°N. The comparison of the observed up-scaled surface *Qh* with the ALMIP-AVG for a single pixel is shown in Fig. 4. The modelled and observed aggregated *Qh* values have been averaged over 10-day periods for this comparison. The *Qh* time series for each site have been weighted by the fraction of their corresponding land cover type over the mesoscale box (approximately 60 km resolution) using remotely sensed data (Timouk et al. 2008). In Fig. 4, dashed curves correspond to the 3-year average (2005–2007) time series for each observation site within the mesoscale domain. Each site represents a very different land cover type: Kelma is a low-lying marshy site during and after the wet season, Eguerit is a rocky site with little vegetation, and the Agoufou site has sparse low vegetation. The aggregated observed fluxes and associated variability are shown by the shaded region. The solid curves enclose a region bounded by ±1 SD about the LSM-AVG *Qh* averaged over 2005–2007. The LSM-average simulated *Qh* response to the wet season and the subsequent dry-down are well correlated with the observed average *Qh*, and the magnitude is well simulated. A detailed analysis of ALMIP LSM evaluation is beyond the scope of this paper (for more details, see Boone et al. 2009).

3 WAMME surface flux evaluation

The analysis in this study focuses on the period from 2004 to 2005 because there is an overlap between the WAMME and ALMIP outputs. Note that WAMME also covers 2003,

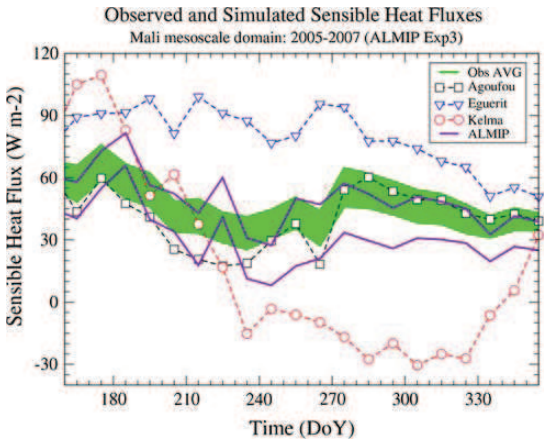

Fig. 4 The 3-year average (2005–2007) observed *Qh* for the three local sites are indicated by the *dashed lines*, and the *shaded green area* corresponds to the spread of the spatially aggregated fluxes (representing the 60 × 60 km^2 supersite domain). The *solid curves* enclose the spread (1 SD) of the ALMIP multi-model *Qh* averaged over 2005–2007 for Exp.3. The observed flux data for this figure were taken from Timouk et al. (2008)

but the satellite-based SAF radiative fluxes were not available for this year. The WAMME evaluation is based on the availability of outputs from May to October. Note that the focus of this study is on seasonal cycles, so that the monthly mean values are examined in this study. Finally, a description of the WAMME models and the experimental setup are given in Xue et al. (this issue): the same model naming convention is used herein. A summary of the WAMME LSM configurations are given in Table 2.

3.1 Comparison of WAMME variables with ALMIP forcing

The precipitation simulation by the WAMME models is of key importance for the surface fluxes, especially in the Sahel were the atmospheric demand and large incoming radiative energy cause most of the precipitation to be evaporated from the surface (as shown in Sect. 2). The WAMME simulated precipitation for the entire ALMIP domain averaged over the core monsoon period JJAS 2004 is compared to the TRMM precipitation in Fig. 5 in the form of scatter plots (the correlation, root mean square difference or RMS and the bias are shown in each panel). The majority of the WAMME models have a positive precipitation bias. NCEP2 (NCEP reanalysis version 2) has one of the lowest at −0.1 kg m^{-2} day^{-1}, but NCEP2 replaced model precipitation at the surface with a rainfall product (see Xue et al., this issue). The inter-rainfall product variability for several standard satellite and gauge based products is considerably smaller than the inter model

Table 2 As in Table 1 except for the WAMME LSMs

A recent model reference is given (the atmospheric model references can be found in Xue et al. 2009). The default LSM configuration used is shown in the rightmost column. The LSMs each used their respective vegetation and soil parameters

WAMME GCM/RCM Acronym	LSM acronym and reference	WAMME configuration
NCEP	NCEP: Pan and Mahrt (1987)	2L, 1 tile, 1E
CFS	NOAH: Chen and Dudhia (2001)	4L, 1 tile, 1E
GFS	NOAH (as above)	4L, 1 tile, 1E
COLA	SSiB: Xue et al. (1991)	3L, 1 tile, 2E
UCLA	SSiB (as above)	3L, 1 tile, 2E
UCLA MRF	SSiB (as above)	3L, 1 tile, 2E
JMA	SiB: Sellers et al. (1986)	3L, 1 tile, 2E
NASA FVGCM	CLM: Dai et al. (2003)	10L, 1 tile, 2E
NCAR CAM	CLM: (as above)	10L, 1 tile, 2E
MOHC	JULES: Essery et al. (2003)	4L, 1 tile, 1E
NASA GMAO	MOSAIC: Koster and Suarez (1996)	3L, 8 tiles, 1E
MM5	NOAH: Chen and Dudhia (2001)	4L, 1 tile, 1E
NASA GISS	GISS: Rosenzweig and Abramopoulos (1997)	6L, 1 tile, 2E
RegCM	BATS: Dickinson et al. (1993)	3L, 1 tile, 2E

variability (see Xue et al., this issue: this is also discussed in more detail in the next paragraph). A high correlation implies that the position and strength of the JJAS-averaged meridional precipitation gradient is similar between the WAMME model and TRMM, and two models (UCLA, and MOHC HadRM3P-NCEP) have both a high correlation (above 0.8) and a relatively low bias (less than 1 kg m^{-2} day^{-1}). It is interesting to note that the best statistics overall are obtained by the GCM ensemble (Fig. 5b). The significance of the ensemble performance is detailed in Xue et al. (this issue).

In fact, it should be noted that the results presented here are not exclusive to TRMM. Indeed, the agreement between different commonly used satellite rainfall products at the monthly scale is much better than that among the WAMME models, so any one of several can be used to evaluate the model performances (depending on the spatial and temporal resolution requirements for evaluation). An example is shown for the Sahel in Fig. 6: thick lines correspond to the commonly used products TRMM, Global Precipitation Climatology Centre (GPCC: Schneider et al. 2008), Global Precipitation Climatology Project (GPCP: Adler et al. 2003), and Climate Prediction Center RainFall Estimation version 2.0 (CPC-RFE2: Laws et al. 2004). The thin lines correspond to the WAMME simulated rain rates. Note that the rainfall simulation problem is also present in operational NWP models (the ECMWF curve based on 12–36 h forecasts is also shown, and it underestimates the rainfall primarily because the latitude of the core of the active precipitation zone is south of the Sahel. This problem is well known at ECMWF: A. Beljaars, personal communication).

The spatial correlations of the downwelling shortwave radiation and the precipitation (averaged over JJAS 2004) are shown in Fig. 7 (where the same letters are used to identify the WAMME models as in Fig. 5). Of the 17 simulations shown, the majority of them show a fair consistency in that better shortwave radiation simulations correspond to better precipitation simulations (compared to the satellite-based product OSI-SAF). Once again, the GCM ensemble is the best (symbol b). Three of the four models with the lowest shortwave correlation tend to simulate the monsoon too far north or south compared to the ALMIP forcing, while the remaining one (NCEP-GFS) simulates a reasonable position but with widespread high precipitation rates within the active monsoon region. Note that the inter-model variability exceeds the inter-annual differences for the 2 years considered, so the conclusions are essentially the same for 2004 as 2005 (not shown here). The spatial and temporal distributions of the precipitation and incoming solar energy obviously modulate the surface fluxes, especially in the transition zone from the dessert to vegetated areas (in the Sahel). This will e examined further in the next section.

3.2 WAMME simulated surface fluxes

The key surface flux which couples the surface to the atmosphere via the hydrological cycle is the latent heat flux. The WAMME model JJAS average latent heat flux, *Qle,* for 2004 is shown in Fig. 8 (the ALMIP *Qle* is shown in Fig. 8w). Looking at the spatial patterns and magnitudes, it is seen that the GCM ensemble compares best with ALMIP (consistent with the analysis in the previous section, see Fig. 7). Three models have relatively high *Qle* rates up to 20°N owing to the penetration of the monsoon too far north (MRI-JMA, Cornell MM5, NCAR CAM-CLM3 and MOHC HadAM3), two models have a monsoon

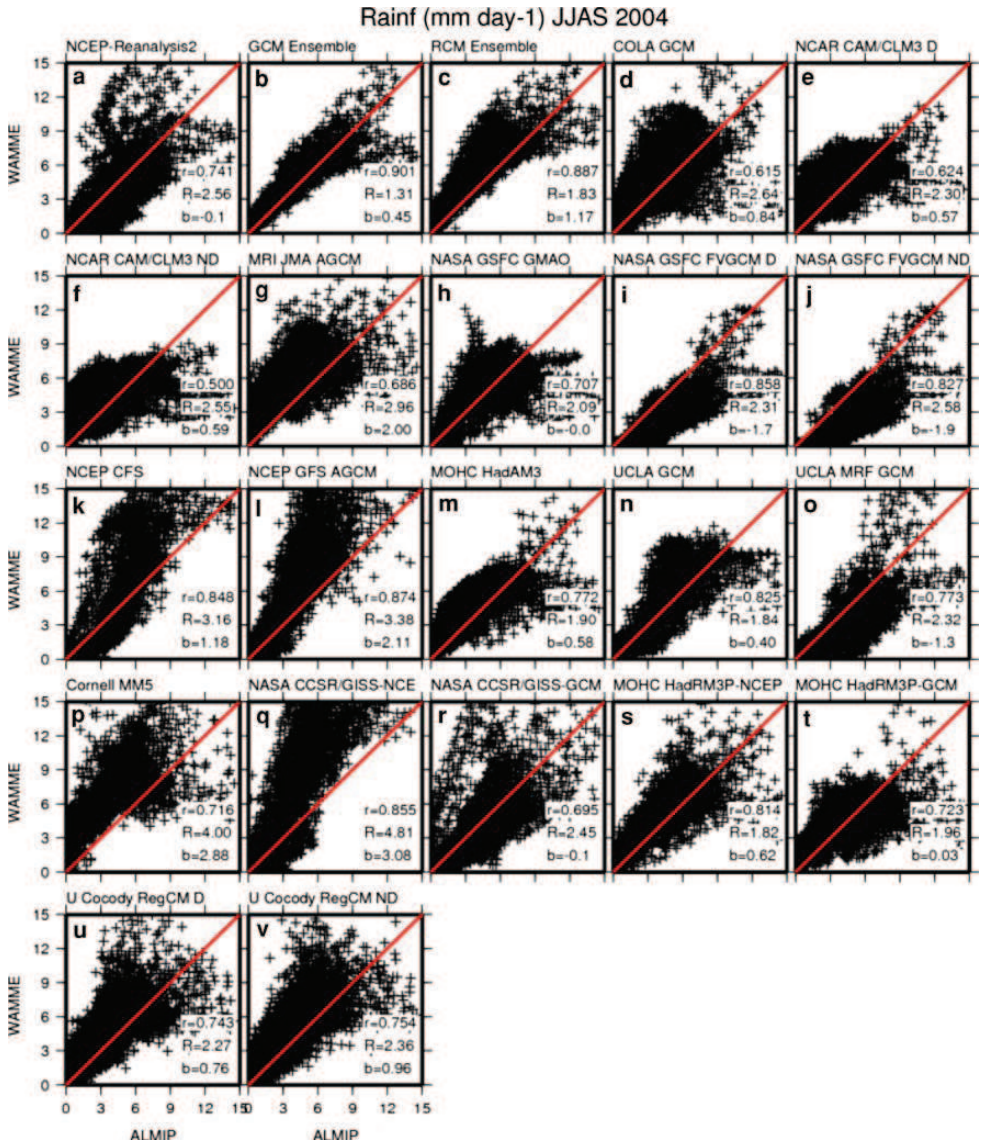

Fig. 5 Scatter plots of the WAMME simulated rainfall verses the values from ALMIP (based on TRMM 3B42). The statistics are computed over the 4 month core monsoon period (June–September). The statistics shown are the correlation, *r*, the root mean square difference, *R*, and the bias, *b*

which stays too far south (UCLA-MRF and NASA GSFC FVGCM), while the remaining models are more consistent with ALMIP. Because of the significant amount of precipitation recycling north of about 10°N because of large atmospheric demand, the evaporation and precipitation are highly correlated. The meridional *Qle* gradient varies significantly among the models, and this will be discussed in more detail later in this section.

The statistical comparison of the JJAS 2004 *Qle* between the WAMME models and ALMIP is shown in Fig. 9. The lowest bias and root mean square difference is for NCEP2, which is reassuring since the surface received a satellite-based precipitation product as opposed to the model precipitation. The best overall agreement with ALMIP in terms of all three statistics is once again the GCM ensemble, although the RCM ensemble is fairly close.

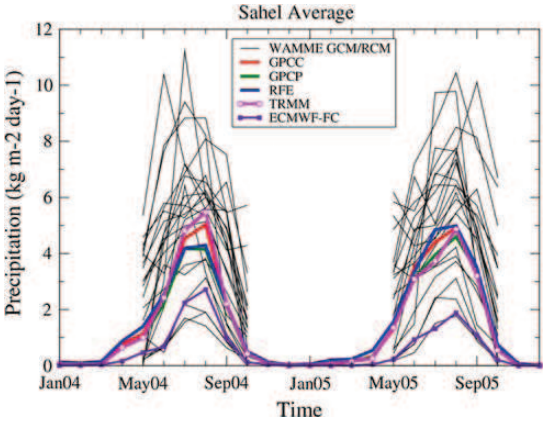

Fig. 6 Comparison of the spatial correlation between WAMME and ALMIP for the downwelling solar radiation (ordinate) and the precipitation. The *boxed region* indicates models which performed the best

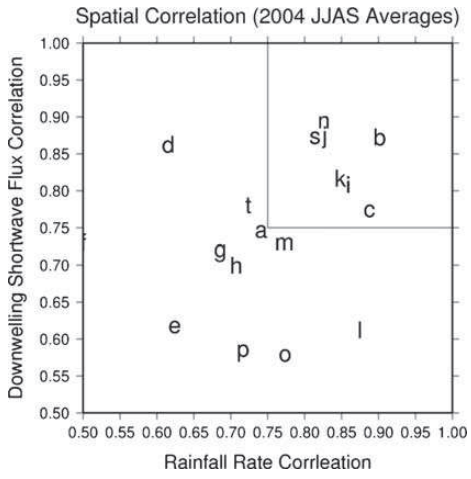

Fig. 7 The Sahel average rainfall monthly time series for 2 years: different precipitation products are represented by *thick curves*, and the WAMME model simulations are indicated by the *thin black curves*. The ECMWF forecast simulation is also indicated

Because of the positive precipitation bias of the WAMME models, there is also a positive *Qle* bias with many models having maximum values of approximately 50% larger than ALMIP maximum values. The overall WAMME *Qle* positive bias is probably also related to the fact that most of the models tend to simulate the monsoon too far north, where atmospheric demand is larger so that precipitation recycling should be intensified.

Hovmoller plots of *Qle* for 2004 (from May to October) are shown in Fig. 10, where the *Qle* has been averaged from −10° to 10°E longitude. The ALMIP *Qle* temporal evolution is asymmetric, with considerably larger *Qle* rates during the monsoon retreat than during any other period. This results as water stored in the root zone is evaporated after the precipitation rates have diminished. The large *Qle* results from a combination of ample soil moisture, significant incoming solar radiation and relatively large atmospheric demand (i.e. relatively dry atmospheric conditions). There is also a relative ALMIP *Qle* minimum transitioning from July to August south of 10° N due to lower precipitation and incoming radiation and humid conditions. In contrast with ALMIP, most of the WAMME models have a fairly symmetric *Qle* temporal evolution, with only COLA, MOHC HadAM3, NCEP-GFS, NCAR CAM/CLM3 and Cornell MM5 having maximum *Qle* rates occurring during the monsoon retreat. NCEP2 has the best overall agreement in terms of *Qle* meridional gradient and northward extent and timing, but this is expected as the precipitation is not from the atmospheric model (it is satellite based as for ALMIP). Therefore for most of the models, the soil water reserve does not seem to be greatly impacting the late season *Qle*. In general agreement with ALMIP, most of the models have a relative *Qle* minimum south of 10°N during the monsoon period, but the exact position in time, magnitude and spatial extent are quite variable.

Of key importance (as mentioned in the introduction) for the monsoon intensity, is the meridional gradient of the surface fluxes. The ratio of *Qh* to the *Rnet* is used in order to explore the surface energetics in a relative sense. The corresponding meridional gradient for each of the WAMME models (averaged from −10° to 10°E longitude) for three times (onset in June, peak monsoon activity in August and post monsoon in October) are shown in Fig. 11 together with the ALMIP values. Several WAMME models have been highlighted (using thick curves) as a reference. During the onset period for both years, ALMIP has more energy going into sensible than latent heating compared to WAMME. Again, this is probably mostly related to the lower ALMIP precipitation rates. Also, quite a few models already have the active monsoon region extending up to approximately 13°N indicated by the inflection point in many of the curves. Although there is considerable scatter, most of the models are similar to ALMIP in August (except for those which place rainfall north of 20°N, indicated by the very low ratios north of 15°N). Ratios range from approximately 0.3 to 0.7 from south to north. October has the most inter-model scatter north of about 12°N, with ratios ranging from 0.2 to nearly 1.0 at 20°N. In contrast, the models have the best agreement with each other and with ALMIP south of 10°N. This is probably because the relatively low incoming solar radiation is preferentially used for evaporation over the relatively wet and well vegetated surfaces. One model of note is NCEP2, which has a markedly different behaviour than all of the other

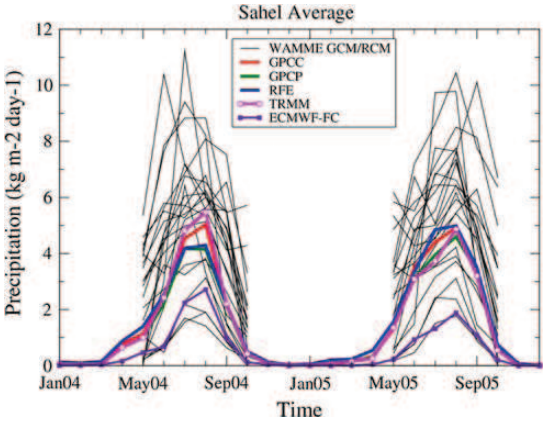

Fig. 6 Comparison of the spatial correlation between WAMME and ALMIP for the downwelling solar radiation (ordinate) and the precipitation. The *boxed region* indicates models which performed the best

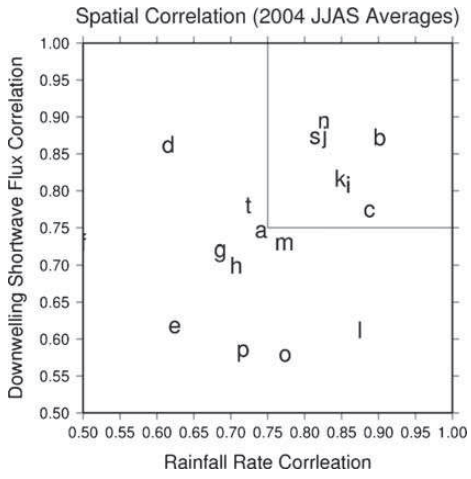

Fig. 7 The Sahel average rainfall monthly time series for 2 years: different precipitation products are represented by *thick curves*, and the WAMME model simulations are indicated by the *thin black curves*. The ECMWF forecast simulation is also indicated

Because of the positive precipitation bias of the WAMME models, there is also a positive *Qle* bias with many models having maximum values of approximately 50% larger than ALMIP maximum values. The overall WAMME *Qle* positive bias is probably also related to the fact that most of the models tend to simulate the monsoon too far north, where atmospheric demand is larger so that precipitation recycling should be intensified.

Hovmoller plots of *Qle* for 2004 (from May to October) are shown in Fig. 10, where the *Qle* has been averaged from −10° to 10°E longitude. The ALMIP *Qle* temporal evolution is asymmetric, with considerably larger *Qle* rates during the monsoon retreat than during any other period. This results as water stored in the root zone is evaporated after the precipitation rates have diminished. The large *Qle* results from a combination of ample soil moisture, significant incoming solar radiation and relatively large atmospheric demand (i.e. relatively dry atmospheric conditions). There is also a relative ALMIP *Qle* minimum transitioning from July to August south of 10° N due to lower precipitation and incoming radiation and humid conditions. In contrast with ALMIP, most of the WAMME models have a fairly symmetric *Qle* temporal evolution, with only COLA, MOHC HadAM3, NCEP-GFS, NCAR CAM/CLM3 and Cornell MM5 having maximum *Qle* rates occurring during the monsoon retreat. NCEP2 has the best overall agreement in terms of *Qle* meridional gradient and northward extent and timing, but this is expected as the precipitation is not from the atmospheric model (it is satellite based as for ALMIP). Therefore for most of the models, the soil water reserve does not seem to be greatly impacting the late season *Qle*. In general agreement with ALMIP, most of the models have a relative *Qle* minimum south of 10°N during the monsoon period, but the exact position in time, magnitude and spatial extent are quite variable.

Of key importance (as mentioned in the introduction) for the monsoon intensity, is the meridional gradient of the surface fluxes. The ratio of *Qh* to the *Rnet* is used in order to explore the surface energetics in a relative sense. The corresponding meridional gradient for each of the WAMME models (averaged from −10° to 10°E longitude) for three times (onset in June, peak monsoon activity in August and post monsoon in October) are shown in Fig. 11 together with the ALMIP values. Several WAMME models have been highlighted (using thick curves) as a reference. During the onset period for both years, ALMIP has more energy going into sensible than latent heating compared to WAMME. Again, this is probably mostly related to the lower ALMIP precipitation rates. Also, quite a few models already have the active monsoon region extending up to approximately 13°N indicated by the inflection point in many of the curves. Although there is considerable scatter, most of the models are similar to ALMIP in August (except for those which place rainfall north of 20°N, indicated by the very low ratios north of 15°N). Ratios range from approximately 0.3 to 0.7 from south to north. October has the most inter-model scatter north of about 12°N, with ratios ranging from 0.2 to nearly 1.0 at 20°N. In contrast, the models have the best agreement with each other and with ALMIP south of 10°N. This is probably because the relatively low incoming solar radiation is preferentially used for evaporation over the relatively wet and well vegetated surfaces. One model of note is NCEP2, which has a markedly different behaviour than all of the other

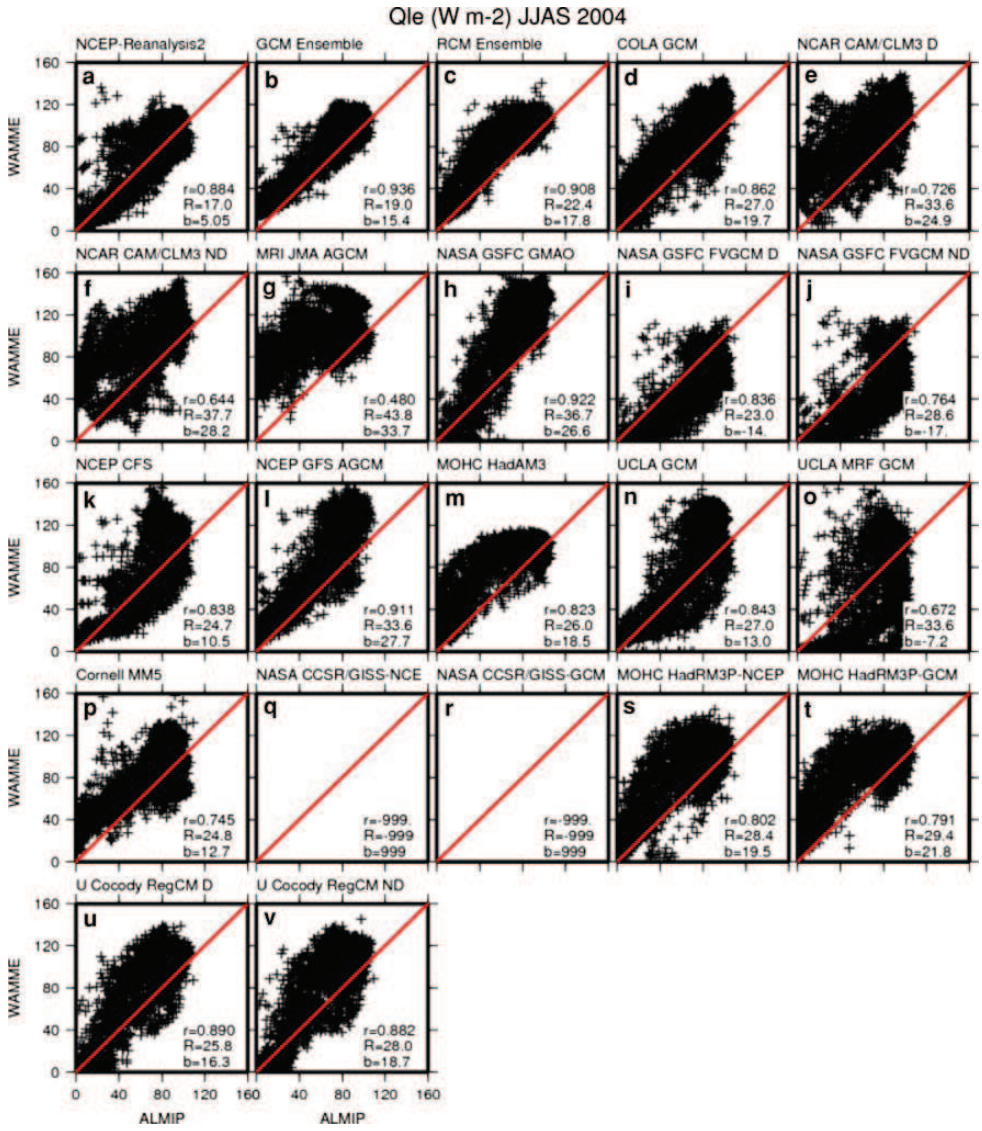

Fig. 9 As in Fig. 4 except for the latent heat flux

compared to ALMIP (owing to rainfall); however, SWIp values are nearly unity in a large area south of 10°N. In fact, this is a common trait in most of the WAMME models. In contrast, Kohler et al. (2009) showed that at a site located in Burkina Fasso (approximately 10° and −3°) during the special observing period in 2006, the daily average Bowen ratio (ratio of sensible to latent heat flux) tended to have minimum values after rainfall events no lower than about 0.27, which corresponds to a maximum SWIp as defined here of approximately 0.78 (consistent with the ALMIP values, which are less than 0.8). This indicates that significant sensible heating of the atmosphere still takes place south of 10°N during the monsoon season in contrast to what is seen in the majority of WAMME models.

4 Conclusions and perspectives

Surface energy fluxes simulated by an ensemble of land surface models from ALMIP have been used as a proxy for the best estimate of the "real world" values in order to

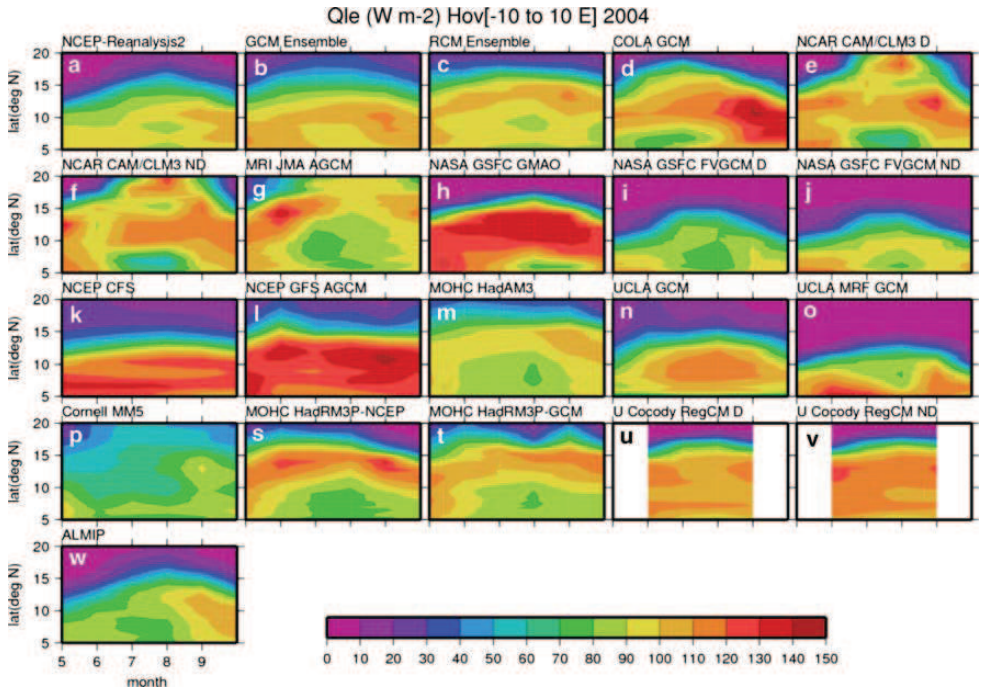

Fig. 10 WAMME model latent heat flux Hovmoller plots for 2004 averaged from −10° to 10°E for 2004. The ALMIP Hovmoller is shown in panel w

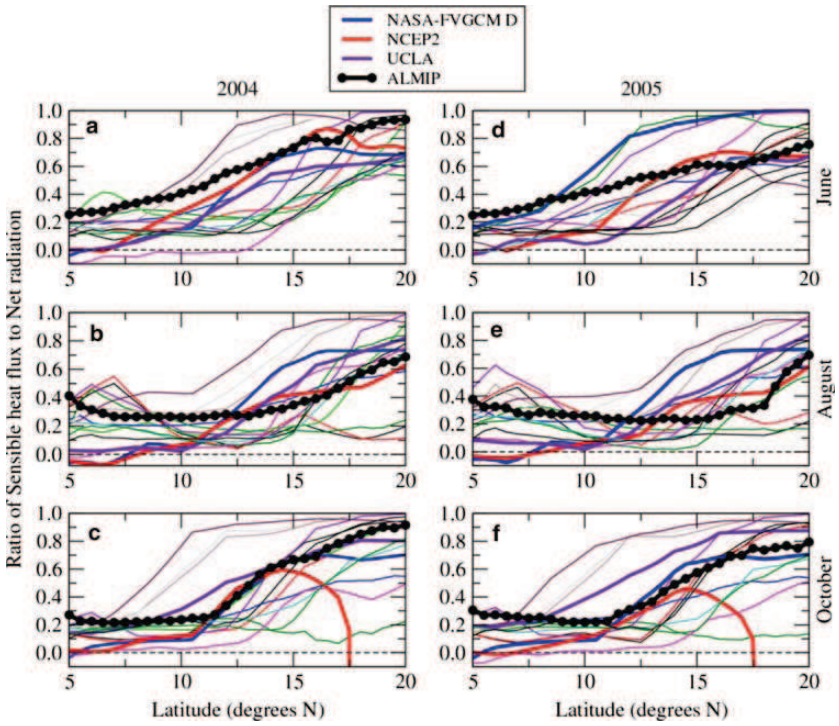

Fig. 11 Meridional profiles of the ratio of the sensible heat flux to the net radiation for three different months averaged from −10° to 10°E. The *thick black curve* corresponds to ALMIP. Several WAMME models are indicated

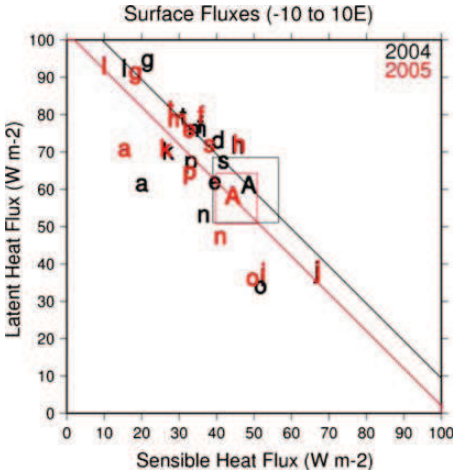

Fig. 12 A comparison of the latent and sensible heat fluxes averaged from −10° to 10°E and from May through October. The WAMME symbols are the same as those in Fig. 8. The A is used to indicate ALMIP. *Boxes* represent the ALMIP range. *Diagonal lines* represent the net radiation simulated by ALMIP

evaluate GCM and RCM simulations under the auspices of the WAMME project, since such large-scale observations do not exist. The ALMIP models have been forced in off-line mode using satellite and gauge based precipitation estimates from TRMM 3B42, downwelling satellite based radiative flux products from OSI and LAND-SAF, and atmospheric state variables from NWP.

An ensemble average is computed for all of the surface energy and water budget components, and the inter-model variability is examined for two annual cycles. The LSM fluxes agree well with a coefficient of variation for latent heat flux ranging from approximately 5–15% over most of West Africa, with the best agreement over the semi-arid Sahel where precipitation recycling is most significant. The ensemble signal to noise ratio of the surface turbulent fluxes is fairly large over most of the region, with the exception of the equatorial rain forest. This is related to the fact that soils are deepest (impacting hydrology and water storage) and vegetation processes (such as radiative transfer and root zone water uptake) and interactions with the under story are more complex. The simulated fluxes over this region have a larger uncertainty (owing to more model disagreement), however, the focus is on the WAM so that the WAMME analysis is mostly done outside of this area.

The WAMME model simulated net radiation agrees rather well with ALMIP for most of the WAMME models, however, the partitioning of this energy into turbulent fluxes is different from ALMIP and is quite variable. The main reason for the difference with respect to ALMIP is that the WAMME models have a positive precipitation bias compared to ALMIP. Because there is ample energy, this leads

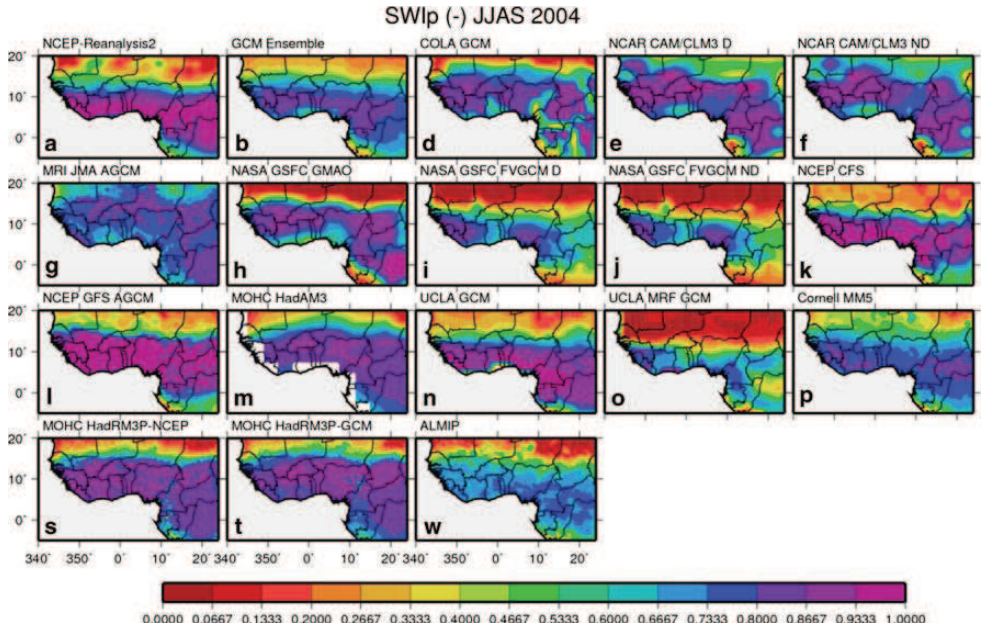

Fig. 13 The WAMME Soil Wetness Index proxy (SWIp) averaged from June through September (JJAS) for 2004. The corresponding ALMIP field is shown in panel w

to larger latent heat fluxes and very little rainfall is being stored or becomes runoff in the WAMME models. This seems to be due, in part, to further northward placement of monsoon in areas with larger potential energy for evaporation or most of the WAMME models. Further research is needed to determine how much the surface contributes to this displacement of the WAM in the WAMME models. NCEP2 is a special case. Surface latent heat fluxes agree well with ALMIP compared to most of the WAMME models, which is comforting since, like ALMIP, the precipitation is not based on NWP (but rather a mixed satellite-gauge approach). But the surface net radiation is quite different (primarily owing to albedo differences), so that sensible heat fluxes are among the lowest of all the WAMME models (and in contrast to ALMIP estimates).

In terms of the annual cycle over West Africa, ALMIP produces the maximum latent heat flux during the monsoon retreat as stored water is evaporated before solar radiation reaches the boreal winter minima: only six of the WAMME models have this feature, and it is generally rather weak. Also, the starting point for the monsoon (in May) is further north than ALMIP for all of the WAMME models except for the two models which keep the monsoon too far south. Thus before onset, the maximum low level MSE gradient is further to the north than ALMIP for most of the WAMME models.

The meridional ratio of sensible heat flux to the net radiation during onset (June) (from 5° to 20°N) is larger in ALMIP than in the WAMME models, mainly because the monsoon starts further south and temrally lags most of the WAMME models (the monsoon jump in TRMM is generally more rapid than in the WAMME models). The best general agreement with ALMIP is in August, when the meridional gradient is generally the lowest. During the monsoon retreat, most of the WAMME models agree quite well with ALMIP south of 10°N (the aforementioned ratio is between 0.1 and 0.2 for most models), while north of 10°N there is the greatest dispersion of WAMME models for the 3 months considered. This seems to be related to large differences in soil water storage and it's extraction within the WAMME models.

In order to truly respond to questions regarding the coupling between the land surface and the atmosphere using GCMs and RCMs, special experiments in which the models are constrained by offline soil moisture (e.g. Douville et al. 2001) or offline surface fluxes (perhaps using a flux replacement method, such as that presented by Dirmeyer and Zhao 2004) should be done focusing on this region using a multi-model GCM or RCM approach together with ALMIP outputs. This effort would also be complemented by the large unique dataset consisting in both surface and atmospheric data measured during the AMMA field campaign.

Acknowledgments The authors would like to acknowledge the support of the data providers, notably R. Lacaze, B. Geiger, D. Carrer and J.-L. Roujean, who have offered considerable assistance with respect to using the LAND-SAF downwelling radiative flux products. A. Marsouin provided guidance on the OSI-SAF radiation product. We wish to extend our gratitude to the POSTEL Service Centre (http://postel.mediasfrance.org) at MEDIAS-France for customising and providing the LSA SAF products. We gratefully acknowledge the European Centre for Medium-Range Weather Forecasts for the use of the ECMWF forecast data. We would like to acknowledge the hard work of the ALMIP Working Group members: G. Balsamo, A. Beljaars, C. Delire, P. Harris, C. Taylor, T. Orgeval, J. Polcher, A. Ducharne, A. Nørgaard, I. Sandholt, S. Gascoin, Y. Gusev, O. Nasonova, S. Saux-Picart, C. Ottle, and B. Decharme, and the WAMME Working Group members. Based on a French initiative, AMMA has been established by an international group and is currently funded by a large number of agencies, especially from France, the UK, and Africa. It has been the beneficiary of a major financial contribution from the European Community's Sixth Framework Research Programme.

References

Adler RF, Huffman GJ, Chang A, Ferraro R, Xie P, Janowiak J, Rudolf B, Schneider U, Curtis S, Bolvin D, Gruber A, Susskind J, Arkin P (2003) The Version 2 Global Precipitation Climatology Project (GPCP) monthly precipitation analysis (1979-present). J Hydrometeorol 4:1147–1167

Balsamo G, Viterbo P, Beljaars A, van den Hurk B, Hirsch M, Betts A, Scipal K (2009) A revised hydrology for the ECMWF model: verification from field site to terrestrial water storage and impact in the Integrated Forecast System. J Hydrometeorol 10:623–643

Boone A, Masson V, Meyers T, Noilhan J (2000) The influence of the inclusion of soil freezing on simulations by a soil–vegetation–atmosphere transfer scheme. J Appl Meteorol 9:1544–1569

Boone A, de Rosnay P, Basalmo G, Beljaars A, Chopin F, Decharme B, Delire C, Ducharne A, Gascoin S, Grippa M, Guichard F, Gusev Y, Harris P, Jarlan L, Kergoat L, Mougin E, Nasonova O, Norgaard A, Orgeval T, Ottlé C, Poccard-Leclercq I, Polcher J, Sandholt I, Saux-Picart S, Taylor C, Xue Y (2009) The AMMA land surface model intercomparison project. Bull Amer Meteorol Soc. doi:10.1175/2009BAMS2786.1

Charney J, Stone PH, Quirk WJ (1975) Drought in the Sahara: a biogeophysical feedback mechanism. Science 187:434–435

Chen F, Dudhia J (2001) Coupling an advanced land surface-hydrology model with the Penn State-NCAR MM5 modelling system. Part I: model implementation and sensitivity. Mon Weather Rev 129:569–585

Coudert B, Ottlé C, Boudevillain B, Guillevic P, Demarty J (2006) Contribution of thermal infrared remote sensing data in multi-objective calibration of a dual source SVAT model. J Hydrometeorol 7:404–420

Cunnington WM, Rowntree PR (1986) Simulations of the Saharan atmosphere—dependence on moisture and albedo. Q J R Meteorol Soc 112:971–999

d'Orgeval T, Polcher J, de Rosnay P (2008) Sensitivity of the West African hydrological cycle in ORCHIDEE to infiltration processes. Hydrol Earth Syst Sci Discuss 5:2251–2292

Dai Y, Zeng X, Dickinson RE, Baker I, Bonan GB, Bosilovich MG, Denning AS, Dirmeyer PA, Houser PR, Niu G, Oleson KW, Schlosser CA, Yang Z-L (2003) The common land model. Bull Am Meteorol Soc 84:1013–1023

de Rosnay P, Polcher J, Bruen M, Laval K (2002) Impact of a physically based soil water flow and soil–plant interaction

representation for modeling large scale land surface processes. J Geophys Res 107(D11), 4118. doi:10.1029/2001JD000634

de Rosnay P, Drusch M, Boone A, Balsamo G, Decharme B, Harris P, Kerr Y, Pellarin T, Polcher J, Wigneron JP (2009) Microwave Land Surface modelling evaluation against AMSR-E data over West Africa. The AMMA Land Surface Model Intercomparison Experiment coupled to the Community Microwave Emission Model (ALMIP-MEM). J Geophys Res 114, D05108. doi: 10.1029/2008JD010724

Decharme B (2007) Influence of the runoff representation on continental hydrology using the NOAH and the ISBA land surface models. J Geophys Res 112:D19108. doi:10.1029/2007JD008463

Dickinson RE, Henderson-Sellers A, Kennedy PJ (1993) Biosphere–Atmosphere Transfer Scheme (BATS) version 1e as coupled to the NCAR Community Climate Model. NCAR Technical Note NCAR/TN-387 + STR, 72

Dirmeyer PA, Zhao M (2004) Flux replacement as a method to diagnose coupled land–atmosphere model feedback. J Hydrometeorol 5:1034–1048

Dirmeyer PA, Dolman AJ, Sato N (1999) The pilot phase of the Global Soil Wetness Project. Bull Am Meteorol Soc 80:851–878

Dirmeyer PA, Gao X, Zhao M, Guo Z, Oki T, Hanasaki N (2006) GSWP-2: multimodel analysis and implications for our perception of the land surface. Bull Am Meteorol Soc 87:1381–1397

Douville H, Chauvin F, Broqua H (2001) Influence of soil moisture on the Asian and African monsoons. Part I: mean monsoon and daily precipitation. J Clim 14:2381–2403

Douville H, Conil S, Tyteca S, Voldoire A (2007) Soil moisture memory and West African monsoon predictability: artefact or reality? Clim Dyn 28:723–742

Eltahir EAB, Gong C (1996) Dynamics of wet and dry years in West Africa. J Clim 9:1030–1042

Essery RLH, Best M, Betts R, Cox P, Taylor CM (2003) Explicit representation of subgrid heterogeneity in a GCM land surface scheme. J Hydrometeorol 4:530–543

Gao X, Dirmeyer PA (2006) A multimodel analysis, validation, and transferability study of global soil wetness products. J Hydrometeorol 7:1218–1236

Geiger B, Meurey C, Lajas D, Franchistguy L, Carrer D, Roujean J-L (2008) Near real-time provision of downwelling shortwave radiation estimates derived from satellite observations. Meteorol Appl 15:411–420

Guo Z, Dirmeyer PA, Koster RD, Bonan G, Chan E, Cox P, Gordon CT, Kanae S, Kowalczyk E, Lawrence D, Liu P, Lu C-H, Malyshev S, McAvaney B, McGregor JL, Mitchell K, Mocko D, Oki T, Oleson KW, Pitman A, Sud YC, Taylor CM, Verseghy D, Vasic R, Xue Y, Yamada T (2006) GLACE: the global land–atmosphere coupling experiment. Part II: analysis. J Hydrometeorol 7:611–625

Gusev EM, Nasonova ON, Kovalev EE (2006) Modeling the components of heat and water balance for the land surface of the globe. Water Resour 33:616–627

Henderson-Sellers A, Pitman A, Love P, Irannejad P, Chen T (1995) The project for intercomparison of land surface parameterization schemes (PILPS): phases 2 and 3. Bull Amer Meteor Soc 76:489–504

Hourdin F, Guichard F, Favot F, Marquet P, BooneA, Lafore J-P, Redelsperger J-L, Ruti P, Dell'Aquila A, Doval TL, Traore AK, Gallee H (2009) AMMA-Model Intercomparison Project. Bull Am Meteorol Soc (in press)

Huffman GJ, Adler RF, Bolvin DT, Gu G, Nelkin EJ, Bowman KP, Hong Y, Stocker EF, Wolff DB (2007) The TRMM multi-satellite precipitation analysis: Quasi-global, multi-year, combined-sensor precipitation estimates at fine scale. J Hydrometeorol 8:38–55

Jobard I, Chopin F, Bergés JC, Ali A, Lebel T, Desbois M (2007) Presentation of the EPSAT-SG method and comparison with other satellite precipitation estimations in the frame of Precip-AMMA. Geophysical Research Abstracts, vol 9, 10062, SRef-ID: 1607–7962/gra/EGU2007-A-10062. European Geosciences Union

Kang H–S, Xue Y, Collatz G (2007) Impact assessment of satellite-derived leaf area index datasets using a general circulation model. J Clim 47:993–1013

Kohler M, Kalthoff N, Kottmeier C (2009) The impact of soil moisture modifications on CBL characteristics in West Africa: a case study from the AMMA campaign. QJR Meteorol Soc (in press). doi:10.1002/qj.430

Koster RD, Suarez MJ (1996) Energy and water balance calculations in the MOSAIC LSM. NASA Technical Memorandum 104606, 9, 76

Koster RD, Suarez MJ, Ducharne A, Kumar P, Stieglitz M (2000) A catchment-based approach to modeling land surface processes in a GCM—Part 1: model structure. J Geophys Res 105:24809–24822

Koster RD, Dirmeyer PA, Hahmann AN, Ijpelaar R, Tyahla L, Cox P, Suarez MJ (2002) Comparing the degree of land–atmosphere interaction in four atmospheric general circulation models. J Hydrometeorol 3:363–375

Koster RD, Guo Z, Dirmeyer PA, Bonan G, Chan E, Cox P, Davies H, Gordon CT, Kanae S, Kowalczyk E, Lawrence D, Liu P, Lu C-H, Malyshev S, McAvaney B, Mitchell K, Mocko D, Oki T, Oleson KW, Pitman A, Sud YC, Taylor CM, Verseghy D, Vasic R, Xue Y, Yamada T (2006) GLACE: the global land–atmosphere coupling experiment. Part I: overview. J Hydrometeorol 7:590–610

Koster RD, Guo Z, Yang R, Dirmeyer PA, Mitchell K, Puma MJ (2009) On the nature of soil moisture in land surface models. J Clim (in press). doi:10.1175/2009JCLI2832.1

Laval K, Picon L (1986) Effect of a change of the surface albedo of the sahel on climate. J Atmos Sci 43:2418–2429

Laws KB, JE Janowiak, GJ Huffman (2004) Verification of rainfall estimates over Africa using RFE, NASA MPA-RT and CMORPH. In: American Meteorological Society 18th Conference on Hydrology, Seattle, WA, January 2004

Li W, Xue Y, Poccard I (2007) Numerical investigation of the impact of vegetation indices on the variability of West African summer monsoon. J Meteorol Soc Jpn 85:363–383

Masson V, Champeaux J-L, Chauvin F, Meriguet C, Lacaze R (2003) Global database of land surface parameters at 1-km resolution in meteorological and climate models. J Clim 16:1261–1282

Noilhan J, Mahfouf J-F (1996) The ISBA land surface parameterization scheme. Glob Planet Change 13:145–159

Pan H–L, Mahrt L (1987) Interaction between soil hydrology and boundary layer developments. Boundary Layer Meteorol 38:185–202

Parker DJ, Thorncroft CD, Burton RR, Diongue-Niang A (2005) Analysis of the African easterly jet, using aircraft observations from the JET2000 experiment. Q J R Meteorol Soc 131:1461–1482

Philippon N, Fontaine B (2002) The relationship between the Sahelian and previous 2nd Guinean rainy seasons: a monsoon regulation by soil wetness? Ann Geophys 20:575–582

Redelsperger J-L, Thorncroft CD, Diedhiou A, Lebel T, Parker DJ, Polcher J (2006) African Monsoon Multidisciplinary Analysis: an international research project and field campaign. Bull Am Meteorol Soc 87:1739–1746

Rosenzweig C, Abramopoulos F (1997) Land-surface model development for the GISS GCM. J Clim 10:2040–2054

Rowell DP, Blondin C (1990) The influence of soil wetness distribution on short range rainfall forecasting in the West African Sahel. Q J R Meteorol Soc 116:1471–1485

Schneider U, Fuchs T, Meyer-Christoffer A, Rudolf B (2008) Global precipitation analysis products of the GPCC. Global Precipitation Climatology Centre (GPCC), DWD, Internet Publikation, 1–12

Sellers PJ, Mintz Y, Dalcher A (1986) A simple biosphere model (SiB) for use within general circulation models. J Atmos Sci 43:505–531

Steiner AL, JS Pal, SA Rauscher, JL Bell, NS Diffenbaugh, A Boone, LC Sloan, F Giorgi (2009) Land surface coupling in a regional climate simulations of the West African monsoon. Clim Dyn. doi 10.1007/s00382-009-0543-6

Sud YC, Fennessy M (1982) A study of the influence of surface albedo on July circulation in semi-arid regions using the GLAS GCM. J Climatol 2:105–125

Timouk F, L Kergoat, E Mougin, C Lloyd, E Ceschia, P de Rosnay, P Hiernaux, V Demarez (2008) Response of sensible heat flux to water regime and vegetation development in a central Sahelian landscape. J Hydrol 1–43. doi: 10.1016/j.jhydrol.2009.04.022

Walker J, Rowntree PR (1977) The effect of soil moisture on circulation and rainfall in a tropical model. Q J R Meteorol Soc 77:353–378

Xue Y, Shukla J (1996) The influence of land surface properties on Sahel climate. Part II: afforestation. J Clim 9:3260–3275

Xue Y, Sellers PJ, Kinter JL III, Shukla J (1991) A simplified biosphere model for global climate studies. J Clim 4:345–364

Xue Y, Hutjes RWA, Harding RJ, Claussen M, Prince SD, Lebel T, Lambin EF, Allen SJ, Dirmeyer PA, Oki T (2004) The Sahelian climate. Vegetation, water, humans and the climate: a new perspective on an interactive system. Springer, Heidelberg, pp 59–78

Xue Y, K-M Lau, KH Cook, D Rowell, A Boone, J Feng, T Bruecher, FDe Sales, P Dirmeyer, LM Druyan, A Fink, M Fulakeza, Z Guo, S M Hagos, SS Ibrah, K-M Kim, A Kitoh, A Konare, V Kumar1, P Lonergan, M Pasqui1, I Poccard-Leclercq, N Mahowald, W Moufouma-Okia, P Pegion, JK Schemm, SD Schubert, A Sealy, WM Thiaw, A Vintzileos, EK Vizy, S Williams, M-L C Wu (2009) The West African Monsoon Modeling and Evaluation project (WAMME) and its First Model Intercomparison Experiment. Clim Dyn (under revision)

Zeng N, Neelin J, Lau K-M, Compton J (1999) Enhancement of interdecadal climate variability in the Sahel by vegetation interaction. Science 286:1537–1540

VOLUME 13 JOURNAL OF HYDROMETEOROLOGY DECEMBER 2012

The Hydrological Modeling and Analysis Platform (HyMAP): Evaluation in the Amazon Basin

AUGUSTO C. V. GETIRANA*

LEGOS/CNES-CNRS-IRD-UPS, and CNRM-GAME/Météo-France, Toulouse, France

AARON BOONE

CNRM-GAME/Météo-France, Toulouse, France

DAI YAMAZAKI

University of Tokyo, Tokyo, Japan

BERTRAND DECHARME

CNRM-GAME/Météo-France, Toulouse, France

FABRICE PAPA AND NELLY MOGNARD

LEGOS/CNES-CNRS-IRD-UPS, Toulouse, France

(Manuscript received 7 February 2012, in final form 12 June 2012)

ABSTRACT

Recent advances in global flow routing schemes have shown the importance of using high-resolution topography for representing floodplain inundation dynamics more reliably. This study presents and evaluates the Hydrological Modeling and Analysis Platform (HyMAP), which is a global flow routing scheme specifically designed to bridge the gap between current state-of-the-art global flow routing schemes by combining their main features and introducing new features to better capture floodplain dynamics. The ultimate goals of HyMAP are to provide the scientific community with a novel scheme suited to the assimilation of satellite altimetry data for global water discharge forecasts and a model that can be potentially coupled with atmospheric models. In this first model evaluation, HyMAP is coupled with the Interactions between Soil–Biosphere–Atmosphere (ISBA) land surface model in order to simulate the surface water dynamics in the Amazon basin. The model is evaluated over the 1986–2006 period against an unprecedented source of information, including in situ and satellite-based datasets of water discharge and level, flow velocity, and floodplain extent. Results show that the model can satisfactorily simulate the large-scale features of the water surface dynamics of the Amazon River basin. Among all stream gauges considered, 23% have Nash–Sutcliffe coefficients (NS) higher than 0.50 and 68% above zero. About 28% of the stations have volume errors lower than 15%. Simulated discharges at Óbidos had NS = 0.89. Time series of simulated floodplains at the basin scale agrees well with satellite-based estimates, with a relative error of 7% and correlation of 0.89. These results indicate nonnegligible improvements in comparison to previous studies for the same region.

1. Introduction

A better understanding of freshwater flux and storage over the continents has been the subject of numerous studies in the last few decades. Indeed, understanding surface water dynamics (including floodplain, wetlands, inundations, etc.) is fundamental given its role in the continental water and energy cycle. For instance, it has

* Current affiliation: Hydrological Sciences Laboratory, NASA Goddard Space Flight Center, Greenbelt, Maryland.

Corresponding author address: Augusto Getirana, Hydrological Sciences Laboratory, NASA Goddard Space Flight Center, 8800 Greenbelt Road, Greenbelt, MD 22071.
E-mail: augusto.getirana@nasa.gov

DOI: 10.1175/JHM-D-12-021.1

been demonstrated that wetland areas, covering about 5% of the earth's land surface (Prigent et al. 2007), can play an important role within the climate system variability. Continental surface waters also influence the surface energy balance and feedback effects between the land surface and atmosphere (Krinner 2003; Mohamed et al. 2005). They also play an important role on water discharges of large rivers, sediment dynamics (Dunne et al. 1998), and freshwater chemistry (e.g., Melack et al. 2004). Finally, wetlands have been shown to have a significant impact on the interannual variability of global methane emissions (Bousquet et al. 2006).

The numerical modeling of the horizontal fluxes of land surface waters is traditionally performed by flow routing schemes (FRSs), which are often driven by surface runoff R and subsurface runoff (or baseflow, B) rates derived from land surface models (LSMs), or coupled with hydrological models composed of simplified vertical energy and water balance schemes.

The first attempts in simulating global land surface hydrology were based on linear relationships between water volume storage and discharge, assuming linear reservoirs with constant residence times (e.g., Vörösmarty et al. 1989), constant (e.g., Oki and Sud 1998), and variable flow velocity v based on empirical equations based on river morphology and topography gradient (e.g., Miller et al. 1994). The coarse spatial resolutions used by these models, varying between 0.5° and 2.5°, were mainly due to computational limitations or in order for the models to be compatible with typical general circulation models (GCMs) at that time.

Recent studies have improved the parameterization of FRS by considering the flow routing at the subgrid scale using linear reservoirs; flow routing between grid cells based on simplified formulations of the Saint–Venant equations, such as the kinematic and diffusive wave equations; interactions between rivers and floodplains; and evaporation from open waters (Döll et al. 2003; Decharme et al. 2012; Yamazaki et al. 2011). Also, recent advances in data availability, resolution, and processing allow one to simulate land surface hydrology globally at a 0.25°–0.50° spatial resolution and subdaily time steps. In particular, a few parameterizations can represent floodplain dynamics in FRS by taking into account topographic information from high-resolution digital elevation models (DEMs) in order to characterize the flooded area × water height relation within a grid cell. These schemes are based on statistical functions (e.g., Coe et al. 2008; Dadson et al. 2010) or elevation profiles (Decharme et al. 2012; Yamazaki et al. 2011), and are able to represent both the water storage and water fluxes between rivers and floodplains within a grid cell at the large scale. However, they still do not account for water fluxes through inundated areas. On the other hand, it has been demonstrated that floodplains can alter the water transport in large basins such as the Amazon basin (Richey et al. 1989). This physical process is explicitly represented by meso- and regional-scale hydrodynamic models (e.g., Estrela and Quintas 1994; Horritt and Bates 2002; Biancamaria et al. 2009; Paiva et al. 2012), but the application of such approaches at the global scale is computationally prohibitive.

While coupling LSMs and FRSs in online mode can require complex programming, the implementation of offline LSM–FRS systems is a straightforward solution for reproducing horizontal water fluxes from LSM outputs over the continents. The offline mode coupling consists in, as a first step, running a given LSM and then, as a postprocessing step, using R and B derived from the land surface model as inputs of the FRS. This two-step procedure allows one to promptly convert runoff from any land surface model into streamflow. On the other hand, offline mode runs prevent LSMs from benefitting from FRS feedbacks, such as the spatiotemporal distribution of wetlands and flooded zones, which could account for a better simulation of evapotranspiration and soil moisture—particularly, considering that evaporation from floodplains in the vertical water and energy balance of an LSM can significantly improve water discharge simulations, as demonstrated by Decharme et al. (2012).

The aforementioned issues are addressed in the present paper. A new global FRS, the Hydrological Modeling and Analysis Platform (HyMAP), is presented and evaluated. HyMAP was specially developed to route LSM outputs in offline mode, taking into account water surface dynamics and representing the runoff and baseflow time delays, the interaction between rivers and floodplains, floodplain water flow among grid cells, and evaporation from open waters.

As a first experiment, HyMAP is coupled with the Interactions between Soil–Biosphere–Atmosphere (ISBA) LSM (Noilhan and Mahfouf 1996) in offline mode and has its performance evaluated in the Amazon basin over the 1986–2006 period at 0.25° spatial resolution. The Princeton University 3-hourly atmospheric dataset (Sheffield et al. 2006) is used as input to force the system. The model is extensively evaluated using both in situ and satellite-based observations, including in situ water discharge and flow velocity made available by the Brazilian Water Agency [Agência Nacional de Águas (ANA)], along with radar altimetry data acquired by *Envisat* and multisatellite-derived estimates of inundation extent at a 0.25° spatial resolution (Prigent et al. 2007; Papa et al. 2010). This paper is organized into five sections. Section 2 presents a detailed description of HyMAP and the model parameterization. The

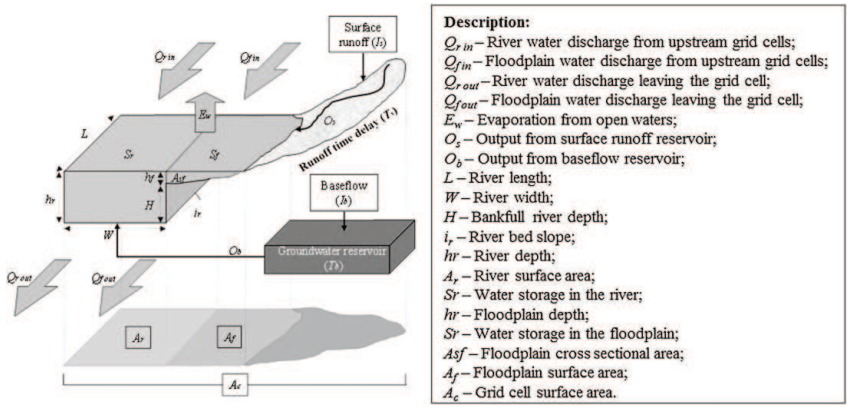

FIG. 1. Schematic of a river channel reservoir and a floodplain reservoir within a grid cell as represented in HyMAP.

experimental design, forcings, and evaluation datasets are described in section 3. Results and discussion are shown in section 4, and the conclusions are provided in section 5.

2. HyMAP: The Hydrological Modeling and Analysis Platform

HyMAP is a global-scale flow routing scheme specifically designed to be coupled with any LSM in offline mode. The model has been developed in the framework of the future Surface Water and Ocean Topography (SWOT) mission, planned to be launched within the decade and which will provide high-resolution characterization of water surface elevations with two-dimensional global maps of terrestrial surface water extent and storage changes (Alsdorf et al. 2007). The objective is to have a modeling system capable of assimilating SWOT data toward a near-real-time global estimation of water discharge.

HyMAP is inspired by the Catchment-based Macroscale Floodplain (CaMa-Flood) model (Yamazaki et al. 2011) and ISBA–Total Runoff Integrating Pathways (TRIP; Decharme et al. 2012) global flow routing schemes in that it simulates the horizontal water fluxes over continental surfaces where the runoff and baseflow (in this study, baseflow represents the vertical flux from unsaturated soil layer to saturated layer) generated by an LSM are routed through a prescribed river network to oceans or inland seas. The model simulates water level, discharge, and storage in rivers and floodplains at the daily time step with internal computational time steps that can be adjusted between a few minutes to several hours. The model is composed of four modules accounting for 1) the surface runoff and groundwater baseflow time delays, 2) a river–floodplain interface, 3) flow routing in river channels and floodplains, and 4) evaporation from open water surfaces. The main advances in the representation of physical processes in comparison to the previous two models are the introduction of time delays for both runoff and baseflow (section 2a), a floodplain elevation profile accounting for the representation of river surfaces (section 2b), the flow routing within the floodplain (section 2c), and the computation of surface water evaporation in offline LSM–FRS systems (section 2d). Also, HyMAP combines a relatively high spatial resolution of 0.25° with spatially distributed parameters. Figure 1 presents a schematic with the main variables of the model.

The runoff and baseflow generated by an LSM pass through the surface water or groundwater linear reservoirs, respectively, and then are routed using a kinematic wave formulation through a prescribed river network to oceans or inland seas. The river network is represented by a river channel reservoir and a floodplain reservoir in each grid cell. Similar to CaMa–Flood, river channel and floodplain are treated as continuous reservoirs in that water spilling from the river channel is stored in the floodplain. At each time step, the inflow water is redistributed between the river channel and floodplain reservoirs following stage–volume relationships derived from the topography of each grid cell. The outflow is then calculated independently for both floodplain and river considering different water depths and roughness coefficients.

Lowland topography and river network characteristics such as river length and slope are prescribed on

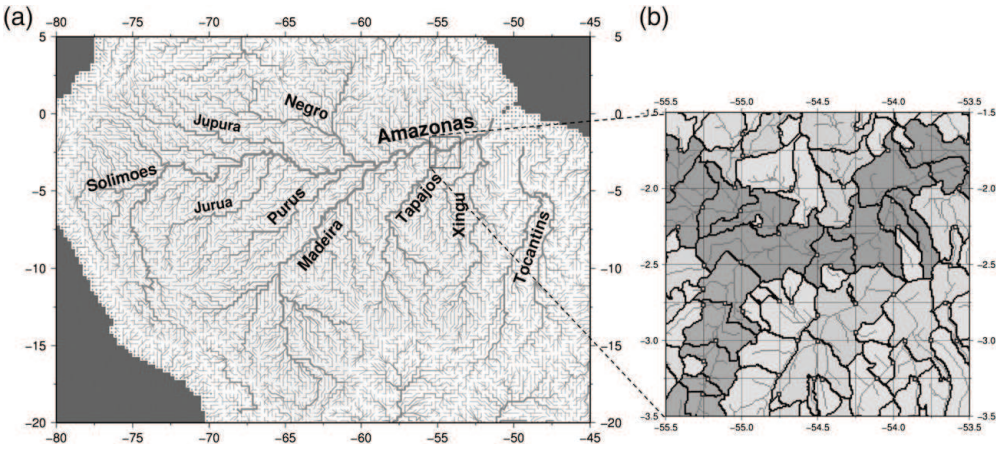

FIG. 2. Products of the upscaling procedure using the FLOW algorithm: (a) the river network map for the Amazon River and (b) subgrid topographic parameters. In (b), small squares represent outlet pixels, thick gray lines indicate river channel pixels, and black lines indicate the unit catchment attributed to each grid cell. Gray tones distinguish unit catchments of main river reaches and other tributaries.

a subgrid-scale basis according to the Flexible Location of Waterways (FLOW) method (Yamazaki et al. 2009). The fine-resolution flow direction map is given by the 1-km-resolution Global Drainage Basin Database (GDBD; Masutomi et al. 2009). The upscaling procedures for delineating coarse-resolution drainage areas and for extracting other river network parameters—such as flow directions, river length, and slope from GDBD—are described in Yamazaki et al. (2011). Figure 2 shows the river network map for the Amazon River and a snapshot of the subgrid data processing as prescribed by FLOW.

River width and bankfull height are derived from empirical relationships, which are functions of the average discharge. Water flow among grid cells is computed for both rivers and floodplains using the kinematic wave equation. Floodplain slope is the same as river's for simplicity. Manning's coefficients are spatially distributed according to river geometry and global land cover types.

Decharme et al. (2012), using ISBA–TRIP in online mode, have demonstrated that the evaporation from floodplains are essential to better estimate the water balance in arid regions subjected to monsoon regimes, such as the Parana and Niger River basins. The authors showed that considering floodplains can significantly increase the evapotranspiration, thereby decreasing the mean discharge in such regions, which was shown to improve results. The calculation of evaporation from open waters in offline mode can be performed in flow routing schemes if physical relationships between water surface and atmosphere are simplified. A Penman–Monteith formula is used in HyMAP to compute the evaporation from open waters. The next sections give a detailed description of the model features.

a. Module 1: The runoff and baseflow time delays

The concentration time (or time delay factor) is a physically based process representing the subgrid-scale routing. For each grid cell, both surface runoff I_s [mm $(\Delta t)^{-1}$] and baseflow I_b [mm $(\Delta t)^{-1}$] derived from an LSM pass through separate linear reservoirs with appropriate time delay factors. These values can vary from a few hours to several days, depending on hydrogeological characteristics of the catchment. The linear reservoir outflows can be represented by the following equation:

$$O_{s,b} = \frac{V_{s,b}}{T_{s,b}}, \tag{1}$$

where the subscripts s and b represent surface runoff and baseflow variables, respectively. The quantity $O_{s,b}$ [mm $(\Delta t)^{-1}$] stands for the outflow at time step t, $V_{s,b}$ (mm) the water stored in the linear reservoir, and $T_{s,b}$ the concentration time of the grid cell. The V is updated twice at each time step: at the beginning, adding the inflow $I_{s,b}$, and at the end, subtracting $O_{s,b}$.

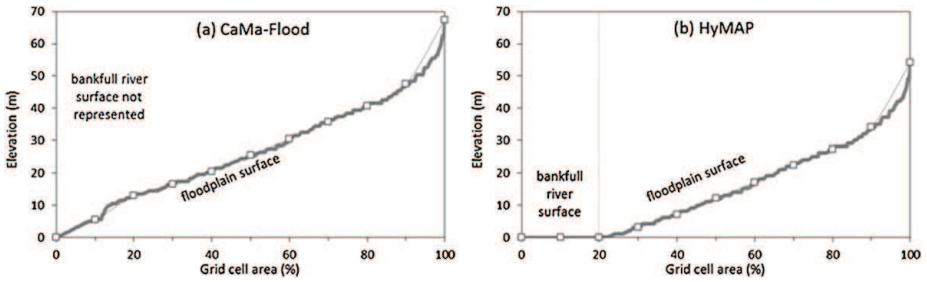

FIG. 3. Floodplain elevation profile represented in (a) CaMa–Flood (Yamazaki et al. 2011) and (b) HyMAP.

The baseflow time delay factor T_b is assumed to be spatially uniform and constant in time. The current parameterization of HyMAP coupled with ISBA defines T_b = 45 days. This value can be changed when other LSMs are used to force the flow routing scheme. The quantity T_s is computed for each grid cell from Kirpich (1940):

$$T_{s_j} = 3600\left(0.868\frac{\Delta x_j^3}{\Delta h_j}\right)^{0.385}, \qquad (2)$$

where Δx_j (km) is the distance between the farthest point within a grid cell and its outlet, and Δh_j (m) is the difference between the maximum and minimum elevations of the pathway. Both Δx_j and Δh_j are derived from the high-resolution DEM. At a 0.25° resolution, T_s values are quite low in comparison with T_b, varying from several minutes to a few days. Finally, the total discharge produced in each grid cell Q_c [m^3 $(\Delta t)^{-1}$] is computed as

$$Q_c = (O_s + O_b)A_c, \qquad (3)$$

where A_c stands for the gridcell area.

b. Module 2: The river–floodplain interface

The numerical representation of river channels and floodplains are similar to that in CaMa–Flood (Yamazaki et al. 2011) and ISBA–TRIP (Decharme et al. 2012). The river channel reservoir of a grid cell is defined using three parameters: channel length L (m); channel width W (m); and bank height H (m). If the actual water height in the river channel h_r (m) is higher than H, water is exchanged between river and floodplain reservoirs. This process is considered instantaneous at each time step so that water surface elevations of the river channel and the floodplain are the same.

A floodplain reservoir has a parameter for the unit catchment area A_c and a floodplain elevation profile, $h_f = f(A_f)$. The topographic parameters used to create the elevation profile are derived from the 30 arc-second Shuttle Radar Topography Mission (SRTM30) DEM processed with the FLOW method (Yamazaki et al. 2009). The errors of SRTM30 DEM due to the limitations of satellite radar sensing (e.g., vegetation canopies, subpixel-sized structures, and random radar speckle) are removed as much as possible before applying the FLOW algorithm for deriving the topographic parameters. The method applied for SRTM30 error correction is summarized in Yamazaki et al. (2012).

Some examples of floodplain elevation profile suggested by Decharme et al. (2012) and Yamazaki et al. (2011) consider that all of the surface area within a grid cell can be potentially flooded, neglecting the existence of the river surface (Fig. 3a). Indeed, it is a difficult task to define reliable river surfaces globally since river geometry is generally defined using statistical relationships: no global land cover dataset with sufficient spatial resolution is currently available to derive precise river widths. In this sense, a simple solution is suggested in this study. First, the bankfull river surface is defined as the product between the river length derived from the DEM processing and the river width obtained from an empirical equation (see below). Also, it is assumed that rivers are always composed by the lowest subgrid pixels within a grid cell. Then, the elevation of the highest ''river pixel'' is subtracted from the elevation profile (Fig. 3b). In this sense, for any river water storage more than zero, the grid cell will have a minimum water surface corresponding to the river surface area.

The river channel and floodplain water exchanges at each time step are represented as follows:

$$\text{if} \quad S_{r_{\max}} \le S, \quad \begin{aligned} S_r &= S \\ h_r &= S_r/(W \times L) \\ S_f &= 0 \\ h_f &= 0 \\ A_f &= 0, \end{aligned} \qquad \text{and} \qquad (4)$$

$$\text{if} \quad S_{r_{\max}} > S, \quad \begin{aligned} S_r &= S - S_f \\ h_r &= S_r/(W \times L) \\ S_f &= \int_0^{A_f} [h_f - h(A_f)]\, dA \\ h_f &= h_r - H \\ A_f &= h^{-1}(h_f), \end{aligned} \tag{5}$$

where subscripts r and f represent river channel and floodplain variables, respectively. The quantity S (m^3) stands for the total water storage in the grid cell, S_r (m^3) and S_f (m^3) the river channel and floodplain water storages, h_r (m) and h_f (m) water depths, W (m) the river width, L (m) the river length, and A_f (m^2) the flooded area. The $S_{r_{\max}}$ (m^3) stands for the river bankfull water storage, and is given as $S_{r_{\max}} = H \times W \times L$, where H (m) is the river bankfull height.

The temporal change of water storage in river channels and floodplains of a grid cell S is defined by the continuity Eq. (6) considering linear reservoir outputs, river and floodplain discharges to the downstream grid point, river and floodplain discharges from the upstream grid points, and evaporation from the floodplains:

$$S^t = S^{t-1} + \left[Qc^{t-1} + \sum_{k=1}^{\text{nUp}} (Q_{r,k}^{t-1} + Q_{f,k}^{t-1}) - Q_r^{t-1} - Q_f^{t-1} - E^{t-1} \right] dt, \tag{6}$$

where t is time, and dt represents the time step. The index k stands for the nUp upstream grid cells of the target grid point.

c. Module 3: Flow routing in river channels and floodplains

Water discharge in both the river and the floodplain is calculated by the kinematic wave equation. Using the Manning formula for a rectangular cross section and large width-to-depth ratio, water discharge in the river channel Q_r ($m^3\ s^{-1}$) can be defined as

$$Q_r = \frac{1}{n_r} i_r W_r h_r^{5/3}, \tag{7}$$

where n_r is the roughness coefficient for rivers; i_r is a constant riverbed slope derived from topographic information and corresponds to the slope between the target and downstream grid cells.

Similarly, water discharge in the floodplains Q_f ($m^3\ s^{-1}$) is given as

$$Q_f = As_f v_f = \overline{w}_f \overline{h}_f v_f, \tag{8}$$

where As_f (m^2) is the floodplain cross-sectional area, v_f (m s^{-1}) the mean flow velocity through the floodplain section, and w_f (m) and h_f (m) stand for the mean width and depth of the floodplains, respectively, which are computed as follows:

$$\overline{w}_f = \frac{A_f}{L} \quad \text{and} \tag{9}$$

$$\overline{h}_f = \frac{S_f}{L\overline{w}_f} = \frac{S_f}{A_f}. \tag{10}$$

The quantity v_f can be defined by using Eqs. (8) and (9) in the Manning formula:

$$v_f = n_f^{-1} (i_f^{1/2}) \left(\frac{S_f}{A_f} \right)^{2/3}, \tag{11}$$

where n_f is the Manning roughness coefficient for floodplains that varies according to the vegetation type (see below) and, for simplicity, i_f is considered equal to i_r.

Finally, combining Eqs. (7) and (10) yields

$$Q_f = \frac{1}{n_f} i_f \frac{S_f^{5/3}}{L A_f^{2/3}}. \tag{12}$$

1) River width and depth

Although flow routing schemes are very sensitive to the accuracy of river geometry, these data are very scarce on the global scale. In this sense, empirical methods are normally employed to determine river width and depth spatially. These methods can be functions of hydrological or geomorphological characteristics (e.g., drainage area and water discharge) and have been largely used in the literature for large-scale hydrological modeling (e.g., Arora and Boer 2001; Coe et al. 2008; Decharme et al. 2012; Yamazaki et al. 2011). In HyMAP, river width is defined for each grid cell based on an empirical relationship between W and the mean annual discharge:

$$W = \max(10, \beta \times Q_{\text{med}}^{0.5}), \tag{13}$$

where Q_{med} ($m^3\ s^{-1}$) is the annual mean discharge in each grid cell estimated using the global runoff database from Cogley (2003). As suggested by Decharme et al. (2012), β is defined for five different hydrological regions of the world (see Fig. 4). For equatorial or subtropical basins, which include the Amazon basin, $\beta = 18$. The H is computed via a linear relationship with W:

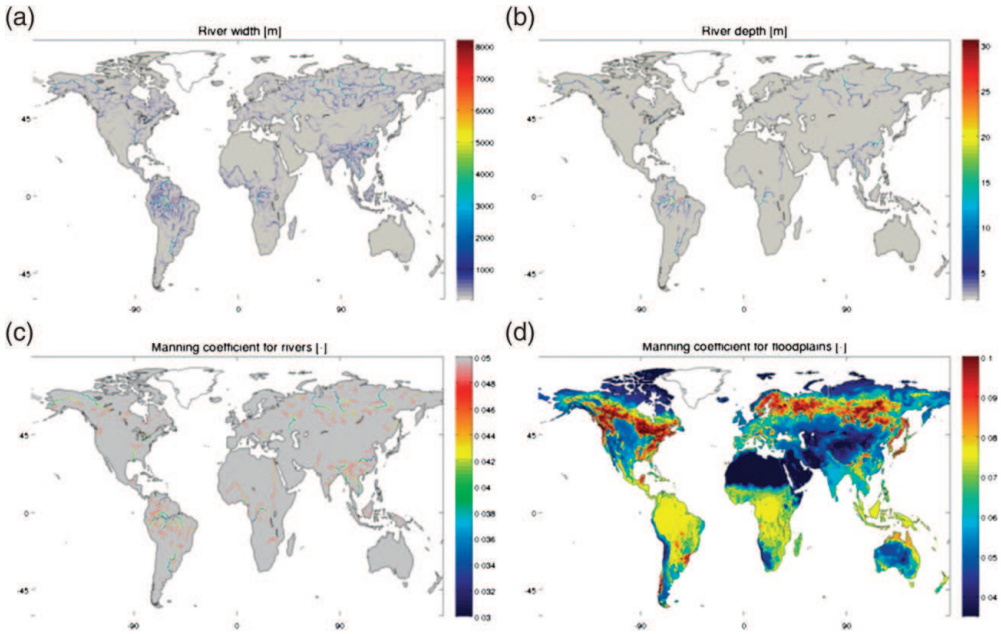

FIG. 4. Global distribution of HyMAP parameters at a 0.25° spatial resolution: (a) river width derived from Eq. (13); (b) river depth derived from Eq. (14); (c) Manning roughness coefficient for rivers, as described by Eq. (15); and (d) Manning roughness coefficient for floodplains, Eq. (16).

$$H = \max(2.0, \alpha \times W) \quad \alpha = 3.73 \times 10^{-3}. \tag{14}$$

2) MANNING COEFFICIENT FOR RIVER CHANNELS AND FLOODPLAINS

The Manning roughness coefficient n is an empirical parameter and general values can be prescribed for most types of channels and surfaces. For practical reasons, in many studies, n is considered constant for the whole domain, with values of about $n = 0.03$ for open channels. HyMAP considers the spatial variability of n in both rivers and floodplains as functions of land cover and water depth. In this study, the Manning coefficient of river channels n_r varies according the following formula:

$$n_r = n_{\min} + (n_{\max} - n_{\min})\left(\frac{H_{\max} - h}{H_{\max} - H_{\min}}\right)^{1/3}$$
$$n_{\min} = 0.03 \quad n_{\max} = 0.05, \tag{15}$$

where $n_{\max}$ and $n_{\min}$ are the maximum and the minimum values of the Manning coefficient selected from values suggested in the literature (Chow 1959) and $H_{\max}$ and $H_{\min}$ the maximum and minimum river depths as provided by Eq. (9).

The Manning coefficient for floodplains n_f is spatially distributed as a function of 12 land cover types at 0.25° resolution derived from the 1-km ECOCLIMAP dataset (Masson et al. 2003). The n_f values are larger in tropical forests and lower for bare soils and rocks. The 12 vegetation types are described in Table 1. A similar solution, as suggested by Decharme et al. (2012), is used:

$$n_f = \sum_{k=1}^{12} (\mathrm{lcov}_i \times n_{f_i}), \tag{16}$$

where lcov_i stands for the gridcell fraction of each vegetation type i listed in Table 1 and n_{f_i} the respective Manning roughness coefficient for floodplains. Figure 4 shows the global distribution of both n_r and n_f. Manning values for floodplains have also been determined based on previous studies found in the literature.

d. *Module 4: Evaporation from floodplains*

A simple approach is used to estimate the evaporation from the open waters E_w (m^3 day^{-1}). First, the potential evaporation E (mm day^{-1}) is calculated by the Penman–Monteith equation once a day, by setting the surface resistance to zero:

TABLE 1. Land cover types and respective Manning roughness coefficients for floodplains n_f. The land cover classification is specified by the 1-km ECOCLIMAP dataset (Masson et al. 2003).

	Land cover types	Manning roughness coefficient
1	Flat bare soil	0.035
2	Rocks	0.035
3	Permanent snow and ice	0.035
4	Tropical forest	0.075
5	Coniferous forest	0.100
6	Broadleaf evergreen forest	0.100
7	C3 crops	0.050
8	C4 crops	0.050
9	Irrigated crops	0.050
10	Grassland	0.050
11	Tropical grassland	0.075
12	Park mashes	0.075

$$E = \left(\frac{\Delta \times A + \rho_A \times c_p \times \dfrac{D}{r_a}}{\Delta + \gamma} \right) \times \frac{M}{\lambda \times \rho_W}, \quad (17)$$

where Δ (kPa $°C^{-1}$) is the gradient of the saturated vapor pressure–temperature function; A (MJ m^{-2} s^{-1}) is the available energy; ρ_A (kg m^{-3}) and ρ_W (kg m^{-3}) are the specific mass of air and water, respectively; c_p is the specific heat of moist air (MJ kg^{-1} $°C^{-1}$); D (kPa) is the vapor pressure deficit; γ (kPa $°C^{-1}$) is the psychrometric constant; r_a (s m^{-1}) is the aerodynamic resistance; λ (MJ kg^{-1}) is the latent heat of vaporization; and M is a time step unit conversion from m s^{-1} to mm Δt^{-1}. Available energy and aerodynamic resistance can be calculated following Shuttleworth (1993). For simplification purposes, water albedo and emissivity were fixed as 0.07 and 1, respectively.

Then, the real or actual evapotranspiration rate ET (mm day^{-1}) diagnosed by the LSM, is subtracted from E and the result is multiplied by the water surface A_f, resulting in the effective evaporation from open waters:

$$E_w = \max[0, (E - \mathrm{ET})A_f]. \quad (18)$$

The computation is done once per day using standard input meteorological forcing variables and assuming that the water in the floodplains and river have the same temperature as the air (a predicted or prescribed surface water temperature is not needed). This is consistent with the neglect of stability corrections in the Penman–Monteith equation (using the daily time step).

3. Experimental design

HyMAP was run over the Amazon basin at the 0.25° spatial resolution during the 1986–2006 period. The model time step was set as 15 min and outputs provided as daily averages. Daily surface runoff and baseflow derived from ISBA are used as inputs in HyMAP. Meteorological forcings and the total evapotranspiration calculated by ISBA are also needed to estimate the remaining energy available for the evaporation from open waters. Since the coupling is performed in offline mode, there is no feedback from HyMAP to ISBA, which implies that floodplains do not cause reinfiltration into the LSM or influence the soil moisture. Main land surface parameters used by ISBA—such as land cover, vegetation parameters, soil textural properties, and topography—are not discussed (a full description can be found in Decharme et al. 2012).

a. Meteorological forcings

The meteorological dataset used as forcing for ISBA is provided by Princeton University on a 3-hourly time step and at a 1° resolution (Sheffield et al. 2006). This dataset is based on the National Centers for Environmental Prediction–National Center for Atmospheric Research (NCEP–NCAR) reanalysis. Sheffield et al. (2006) carried out corrections of the systematic biases in the 6-hourly NCEP–NCAR reanalyses via hybridization with global monthly gridded observations. In addition, the precipitation was disaggregated in both space and time at 1° resolution via statistical downscaling and at 3-hourly time step using information from the 3-hourly Tropical Rainfall Measuring Mission (TRMM) dataset. The 3-hourly precipitation from Sheffield et al. (2006) are then hybridized to match the monthly value from the Global Precipitation Climatology Center (GPCC) Full Data Product V4, as proposed in Decharme et al. (2012).

b. Evaluation dataset

1) IN SITU OBSERVATIONS

Daily observed water discharge data at 172 gauging stations operated by the Brazilian Water Agency (ANA) are used to evaluate HyMAP streamflows. These gauging stations have time series with at least one year of observations within the 1986–2006 period. Observed water discharge at both Jatuarana and Careiro stations, located along the Amazon River, can be summed providing the water discharge downstream Negro River's confluence. The ''new station'' is called Jatuarana+ Careiro or station 2.

Observed flow velocities (v) at 153 gauging stations with areas bigger than 15 000 km^2 are also considered in the evaluation procedure. These data are also maintained by ANA and acquired only a few times per year in order to calibrate rating curves. Available v values are averages of numerous instantaneous and quasi-instantaneous

measurements, which are, in most cases, obtained by acoustic Doppler current profiler (ADCP) or Pygmy meter measurements within the river cross section. The selected gauging stations have between 5 and 151 daily flow velocity observations within the 1986–2006 period, totaling 9149 observations. Drainage areas of both water discharge and flow velocity gauging stations range from 1000 to 4 670 000 km^2. Errors of in situ data are generally on the order of 10%–15% and can be mainly caused by imperfect samplings at actual cross sections with considerable velocity gradients.

2) RADAR ALTIMETRY DATA

Data provided by the altimeter on board the *Envisat* satellite are considered in this study. *Envisat* orbits on a 35-day temporal resolution (duration of the orbital cycle) from latitude 81.5°N to 81.5°S, and 70-km intertrack spacing at the equator. The ranges used in this study are those issued by the ICE-1 algorithm (Bamber 1994). Errors in altimetric time series along rivers within the Amazon basin are in the order of tens of centimeters. *Envisat* data are freely available on the Hydroweb server (http://ctoh.legos.obs-mip.fr/products/hydroweb) (Crétaux et al. 2011). Altimetric data at 294 virtual stations (VS) located within Amazon basin are considered in this study. Selected VS cover most Amazon River's tributaries and other small rivers, with drainage areas ranging from 10 000 to 5 238 800 km^2. Time series vary from 34 to 41 altimetric observations for the 2002–06 period.

3) FLOODPLAIN EXTENT FROM MULTISATELLITE TECHNIQUE

Floodplains simulated by HyMAP were evaluated against the multisatellite estimates of surface water extent from Papa et al. (2010). This dataset, called P10 hereafter, is available at a monthly time step for 1993–2004, with a spatial resolution of 773 km^2 (i.e., equal-area grid of 0.25° × 0.25° at the equator). It was generated from a complementary multiple satellite observations, including passive [Special Sensor Microwave Imager (SSM/I)] and active [European Remote Sensing (ERS) series satellites] microwaves, along with visible and near-infrared imagery [Advanced Very High Resolution Radiometer (AVHRR)].

Because the dataset makes no distinction between floodplains and other kinds of surface water bodies—including lakes, anthropogenic and natural reservoirs, or irrigated agriculture—Decharme et al. (2012) show that a hybrid version of P10 is more suitable to be directly compared with the simulated floodplain extents derived from flow routing schemes such as HyMAP or ISBA–TRIP. Following a similar approach, the Global Lakes and Wetland Database (GLWD) and the Monthly Irrigated and Rainfed Crop Areas (MIRCA2000) products were used to build an alternative product to P10 that is more comparable with model simulations. The GLWD data (Lehner and Döll 2004) gives the global distribution of 12 types of surface water bodies, including lakes, wetland, and floodplains at 30-arc-second resolution (~1 km at the equator), and the MIRCA2000 product (Portmann et al. 2010) provides the classification of 26 irrigated crops for each month of a year around the year 2000 at 5-arc-minute resolution (~9.2 km at the equator). In this study, both products are resized to fit the 0.25° model grid. Decharme et al. (2012)'s technique consists of subtracting the GLWD lakes and bogs, fen, and mire areas (LGLWD), as well as the MIRCA2000 annual cycle I_{mth}, from P10 where the GLWD rivers, floodplains, and intermittent lake/floodplain areas (FGLWD) exist:

$$\mathrm{FLD}_{\mathrm{obs}}(t) = \delta \times \max[0, \mathrm{P10}(t) - L_{\mathrm{GLWD}} - I_{\mathrm{mth}}] \,\Big|\, \begin{matrix} \delta = 1 & \forall & F_{\mathrm{GLWD}} > 0 \\ \delta = 0 & \forall & F_{\mathrm{GLWD}} = 0 \end{matrix}, \tag{19}$$

where $\mathrm{FLD}_{\mathrm{obs}}$ stands for the new final product and t the time step in months.

4. Results and discussion

a. Evaluation of water discharges

About 50% of the stations have drainage areas bigger than 30 000 km^2. This large dataset provides the unique opportunity for thoroughly evaluating a flow routing scheme over the Amazon basin. Based on observations at eight stations (gauging stations 1, 2, 3, 4, 7, 9, 11, and 13), one can notice in Fig. 5 a changing water discharge regime along the Solimões–Amazon main stream. In the upper part of the Solimões River, a large gradient (resulting owing to the relatively close proximity to the Andes) causes the noisy annual cycles with abrupt changes, as seen at stations 13 (Tabatinga), 11 (Teresina), 9 (São Paulo de Olivença), and 7 (Santo Antonio do Içá). In the lower part, high and smooth water discharges at stations 4 (Itapeua), 3 (Manacapuru), 2 (Jatuarana+Careiro), and 1 (Óbidos) are a result of both the diffusive effect of a low gradient in lowlands and water storage in floodplains and

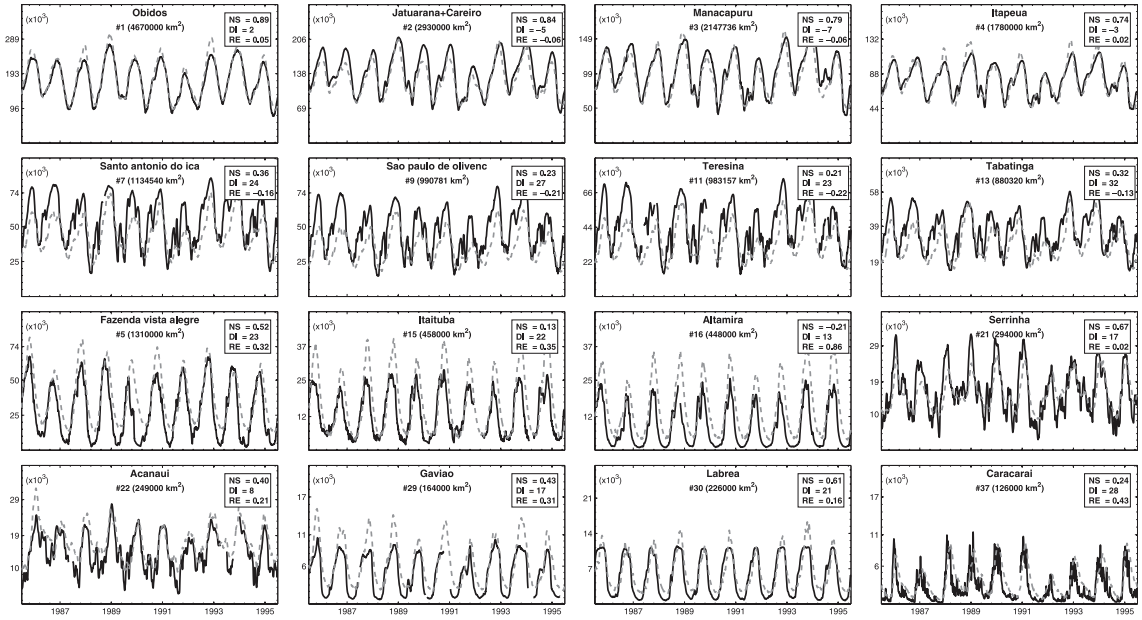

FIG. 5. Hydrographs at 16 gauging stations. Drainage areas and performance coefficients for daily water discharge (NS, DI, and RE) are also provided for selected stations. Values of DI are in days. Model outputs are in dashed gray lines and in situ observations in black. Water discharge units are in 10^3 m^3 s^{-1}. The locations of selected stations are indicated in Fig. 7.

the massive contribution of important tributaries such as the Purus, Madeira, and Negro Rivers.

Daily water discharges have been quantitatively evaluated by means of three performance coefficients: the delay index (DI) (days), the Nash–Sutcliffe coefficient (NS), and the volume error of streamflows (DV). The delay index (DI) (days) is used to measure errors related to time delay between simulated and observed hydrographs. The DI is computed using the cross-correlation function Rxy (m) from simulated (x) and observed (y) time series, where DI equals the value of the time lag m where Rxy (m) is maximum (Paiva et al. 2012). The quantities NS and DV are represented by the following equations:

$$\mathrm{NS} = 1 - \frac{\sum_{t=1}^{\mathrm{nt}} (y_t - x_t)^2}{\sum_{t=1}^{\mathrm{nt}} (y_t - \overline{y})^2} \quad \text{and} \tag{20}$$

$$\mathrm{DV} = \frac{\sum_{t=1}^{\mathrm{nt}} x_t - \sum_{t=1}^{\mathrm{nt}} y_t}{\sum_{t=1}^{\mathrm{nt}} y_t}, \tag{21}$$

where t is the time step; nt the total number of days with observed data; x and y are, respectively, the simulated and target (observed) signals at time step t; and $\overline{y}$ is the mean value of the target signals for the entire period. The NS ranges from $-\infty$ to 1, where 1 is the optimal case and 0 is when simulations represent observed signals as well as the mean value. One can obtain RE values in percentage by multiplying by 100.

Results show that HyMAP can satisfactorily reproduce water discharges along the Solimões–Amazon main stream, representing well the aforementioned discharge characteristics. At Óbidos, the gauging station representing most of the Amazon basin outflow, located about 800 km upstream from the river mouth, discharges are very well simulated with NS = 0.89. This result shows improvements in comparison with previous daily water discharge simulations at Óbidos, where NS values reached 0.78 and 0.83 with kinematic and diffusive wave equations, respectively (Yamazaki et al. 2011). Simulations with ISBA–TRIP resulted in NS values of 0.69 in offline mode (i.e., without floodplains) and 0.83 in online mode (i.e., with floodplains accounting for soil moisture and evaporation from open waters). The slightly improved performance with this model can be partially explained by the fact that both of the aforementioned models are simpler than HyMAP with respect to the horizontal water flow parameterization such as a limited representation of physical processes, global-scale parameter estimation, and, in the case of ISBA–TRIP, coarser spatial resolution. Simulated wave peaks are in phase with observations with a mean delay of only two days (DI = 2). Mean simulated water discharge overestimates the observations by about 5%. This error is easily perceptible during peaks and can be mainly attributed to forcing uncertainties over the basin. HyMAP also performed very well at stations 2, 3, and 4, all of which are located along the lower Solimões–Amazon main stream, with NS values varying from 0.74 to 0.84 and relative errors (RE) from −6% to 2%. On average, simulated discharge peaks occur 3–7 days before observations at these stations. Except for station 2, all of these gauging stations experience slightly overestimated peaks, as shown in Fig. 5.

Simulated discharges at gauging stations 7, 9, 11, and 13 have NS coefficients between 0.21 (station 13) and 0.36 (station 7). Simulations represent well dry seasons but underestimate peaks systematically, resulting in negative volume errors RE ranging from −13% (station 13) to −22% (station 11). Overall, HyMAP has very good discharge simulations at the basinwide scale. Better results are obtained in larger rivers while smaller tributaries had medium or poor performances. This is expected and fairly typical of such large-scale models since the precipitation and basin parameter errors are larger at small scales. As shown in Fig. 6, among all stream gauges used in the evaluation process, 39 (or 23% of the total) have NS higher than 0.50 and 117 (or 68%) have values above zero. About 28% of the stations have volume errors lower than 15% and they are located mostly in the western and central parts of the basin. As shown in Fig. 7, the overestimated mean discharges in most rivers draining over the southern part of the basin are probably a result of errors in the forcings. For instance, the mean discharges in the Madeira River are overestimated in about 32% at Fazenda Vista Alegre (station 5). Similar results are obtained for the Purus (RE = 32% at Gavião—station 29), Tapajós (RE = 35% at Itaituba—station 15), and Xingu (RE = 82% at Altamira—station 16). At these same stations, DI values are of 23, 22, and 13 days, respectively, and NS values of 0.43, 0.13, and −0.21. Good results are obtained for the Negro River at Serrinha (station 21), with NS = 0.67, DI = 2 days, and RE = 2%. High delay indexes can be explained by both the use of a single T_b value for the whole basin and the kinematic wave assumption in flat water surfaces.

b. *Evaluation of water levels*

The water level evaluation at 294 *Envisat* virtual stations gives a wide overview of model performance at the basin scale. Three performance coefficients have been used to evaluate simulated water levels: the correlation

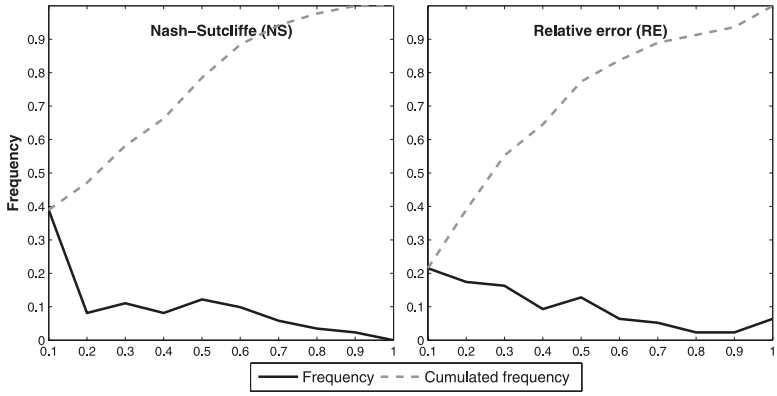

FIG. 6. The histogram of the normalized frequency of (left) the Nash–Sutcliffe coefficient (NS) and (right) absolute values of relative error (RE) of daily water discharges at 172 gauging stations. The range is from 0 to 1 with a bin size of 0.1. The best overall simulations are skewed the most to the right. Negative NS values are included in values between zero and 0.1.

coefficient (r), the tangent derived from a linear regression between simulated and observed signals (α), and the NS coefficient of unbiased water levels (NSA). The quantity NSA is defined as follows:

$$\mathrm{NSA} = 1 - \frac{\sum_{t=1}^{\mathrm{nt}} [(y_t - \overline{y}) - (x_t - \overline{x})]^2}{\sum_{t=1}^{\mathrm{nt}} (y_t - \overline{y})^2}, \qquad (22)$$

where $\overline{x}$ stands for the mean value of the simulated signals for the entire period. Similarly to NS, NSA ranges from $-\infty$ to 1, where 1 is the optimal case. The following correction has been applied to α:

$$\begin{matrix} \alpha & \text{if} \quad \alpha \leq 1 \\ \alpha^{-1} & \text{if} \quad \alpha > 1 \end{matrix}. \qquad (23)$$

In this sense, the optimal α value is one and any other result below unity means that the amplitude of one of the signals is overestimated or underestimated.

As shown in Fig. 8, good correlations between simulated and observed water levels are found in most of the main rivers. This indicates that the model can properly represent the water level interannual variations. The averaged r of 18 VS along the central and low Solimões–Amazonas Rivers is 0.91, ranging from 0.83 (VS-36) to 0.96 (VS-24). These results present improvements in comparison to previous model evaluations with radar altimetry data over the Amazon River (Coe et al. 2008), where the averaged correlation between Ocean Topography Experiment (TOPEX)/Poseidon and water level simulations at eight VS along the same river reach is 0.70.

About 54% of VS have r values greater than or equal to 0.75 and 58% have NSA values higher than or equal to 0.50. Most of these stations are located over main rivers with large drainage areas. As shown in Fig. 8, virtual stations located in headwater catchments and on the western side of the basin, such as the Japurá River, the upper reaches of rivers draining the Andes and the lower Negro River, perform worse. The spatial distribution of coefficient a indicates that the amplitudes between simulated and observed water levels are in agreement in the Madeira and Branco Rivers and along the central Solimões and Negro Rivers. However, a significant discrepancy can be seen in other areas of the basin.

Water level errors in headwater catchments can be explained using arguments similar to those used for discharge error: mainly owing to meteorological forcing uncertainties at refined scales and simplified model physics. In other places, the degraded model performance (indicated by the low a coefficients) is also due to the application of a unique equation defining river geometry. Indeed, river width can have a great impact on water level amplitudes, as demonstrated in Getirana et al. (2012). In some specific cases, such as the lower Amazon River, low a values do not prevent the model from obtaining very good performances in terms of discharge. For example, even if the virtual station VS-10 had $a = 0.48$ (see Fig. 8), the simulated water discharge at Óbidos station (located a few kilometers away) resulted in NS = 0.89. The 1-month delay observed in the water discharge time series at the Caracaraí station is also evident in the simulated water levels at virtual

stations along the Branco River (e.g., VS-227). This indicates that the hydrological regime of this basin might be controlled by surface water rather than groundwater, implying that a high volume of baseflow stored in the baseflow reservoir can cause a significant flood wave delay.

c. Evaluation of flow velocities

Previous regional and global flow routing schemes compute flow velocity assuming a time-independent v parameterized as a function of one or more river physical characteristics, including slope and mean discharge (e.g., Vörösmarty et al. 1989; Miller et al. 1994; Sausen et al. 1994; Hagemann and Dümenil 1998). Other approaches have used traditional equations such as the Manning formula (e.g., Arora et al. 1999; Decharme et al. 2012; Yamazaki et al. 2011) and adaptations of the Chezy formula (e.g., Coe et al. 2008). These models simulate water flow only in river banks, while floodplains (if represented) are considered as static reservoirs. HyMAP calculates flow velocities in both rivers and floodplains by using Manning's formula with roughness coefficients adapted to the land cover type. Results show that flow velocities along the Solimões–Amazon main stream vary from 0.8 to 1.6 m s^{-1}, with lower values occurring between September and November and high values between March and May. These results are in agreement with other models based on similar formulations (e.g., Decharme et al. 2012; Yamazaki et al. 2011).

However, observations at gauging stations reveal that v values are higher than those given by the model. According to Fig. 9, simulated velocities are underestimated in large rivers, where the mean error e, computed as the ratio between mean simulated $\overline{v}_{sim}$ and observed $\overline{v}_{obs}$ flow velocities ($e = \overline{v}_{sim}/\overline{v}_{obs}$) is less than 1. In some regions, such as the southern Amazon basin, mean simulated v values are overestimated ($e > 1$). These differences are mainly due to (i) the simplified representation of river geometry and (ii) errors in the forcing data. Water depth h is the only time-dependent variable in the Manning's formula, while the roughness coefficient n and river slope i_r are constant. This means that changes in v is directly proportional to h. At each time step and grid cell, h is computed as a function of the river width W, length L, and water storage S_{riv} [Eqs. (4) and (5)]. Overestimated runoff and baseflow may result in higher water storage and, as a consequence, a higher h value. This explains the overestimation of both water discharge (RE > 0) and flow velocities ($e > 1$) at most gauging stations located in the southern Amazon basin (including Xingu, Tapajós, and Madeira River basins), as one can see in Fig. 9.

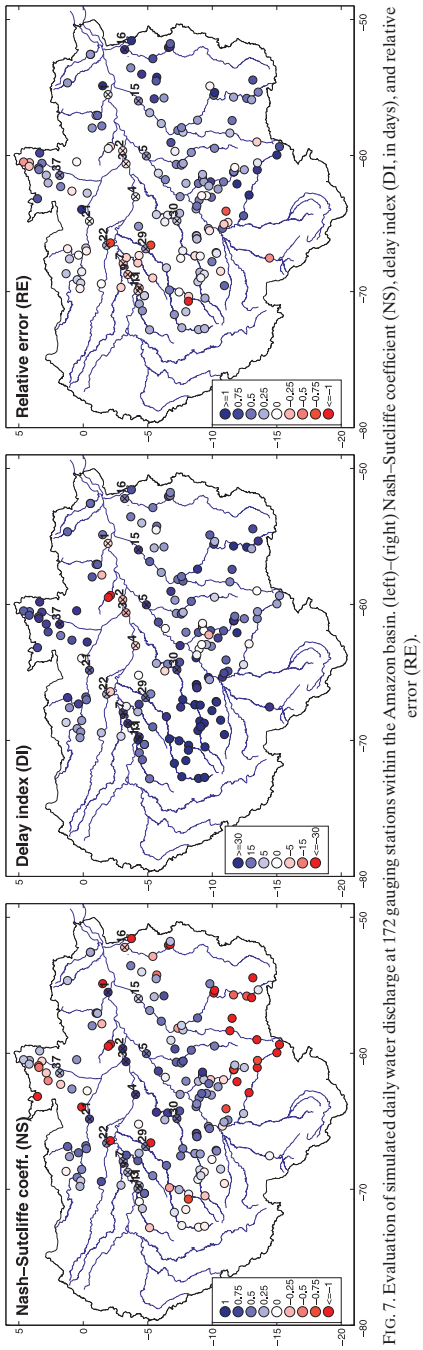

FIG. 7. Evaluation of simulated daily water discharge at 172 gauging stations within the Amazon basin. (left)–(right) Nash–Sutcliffe coefficient (NS), delay index (DI, in days), and relative error (RE).

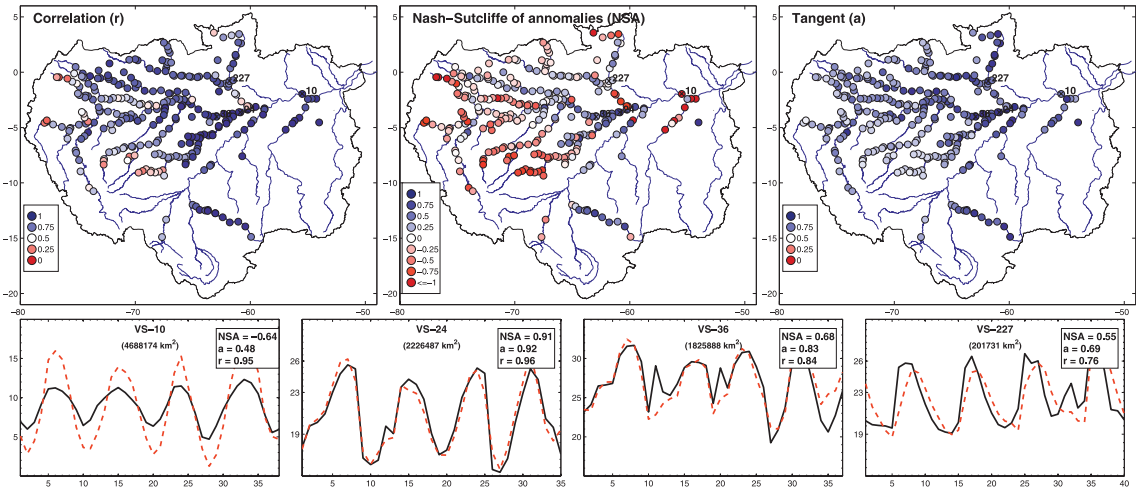

FIG. 8. Evaluation of simulated water levels against *Envisat* altimetric data. (top) Correlation (*r*), Nash–Sutcliffe coefficient of anomalies (NSA), and tangent (*a*) of simulated water levels at 294 virtual stations. (bottom) Water level time series at VS-10, VS-24, VS-36, and VS-227. Water level units are in meters and the abscissas in *Envisat* cycles available in the 2002–06 period. Model outputs are in dashed red lines and satellite observations in black.

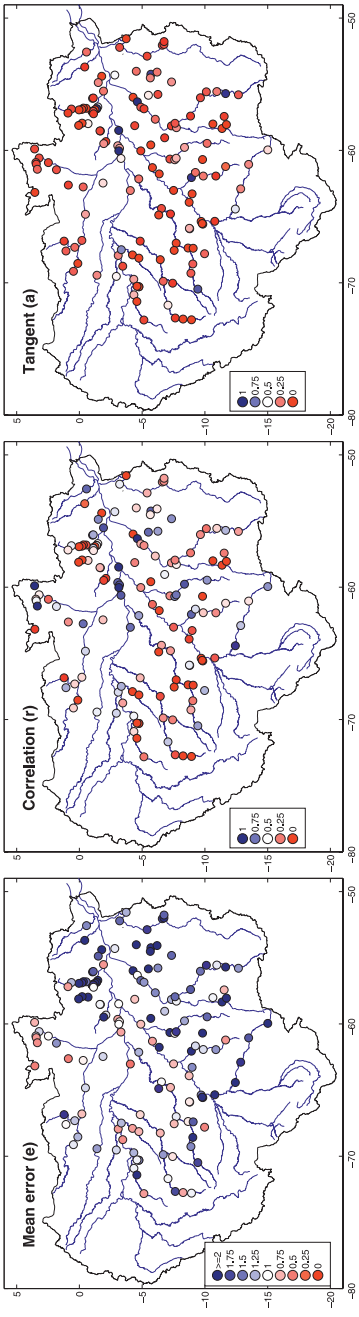

FIG. 9. Evaluation of simulated flow velocities at 153 gauging stations within the Amazon basin. (left)–(right) Mean error (*e*), correlation (*r*), and tangent (*a*).

d. Evaluation of floodplain extent

Figure 10 compares the spatial distribution of floodplains over the entire Amazonian basin from the model with the satellite-derived estimates for two distinct time periods: the dry (October 1995) and humid (June 1996) seasons. The simulated floodplain extent agrees with satellite-based estimates along the major river channels such as the Solimões, Amazon, Negro, Purus, and Madeira Rivers. However, differences are present in the Northern Negro and Branco River basins and southern Xingu River basin. Also, simulations show a very dispersed floodplain spatial distribution, which is not observed in the satellite-based estimates. These inconsistencies might be due to the model parameterizations and algorithms used to process satellite data, as discussed later in this section.

Note that the visual comparison of flooded areas is not straightforward because of the discrepancy between the satellite product's rectangular grid and the model's unit catchment (as shown in Fig. 2b). This means that, in some cases, a single unit catchment can represent surface areas corresponding to several satellite rectangular grid cells. This situation is most frequent in the main rivers, where large satellite-derived floodplain extents (e.g., Solimões–Amazon Rivers in the central Amazon area) are represented by a few unit catchments. For these reasons, a comparison of time series of averaged flood extent at the basin scale is more suited for an evaluation purpose.

The simulated time series compared well with observations at the basin scale during the 1993–2004 period with NS = 0.57, $r = 0.89$, and RE = 7%. In particular, the extreme events observed in 1997 and 1998, associated with El Niño and La Niña events, respectively (Fig. 11), are extremely well reproduced. However, note that the yearly maximum in simulated total flooded area is slightly overestimated when compared to observations, with larger discrepancies for 1999–2001. Moreover, model performance also varies regionally. For a more quantitative comparison, five other subregions are considered in order to evaluate the monthly averaged flooded areas over the 1993–2004 period: the central Amazonian floodplains (defined as the rectangle from 0°S–54°W to 8°S–72°W), and the Negro, Madeira, Xingu, and upper Solimões River basins. Among the five subregions defined within the Amazon basin, the best results were found for the Negro River basin, with relatively high correlation (0.85) and Nash–Sutcliffe coefficients (0.58), and low relative error (RE = −11%). In the central Amazon basin—which includes the Amazon River and parts of the Solimões, Negro, and lower Madeira River basins—the seasonality is well represented ($r = 0.85$), but the simulated flooded area is underestimated, on

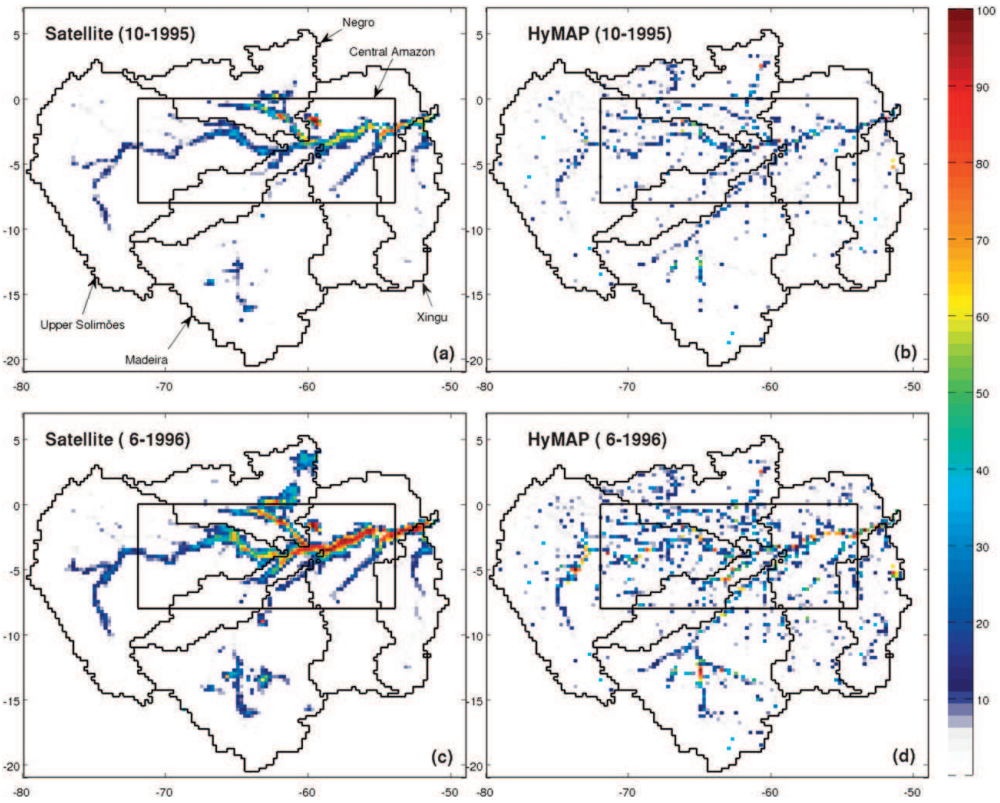

FIG. 10. Floodplain extent in the Amazon basin for (top) October 1995 and (bottom) June 1996. (left) Multisatellite observations (Papa et al. 2010) and (right) HyMAP outputs. Six regions considered to evaluate model outputs are contoured: the entire Amazon basin, central Amazonian floodplains (0°–8°S, 54°–72°W), and the Negro, Madeira, Xingu, and upper Solimões River basins. Units are in %.

average, by 21%. The underestimation found in the central Amazon and Negro River basins are compensated by an overestimation in other areas such as the upper Solimões and tributary river basins located in the lower Amazon basin, such as Xingu. In the upper Solimões River basin, seasonal variation is well represented (r = 0.84), although HyMAP overestimates flood extent in both wet and dry seasons (RE = 59%). Peaks are significantly overestimated in this region during the years 1993/94 and 1999–2001, leading to high peaks during the same periods at the basinwide scale. In the case of the Xingu River basin, modeled floodplain extent agrees with the satellite product during the dry seasons, but it is overestimated during the wet seasons, with a relative error (RE = 83%). Both Xingu and upper Solimões overestimate the amplitude and flooding during the wet seasons, explaining the low *NS* values.

To evaluate the interannual variability, anomalies of the floodplain extent averaged over the six regions are shown in Fig. 12. The correlation r and root-mean-square error (rmse) for each of the time series are also presented. Simulated monthly anomalies over the entire basin had r = 0.45 and rmse = 0.34, which demonstrate a reasonable improvement in comparison with Decharme et al. (2012) using ISBA–TRIP (r = 0.28 and rmse = 0.40). Regionally, r values vary from 0.37 (upper Solimões) to 0.69 (Madeira) and rmse from 0.33 (Xingu) to 0.84 (Madeira). The best overall simulation of monthly anomalies of floodplain extent is obtained again in the Negro River basin, with r = 0.58 and rmse = 0.50.

Differences between simulations and remote sensing–derived estimates may be due to different sources of uncertainty. First, uncertainties in the model parameterization might explain a large part of the differences.

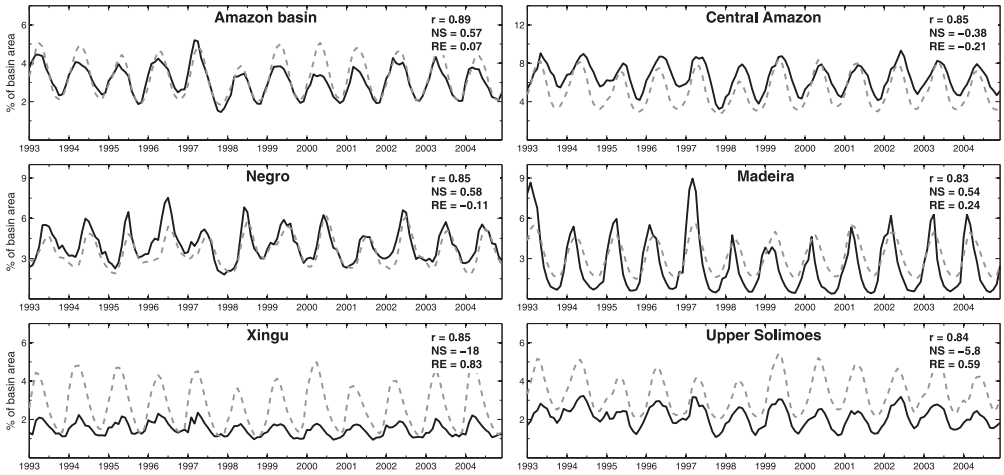

FIG. 11. Monthly averaged flooded extent over the 1993–2004 period for the six areas defined in Fig. 1. Model outputs are in dashed gray lines and satellite observations in black. The correlation (r), Nash–Sutcliffe coefficient (NS), and relative error (RE) are given for each series.

Previous evaluations of global-scale flow routing schemes have shown that the floodplain extent is very sensitive to changes in river geometry and roughness coefficient (Decharme et al. 2012; Yamazaki et al. 2011). Slightly reducing river depth and width can result in drastic increases in flooded areas, and vice versa. Inaccurate runoff and baseflow are other important sources of error in the flood extent simulation, over- or underestimating water stored in the river channels and, as a consequence, changing the floodplain dynamics. In addition, surface elevation errors, which are frequently found in current DEMs, can alter the relation (floodplain area × water level × water storage). The kinematic wave assumption can also impact the performance of simulated flood extent since it does not represent the backwater effects often present in certain locations of the Amazon basin.

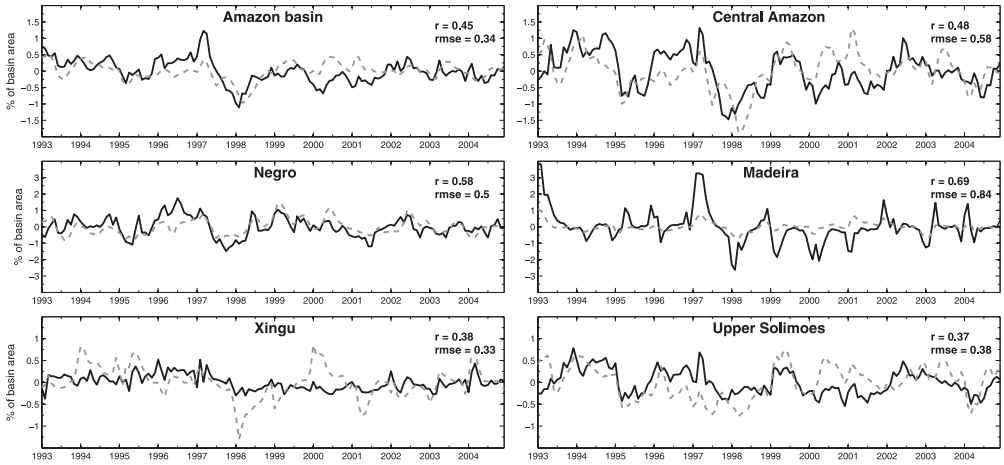

FIG. 12. As in Fig. 11, but for the monthly flooded area anomalies (mean seasonal cycle removed) and with the correlation (r) and the root-mean-square error (rmse) given for each series.

However, Yamazaki et al. (2011) show little difference in the basin-scale flood extent when kinematic and diffusive wave approaches are compared, suggesting that the kinematic wave assumption might have only a second order influence on floodplain dynamics. On the other hand, the satellite-derived products can also be sources of uncertainties. Prigent et al. (2007) and Papa et al. (2010) showed that the algorithm developed to retrieve floodplain extent from satellites still has difficulties in detecting inland water bodies covering less than ~80 km^2 of 25-km equal-area grid cells and it still has the tendency to underestimate small surface water-covered areas with less than 10% fractional coverage. The actual floodplain areas can be larger than those used as the reference.

e. Analysis of the water storage components

The understanding of the spatiotemporal distribution of water storage is essential to improved water resource management. HyMAP can provide useful insights of water storage in the different surface reservoirs within grid cells (runoff and baseflow time delays and river and floodplain reservoirs). According to the model outputs, as shown in Fig. 13, water is mainly stored in the runoff and baseflow ($R+B$) reservoirs at the basin scale, with a mean volume storage of 678 km^3. This means that 46% of the total runoff and baseflow derived from ISBA is flowing within grid cells before reaching the main river network. The water storage in $R+B$ reservoirs has a high amplitude, varying from about 260 up to 1220 km^3. The rivers store the second largest water volume in the Amazon basin, with about 41% (or 605 km^3) of the total runoff and baseflow. Finally, the average water storage in floodplains is about 13% (185 km^3). Water partitioning can be different in other regions within the Amazon basin according to physical characteristics of catchments and rivers.

Water stored in the central Amazon basin corresponds to 52% (765 km^3) of the total storage of the Amazon basin. This large volume is mainly stored in rivers, containing more than half (407 km^3) of the total water of this region. This is due to the large dimensions of the Amazon River and its tributaries within the selected area. In all other selected areas, $R+B$ reservoirs store the main water volume.

In the Negro River basin, water storage in rivers has a low amplitude compared to the water stored in the floodplain reservoir. This means that, once water reaches the river network, floodplain water storage is highly sensitive to the wet seasons. However, the $R+B$ reservoirs still represent the main water storage, with 57% (106 km^3) of the total runoff and baseflow produced in the basin. Floodplain water storage in the Madeira River basin is also sensitive to the wet seasons, with amplitudes higher than water storage in the rivers.

It must be highlighted that the water storage represented here corresponds to horizontal water fluxes only (i.e., runoff and baseflow). Other water reservoirs include soil moisture and precipitation intercepted by the vegetation canopy and are not discussed in this study. In addition, it should be noted that the values found here can vary significantly according to the parameter setting for river geometry.

f. Water discharge in floodplains

Figure 14 shows the annual cycles of simulated absolute water discharges in floodplains (Q_{fld}) and floodplain–river discharge fractions (Q_{frc}) averaged over the entire Amazon basin and the other five regions previously defined in Fig. 10. The Q_{fld} peaks vary from one region to another, according to the hydrological regime. The Madeira and Xingu River basins, located in the Southern Hemisphere, have Q_{fld} peaks in March–April. The Madeira River basin has the highest mean floodplain–river discharge fraction (Q_{frc} = 7.8%), with peaks above 15% representing more than 400 m^3 s^{-1}, while the Negro River basin, located in the Northern Hemisphere, has the highest water discharge in floodplains in July–August (~450 m^3 s^{-1}) and has the second highest Q_{frc}, with a mean value of 7%, and peaks as high as 14%. The upper Solimões River basin is spatially distributed in both Hemispheres, resulting in peaks occurring in April–June. The presence of meaningful nonflooded areas in this region (according to model outputs, on average, only ~3% is covered with water) contribute to a low mean Q_{fld} of about 83 m^3 s^{-1}, corresponding to Q_{frc} = 2.2%. Results are similar in the entire Amazon basin, with low mean Q_{fld} and Q_{frc} of ~128 m^3 s^{-1} and 3%, respectively. During wet seasons, Q_{fld} averaged over the entire Amazon basin is 280 m^3 s^{-1}, representing about 6% of the total water discharge, and in the dry seasons, Q_{fld} is reduced to values as low as 25 m^3 s^{-1}, or ~1% of the total water discharge. The highest Q_{fld} values occur in the central Amazon basin, where most floodplains are located. The mean Q_{fld} value in this region is 228.5 m^3 s^{-1} and peaks reach values above 500 m^3 s^{-1}. It must be highlighted that these values are averages for the entire regions and that Q_{fld} can be much higher in grid cells representing the main rivers. For example, the mean Q_{fld} values along the Solimões–Amazon main stream can be as high as 2750 m^3 s^{-1} (not shown). However, this discharge is negligible compared to the total water flow in the same reach (171 200 m^3 s^{-1}), resulting in a low Q_{frc} value of 1.6%. In contrast, a previous study based on the Muskingum method (Richey et al. 1989) estimated that up to 30% of the discharge of the Amazon River is routed through the floodplains. However, to the knowledge of the authors, no observed floodplain discharge is

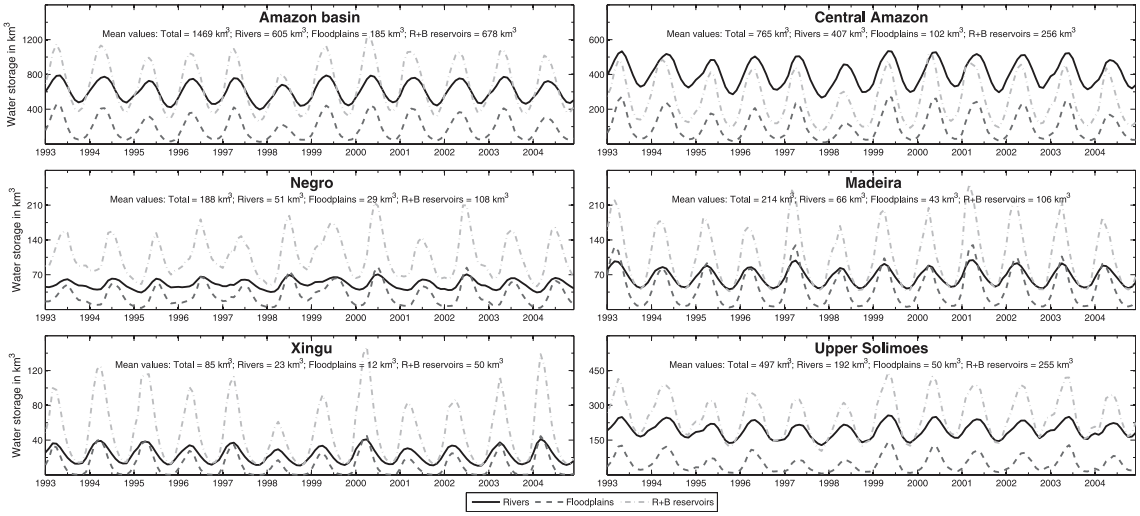

FIG. 13. Monthly water storage in the river, floodplain, and surface $R+B$ reservoirs in the Amazon basin and other five regions.

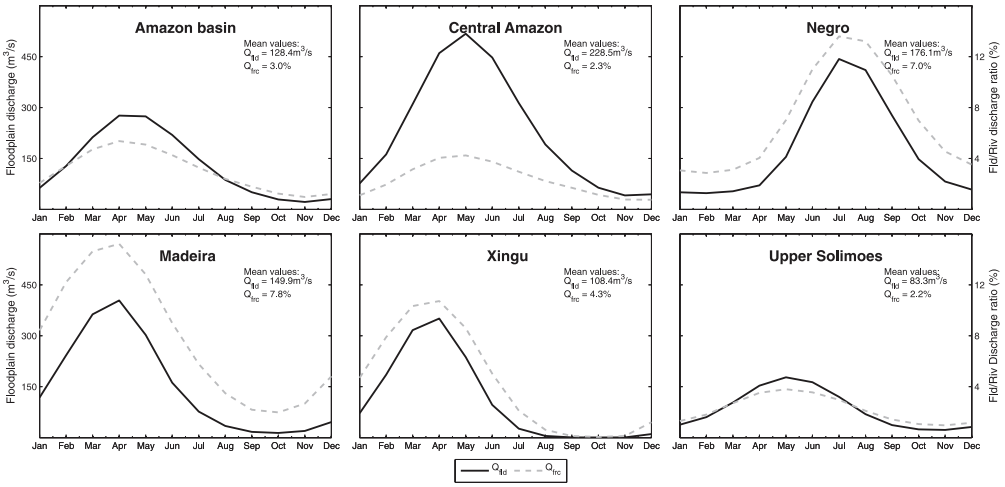

FIG. 14. Annual cycles of simulated floodplain water fluxes averaged for the Amazon basin and other five regions. Solid lines represent absolute water discharge discharges (Q_{fld}) in $\mathrm{m^3\ s^{-1}}$ and dashed lines floodplain–river discharge fraction (Q_{frc}) in %.

currently available, and thus it is not feasible to confirm these estimates.

g. Evaporation from open waters

The total evapotranspiration from ISBA averaged over the entire Amazon basin is about 2.8 mm $\mathrm{day^{-1}}$ while the potential evaporation from open waters, derived from the modified Penman–Monteith equation without surface resistance [Eq. (17)], is 3.4 mm $\mathrm{day^{-1}}$. Following Eq. (18), the remaining energy for evaporation from open waters E_w is 0.8 mm $\mathrm{day^{-1}}$. This rate is valid for the case where the basin surface area is completely covered with water during the entire study period. However, as discussed before, open waters in the basin represent 2%–5% of the total surface area, resulting in low mean E_w values across the basin. As shown in Fig. 15, maximum and minimum E_w values simulated by HyMAP and averaged for the Amazon basin occur in April (~0.034 mm $\mathrm{day^{-1}}$) and July–August (~0.013 mm $\mathrm{day^{-1}}$), respectively.

Mean rates can be much higher in some locations, corresponding to an open water surface area. Monthly E_w values can be as high as 1.2 mm $\mathrm{day^{-1}}$ in some locations of the southern Madeira River basin in both dry and wet seasons. Other areas in the central Amazon basin can also have monthly rates above 1 mm $\mathrm{day^{-1}}$ during the wet seasons. Considering the differential evaporation from open waters has a relatively low effect on the water discharge at the scale of the entire Amazon basin (the mean E_w rate simulated by HyMAP is ~0.02 mm $\mathrm{day^{-1}}$, representing ~1600 $\mathrm{m^3\ s^{-1}}$ or about 0.8% of the total water discharge produced in the basin). However, even if evaporation from open waters may not be significant compared to the water discharge in the Amazon basin, it has been shown that E_w has a significant impact in the water balance in arid regions such as the Niger River basin (e.g., Decharme et al. 2012).

h. Effects of floodplain dynamics on water discharge

To evaluate the effects of floodplain dynamics on water discharge, two experiments have been proposed: (i) no dynamics in flooded areas (NODYN) [$v_f = 0$ in Eq. (11)] (i.e., floodplains are merely considered as river overflow reservoirs, following the same approaches as those in current versions of ISBA–TRIP and CaMa–Flood) and (ii) floodplains are completely removed from the system (NOFLD) (i.e., water flows only through rivers). The previously presented model output is considered as the reference simulation (SIM). An evaluation is performed at four gauging stations along the Solimões–Amazon River (Óbidos, Jaturana+Careiro, Manacapuru, and Tabatinga), as shown in Fig. 16.

At Óbidos, NS coefficients provided by NODYN (NS = 0.84) and NOFLD (NS = 0.78) are lower than those resulting from SIM. Flood waves are delayed by about 20 days at Óbidos when water flow in floodplains is not considered. This is caused by the increased water storage in floodplain reservoirs, which smooths and delays the hydrographs. Increases in water storage in floodplains slightly increases E_w rates and reduces volume errors (DV = 4.9%) in comparison with SIM

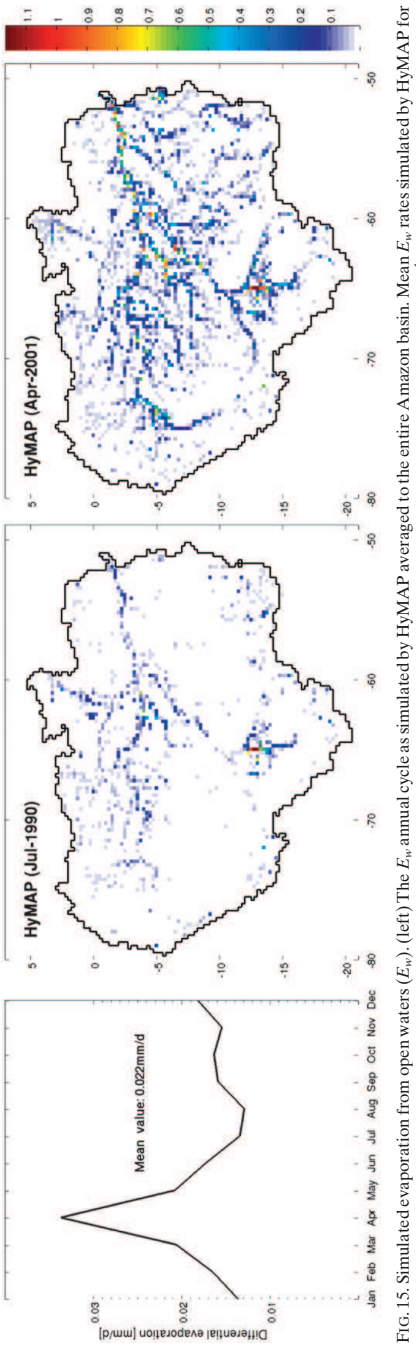

FIG. 15. Simulated evaporation from open waters (E_w). (left) The E_w annual cycle as simulated by HyMAP averaged to the entire Amazon basin. Mean E_w rates simulated by HyMAP for (middle) July 1990 (low evaporation rate) and (right) April 2001 (high evaporation rate). Units are in mm day^{-1}.

(DV = 5.1%). The opposite effect is seen for NOFLD. Neglecting floodplains results in an 18-day advance of the flood wave provoked by a significant augmentation of water storage in rivers and therefore of water depths h and flow velocity v (as discussed in section 4d, the flow velocity v is directly proportional to h). Since open waters are significantly reduced, an increasing of volume error (DV = 5.8%) is seen for NOFLD. Results at Jatuarana+Careiro are similar, with reduced NS values for both NODYN (0.81) and NOFLD (0.75), differences in time lags (DI values equal to 11 and −19 days, respectively), and volume errors (DV values equal to −6.3% and −5.7%, respectively). A slight increase of NS values is observed at Manacapuru with the experiment NODYN (NS = 0.82), probably caused by the change of time delay (DI = 9 days). NOFLD at Manacapuru has the same characteristics which were found at the other gauging stations with reduced NS (0.66), negative DI (−20 days), and higher DV (−5.2%). At Tabatinga station, the noise introduced by neglecting floodplain storage does not prevent obtaining a better NS (0.48) value with NOFLD. This is explained by the reduced time lag obtained in this experiment (DI = 16 days). Poor results are obtained with NODYN with NS close to zero and DI = 49 days.

5. Conclusions

This paper presents the Hydrological Modeling and Analysis Platform (HyMAP), a new parameterization of horizontal water flow over continental surfaces capable of routing surface runoff R and baseflow B provided by LSMs in offline mode. The model is a result of the integration and improvement of known approaches described by previous state-of-the-art global FRS and new features suggested in this paper, which include the representation of time delays for both R and B, the use of the kinematic wave equation to route water in rivers and floodplains separately, and the evaporation from open waters.

HyMAP was run for the Amazon basin at the daily time step and a 0.25° spatial resolution. A full evaluation of main variables such as water discharge and level, floodplain extent, and flow velocity is performed against a large dataset of in situ observations and satellite-derived products. In addition, water discharge in floodplains, evaporation from open waters, storage in reservoirs, and impact of floodplain dynamics on simulated water discharges are presented and discussed.

Results show that the model simulates well the discharge and water levels in the main rivers of the Amazon basin, with an overall performance better than previous modeling attempts. Nevertheless, as discussed in this

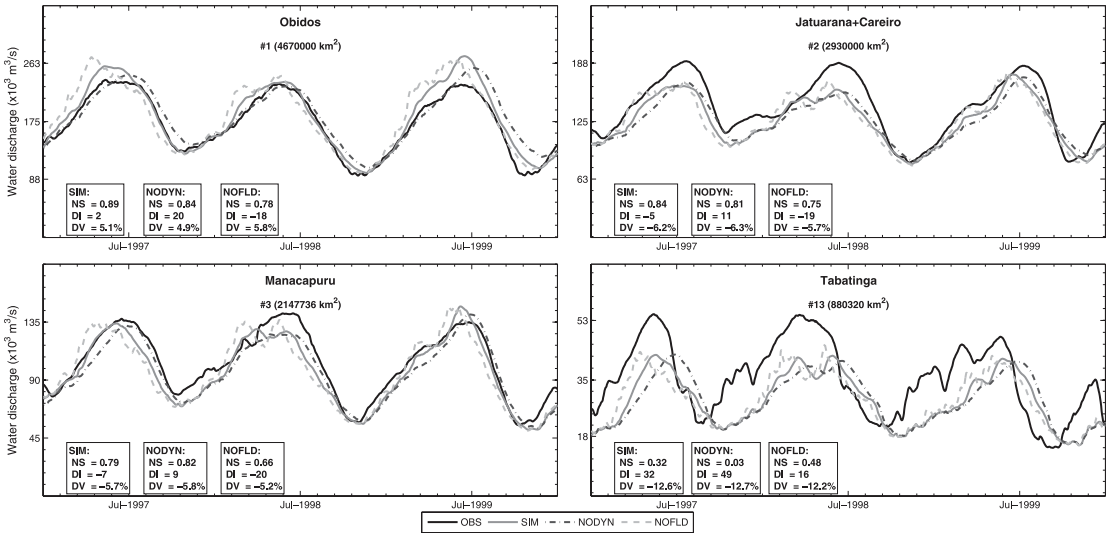

FIG. 16. Hydrographs at four gauging stations along the Solimões–Amazon River (Óbidos, Jaturana+Careiro, Manacapuru, and Tabatinga) resulting from experiments evaluating effects of floodplain dynamics on water discharges.

paper, smaller catchments present problems mainly related to scale issues and forcing errors. This happens because, as a general rule, the larger the studied domain, the coarser the spatial resolution and the more the processes must be simplified. Moreover, the lack of adequate global datasets prevents a better parameterization of the baseflow time delay (T_b) and river geometry (i.e., river width W and length L). These parameters account for most of the surface water stored in the basin, thus representing the major reservoirs.

For the first time, simulated flow velocity was evaluated against observations over the entire Amazon basin. Even though HyMAP and previous modeling attempts are similar, it has been shown that simulated v presents significant errors, possibly owing to uncertainties in the river geometry and simplifications of physical processes. Other sources of error are the kinematic wave assumption, which is not capable of simulating hysteresis caused by backwater effects in flat water surfaces. This limitation can also explain uncertainties in water levels and, to a lesser degree, in the floodplain extent. On the other hand, the use of a diffusive wave approach requires a much finer temporal resolution in order to avoid numerical instabilities. A choice for the kinematic wave equation was made in this study. However, further analyses must be performed to fully evaluate the limitations of each approach.

Satellite-derived and simulated interannual variability of floodplain extent matches well at the basin scale. However, significant differences can be noticed locally. Indeed, open water surfaces are closely dependent on river geometry and topography. The geometry defines whether river overflow may occur and the topography, which prescribes floodplain surface profile within a grid cell, determines the flooded area given an overflowed water volume. But both of them present limitations owing to problems with the needed input data.

Current satellite-based DEMs are not adequate to provide accurate floodplain elevation profiles. The SRTM30 DEM used to represent the topography and processed with FLOW to provide hydrological information has large uncertainties. For example, SRTM30 DEM data over South America have a mean absolute height accuracy of 1.7 m, with 90% of the errors being less than 7.5 m (Rodriguez et al. 2005, 2006). A few attempts have been proposed in the literature to reduce the SRTM30 uncertainty by degrading the spatial resolution (e.g., Wilson et al. 2007) and using land cover maps to identify the presence of forests (e.g., Coe et al. 2008). However, DEM errors remain as one of the main sources of uncertainty in modeling the interactions between rivers and floodplains.

Another issue that plays an important role in flooded areas is the model spatial resolution. Even relatively higher spatial resolutions may not adequately represent wide floodplains with only one grid cell, and as a consequence, open water extents are underestimated. For such cases, two-dimensional approaches capable of simulating floodplain water flow among neighboring grid cells might be necessary. These techniques have been largely used at smaller scales (e.g., Estrela and Quintas 1994; Horritt and Bates 2002) and must be adapted for use in global models in the future. Another solution is the use of DEM processing approaches called "burning methods" to change floodplain flow directions to correspond to the closest river stream. In particular, the floodplain burning approach, which takes into account river and floodplain maps, can be an efficient way to gradually change high-resolution DEM pixel elevations in flooded areas (Getirana et al. 2009a,b). This would concentrate the whole floodplain extent of a given river reach in only one grid cell.

It has been shown that about 3% of the water found the river network in the Amazon basin flow through the floodplains. This is the first estimate at the basin scale since other large-scale flow routing schemes do not take into account water dynamics in floodplains. Also, discharge estimates through floodplains are highly sensitive and limited by numerous aspects related to model parameters representing river geometry, flow dynamics, and DEM errors, and these results must be considered as first estimates.

However, as DEM precision and model physics improve, this value may change. In addition, the assimilation of two-dimensional water surface dynamics provided by SWOT will significantly refine floodplain water flow simulations. Briefly, when compared to previous global flow routing schemes, HyMAP shows visible improvements in simulating horizontal water flow over the continents and its use in general water resources studies and flood hazards is recommended.

This study has been developed as part of the SWOT (Alsdorf et al. 2007) Virtual Mission and the choices of the dynamics and processes included in HyMAP have been made, in some measure, to be able to use SWOT data. Current developments in the framework of this study include the use of an optimization scheme considering different data sources, such as radar altimetry, to improve the modeling, understanding, and streamflow forecasts in poorly gauged or ungauged basins (Getirana et al. 2012). Future applications include the development of a water height change assimilation approach using data provided by the SWOT mission (Mouffe et al. 2011). Also, the model is currently being implemented in the Land Information System (LIS) (Kumar et al. 2006). This effort is the first step to have HyMAP running in online mode with a variety of LSMs and climate models.

Acknowledgments. The first author would like to thank the Centre National d'Études Spatiales (CNES) for the financial support. The study benefited from data made available by Agência Nacional de Águas (ANA) and by the European Space Agency (ESA) under the form of Geophysical Data Records (GDRs). The multimission database of GDRs is maintained by the Centre de Topographie des Océans et de l'Hydrosphère (CTOH) at LEGOS. Grateful acknowledgments are also due to G. Cochonneau (IRD), M.C. Gennero (LEGOS), and R. Alkama (Météo-France) for their help in data acquisition and processing and P. Bates (Univ. Bristol) and an anonymous reviewer for their valuable comments.

REFERENCES

Alsdorf, D. E., E. Rodríguez, and D. P. Lettenmaier, 2007: Measuring surface water from space. *Rev. Geophys.,* **45,** RG2002, doi:10.1029/2006RG000197.

Arora, V. K., and G. J. Boer, 2001: Effects of simulated climate change on the hydrology of major river basins. *J. Geophys. Res.,* **106** (D4), 3335–3348.

——, F. H. S. Chiew, and R. B. Grayson, 1999: A river flow routing scheme for general circulation models. *J. Geophys. Res.,* **104** (D12), 14 347–14 357.

Bamber, J. L., 1994: Ice sheet altimeter processing scheme. *Int. J. Remote Sens.,* **15**, 925–938.

Biancamaria, S., P. D. Bates, A. Boone, and N. M. Mognard, 2009: Large-scale coupled hydrologic and hydraulic modelling of the Ob river in Siberia. *J. Hydrol.,* **379,** 136–150, doi:10.1016/j.jhydrol.2009.09.054.

Bousquet, P., and Coauthors, 2006: Contribution of anthropogenic and natural sources to atmospheric methane variability. *Nature,* **443,** 439–443, doi:10.1038/nature05132.

Chow, V. T., 1959: *Open-Channel Hydraulics.* McGraw-Hill, 680 pp.

Coe, M. T., M. H. Costa, and E. A. Howard, 2008: Simulating the surface waters of the Amazon River basin: Impacts of new river geomorphic and flow parameterization. *Hydrol. Processes,* **22,** 2542–2553, doi:10.1002/hyp.6850.

Cogley, J. G., 2003: GGHYDRO—Global hydrographic data, release 2.3. Trent Tech. Note 2003-1, 11 pp. [Available online at http://people.trentu.ca/~gcogley/glaciology/index.htm.]

Crétaux, J. F., and Coauthors, 2011: SOLS: A lake database to monitor in the near real time water level and storage variations from remote sensing data. *Adv. Space Res.,* **47,** 1497–1507.

Dadson, S. J., I. Ashpole, P. Harris, H. N. Davies, D. B. Clark, E. Blyth, and C. M. Taylor, 2010: Wetland inundation dynamics in a model of land surface climate: Evaluation in the Niger inland delta region. *J. Geophys. Res.,* **115,** D23114, doi:10.1029/2010JD014474.

Decharme, B., R. Alkama, F. Papa, S. Faroux, H. Douville, and C. Prigent, 2012: Global off-line evaluation of the ISBA-TRIP flood model. *Climate Dyn.,* **38** (7–8), 1389–1412, doi:10.1007/s00382-011-1054-9.

Döll, P., F. Kaspar, and B. Lehner, 2003: A global hydrological model for deriving water availability indicators: Model tuning and validation. *J. Hydrol.,* **270,** 105–134, doi:10.1016/S0022-1694(02)00283-4.

Dunne, T., L. A. K. Mertes, R. H. Meade, J. E. Richey, and B. R. Forsberg, 1998: Exchanges of sediment between the flood plain and channel of the Amazon River in Brazil. *GSA Bull.,* **110,** 450–467.

Estrela, T., and L. Quintas, 1994: Use of GIS in the modelling of flows on floodplains. *Proceedings of the Second International Conference on River Flood Hydraulics,* Wiley, 177–189.

Getirana, A. C. V., M.-P. Bonnet, and J.-M. Martinez, 2009a: Evaluating parameter effects in a DEM 'burning' process based on land cover data. *Hydrol. Processes,* **23,** 2316–2325, doi:10.1002/hyp.7303.

——, ——, O. C. Rotunno Filho, and W. J. Mansur, 2009b: Improving hydrological information acquisition from DEM processing in floodplains. *Hydrol. Processes,* **23,** 502–514, doi:10.1002/hyp.7167.

——, A. Boone, and N. Mognard, 2012: Automatic calibration of a flow routing scheme constrained by radar altimetry data. *Extended Abstracts, 20 Years of Progress in Radar Altimetry Symp.,* Venice, Italy, European Space Agency, 119. [Available online at http://www.congrexprojects.com/docs/12c01_docs/20ypra_abstracts_12_08_27_v9.pdf.]

Hagemann, S., and L. Dümenil, 1998: A parameterization of lateral water flow for the global scale. *Climate Dyn.,* **14,** 17–41.

Horritt, M. S., and P. D. Bates, 2002: Evaluation of 1D and 2D numerical models for predicting river flood inundation. *J. Hydrol.,* **268,** 87–99, doi:10.1016/S0022-1694(02)00121-X.

Kirpich, Z. P., 1940: Time of concentration of small agricultural watersheds. *Civ. Eng.,* **10,** 362.

Krinner, G., 2003: Impact of lakes and wetlands on boreal climate. *J. Geophys. Res.,* **108,** 4520, doi:10.1029/2002JD002597.

Kumar, S. V., and Coauthors, 2006: Land information system: An interoperable framework for high resolution land surface modeling. *Environ. Modell. Software,* **21,** 1402–1415, doi:10.1016/j.envsoft.2005.07.004.

Lehner, B., and P. Döll, 2004: Development and validation of a global database of lakes, reservoirs and wetlands. *J. Hydrol.,* **296,** 1–22.

Masson, V., J.-L. Champeaux, C. Chauvin, C. Meriguet, and R. Lacaze, 2003: A global database of land surface parameters at 1-km resolution in meteorological and climate models. *J. Climate,* **16,** 1261–1282.

Masutomi, Y., Y. Inui, K. Takahashi, and U. Matsuoka, 2009: Development of highly accurate global polygonal drainage basin data. *Hydrol. Processes,* **23,** 572–584.

Melack, J. M., L. L. Hess, M. Gastil, B. R. Forsberg, S. K. Hamilton, I. B. T. Lima, and E. M. L. M. Novo, 2004: Regionalization of methane emissions in the Amazon basin with microwave remote sensing. *Global Change Biol.,* **10,** 530–544.

Miller, J., G. Russell, and G. Caliri, 1994: Continental scale river flow in climate models. *J. Climate,* **7,** 914–928.

Mohamed, Y. A., B. J. J. M. van den Hurk, H. H. G. Savenije, and W. G. M. Bastiaanssen, 2005: Impact of the Sudd wetland on the Nile hydroclimatology. *Water Resour. Res.,* **41,** W08420, doi:10.1029/2004WR003792.

Mouffe, M., A. C. V. Getirana, S. Ricci, C. Lion, S. Biancamaria, N. Mognard, A. Boone, and P. Rogel, 2011: Towards SWOT data assimilation for hydrology: Automatic calibration of global flow routing model parameters in the Amazon basin. American Geophysical Union, Fall Meeting 2011, Abstract H23G-1364.

Noilhan, J., and J.-F. Mahfouf, 1996: The ISBA land surface parameterisation scheme. *Global Planet. Change,* **13** (1–4), 145–159, doi:10.1016/0921-8181(95)00043-7.

Oki, T., and Y. C. Sud, 1998: Design of total runoff integrating pathways (TRIP)—A global river channel network. *Earth Interact.,* **2**. [Available online at http://EarthInteractions.org.]

Paiva, R. C. D., W. Collischonn, and D. C. Buarque, 2012: Validation of a full hydrodynamic model for large-scale hydrologic modelling in the Amazon. *Hydrol. Processes,* doi:10.1002/hyp.8425, in press.

Papa, F., C. Prigent, F. Aires, C. Jimenez, W. B. Rossow, and E. Matthews, 2010: Interannual variability of surface water extent at the global scale, 1993–2004. *J. Geophys. Res.,* **115,** D12111, doi:10.1029/2009JD012674.

Portmann, F. T., S. Siebert, and P. Döll, 2010: MIRCA2000—Global monthly irrigated and rainfed crop areas around the year 2000: A new hight-resolution data set for agricultural and hydrological modeling. *Global Biogeochem. Cycles,* **24,** GB1011, doi:10.1029/2008GB003435.

Prigent, C., F. Papa, F. Aires, W. B. Rossow, and E. Matthews, 2007: Global inundation dynamics inferred from multiple satellite observations, 1993–2000. *J. Geophys. Res.,* **112,** D12107, doi:10.1029/2006JD007847.

Richey, J. E., L. A. K. Mertes, T. Dunne, R. Victoria, B. R. Forsberg, A. C. F. N. S. Tancredi, and E. Oliveira, 1989: Source and routing of the Amazon River flood wave. *Global Biogeochem. Cycles,* **3,** 191–204.

Rodriguez, E., C. S. Morris, J. E. Belz, E. C. Chapin, J. M. Martin, W. Daffer, and S. Hensley, 2005: An assessment of the SRTM topographic products. Jet Propulsion Laboratory Tech. Rep. JPL D-31639, 143 pp.

——, ——, and ——, 2006: A global assessment of the SRTM performance. *Photogramm. Eng. Remote Sens.,* **72,** 249–260.

Sausen, R., S. Schubert, and L. Dumenil, 1994: A model of river runoff for use in coupled atmosphere-ocean models. *J. Hydrol.,* **155,** 337–352.

Sheffield, J., G. Goteti, and E. F. Wood, 2006: Development of a 50-year high-resolution global dataset of meteorological forcings for land surface modeling. *J. Climate,* **19,** 3088–3111.

Shuttleworth, W. J., 1993: Evaporation. *Handbook of Hydrology,* D. Maidment, Ed., McGraw-Hill, 1–4.

Vörösmarty, C. J., B. Moore III, A. L. Grace, and M. P. Gildea, 1989: Continental scale models of water balance and fluvial transport: An application to South America. *Global Biogeochem. Cycles,* **3,** 241–265.

Wilson, M., P. Bates, D. Alsdorf, B. Forsberg, M. Horritt, J. Melack, F. Frappart, and J. Famiglietti, 2007: Modeling large-scale inundation of Amazonian seasonally flooded wetlands. *Geophys. Res. Lett.,* **34,** L15404, doi:10.1029/2007GL030156.

Yamazaki, D., T. Oki, and S. Kanae, 2009: Deriving a global river network map and its sub-grid topographic characteristics from a fine-resolution flow direction map. *Hydrol. Earth Syst. Sci.,* **13,** 2241–2251, doi:10.5194/hess-13-2241-2009.

——, S. Kanae, H. Kim, and T. Oki, 2011: A physically based description of floodplain inundation dynamics in a global river routing model. *Water Resour. Res.,* **47,** W04501, doi:10.1029/2010WR009726.

——, C. A. Baugh, P. D. Bates, S. Kanae, D. E. Alsdorf, and T. Oki, 2012: Adjustment of a spaceborne DEM for use in floodplain hydrodynamic modeling. *J. Hydrol.,* **436–437,** 81–91.

Hydrol. Earth Syst. Sci., 18, 4485–4507, 2014
www.hydrol-earth-syst-sci.net/18/4485/2014/
doi:10.5194/hess-18-4485-2014

Hydrology and Earth System Sciences Open Access

Assimilation of satellite data to optimize large-scale hydrological model parameters: a case study for the SWOT mission

V. Pedinotti[1,2], A. Boone[1], S. Ricci[3], S. Biancamaria[4], and N. Mognard[2]

[1]CNRM/GAME, Météo-France, CNRS, URA 1357, Toulouse, France
[2]Centre National d'études spatiales (CNES), Toulouse, France
[3]CERFACS/URA 1875, 42 Avenue Gaspard Coriolis, 31057 Toulouse CEDEX, France
[4]CNRS, LEGOS, UMR5566 CNRS-CNES-IRD-Université Toulouse III, France

Correspondence to: V. Pedinotti (vanessa.pedinotti@gmail.com)

Received: 3 March 2014 – Published in Hydrol. Earth Syst. Sci. Discuss.: 30 April 2014
Revised: 20 September 2014 – Accepted: 23 September 2014 – Published: 10 November 2014

Abstract. During the last few decades, satellite measurements have been widely used to study the continental water cycle, especially in regions where in situ measurements are not readily available. The future Surface Water and Ocean Topography (SWOT) satellite mission will deliver maps of water surface elevation (WSE) with an unprecedented resolution and provide observation of rivers wider than 100 m and water surface areas greater than approximately 250 × 250 m over continental surfaces between 78° S and 78° N. This study aims to investigate the potential of SWOT data for parameter optimization for large-scale river routing models. The method consists in applying a data assimilation approach, the extended Kalman filter (EKF) algorithm, to correct the Manning roughness coefficients of the ISBA (Interactions between Soil, Biosphere, and Atmosphere)-TRIP (Total Runoff Integrating Pathways) continental hydrologic system. Parameters such as the Manning coefficient, used within such models to describe water basin characteristics, are generally derived from geomorphological relationships, which leads to significant errors at reach and large scales. The current study focuses on the Niger Basin, a transboundary river. Since the SWOT observations are not available yet and also to assess the proposed assimilation method, the study is carried out under the framework of an observing system simulation experiment (OSSE). It is assumed that modeling errors are only due to uncertainties in the Manning coefficient. The true Manning coefficients are then supposed to be known and are used to generate synthetic SWOT observations over the period 2002–2003. The impact of the assimilation system on the Niger Basin hydrological cycle is then quantified. The optimization of the Manning coefficient using the EKF (extended Kalman filter) algorithm over an 18-month period led to a significant improvement of the river water levels. The relative bias of the water level is globally improved (a 30 % reduction). The relative bias of the Manning coefficient is also reduced (40 % reduction) and it converges towards an optimal value. Discharge is also improved by the assimilation, but to a lesser extent than for the water levels (7 %). Moreover, the method allows for a better simulation of the occurrence and intensity of flood events in the inner delta and shows skill in simulating the maxima and minima of water storage anomalies, especially in the groundwater and the aquifer reservoirs. The application of the assimilation method in the framework of an observing system simulation experiment allows evaluating the skill of the EKF algorithm to improve hydrological model parameters and to demonstrate SWOT's promising potential for global hydrology issues. However, further studies (e.g., considering multiple error sources and the difference between synthetic and real observations) are needed to achieve the evaluation of the method.

1 Introduction

The impact of climate variability on land water storage is becoming an increasingly crucial issue for the development of future water resource management strategies. In order to investigate this impact, continental hydrologic systems (CHSs) can be used to simulate water dynamics above and

below the land surface as a response to environmental forcing. CHSs are generally made of a land surface model (LSM) which computes the water and energy budget at the surface–atmosphere interface, coupled with a river routing model (RRM) which distributes the runoff to the river and the soil storage components. At regional or global scales, the realistic representation of major surface hydrologic and hydrodynamic processes is very challenging and requires the use of computationally efficient, easily parameterized, comparatively simple and physically based routing methodologies. However, land surface hydrologic processes are highly heterogeneous in space and time and are therefore difficult to parameterize given the huge dimensions of atmospheric general circulation model (AGCM) grid areas. Observational data describing the water dynamics and storage variations are required to evaluate CHS-simulated diagnostics, and to calibrate these models. In situ data have been extensively used, but they are limited by their temporal and spatial coverage. In addition to the information provided by in situ measurements, satellite remote sensing instruments have been developed and are continually improved. These instruments generally provide a large spatial coverage which is more appropriate for global applications, especially in areas where in situ data are scarce. Such areas are generally sparsely inhabited, with reduced infrastructures and possible geopolitical issues, such as large portions of the African continent or part of the Arctic (Alsdorf et al., 2007). Applications using satellite remote sensing techniques lead to many promising perspectives for improving the observation of land surface and hydrological variables and processes.

Hydrological models require information about continental water dynamics and storage variations above and below the surface for calibration and evaluation of the simulated water budget. To this end, diverse types of monitoring data are needed. In situ discharge data, for example, give information of 1 spatial dimension, which quantifies water fluxes in a specific river channel, but do not give any direct information about runoff or lateral inflow. Yet, hydrologically complex areas, such as wetlands and floodplains which are processes of three spatial dimensions, cannot be adequately resolved using observations of 1 spatial dimension (Alsdorf et al., 2007). Spatially distributed observations are required, such as those provided by satellites which give 2-dimensional information about surface water dynamics. Recently, efforts have been made to build global maps of floodplain variability and extent, providing an additional metric for CHS evaluation (Papa et al., 2010). Nadir altimetry has also constituted a valuable progress for the monitoring of surface water dynamics and elevation (TOPEX/Poseidon, Envisat, Jason 1 and 2; Baup et al., 2007; Santos Da Silva et al., 2012).

Although useful, current satellite altimetry spatial resolution does not resolve small-scale land water dynamics thereby limiting our understanding of large-scale hydrologic and hydrodynamic processes. The future NASA–CNES–CSA Surface Water and Ocean Topography (SWOT) satellite mission will be launched in 2020 and will deliver maps of water surface elevation (WSE), slope and extent with an unprecedented resolution of 100 m.

For continental hydrology, the SWOT mission has the potential to help deal with critical issues, such as monitoring transboundary basins and the development of management strategies in a changing world. It is necessary to determine how the SWOT data can be used to improve hydrological simulations and to better predict continental water storage.

Data assimilation (DA) has been shown to be a promising technique for improving river modeling (Andreadis et al., 2007; Durand et al., 2010; Biancamaria et al., 2011; Yoon et al., 2012). Commonly used in operational meteorology and oceanography, DA combines data coming from various sources, such as numerical models or observations, while taking into account measurement errors and model uncertainties for a better description and prediction of the system. However, these methods are not yet extensively used in hydrology and related works are rare, especially for large-scale applications. Drusch et al. (2009) used observations of 2 m air temperature and soil moisture to evaluate a Kalman filter-based soil moisture analysis system and its impact on the operational ECMWF (European Centre for Medium-Range Weather Forecasts)-integrated forecast system. They showed that the impact of EKF on the forecast skill of the operational weather forecast model was neutral in terms of forecast score but gave the promising possibility to better constrain the soil water content with more accurate soil moisture estimates. Pereira-Cardenal et al. (2011) investigated the potential of using Envisat water levels observations in a real time or near-real time by applying an ensemble Kalman filter in order to update semidistributed hydrological model state variables. The method was applied to the Syr Darya River basin, a complex mountainous region covering approximately 7000 km^2. They showed that data assimilation allowed for a better real-time estimation of reservoir levels over the region. However, because of the state updating procedure used in this study, which consisted in adding or abstracting water from reservoirs, the method is limited to medium-range forecasting. It is not suitable for long-term water resources scenario calculations, where mass balance has to be maintained. More recently, Michailovsky et al. (2013) used radar altimetry data from the Envisat mission for updating the storage of a routing model of the main reach of the Brahmaputra River driven by the outputs of a calibrated rainfall–runoff model showing the potential for the use of altimetric data in combination with hydrological models for flow modeling in large rivers.

However, in situ flow data were required for the calibration of the rainfall–runoff model which may still be a limitation in some areas with poor data availability such as the Niger River. Salamon and Feyen (2009) used the residual resampling particle filter to assess parameter, precipitation and predictive uncertainty in the distributed rainfall–runoff hydrological model LISFLOOD for the Meuse catchment using discharge measurements. They showed that the equifi-

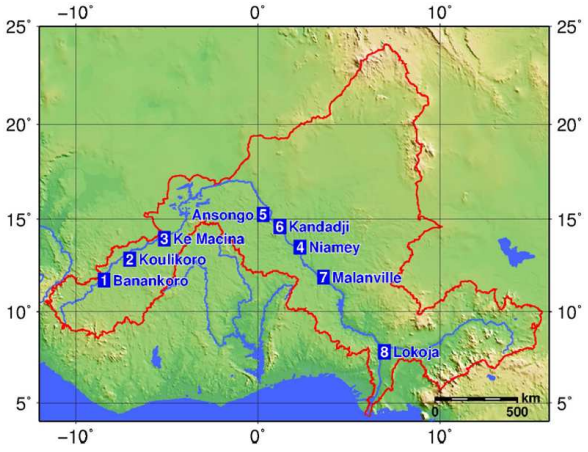

Figure 1. The Niger River basin. The spatial resolution is $0.5° \times 0.5°$. The red contour marks the boundary of the Niger Basin. The squares correspond to the following locations: (1) Banankoro, (2) Koulikoro, (3) Ke Macina, (4) Niamey, (5) Ansongo, (6) Kandadji, (7) Malanville and (8) Lokoja. Terrain elevations come from ETOPO2 (m).

nality hypothesis (several different parameter sets can lead to a good estimation of the discharge) was a limitation to the correction of a distributed hydrological parameter even in a physically based hydrologic model. Moreover, they emphasized the strong effect of rainfall uncertainties on the analysis. Finally, the results showed that accounting for parameter uncertainty only during a calibration phase was not sufficient to properly predict uncertainty, limiting the application of the method for hydrologic forecasting over longer time periods. The aforementioned applications of DA in hydrological modeling have shown the potential of using remote sensing data in order to improve the model states or the parameters. However, they also showed the limitations due to the generally low spatial and temporal resolutions of these data sets. Hydrological model uncertainties can come from several sources, such as model structure, input parameters or input data (mostly precipitation), leading to the development of different DA methodologies. Depending on the study, DA either aims at optimizing the model input parameters or at directly correcting the model state (generally done in operational forecast applications for example). The current study investigates benefits of assimilating SWOT virtual water levels in order to improve input parameters of a large-scale hydrological model within the context of a prelaunch study. The domain study area is the transboundary Niger Basin (Fig. 1) which crosses a large part of the Sahel and is a critical source of water in this semiarid region. The West African region is also characterized by an increasing population, putting larger pressure on the already limited freshwater resources. The hydrology of this basin is modulated by the West African monsoon (WAM) seasonal and interannual variability which is characterized by extreme events such as droughts and floods which can have dramatic impacts on society and the regional economy. However, the lack of field measurements limits the understanding of the salient hydrological processes in the Niger Basin. For these reasons, it is an ideal test bed for studying global hydrological issues. In a previous study, a Niger Basin hydrological model application was set up using the ISBA (Interaction Sol-Atmosphere-Biosphere)-TRIP (Total Runoff Integrating Pathways) distributed hydrological model. Along with river routing, this model includes a flooding scheme and a linear unconfined aquifer reservoir (Pedinotti et al., 2012). The model parameters were estimated using geomorphologic relationships to characterize the river characteristics. The modeling evaluation showed that the model was able to reasonably reproduce the major hydrologic and hydrodynamic processes. The model outputs were compared to in situ discharge as well as satellite-derived flood extent, total continental water storage changes and river height changes. The importance of floodplains was also demonstrated, since they have a considerable impact on discharge downstream of the inland Niger Delta. The confined aquifer improves the recession law, i.e., the curve of the decreasing flow and the simulation of low flows. However, some model deficiencies remain which can be due to forcing or model uncertainties; among these sources of error are the uncertainties of TRIP hydrological parameters. Indeed, these distributed parameters are defined by empirical relationships using available observations which are adapted towards obtaining the best results over the entire globe. However, such relationships might not give the best results locally (for a particular basin). Studies showed that empirical equation does not work well even within one basin and significant errors can be found at subbasin or reach scales (e.g., Miller et al., 2014; Yamazaki et al., 2014). These relationships thus lead to nonnegligible errors which could be reduced using satellite data. Such data can potentially be used to estimate spatial parameters for each particular basin and then contribute to the development of a global database describing major river characteristics. Pedinotti et al. (2012) performed sensitivity tests to determine the main sources of uncertainty among the TRIP parameters. These tests have shown that the model was sensitive to modifications of some key river parameters (river height and depth as well as Manning coefficient) and that a good estimation of those parameters was required to optimize the simulation errors. The aim of the current study is to investigate how SWOT water level products can be used to optimize the Manning coefficient. Unlike river depth and width, which can be estimated through direct measurements, the Manning coefficient can be estimated only indirectly, using bathymetry and flow velocity measurements. Several studies have discussed the importance and difficulty of estimating the Manning coefficient (Chow et al., 1989; Bates and de Roo, 2000). The sensitivity of the Manning equation to several river parameters including the roughness coefficient was investigated by Pistocchi and Pen-

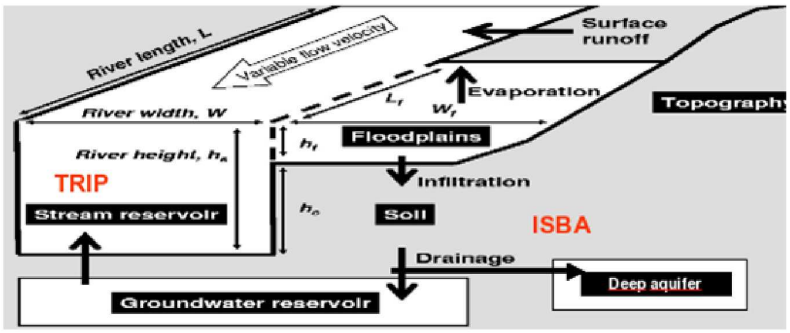

Figure 2. The TRIP model configuration in ISBA.

nington (2006). In addition to the concern about accurately estimating the Manning coefficient value, they highlighted the importance of considering its spatial distribution instead of a unique value as it is done in some hydrological models (Arora and Boer, 1999). Moreover, the Manning coefficient is often used as an adjustment variable for model calibration which can lead to additional errors (e.g., Biancamaria et al., 2009). Hunter et al. (2007) indicated that very frequently in models errors on topography and roughness dominate errors from equation approximation. The estimation of the Manning coefficient is thus considered in the literature as one of the major issues limiting the performance of hydrological models and, to the authors knowledge, there have been very few attempts to evaluate the potential of satellite data to correct it. Therefore, it was chosen as the main parameter to be investigated in the DA study presented in this study. Since SWOT observations are not yet available and to assess the usefulness of data assimilation, this study is carried out within the framework of an OSSE (observing system simulation experiment) using the TRIP model for the simulation of the Niger hydrodynamics. SWOT virtual measurements are produced using a reference ISBA-TRIP simulation. Here, it is assumed that modeling errors are only due to one key parameter which cannot be directly estimated via observational data: the Manning roughness coefficient (the other sources of modeling errors are not considered here, and the reasons will be explained in Sect. 4.1). The impact of the assimilation system on the Niger River model is then quantified. First, a brief presentation of the study domain and the model is made in Sect. 2. In this section, the Manning coefficient is also defined and its spatial distribution used for the true simulation is shown. Then, the production of the SWOT virtual water level is described in Sect. 3. The methodology used to build the assimilation scheme is explained, and the main variables of the assimilation problem are described in Sect. 4. Finally, the impact of the assimilation on the main hydrological variables of the Niger Basin is discussed in Sect. 5.

2 Study domain and model description

2.1 The Niger River basin

Originating in the Guinean highlands within the Upper Guinea (Haute Guinée) and Forested Guinea (Guinée Forestière) regions located in the Fouta Djallon mountain range, the Niger River is the third longest river in Africa (4200 km), after the Nile and the Congo. Its outlet is located in Nigeria, discharging through a massive delta into the Gulf of Guinea. On its way through Mali, it crosses a vast floodplain region called the inland delta. The inland delta has an average surface area of 73 000 km^2, and it dissipates a significant proportion of the flow of the river through absorption and evaporation (it is estimated that about 40 % of water is lost through the inland delta by evaporation and/or infiltration; Andersen et al., 2005). From the headwaters to the Niger Delta (taking into account the hydrologically active area), the basin has an average area of about 1.5 million km^2. The Niger River is shared by nine countries and is the main source of water for about 100 million people living principally from agriculture and farming. During the 1970s and 1980s, West Africa faced extreme climate variations with extended drought conditions followed by floods; therefore, there is a need to better understand the functioning of this basin for water management purposes. The complexity of modeling the Niger Basin is mainly due to the fact that it crosses very different climatic zones, from the tropical humid Guinean coast where it generally rains every month of the year, to the desertic Saharan region. The main source of water over the basin is due to the WAM which is characterized by a marked annual cycle and significant interannual variability, leading to the succession of extreme events such as droughts and floods. In addition to modeling issues due to rainfall uncertainties, the representation of processes such as infiltration and evaporation from floodplains is also very important in modeling the Niger River.

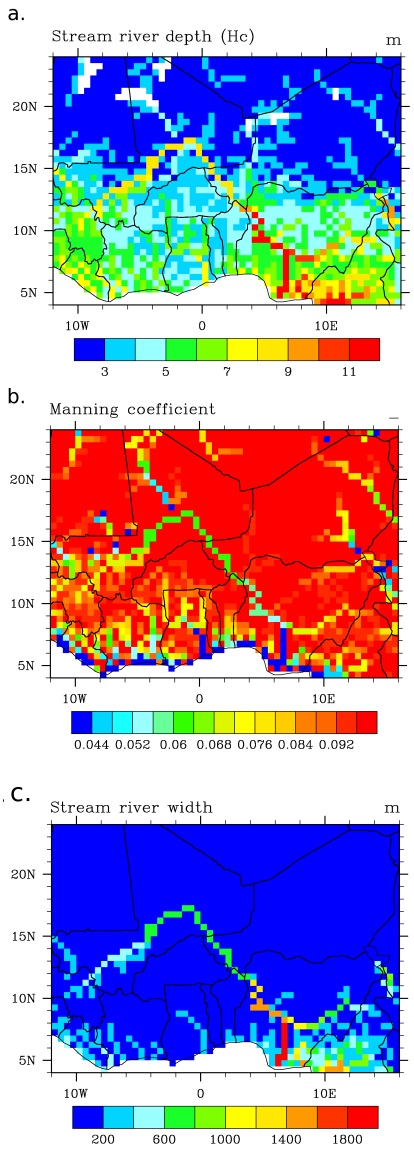

Figure 3. The spatial distribution of river depth (m) **(a)**, Manning coefficient **(b)**, and river width (m) **(c)** parameters in ISBA-TRIP.

2.2 Review of the ISBA-TRIP model

ISBA is a state-of-the-art land surface model which calculates the time evolution of the surface energy and water budgets (Noilhan and Planton, 1989). It represents the natural land surface component of the SURface-EXternalized (SURFEX) coupling platform at Météo-France (Masson et al., 2013). In the current study, we use the three-layer force-restore soil hydrology option (Boone et al., 1999). The options are also activated for a comprehensive representation of subgrid hydrology in order to account for the heterogeneity of precipitation, topography and vegetation in each grid cell. A TOPMODEL approach (Beven and Kirkby, 1979) has been used to simulate a saturated fraction, f_{sat}, over which precipitation is entirely converted into surface runoff (Decharme et al., 2006). Infiltration is computed via two subgrid exponential distributions of rainfall intensity and soil maximum infiltration capacity (Decharme and Douville, 2006). The TRIP original RRM was developed by Oki and Sud (1998) at University of Tokyo. It was first used at Météo-France to convert the model simulated runoff into river discharge using a global river channel network at a 1° resolution. More recently, a 0.5° resolution global river network has been developed which is used for this study. The TRIP schematic concept is presented in Fig. 2 and more details can be found in Pedinotti et al. (2012). The ISBA-TRIP CHS was recently improved to take into account a simple groundwater reservoir, which can be seen as a simple soil-water storage, and a variable stream flow velocity computed via the Manning equation (Decharme et al., 2010). In addition, ISBA-TRIP includes a two-way flood scheme in which a flooded fraction of the grid cell can be determined (Decharme et al., 2008, 2011). The flood dynamics are described through the daily coupling between the ISBA land surface model and TRIP RRM, including a prognostic flood reservoir. This reservoir fills when the river height exceeds the critical river bank full height (Fig. 3a), h_{c} (m). The flood interacts with the soil hydrology through infiltration, with the overlying atmosphere through precipitation interception and through free-water-surface evaporation. For the Niger application, Pedinotti et al. (2012) added a simple, linear, confined aquifer reservoir to account for the long-term water storage in deep and more or less confined aquifers. This reservoir was built on the example of the groundwater reservoir, but with a significantly longer time-delay factor. The confined aquifer is supplied by a fraction $(1-\alpha)$ of the drainage from ISBA, the remaining fraction (α) going to the groundwater reservoir.

2.3 TRIP specific parameters

The Manning coefficient characterizes the roughness so that it modulates the surface water velocity and thus water levels and discharge, via the Manning formula. However, it is difficult to estimate via in situ measurements or remote sensing techniques. In ISBA-TRIP, the Manning friction coefficient, n_{riv}, varies linearly and proportionally to the river width, W (m), from 0.04 near the river mouth to 0.1 (Decharme et al., 2011) in the upstream grid cells (Fig. 3b):

$$n_{\mathrm{riv}} = n_{\mathrm{min}} + (n_{\mathrm{max}} - n_{\mathrm{min}}) \left(\frac{W_{\mathrm{mouth}} - W}{W_{\mathrm{mouth}} - W_{\mathrm{min}}} \right), \quad (1)$$

where n_{riv} represents the grid cell average Manning coefficient, n_{max} and n_{min} the maximum and minimum values of the Manning friction coefficient (equal to 0.1 and 0.04, re-

spectively), $W_{\min}$ (m) the minimum river width value and W_{mouth} (m) is the width of the mouth in each basin of the TRIP network ($W_{\text{mouth}} = 2000$ for the Niger Basin). W is an important parameter because it controls both the river flow speed and the floodplain dynamics. It is computed over the entire TRIP network via an empirical mathematical formulation that describes a simple geomorphological relationship between W and the mean annual discharge at each river cross section (Knighton, 1998; Arora and Boer, 1999; Decharme et al., 2011):

$$W = \max\left(30, \beta \times Q_{\text{yr}}^{1/2}\right), \quad (2)$$

where Q_{yr} ($\text{m}^3\,\text{s}^{-1}$) is the annual mean discharge in each grid cell estimated using the global runoff database from Cogley (1979). As discussed in Decharme et al. (2011), the β coefficient can vary drastically from one basin to another. β is equal to 20 for the branch of the river going from the river mouth (5° N) to 12° N and is fixed to 10 for the remaining river branch. The spatial distribution of the river width is shown in Fig. 3c. Another critical parameter is the riverbank-full critical height, h_c, which is computed according to the river width via a simple power function (Decharme et al., 2011):

$$h_c = W^{1/3}. \quad (3)$$

The spatial distribution of h_c is shown in Fig. 3a. These relationships are found to work well at the global scale but can lead to significant errors for a specific basin at the regional scale (see the sensitivity tests in Pedinotti et al., 2012). Indeed, the assumption that the river width is proportional to the annual mean discharge can lead to significant errors in flooded areas where the river bed enlarges but the discharge is reduced through the flooding process. Moreover, it is assumed that the Manning coefficient is only dependent on the river width while other factors should be considered, such as the presence of vegetation, debris, soil type, etc. Finally, these parameters are defined as constant in time, which is a significant assumption, especially in a region with a marked seasonal climate variability such as the Niger Basin. Remote sensing opens the possibility of estimating the river width by direct measurements and the critical bank-full height by indirect algorithms (Pavelski and Smith, 2008; Yamazaki et al., 2014; Durand et al., 2008). However, the Manning coefficient will still be difficult to estimate even using remote sensing. This study focuses on finding a methodology to estimate this critical parameter via DA.

3 Satellite observations

The aim of this work is to estimate the potential benefits of using SWOT satellite measurements to provide spatially distributed estimates of the Manning coefficient over the Niger River basin. This section describes this future satellite mission and how virtual SWOT observations have been generated in this study.

3.1 The SWOT mission

SWOT will provide high-resolution images of water surface elevations over the oceans and continental surface water bodies. It will therefore observe continental surface waters at an unprecedented resolution, providing information for a better understanding of surface water dynamics and storage variations. The mission is currently planned to be launched around 2020.

The satellite main payload will be the Ka-band Radar Interferometer (KaRIN), a wide swath SAR (synthetic aperture radar) interferometer. KaRIN will have two antennas separated by a 10 m boom, which will observe two ground swaths of 60 km on each side of the satellite nadir, separated by a 20 km gap. The intrinsic pixel resolution will vary from 60 (near range) to 10 m (far range) across track and will be at best around 5 m along track (however, this value is also dependent upon decorrelation time). Yet, for these intrinsic pixels, water elevation measurements have metric errors, which increase along the swath (depending on the look angle). To increase vertical accuracy, pixels have to be aggregated: over a $1\,\text{km}^2$ area inside the river mask, water elevation has a 10 cm or lower error (Rodríguez, 2012). River slopes will be measured with a $1\,\text{cm}\,\text{km}^{-1}$ resolution, after processing elevations over 10 km river reaches (Rodríguez, 2012). SWOT will be able to observe rivers wider than 100 m (mission requirement) and should be able to observe rivers wider than 50 m (goal). The chosen orbit will be a low earth orbit with a 78° inclination, in order to observe almost all of the continental surfaces (Rodríguez, 2012).

3.2 Observing system simulation experiment (OSSE) and virtual SWOT data

The OSSE framework consists in simulating data that would be observed by the future measurement platform using a numerical model, in order to use it as virtual observations for DA experiments. The main objective of an OSSE is to validate the DA method by using ideal conditions. It is assumed that the state of the system and the error statistics of the model and observations are known and correctly described, which is not the case in real conditions. This method is useful within the framework of the SWOT satellite mission preparation, since it allows a quantification of the satellite data contribution to improve large-scale river modeling (such as for the Niger Basin) before the launch of the satellite. First, a realistic modeling of the studied basin is needed for the OSSE. The model must be able to simulate the major hydrodynamic processes of the basin so that the simulated observations will reasonably represent the reality. The ISBA-TRIP setup evaluated in Pedinotti et al. (2012), with the inclusion

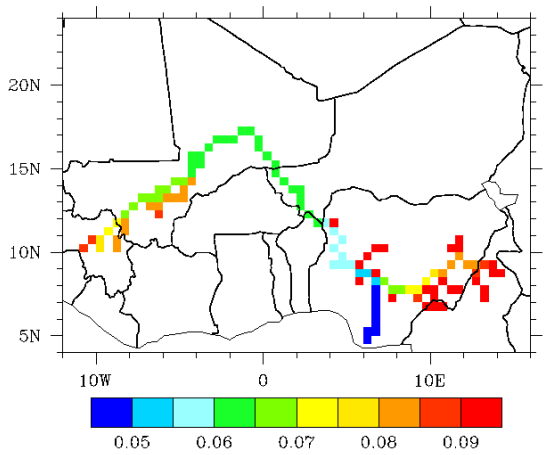

Figure 4. Distribution of the "true" Manning coefficient over the river. This distribution of Manning coefficients was used as an input parameter to run the reference ISBA-TRIP model.

of the flooding scheme and aquifer reservoir, is used to represent the true state of the hydrological system, also referred to as the *reference simulation*. For this so-called "truth", the model and its parameters are assumed to be perfect. An error is then added to this true state to build virtual observations. The background simulation results from the integration of the same model in a different configuration, for instance with a different set of parameters (also called perturbed or background parameters). It gives an a priori description of the system that is an approximation of the truth. In the present study focussed on parameter estimation, the purpose of the DA algorithm is to retrieve an optimal set of model parameters starting with the background parameters, by assimilating the virtual observations. It is important to note that in the present study, the error between the "true" Manning coefficients and the background Manning coefficients does not vary in time.

Within the framework of this SWOT-dedicated study, the true simulation is used to generate the SWOT observations, with the help of a relatively simple simulator developed by Biancamaria et al. (2011). Based on the prescribed orbit and swath, the simulator provides an ensemble of SWOT tracks and related dates. The SWOT tracks are provided for the orbital period and then repeated over the years 2002 and 2003 (assuming the satellite started its first orbit on 1 January 2002). The virtual data are the sum of the ISBA-TRIP water levels at the corresponding grid points and an instrumental error which is added to partially account for the SWOT observation errors (see Sect. 4.2.1 for details). A river mask for the Niger comprising grid cells with a river width above 200 m is defined as illustrated in Fig. 4, which displays the Manning coefficient for the unmasked 110 pixels. It should be noted that the SWOT satellite will not measure water depth but free-surface-water elevation. For DA applications in real conditions, the direct comparison between SWOT and ISBA-TRIP water levels will not be straightforward and will need further investigation. Indeed, the SWOT satellite measures free-surface-water elevation, which cannot be directly compared to the ISBA-TRIP outputs which are stream-water absolute depths in the river channel. The assimilation then requires finding a way to compare these two different variables in order to perform the DA. For example, they can be compared in terms of anomalies relative to a mean value over a long period of time instead of absolute water elevations. This method allows removing the bias due to different reference values of the level where the water elevation is zero. However, in the framework of an OSSE, the same model is used to generate the a priori and observed water levels and this issue can be evaded.

The 22-day repeat orbit and the 140 km swath used in this simulator allowed for a global coverage of the study domain within 22 days. Among the available orbits, two orbits have been preselected by the NASA–CNES project team, for various scientific and technical reasons (mainly to seek a compromise between both the hydrological and oceanographic scientific communities). These two orbits have the same repeat period, but different altitudes, meaning different subcycles. The repeat period corresponds to the minimum time taken by the satellite to fly over exactly the same ground location. Given the orbit parameters and earth's rotational speed, it requires a fixed number of satellite revolutions. For all of these revolutions, the part of the orbit that goes from north to south corresponds to the descending track and the one that goes from south to north corresponds to the ascending track. These ascending and descending tracks cross the Equator at different times during one repeat period. The difference between these crossing times for two adjacent ascending (or descending) tracks during a repeat period is the orbit subcycle. The 970 km altitude orbit has a 3-day subcycle, whereas the 873 km altitude orbit has a 1-day subcycle. These two orbits both have global coverage but with a different time and spatial spread of the satellite tracks during one repeat period. The 1-day subcycle orbit has two adjacent swaths every day, meaning that each river basin will be well sampled in few days, but then there will be no observations for several days (Fig. 5) with the risk of missing short-term events. The 3-day subcycle orbit has two adjacent swaths every 3 days, on average, meaning ground tracks will be more regularly distributed in space and time. Yet, there will be no tracks close in time at any point during the cycle (Fig. 6). Thus, due to their spatial and temporal coverage over the domain, these two orbits present specific advantages and disadvantages that will be investigated within of the DA framework. The OSSE is run over 2 years starting from the beginning of the monsoon season, on 1 June 2002. During each SWOT 22-day repeat, there are about 53 satellite overpasses on the Niger Basin for the 3-day subcycle orbit and 50 for the 1-day subcycle orbit.

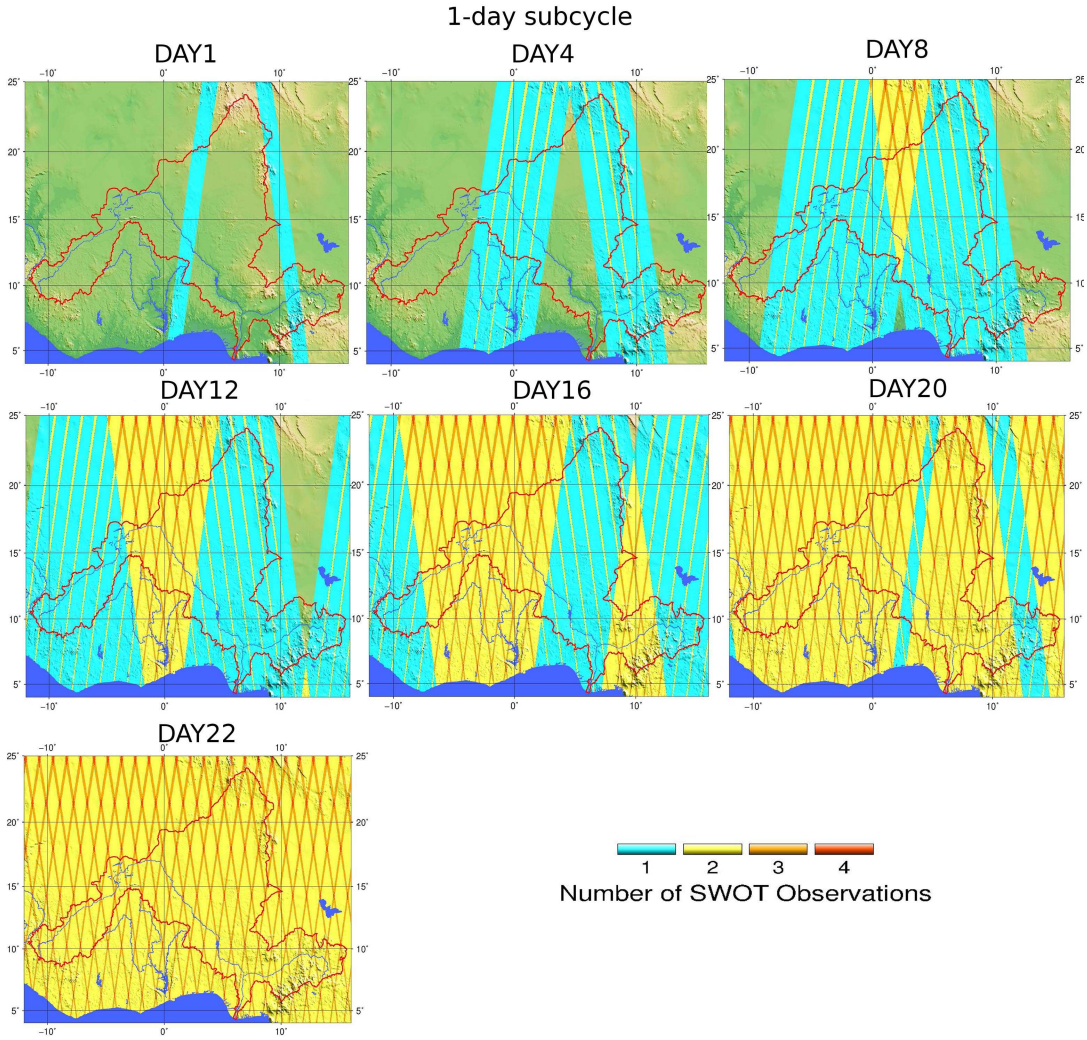

Figure 5. The 22-day repeat, 871 km altitude, 1-day subcycle orbit coverage, data issued from the SWOT data simulator.

4 Data assimilation schemes

4.1 Choice of the control variable

The goal of using assimilation in this study is to correct the TRIP routing input parameters which are associated with uncertainties. The contribution of such corrections is estimated by comparing model outputs (water level, discharge, water storage, etc.) with and without DA. Sensitivity tests in Pedinotti et al. (2012) determined the most sensitive TRIP parameters which impact the major hydrological processes of the Niger Basin. It was shown that a modification of n_{riv} has a significant impact on the simulated hydrological variables over the Niger Basin which can be expected since the Manning coefficient is used for flow calculations in the river stream, via the Manning formula. Due to its close relationship with water levels and discharge, it is one of the most important empirical parameters in the field of hydrology and hydraulics. Thus, a good estimation of this coefficient in the river bed leads to a better reproduction of surface water dynamics. There is a tendency to regard the selection of the Manning coefficient as an arbitrary or intuitive process. Hydrodynamic modelers usually determine the value of the Manning coefficient manually, often using estimations based on visual interpretation of the land cover. The roughness can also be described by geomorphologic relationships, which are related to another parameter for which more information is known (river width for example). In ISBA-TRIP, n_{riv} is assumed to vary linearly with W, from 0.04 near the river mouth to 0.10 in the upstream grid cells (Eq. 1). These geo-

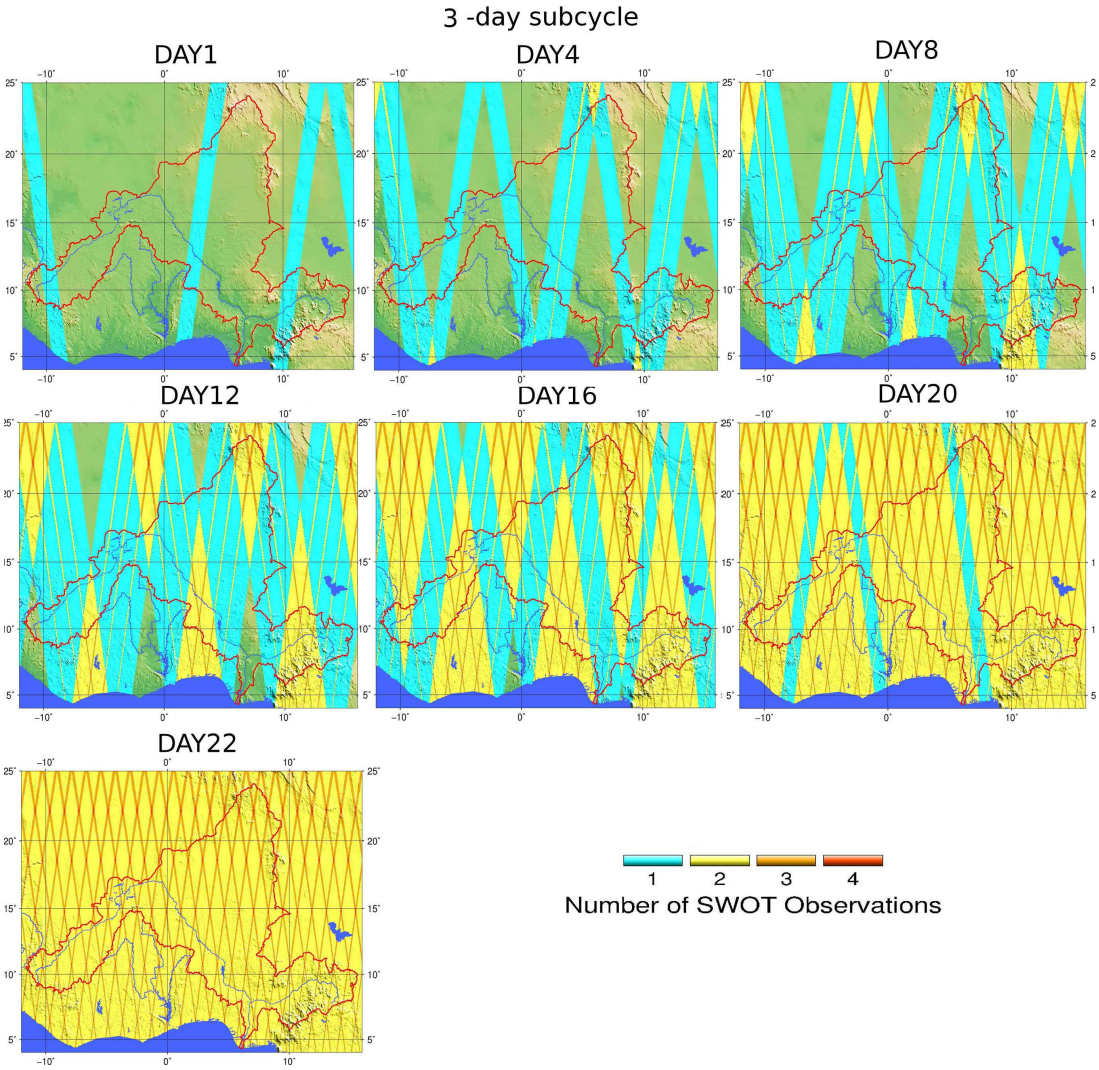

Figure 6. As in Fig. 5, except for a 22-day repeat, 970 km altitude, 3-day subcycle orbit average.

morphologic relationships are used to obtain the spatially distributed Manning coefficient which provides a "global" fit or best estimate. However, the accuracy of these relations can be very uncertain due to the significant heterogeneity of the river and land properties, especially in uncalibrated models. Both approaches can lead to significant errors over a large computational domain which is characterized by multiple land use/cover classes. Although progress in remote sensing will probably improve our estimates of the Manning coefficient (using the two aforementioned approaches), this parameter will not be estimated directly via remote sensing and therefore will remain dependent on the physical relevance of the geomorphologic relationships. Thus, DA appears to be an appealing option for estimating the Manning coefficient using remote sensing data. In reality, the temporal variability of the error on the Manning coefficient is related to the flow dynamics as the river bed morphology can be significantly modified by flood events. Even though this temporal variability is not accounted for in our OSSE framework, the DA analysis is performed sequentially over a 2-day time window which allows for a high variability of the correction on the Manning coefficient. It should be noted that in a real case study where sources of uncertainty are multiple (contrary to our OSSE framework where errors are only due to Manning coefficient perturbations), correcting the Manning coefficient could be interpreted as a way to account for other uncertainties (which are possibly characterized by errors with a higher temporal variability than that of the Manning coefficient).

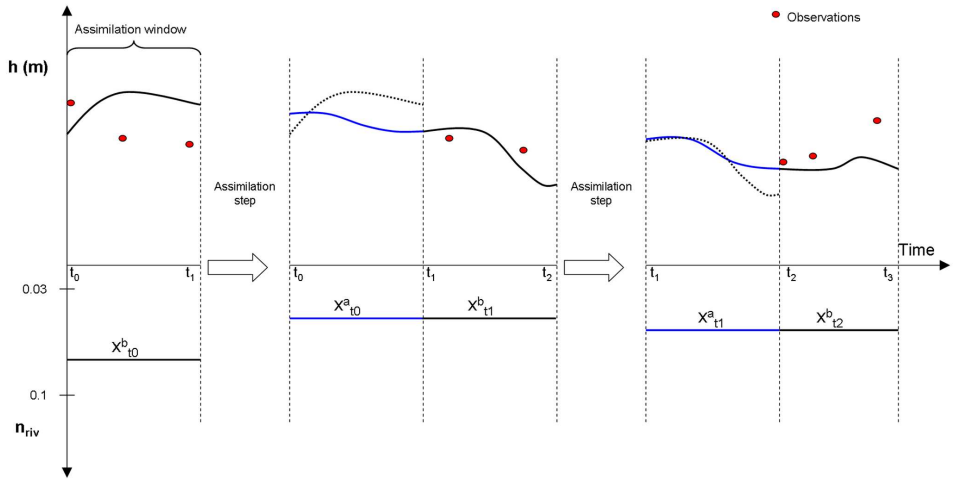

Figure 7. Schematic of the assimilation scheme used in this study. The black line represents the a priori or background trajectory and the blue line is the posterior trajectory after data assimilation. After the DA step, the a priori trajectory is represented by a dashed line to compare with the new trajectory.

The choice of the time window length could be revisited in further studies. However, a longer assimilation window also requires a bigger disc storage capacity and this must be considered when selecting the length of the assimilation window.

In the following section, along-track virtual SWOT data over 2 days are assimilated to correct the Manning coefficient for the unmasked $n_t = 110$ ISBA-TRIP grid points. For each analysis at time t (also called cycle), the control vector is thus a vector of 110 elements noted $\boldsymbol{x}_t$. The framework of the OSSE does not guarantee the physical representativeness of the modeled values, specifically because of the lack of monitoring data. Here, the values have therefore simply been bounded to be within a reasonable range (based on rivers similar to the Niger and the scale of TRIP).

4.2 The extended Kalman filter (EKF)

The assimilation algorithm used for the calculation of the analysis is the EKF, which is presented in this section within the framework of parameter optimization. The true Manning coefficients (known in the framework on an OSSE but unknown in reality) are gathered in the vector $\boldsymbol{x}_t^{\text{true}}$ of size n_t. The vector of the a priori parameters $\boldsymbol{x}_t^{\text{b}}$ for the hydrological models is prescribed by geomorphologic relationships which induce an error $\epsilon_t^{\text{b}} = \boldsymbol{x}_t^{\text{true}} - \boldsymbol{x}_t^{\text{b}}$ of which statistics are described in the background error covariance matrix $\mathbf{B}$. Here, these statistics are assumed to be constant over the assimilation cycles and to follow a Gaussian distribution, centered on 0 with a standard deviation, σ_t^{b}, of 20 % of the average value of the Manning coefficient over the river.

The observation vector $\boldsymbol{y}_t^0$ of dimension p_t contains all the SWOT observations collected during the 2-day assimilation window. The observation operator H projects the control vector onto the observation space. This operator is nonlinear as it is the composition of the hydrological model M and of a selection operator S that simply extracts or interpolates the simulated water levels (over the whole gridded domain) at the observation points. Here $H = SoM$, where S represents the SWOT simulator and M is the integration of the hydrological model over the assimilation window. The relation $\mathbf{y}_t = H(\boldsymbol{x}_t)$ allows describing the true water level vector $\mathbf{y}_t^{\text{true}}$ at the observation points when $\boldsymbol{x}_t^{\text{true}}$ is used and the background hydrological water level vector $\mathbf{y}_t^{\text{b}}$ at the observation points when $\boldsymbol{x}_t^{\text{b}}$ is used. In OSSE, an observation error ϵ_t^0 is added to $\boldsymbol{y}_t^{\text{true}}$ to account for instrumental and representativeness errors. The observation errors are assumed to be decorrelated in space and time, and the observation error standard deviation $(\sigma_t^0)^2$ is set equal to $(\sigma_t^{\text{b}})^2$. The observation error covariance matrix $\mathbf{R}_t$ is thus assumed to be diagonal. Further work should focus on a complete estimation of the observation error statistics in order to allow for along-track correlation of the instrumental errors (Lion, 2012).

The EKF analysis vector $\boldsymbol{x}_t^{\text{a}}$ is defined as a correction to the background vector, where the the innovation vector $\boldsymbol{d}_t = \boldsymbol{y}_t^0 - \mathbf{H}_t(\boldsymbol{x}_t^{\text{b}})$ is multiplied by the gain matrix $\mathbf{K}_t$:

$$\boldsymbol{x}_t^{\text{a}} = \boldsymbol{x}_t^{\text{b}} + \mathbf{K}_t \boldsymbol{d}_t, \tag{4}$$

where $\mathbf{K}_t$ reads

$$\mathbf{K}_t = \mathbf{B}_t \mathbf{H}_t^T (\mathbf{H}_t \mathbf{B}_t \mathbf{H}_t{}^T + \mathbf{R}_t)^{-1}, \tag{5}$$

where $\mathbf{H}_t$ is the tangent linear of $\mathbf{H}$ with respect to $\boldsymbol{x}_t$. The statistics of the analysis error ϵ_t^{a} are determined by the

Table 1. Principal variables, vectors and matrices used in the data assimilation of SWOT water levels (WL). The assimilation window length is N days. The number p of observed water levels during the assimilation window changes for each cycle.

Symbol	Variable	Dimensions
$\boldsymbol{y}_t^0$	Observation vector, containing the SWOT WL observations during the N day assimilation window	p (different for each assimilation cycle)
$\boldsymbol{x}_t^{\mathrm{b}}$	Background vector, containing the corrupted Manning coefficient over the river mask	$n = 110$
$\boldsymbol{x}_t^{\mathrm{a}}$	Analysis vector, containing the corrected values of the Manning coefficient over the river mask	$n = 110$
M_t	ISBA-TRIP (nonlinear)	
$H_t(\boldsymbol{x}_t^{\mathrm{b}})$	ISBA-TRIP simulated water levels, using $\boldsymbol{x}_t^{\mathrm{b}}$ as an input parameter	p
$\mathbf{R}_t$	Observation error covariance matrix (related to water levels)	$p \times p$
$\mathbf{B}_t$	Background error covariance matrix (related to the Manning coefficient)	$n \times n$
A_t	Analysis error covariance matrix	$n \times n$
$\mathbf{H}_t$	Jacobian matrix of H (sensitivity of ISBA-TRIP water levels to the Manning coefficient)	$n \times p$
$\mathbf{K}_t$	Gain matrix	

analysis covariance matrix $\mathbf{A}_t = (\mathbf{I} - \mathbf{K}_t\mathbf{H}_t)\mathbf{B}_t$ (Bouttier and Courtier, 1999). The analysis vectors provide the corrected Manning coefficient values, which can then can be used to integrate the hydrological model and simulate the analyzed water levels over the whole domain. A schematic diagram of the assimilation process is shown in Fig. 7, and the key variables are represented in Eqs. (4) and (5) and listed in Table 1.

4.3 Jacobian matrix calculation

The EKF algorithm relies on the computation of a local approximation of the tangent linear of the observation operator that describes the relationship between the control vector and the observation space, with respect to the control vector. As the size of the control space is limited in this study, a finite difference scheme can be used to perform this approximation, in the vicinity of the background vector. Since the observation operator H includes the model propagation, the calculation of the Jacobian matrix $\mathbf{H}_t$ requires the computation of n_t independent integrations of the hydrological model with a perturbed element for each component of $\boldsymbol{x}_t$.

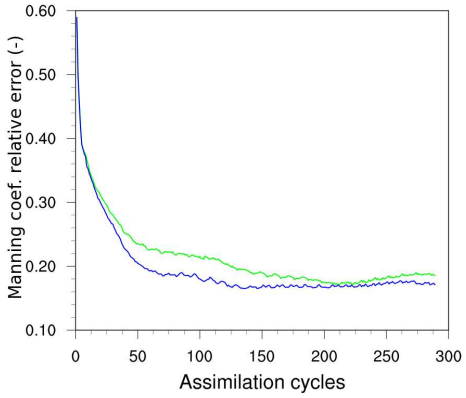

Figure 8. The Manning coefficient relative error averaged over the river versus time with a 1-day subcycle (green) and a 3-day subcycle (blue) orbit SWOT assimilation. The related error is calculated as the ratio $|n_{riv_{\text{with/without assi}}} - n_{\text{riv}_{\text{truth}}}| / n_{\text{riv}_{\text{truth}}}$, where n_{riv} is the Manning coefficient.

$$\mathbf{H}_{t,ij} = \frac{\partial H}{\partial x}_{|_{t,ij}} = \frac{\mathbf{H}(\boldsymbol{x}_t + \Delta x) - \mathbf{H}(\boldsymbol{x}_t - \Delta x)_i}{\Delta x_{t,j}} = \frac{\Delta \boldsymbol{y}_{t,i}^{+} - \Delta \boldsymbol{y}_{t,i}^{-}}{\Delta \boldsymbol{x}_{t,j}^{+} + \Delta \boldsymbol{x}_{t,j}^{-}} \quad (6)$$

In Eq. (6), $\mathbf{H}$ translates the variations of water levels at the observation points induced by the variation of Manning coefficients. $\Delta \boldsymbol{y}_{t,i}^{+}$ and $\Delta \boldsymbol{y}_{t,i}^{-}$ represent the water level variations at the gridded pixel "i" related to variations $\Delta \boldsymbol{x}_{t,j}^{+}$ and $\Delta \boldsymbol{x}_{t,j}^{-}$ of the Manning coefficient at the gridded pixel "j". A centered finite difference scheme was favored over a one-sided scheme as it reduces noise on the evaluation of the local derivative. The computation of $\mathbf{H}_t$ thus requires $2 \times n_t$ integrations of ISBA-TRIP over the assimilation window using elementary perturbed Manning coefficients at the unmasked observation point. The computational cost of $\mathbf{H}$ could be optimized as only perturbations on Manning coefficients at the grid points located upstream of each observation point have an impact on water level at the observation point. In the present work, the $2 \times n_t$ integrations of ISBA-TRIP are achieved sequentially.

5 Results

The impact of DA on the hydrological processes is analyzed using the relative error. For any variable v, the relative error is expressed as

$$\mathrm{err}_v = \left| \frac{v - v_{\text{truth}}}{v_{\text{truth}}} \right|, \quad (7)$$

where v_{truth} refers to the variable v as described in the true simulation.

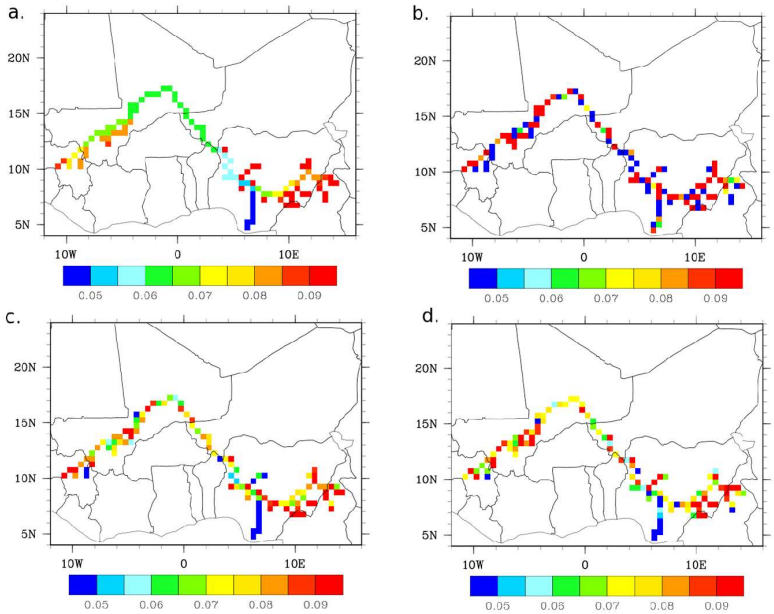

Figure 9. The Manning coefficient distribution **(a)** for the truth, **(b)** the background, **(c)** the 1-day subcycle assimilation at the end of the assimilation period (after 289 assimilation cycles in December 2003) and **(d)** the 3-day subcycle assimilation at the end of the assimilation period (after 289 assimilation cycles in December 2003).

5.1 Impact of assimilation on Manning coefficient

The truth simulation is made using Manning coefficients which are constant in time, meaning that there is no temporal variation of the error on the model parameters; thus, it is expected that the DA analysis leads to a constant value of the corrected Manning close to the "true" values.

However, since the Manning coefficient is spatially distributed, several spatial combinations of these parameters might resolve the assimilation problem which is generally referred to as the equifinality hypothesis. Figure 8 shows the Manning coefficient relative error (averaged over the river) time series for the two orbits. The average relative error of the Manning coefficient is significantly improved during the assimilation period and tends to converge to a stable value (about 0.19 for the 1-day subcycle orbit and 0.17 for the 3-day subcycle orbit), since the error is not significantly changed from January 2003 until the end of the assimilation experiment. The convergence towards the minimum value of the spatially averaged relative error to the true averaged Manning coefficient is slightly faster for the 3-day subcycle orbit than for the 1-day subcycle.

Figure 9 displays the spatial distribution of the Manning coefficient (a) for the truth, (b) the background simulation, (c) the 1-day subcycle assimilation at the end of the study period and (d) the 3-day assimilation at the end of the study period. The general patterns of the Manning coefficient distribution are recovered through the DA; especially, the extreme values of the background distribution are corrected. Also, we notice that the values downstream are better corrected than those upstream of the river, which can be expected since the downstream grid cells take advantage of the cumulated corrections upstream.

The Manning coefficient temporal evolution at the eight gage locations is shown in Fig. 10. It should be noted that in some places and for both subcycles, the "real" Manning coefficient value is only approached and not found through the assimilation cycles, which can be related to the equifinality problem. The 1-day subcycle and 3-day subcycle orbit assimilations converge to the same value in five locations out of eight. In Banankoro, Kandadji and Malanville, however, the coefficient values for the two orbits converge to different values. Banankoro is located upstream of the river, so this difference can be explained by the lack of data upstream of this location for obtaining a robust estimate of the Manning coefficient at this site. Also, the impact of the Manning coefficient on the simulation depends on the rain amount over the observed locations. According to the considered subcycle, the satellite will see different zones and a different number of observations corresponding to different rain events which can lead to the different values obtained for the optimal Manning coefficient in some locations. Also, a "jump" with a frequency of about 20 days is observed in every location and for the two subcycles and might be related to the orbit repetitivity.

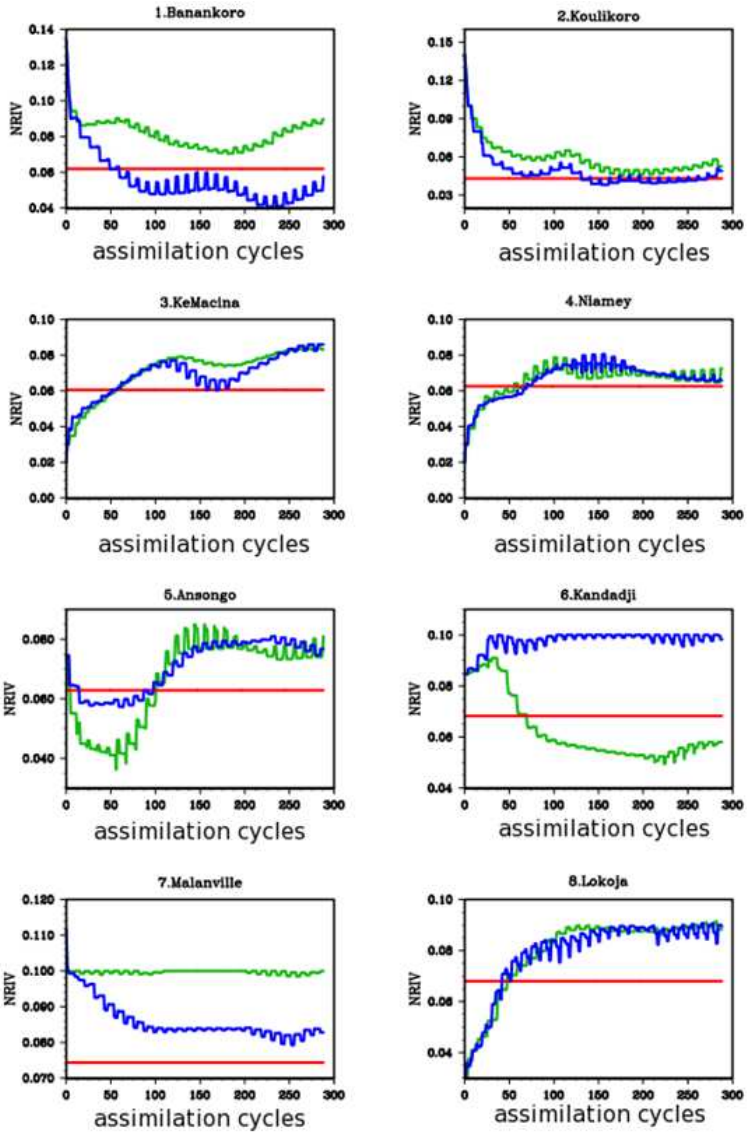

Figure 10. Manning coefficient versus assimilation cycle at eight locations (Fig. 1) for the 3-day subcycle (blue) and 1-day subcycle (green) orbits. The value of the true coefficient is in red.

Table 2. Water level relative error averaged over the river and at the location of the eight gages along the river (each gage is defined by its number specified inside the orange rectangles in Fig. 1). The relative error is calculated as the ratio $(h_{\text{with/without assi}} - h_{\text{truth}}) / h_{\text{truth}}$, where h is the water level (m); assi: assimilation, 3 and 1 d sbc: 3- and 1-day subcycles.

Location no.	River mean	1	2	3	4	5	6	7	8
No assi	0.45	0.35	0.17	0.36	0.55	0.16	0.69	0.68	1.10
3 d sbc	0.12	0.09	0.25	0.11	0.17	0.12	0.12	0.10	0.09
1 d sbc	0.12	0.19	0.10	0.11	0.12	0.13	0.07	0.12	0.18

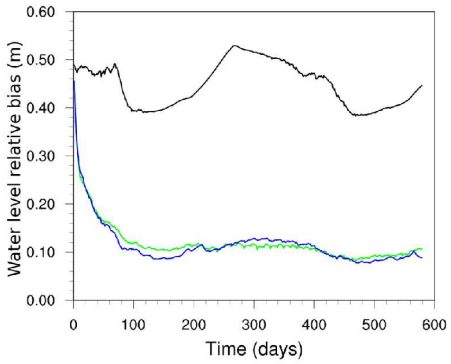

Figure 11. Water level relative error averaged over the river versus time with no assimilation (black), with 1-day subcycle (green) and 3-day subcycle (blue) orbit SWOT assimilations. The relative error is calculated as the ratio $|h_{\text{with/without assi}} - h_{\text{truth}}| / h_{\text{truth}}$, where h is the water level (m).

5.2 Impact of assimilation on water levels

Table 2 gives the water level mean relative error computed with respect to the true water levels, first averaged over the entire river for the 2-year period and then at each of the eight observing stations shown in Fig. 1. Figures 11 and 12 display the water level relative error averaged over the river and at the eight observing stations as a function of time when (i) there is no assimilation (black curve), (ii) after a 1-day subcycle orbit SWOT-observation assimilation (green curve) and (iii) the 3-day subcycle orbit SWOT-observation assimilation (blue curve).

These results show that the DA analysis leads to a significant reduction of the water level relative error over the whole river (the averaged relative error is reduced by more than a factor of 3 with DA) and at the eight gages. In most of the eight locations, there is an improvement of several meters reaching up to 9 m at Lokoja (for an 8 m averaged river depth along the river). As for the Manning coefficient, a noise with a repeat period of 20 days is observed and can be directly related to the noise observed on the Manning coefficient. Also, even in the locations where the analyzed Manning coefficient differs for both subcycles, the same water levels are retrieved for both subcycles, which confirms the equifinality hypothesis.

A great improvement in the water level is achieved with the first assimilation cycles since the background Manning parameters and thus the background water levels initially differ significantly from the true parameter values and water levels. For the following cycles, as the background parameters are set equal to the analysis parameters, the sequential correction results in a convergence towards the optimal Manning coefficients leading to water levels that are coherent with the true water levels. The improvement is larger for stations that are located downstream of the river, possibly because of the cumulated corrections upstream of these stations. Moreover, the hypothesis of a linear relation between width and roughness means that the 20 % standard deviation will lead to a larger absolute error on the roughness for wider rivers. These results are similar for both orbits as illustrated in Fig. 13, which shows the spatially distributed relative error of water levels averaged over the period from June 2002 to December 2003 for the run with (a) no assimilation, (b) a 3-day subcycle assimilation and (c) a 1-day subcycle assimilation. Without assimilation, the relative error over the river ranges between 0 and 1.2. With assimilation, more than 90 % of the river pixels have a relative error smaller than 0.2 for both subcycles, and no pixel has a relative error higher than 0.5.

5.3 Impact of assimilation on river discharge

Table 3 presents the discharge mean relative error computed with respect to the true discharge, first averaged over the entire river for the 2-year period and then at each of the eight observing stations shown in Fig. 1. Figures 14 and 15 display the discharge relative error averaged over the river and the discharge evolution at the eight observing stations as a function of time when (i) there is no assimilation (black curve), (ii) after a 1-day subcycle orbit SWOT-observation assimilation (green curve) and (iii) the 3-day subcycle orbit SWOT-observation assimilation (blue curve). The assimilation contributes to an improvement of the river discharge over the whole basin and at the eight locations, although this improvement is smaller than for water levels which can be expected since the Manning roughness is updated through level measurements. Discharge improvement, even if less significant than for water levels, can represent several hundreds of cubic meters per second globally and up to 3000 $m^3 s^{-1}$ in Lokoja. Discharge obtained after assimilation is somewhat "noisy" (as observed for water level) for both orbits during the wet season. This is likely due to a higher discharge sensitivity to Manning coefficient change during this period. Discharge is improved, in particular, at Lokoja, i.e., the location situated furthest downstream of the river, which is a promising result for coupled land–ocean applications since it shows that the RRM can provide a reasonable estimation of discharge at the river mouth. Similar to what was found for water levels, there is almost no discharge sensitivity to the considered orbit.

Figure 16 shows the spatially distributed relative error of discharge averaged over the period June 2002–December 2003 for the run without assimilation (a), 3-day subcycle assimilation (b) and 1-day subcycle assimilation (c). The discharge relative error is globally improved with better results over the inner delta for the 1-day subcycle orbit. Otherwise, there is no significant difference in results between the two orbits. Without assimilation, the relative error range over the river goes from 0 to 0.4. With assimilation, all pixels have a relative error smaller than 0.2, with 80 % of them having errors of less than 0.1.

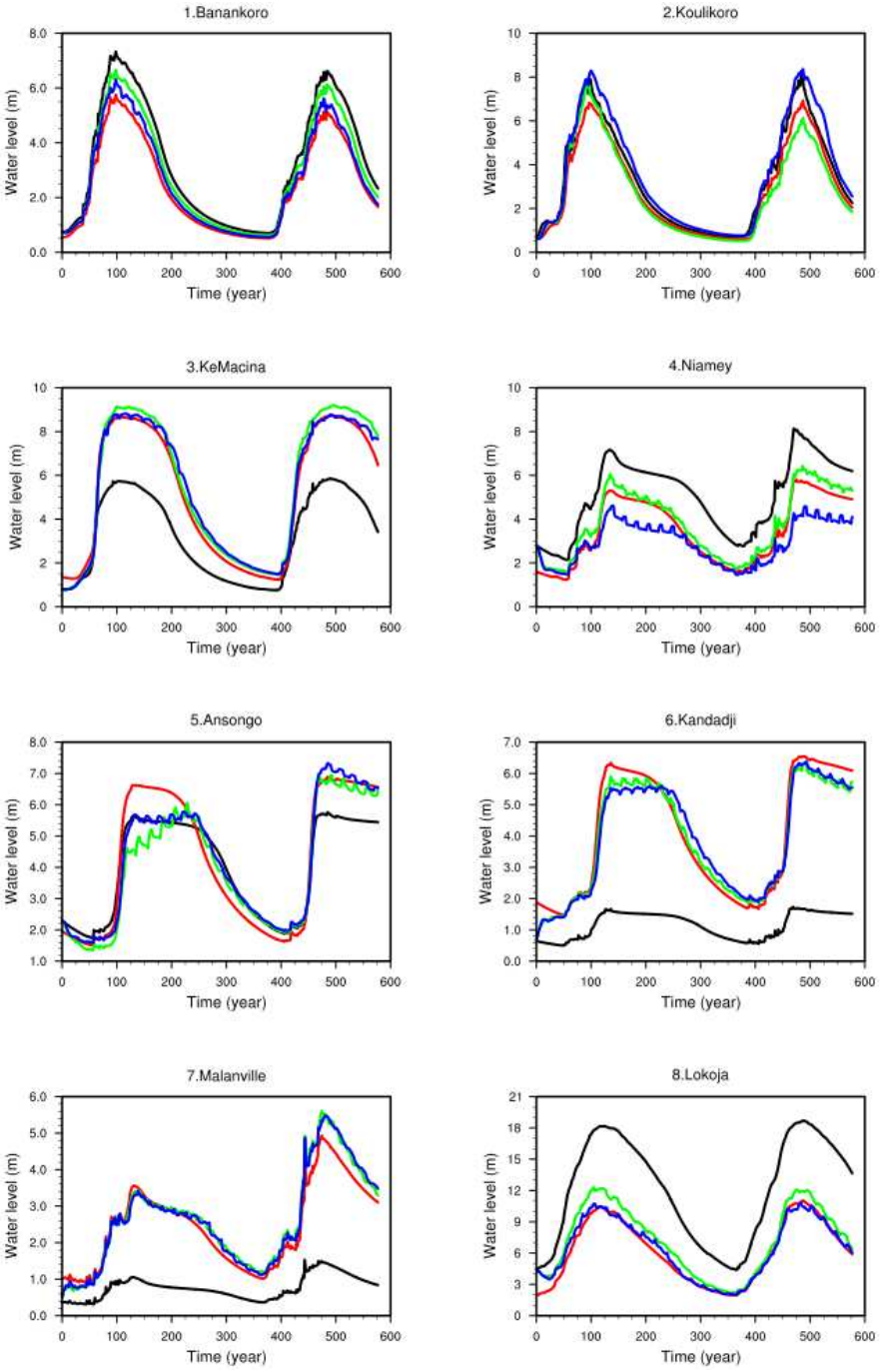

Figure 12. Time evolution of water levels at the eight locations shown in Fig. 1 for the "truth" (red curves), with no assimilation (black curves) and with assimilation of SWOT 1-day subcycle (green) and 3-day subcycle (blue) orbit observations.

Table 3. Discharge relative error averaged over the river and at the location of the eight gages along the river (each gage is defined by its number specified inside the orange rectangles in Fig. 1). The relative error is calculated as the ratio $(q_{\text{with/without assi}} - q_{\text{truth}}) / q_{\text{truth}}$, where q is the discharge ($m^3\ s^{-1}$).

Location no.	River mean	1	2	3	4	5	6	7	8
No assi	0.14	0.06	0.10	0.18	0.22	0.20	0.20	0.15	0.14
3 d sbc	0.08	0.04	0.04	0.11	0.14	0.14	0.14	0.09	0.06
1 d sbc	0.07	0.03	0.03	0.09	0.13	0.13	0.11	0.08	0.06

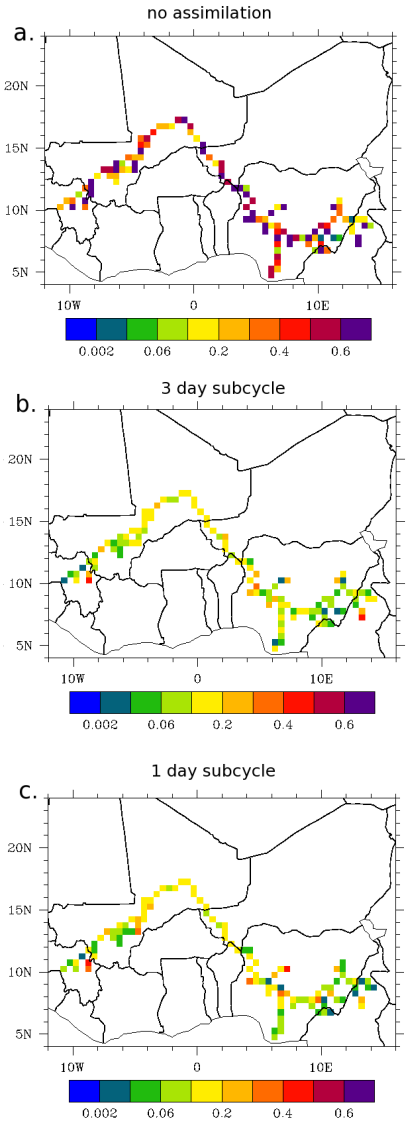

Figure 13. Relative error of water levels averaged over the period of assimilation.

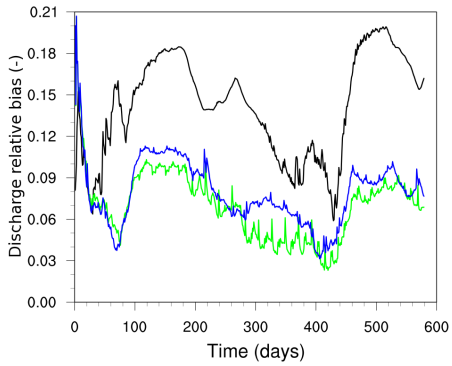

Figure 14. Discharge relative error averaged over the river versus time with no assimilation (black), with 1-day subcycle (orange) and 3-day subcycle (blue) orbit SWOT assimilations. The relative error is calculated as the ratio $(|q_{\text{with/without assi}} - q_{\text{truth}}| / q_{\text{truth}}$, where q is the water level ($m^3\ s^{-1}$).

To better understand the relationship between the water levels and the discharge, the flooded fraction time series at two locations (Ke Macina and Lokoja) is shown in Fig. 17. In Ke Macina, there was no flooded fraction before the assimilation, while there was about 15–20 % for the "truth". At this location, DA leads to a water level increase that generates flooding for both orbits, in agreement with the true run. The amplitude of the flooded fraction simulated with the assimilation for a 3-day subcycle is close to that of the true run while the flooded fraction simulated with assimilation for a 1-day cycle is overestimated. This results because the water level and discharge results slightly overestimate the results from the true run for the 1-day orbit.

Another interesting case is observed in Lokoja, where the model simulates flooding in 25 % of the grid area with no assimilation, which is not observed for the "truth". Here again, by reducing water levels, the assimilation considerably reduces the flooded fraction for the 1-day subcycle orbit and even prevents it from occurring for the 3-day subcycle orbit. No floods are modeled at the other sites for the truth, the run with no assimilation or the runs with assimilation, so these sites are not shown in Fig. 17. These results are valuable since they show that the use of DA corrects the flood

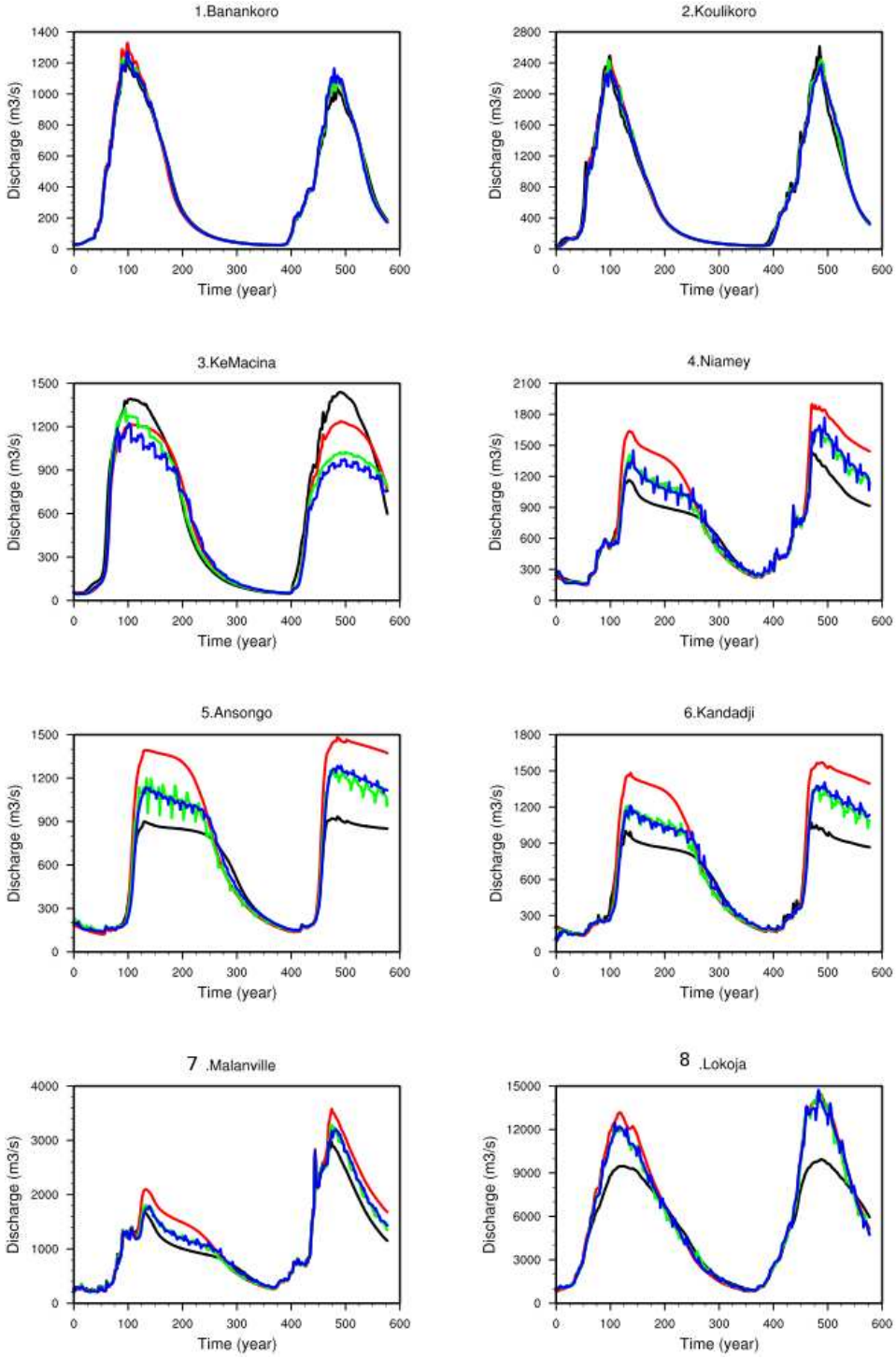

Figure 15. Time evolution of discharge at the location of the eight locations (Fig. 1) for the "truth" (red curves), with no assimilation (black curves) and with assimilation of SWOT 1-day subcycle (green) and 3-day subcycle (blue) orbit observations.

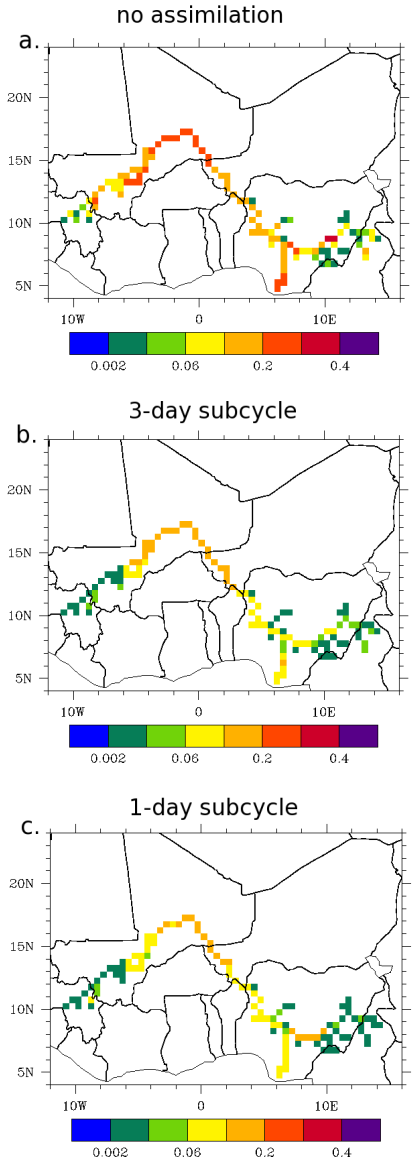

Figure 16. Relative error of discharge averaged over the period of assimilation.

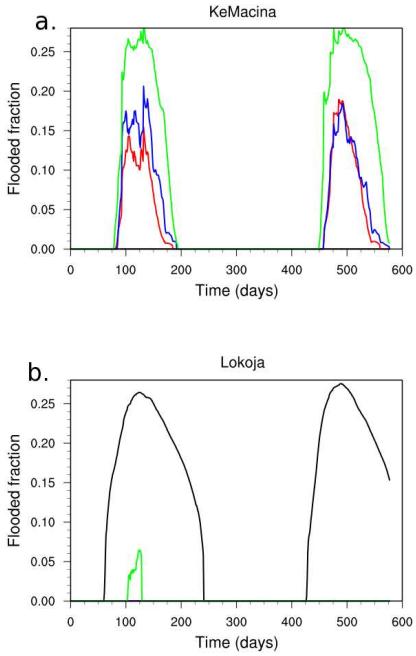

Figure 17. Flooded fraction versus time at Ke Macina and Lokoja, for the truth (red), with no assimilation (black), with assimilation for 3-day subcycles (blue) and 1-day subcycles (green). Note that in Lokoja, there is no flooded fraction represented for the truth and for the run with assimilation with a 3-day subcycle.

prediction for two major sites of the Niger Basin. Indeed, Ke Macina is located just upstream to the entrance of the inner-delta region, while Lokoja is the last in situ station upstream of the river outlet. It should be noted that the discharge response to water level modification depends on whether or not there are floods. For example, at Ke Macina, during the monsoon period, the water level is increased via assimilation, which results in a better fit with the truth simulation and in a discharge decrease. This is coherent with the results of Pedinotti et al. (2012), in which the introduction of floodplains leads to a reduction of the discharge. However, in regions without floodplains, a water level increase leads to a discharge increase (see Kandadji for example).

The frequency of events as a function of the flooded fraction value (ratio of flooded area over pixel area) is shown in Fig. 18 for the truth (a), without assimilation (b), a 1-day subcycle assimilation (c) and a 3-day subcycle assimilation (d). Only the pixels with a flooded fraction greater than 10 % (0.1 on the horizontal axis) are considered. It is shown that without assimilation, the model does not simulate flooded fractions above 0.5, which represents about 8 % of the flood events for the truth simulation. Moreover, without assimilation, the model tends to overestimate the occurrence of smaller events. This is corrected by the assimilation, with a slight tendency to over-estimate flood intensity for the assimilation with the 3-day subcycle orbit, while the 1-day subcycle orbits leads to an excessive occurrence of flooded fractions contained in the [0.2–0.3] range. According to these results, DA allows for a better simulation of the water storage variations and leads to better estimation of flood event occurrence and intensity in the inner-delta area.

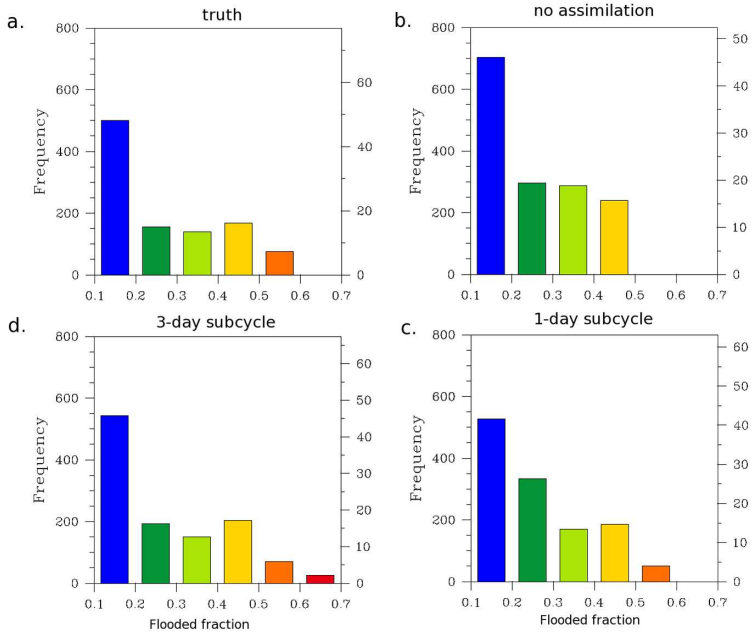

Figure 18. Frequency of flood events over the delta classified by intensity (flooded fraction). Only the pixels with a flooded fraction higher than 10 % are considered for the calculation.

5.4 Water storage variations

Ideally, for water resource management applications and for making reliable future water resource projections, global hydrologic models should be able to reasonably simulate water storage variations in regional to large-scale continental reservoirs including rivers, groundwater, aquifers and floodplains. It is then of interest to see if DA can improve the simulation of these water variations. Figure 19 shows the relative water storage variations in four continental reservoirs (river, floodplains, aquifers and soil) for the truth (red), without assimilation (black), 1-day subcycle (blue) and 3-day subcycle assimilations (green). For each reservoir, the 20-day running average water storage variations are divided by the averaged water storage over the period of assimilation. The maximum relative water storage variation ranges from 6 % in the river reservoir to about 30 % in the floodplain reservoir, which is not negligible. In the four reservoirs, the simulations with assimilation better represent the amplitude and the phase of the water storage variations. The assimilation seems to be useful for better representing anomalies in continental reservoirs, which are subject to many uncertainties. However, it should be noted that the physical representativeness of these storage values is not guaranteed due to the lack of monitoring data.

6 Discussion

Optimization of the Manning coefficient using a DA methodology leads to a significant improvement of the water levels over the Niger River, and also at the eight locations with gages. The relative error of the Manning coefficient is reduced (40 % reduction) and it globally converges towards an optimal value despite potential problems related to equifinality. The relative error of the water level is globally improved (a 30 % reduction) and the amplitude of the water level is closer to the truth with assimilation than without assimilation. Discharge is also improved by the assimilation, but to a lesser extent than for the water levels (7 %). Moreover, the proposed methodology results in a better prediction of flood event occurrence and intensity in the inner delta and better simulates water storage anomaly maxima and minima in several reservoirs, especially the groundwater and the aquifer reservoirs, for which the temporal evolution is difficult to observe. This study is promising since, to our knowledge, no large-scale assimilation applications exist for the optimization of spatially distributed hydrological parameters. It shows SWOT observations would be useful for the improvement of CHSs. This method could lead to a better representation of the water cycle in climate prediction applications, but could also be used for large-scale water resource management applications. Finally, there is no clear advantage difference between the two subcycle orbits used for this study; each has better skill for certain situations.

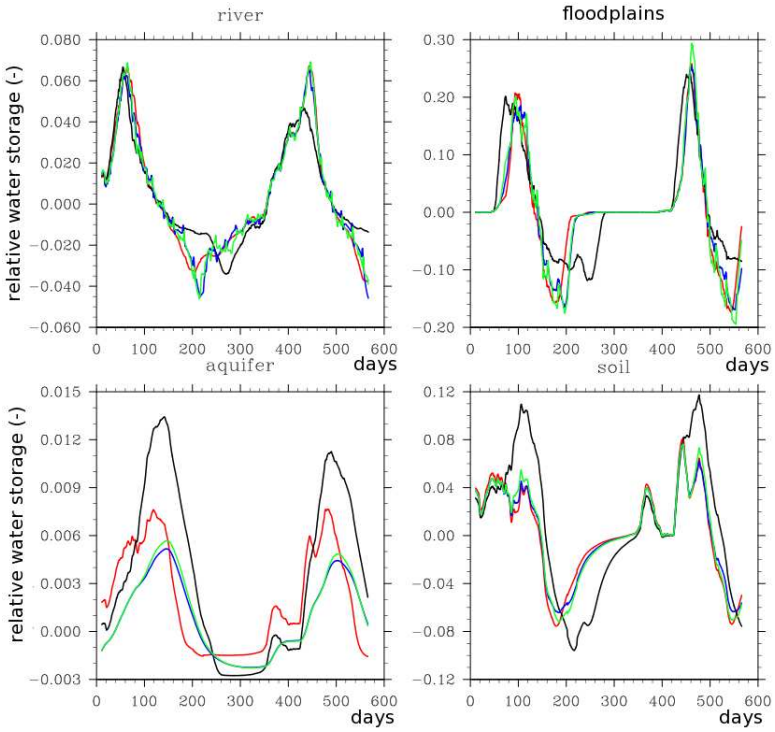

Figure 19. Relative water storage variations in the river, the floodplains, the aquifer and the soil reservoirs for the truth (red), no assimilation (black), 1-day orbit subcycle (green) and 3-day subcycle assimilations (blue). For each reservoir, the 20-day running average water variations are divided by the averaged water storage over the period of assimilation (from June 2002 to December 2003).

This study has some limitations and several assumptions should be noted. The assumption of the white noise error for SWOT observations is probably too optimistic. Furthermore, no correlation of the measurement errors along the swath has been assumed. Estimating satellite observation error sources has been the subject of several studies at the French space agency (CNES) in recent years. Initially, a white noise was introduced within the SWOT water level along track altimetric estimate in order to represent the error due to satellite observations (Biancamaria et al., 2011). Lion (2012) presents methods to simulate, in a more realistic manner, different sources of SWOT satellite observation errors. These errors are generally due to several factors such as satellite attitude, baseline error, phase unwrapping errors, etc. These errors are not always Gaussian and do not always have a mean value of 0. A perspective for improvement of the assimilation methodology proposed in this study is to introduce these errors into the assimilation system in order to get a more realistic estimation of SWOT observation errors and of the error covariance matrix $\mathbf{R}$. However, their introduction in the system is not obvious and requires the use of a different assimilation filter due to the aforementioned Gaussian issue. Indeed, the Gaussian error distribution along SWOT tracks does not ensure that the error of the observation vector, $\boldsymbol{y}^0$, is Gaussian. Yet, the Gaussian nature of the observation error is a strong assumption of the EKF and possible solutions to get around this limitation exist, such as the use of an ensemble Kalman filter or a particle filter.

The hypothesis that the Manning coefficient uncertainties are the only source of model errors is obviously a rather simple assumption since other errors, such as those related to precipitation forcing uncertainties, riverbank-full depth error or the relatively simple ISBA-TRIP physics, can also be the sources of significant modeling errors. It could be potentially interesting to perform the assimilation on an ensemble of perturbed runs in order to take into account several uncertainty scenarios and the estimation of the background modeling matrix could be done using an ensemble method (Evensen et al., 2004). Within the framework of a real-data experiment, accounting for various sources of errors via Manning control will lead to improved Manning values that should not be interpreted as physical values. Modeling assumptions also put a limitation on the DA performance in the context of real-data experiments. For example, it is assumed in the TRIP model that geomorphological parameters such as the Manning coefficient are constant in time, which is a significant assumption, especially in a region with a strong seasonal climate variability, such as the Niger Basin. Hopefully, SWOT

observations will help to correct this problem, for example, using this method to build seasonal climatologies of key parameters. To exploit this possibility, a further OSSE study could be done, in which the "true" Manning coefficient varies seasonally.

Additionally, this study was done within the context of OSSE, in which the truth was issued from a reference ISBA-TRIP simulation. This allowed for an evaluation of the methodology but makes the improvements on roughness, level, flow and storage highly correlated. Moreover, the OSSE does not guarantee the physical representativeness of the corrected values of the Manning coefficient since the background and the observations are issued from the same model. For these reasons, the performance of the DA will need to be re-evaluated with real observations. In the study presented here, the truth and the perturbation are based on the same physical parameterizations: this is not true when real data are used. Therefore, the assimilation should be applied using either real observations of water level, or water level issued from a different model, such as a hydrodynamic model. In further studies, longer assimilation windows could be exploited but also require a bigger storage capacity which must be considered for the choice of the assimilation window size.

Finally, this method must be applied to other ISBA-TRIP parameters and for other large-scale basins to evaluate its global application capability. It is not guaranteed that a methodology, which works for a specific basin, could be used for all other major basins (with different climates, geology, etc.). Ongoing work is focused on applying the methodology herein to other basins. These proposed improvements aim at ensuring that the assimilation methodology will be applicable when real SWOT data area be available.

7 Conclusions

This study presents a simple method for assimilating SWOT virtual water level into a large-scale coupled land-surface hydrology model (TRIP-ISBA) in order to improve estimates of the required global hydrological model input parameters. In this case, the assimilation is used for the correction of a single parameter which is the Manning coefficient. To accomplish this, an OSSE was performed, using virtual SWOT observations of water levels. Two orbits, with different subcycles but with the same 22-day repeat period, have been considered to generate the observations (1-day and 3-day subcycles), each one providing a specific spatial and temporal coverage of the domain. Uncertainties on the estimation of the Manning coefficient are assumed to be the only sources of modeling errors. The EKF algorithm was applied every 2 days (the length of the assimilation window) to compute an optimal Manning coefficient (analysis). The Manning coefficient globally converged for both orbital subcycles to the same average value, the convergence being faster for the 3-day subcycle orbit. The method leads to a global reduction of 40 % of the Manning coefficient error over the river. This correction significantly improved the water levels (the error has been reduced by 30 % for the river) and, to a lesser extent, discharge (7 % of reduction of the error which can be significant for the Niger River in terms of water resources considering that its mean annual discharge is $6000\,m^3\,s^{-1}$). Moreover, the biggest improvements were observed downstream of the river (Lokoja), which is a valuable result for climate applications which require estimation of the discharge at large river mouths.

This method gives a promising perspective for global-scale applications, and it could be extended to other large basins. However, several relatively simple hypotheses have been made, and these should be addressed and refined in future studies. The context of the OSSE allows for the evaluation of the model but does not guarantee the physical representativeness of the corrected values obtained in this study. Moreover, other sources of uncertainties should be assumed for the assimilation, such as rainfall errors and/or riverbank-full depth. Modeling errors such as those from the ISBA land surface parameterization should be considered, such as that pertaining to runoff. It was also considered in this work that observation and modeling errors were not correlated in space and time, which might not be realistic. The use of more realistic errors simulated by Lion (2012) in the framework of the SWOT mission prelaunch investigations will be considered in future studies.

Another perspective consists in the application of this method to other TRIP parameters, or several parameters at a time. Correction of ISBA parameters, such as those controlling subgrid runoff for example, is also planned but must be considered carefully as the impact on the river is less direct. Before the satellite launch, the AirSWOT airborne campaign will provide SWOT-like data sets of water level, which will enable studies using a more realistic SWOT DA application, instead of the observing simulation system experiment presented here. Even if this airborne campaign does not cover the Niger Basin, it will potentially provide a better observation error model. Yet, using more complex observations and model errors might require a modification of the assimilation scheme to overcome extremely stringent EKF filter assumptions of Gaussian unbiased errors. Possible assimilation techniques to test are the ensemble Kalman filter or the particle filter.

Acknowledgements. This work is supported by the African Monsoon Multidisciplinary Analysis (AMMA) project and the Surface Water Ocean Topography (SWOT) satellite mission project of the Centre National d'Etudes Spatiales (CNES). The diverse studies presented in this paper would not have been possible without the valuable contribution of the Autorite du Bassin du Niger(ABN).

Edited by: F. Tian

References

Alsdorf, D. E., Rodriguez, E., and Lettenmaier, D. P.: Measuring surface water from space, Rev. Geophys., 45, RG2002, doi:10.1029/2006RG000197, 2007.

Andersen, I., Dione, O., Jarosewich-Holder, M., and Olivry, J.-C.: The Niger river basin: A vision for sustainable management, World Bank, Washington, DC, 2005.

Andreadis, K. M., Clark, E. A., Lettenmaier, D. P., and Alsdorf, D. E.: Prospects for river discharge and depth estimation through assimilation of swath-altimetry into a raster-based hydrodynamics model, Geophys. Res. Lett., 34, L10403, doi:10.1029/2007GL029721, 2007.

Arora, V. K. and Boer, G. J.: A variable velocity flow routing algorithm for GCMs, J. Geophys. Res., 104, 30965–30979, doi:10.1029/1999JD900905, 1999.

Bates, P. and De Roo, A.: A simple raster-based model for flood inundation simulation, J. Hydrol., 236, 54–57, doi:10.1111/j.1752-1688.2001.tb05522.x, 2000.

Baup, F., Mougin, E., de Rosnay, P., Timouk, F., and Chenerie, I.: Surface soil moisture estimation over the AMMA Sahelian site in Mali using ENVISAT/ASAR data, Remote Sens. Environ., 109, 473–481, doi:10.1016/j.rse.2007.01.015, 2007.

Beven, K. and Kirkby, M.: A physically-based variable contributing area model of basin hydrology, Hydrolog. Sci. B., 24, 43–69, 1979.

Biancamaria, S., Bates, P., Boone, A., and Mognard, N.: Large-scale coupled hydrologic and hydraulic modelling of the Ob river in Siberia, J. Hydrol., 379, 136–150, doi:10.1016/j.jhydrol.2009.09.054, 2009.

Biancamaria, S., Durand, M., Andreadis, K., Bates, P., Boone, A., Mognard, N., Rodriguez, E., Alsdorf, D., Lettenmaier, D., and Clark, E.: Assimilation of virtual wide swath altimetry to improve Arctic river modeling, Remote Sens. Environ., 115, 373–381, doi:10.1016/j.rse.2010.09.008, 2011.

Boone, A., Calvet, J.-C., and Noilhan, J.: Inclusion of a Third Soil Layer in a Land Surface Scheme Using the Force-Restore, Method, J. Appl. Meteorol., 38, 1611–1630, 1999.

Bouttier, F. and Courtier, P.: Data assimilation concepts and methods, ECMWF, 1999.

Chow, V. T., Maidment, D. R., and Mays, L. W.: Applied hydrology, MacGraw-Hill series in water resources and environmental engineering series, 1989.

Cogley, J. G.: The Albedo of Water as a Function of Latitude, Mon. Weather Rev., 107, 775–781, doi:10.1175/1520-0493(1979)107<0775:TAOWAA>2.0.CO;2, 1979.

Decharme, B. and Douville, H.: Introduction of a sub-grid hydrology in the ISBA land surface model, Clim. Dynam., 26, 65–78, doi:10.1007/s00382-005-0059-7, 2006.

Decharme, B., Douville, H., Boone, A., Habets, F., and Noilhan, J.: Impact of an Exponential Profile of Saturated Hydraulic Conductivity within the ISBA LSM: Simulations over the Rhône Basin, J. Hydrometeorol., 7, 61–80, doi:10.1175/JHM469.1, 2006.

Decharme, B., Douville, H., Prigent, C., Papa, F., and Aires, F.: A new river flooding scheme for global climate applications: Off-line evaluation over South America, J. Geophys. Res., 113, D11110, doi:10.1029/2007JD009376, 2008.

Decharme, B., Alkama, R., Douville, H., Becker, M., and Cazenave, A.: Global Evaluation of the ISBA-TRIP Continental Hydrological System. Part II: Uncertainties in River Routing Simulation Related to Flow Velocity and Groundwater Storage, J. Hydrometeorol., 11, 601–617, doi:10.1175/2010JHM1212.1, 2010.

Decharme, B., Alkama, R., Papa, F., Faroux, S., Douville, H., and Prigent, C.: Global off-line evaluation of the ISBA-TRIP flood model, Clim. Dynam., 38, 1389–1412, doi:10.1007/s00382-011-1054-9, 2011.

Drusch, M., Scipal, K., de Rosnay, P., Balsamo, G., Andersson, E., Bougeault, and Viterbo, P.: Towards a Kalman Filter based soil moisture analysis system for the operational ECMWF Integrated Forecast System, Geophys. Res. Lett., 36, L10401,doi:10.1029/2009GL037716, 2009.

Durand, M., Andreadis, K., Alsdorf, D., Lettenmaier, D., Moller, D., and Wilson, M.: Estimation of bathymetric depth and slope from data assimilation of swath altimetry into a hydrodynamic model, Geophys. Res. Lett., 35, L20401, doi:10.1029/2008GL034150, 2008.

Durand, M., Rodriguez, E., Alsdorf, D. E., and Trigg, M.: Estimating River Depth From Remote Sensing Swath Interferometry Measurements of River Height, Slope, and Width, IEEE J. Sel. Top. Appl., 3, 20–31, doi:10.1109/JSTARS.2009.2033453, 2010.

Evensen, G.: Sampling strategies and square root analysis schemes for the EnKF, Ocean Dynam., 54, 539–560, doi:10.1007/s10236-004-0099-2, 2004.

Hunter, N., Bates, P., Horritt, M., and Wilson, M.: Simple spatially-distributed models for predicting flood inundation: A review, Geomorphology, 90, 208–225, doi:10.1016/j.geomorph.2006.10.021, 2007.

Knighton1998] Knighton D.: Fluvial forms and processes : A new perspective, Hodder Arnold Publication, Routledge, 400 pp., 1998.

Lion, C.: Simulation des données SWOT haute résolution et applications à l'étude de l'estuaire de l'Amazone, Ph.D. thesis, Univ. Paul Sabatier – Toulouse III, 2012.

Masson, V., Le Moigne, P., Martin, E., Faroux, S., Alias, A., Alkama, R., Belamari, S., Barbu, A., Boone, A., Bouyssel, F., Brousseau, P., Brun, E., Calvet, J.-C., Carrer, D., Decharme, B., Delire, C., Donier, S., Essaouini, K., Gibelin, A.-L., Giordani, H., Habets, F., Jidane, M., Kerdraon, G., Kourzeneva, E., Lafaysse, M., Lafont, S., Lebeaupin Brossier, C., Lemonsu, A., Mahfouf, J.-F., Marguinaud, P., Mokhtari, M., Morin, S., Pigeon, G., Salgado, R., Seity, Y., Taillefer, F., Tanguy, G., Tulet, P., Vincendon, B., Vionnet, V., and Voldoire, A.: The SURFEXv7.2 land and ocean surface platform for coupled or offline simulation of earth surface variables and fluxes, Geosci. Model Dev., 6, 929–960, doi:10.5194/gmd-6-929-2013, 2013.

Michailovsky, C., Milzow, C., and P., B.-G.: Assimilation of radar altimetry to a routing model of the Brahmaputra River, Water Resour. Res., 49, 1–10, doi:10.1002/wrcr.20345, 2013.

Miller, Z. F., Pavelsky, T. M., and Allen, G. H.: Quantifying river form variations in the Mississippi Basin using remotely sensed imagery, Hydrol. Earth Syst. Sci. Discuss., 11, 3599-3636, doi:10.5194/hessd-11-3599-2014, 2014.

Noilhan, J. and Planton, S.: A Simple Parameterization of Land Surface Processes for Meteorological Models, Mon. Weather Rev., 117, 536–549, 1989.

Oki, T. and Sud, Y. C.: Design of Total Runoff Integrating Pathways (TRIP) – A Global River Channel Network, Earth Interact., 2, 1–37, doi:10.1175/1087-3562(1998)002<0001:DOTRIP>2.3.CO;2, 1998.

Papa, F., Prigent, C., Aires, F., Jimenez, C., Rossow, W. B., and Matthews, E.: Interannual variability of surface water extent at the global scale, 1993–2004, J. Geophys. Res., 115, D12111, doi:10.1029/2009JD012674, 2010.

Pavelsky, T. M. and Smith, L. C.: RivWidth: A software tool for the calculation of river widths from remotely sensed imagery, IEEE Geosci. Remote Sens. Lett., 5, 70–73, 2008.

Pedinotti, V., Boone, A., Decharme, B., Crétaux, J. F., Mognard, N., Panthou, G., Papa, F., and Tanimoun, B. A.: Evaluation of the ISBA-TRIP continental hydrologic system over the Niger basin using in situ and satellite derived datasets, Hydrol. Earth Syst. Sci., 16, 1745–1773, doi:10.5194/hess-16-1745-2012, 2012.

Pereira-Cardenal, S. J., Riegels, N. D., Berry, P. A. M., Smith, R. G., Yakovlev, A., Siegfried, T. U., and Bauer-Gottwein, P.: Real-time remote sensing driven river basin modeling using radar altimetry, Hydrol. Earth Syst. Sci., 15, 241-254, doi:10.5194/hess-15-241-2011, 2011.

Pistocchi, A. and Pennington, D.: European hydraulic geometries for continental scale environmental modelling, J. Hydrol., 329, 553–567, doi:10.1016/j.jhydrol.2006.03.009, 2006.

Rodriguez, E.: SWOT Science Requirements Document, JPL Document, 11, 2012.

Salamon, P. and Feyen, L.: Assessing parameter, precipitation, and predictive uncertainty in a distributed hydrological model using sequential data assimilation with the particle filter, J. Hydrol., 376, 428–442, doi:10.1016/j.jhydrol.2009.07.051, 2009.

Santos Da Silva, J. and Calmant, S.: Mapping of the extreme stage variations using ENVISAT altimetry in the Amazon Basin Rivers, Int. Water Technol. J., 2, 14–25, 2012.

Yamazaki, D., O'Loughlin, F., Trigg, M. A., Miller, Z. F., Pavelsky, T. M., and Bates, P. D.:Development of the Global Width Database for Large Rivers, Water Resour. Res., 50, 3467–3480, doi:10.1002/2013WR014664, 2014.

Yoon, Y., Durand, M., Merry, C., Clark, E., Andreadis, K., and Alsdorf, D.: Estimating river bathymetry from data assimilation of synthetic SWOT measurements, J. Hydrol., 464, 363–375, doi:10.1016/j.jhydrol.2012.07.028, 2012.